THE UNIVERSITY *of* EDINBURGH

Synthesis and Application of Novel Near Infrared Cyanine Dyes and Optical Imaging Agents

Neil Norouzi

Doctor of Philosophy

The University of Edinburgh

2014

Declaration

I, Neil Norouzi, hereby confirm that the research described in this thesis was carried out by myself under the supervision of Prof. Mark Bradley at the University of Edinburgh between September 2009 and June 2013. Where work has been performed either jointly or wholly by others, this is clearly attributed. No part of this thesis has been previously submitted for any other degree or professional qualification.

I am aware of and understand the University's policy on plagiarism and I certify that this thesis is my own work**,** except where indicated by referencing.

Parts of this thesis were published previously as:

Thielbeer, F., Chankeshwara, S. V., Johansson, E. M. V., Norouzi, N and Bradley M. Palladium-mediated bioorthogonal conjugation of dual-functionalised nanoparticles and their cellular delivery. *Chemical Science* **2013**, *4*, 425-431

Norouzi, N. Cyanine Dyes *SynLett* **2013**, *24*, 1307.

Signed: Date:

Acknowledgements

First and foremost I would like to thank Professor Mark Bradley for his guidance, motivation and patience throughout my time in Team Bradley. Thank you to Drs Nicos Avlonitis, Sunay Chankeswara, Jeff Walton and Tashfeen Walton for the helpful advice and useful discussions throughout the years and who taught me every single day.

To the members of the Bradley group itself the list is long. To the forgotten duo of Juan Ma and Adam who made the lab a fun and perhaps interesting environment, I say thank you for the good times early on. To the lunch team of Aurélie, Martha, Andrew, Matt, Martin and more recently Holly, I say thank you for helping lift the pressure while providing the constant motivation that kept me pushing forward. To my long time desk neighbour Thingsoon, thank you for putting up with my terrible jokes for what must have felt like forever. I thank all the Bradley group members, past and present for all our moments and I wish you all the best.

A big thank you to all the team at the QMRI, with special thanks to Prof. Chris Haslett, Dr Kevin Dhaliwal, Dr Neil McDonald, Dr Manuelle Debunne and Miss Emma Schofield, I am ever grateful for your time and effort which made this thesis possible.

I would like to thank my family in the UK, Denmark and Iran who have always supported me throughout my endeavours and I hope that this thesis will do you all justice. Special thanks to my Mum, my Uncles Hassan and Mansour, my Aunty Elahe and sister Eileen. To all my long term friends, Jamie, Callum, Matt, James, Shaun and Graham, poker friends and colleagues out-with the Bradley group, you can stop asking me when I will submit now.

Finally, to Aurélie who has been there for me since day one of this adventure, I could not have done it without you. Thank you for always building my confidence, providing me with the motivation that got me where I am and for always being there for me. This is just the start.

Lay Summary

The use of imaging techniques such as molecular resonance imaging (MRI) is common and widely used for the diagnosis of various diseases. Although extremely useful, they can be time consuming, expensive and can require the use of radioactive molecules. For these reasons the use of optical imaging, a technique in which light is used to visualize the molecular processes or macroscopic tissues such as tumours, is now becoming more widely used.

Currently, fluorescence optical imaging uses light in the visible region of the electromagnetic spectrum. In this region light is uncontrollably absorbed by tissue and biomolecules within the human body and is therefore not efficient at providing a fluorescence signal. To overcome this, near-infra red (NIR) fluorophores have been used as their emission in the NIR region of the electromagnetic spectrum results in less absorption by the body providing stronger signals. NIR fluorophores have obtained great interest over the past 20 years due to their high tissue penetration. Synthesis of new imaging agents is constantly required to increase signal intensity, increase specificity to the target under investigation and lower toxicity. This thesis describes steps towards this through the synthesis of a variety of NIR cyanine dyes and discusses their cellular uptake and toxicity.

One practical application of these NIR fluorophores was the derivitisation of microspheres. Microspheres are small spherical particles which have several interesting properties such as good cell penetration. These spherical polymers are usually around 150 nm in diameter and can be modified with NIR fluorophores. Two types of fluorescent microspheres are reported within this thesis, with discussions into their cellular uptake and localisation.

Synthesis of a fluorescent bacteria detector is also discussed, describing a simple tool to separate Gram negative from Gram positive bacteria in a fast and efficient manner.

Abstract

The use of fluorescent imaging probes for the real time detection of cellular malfunctions, such as enzyme over expression has shown promise. Fluorescent dyes with absorption and emission values below 600 nm are limited in their *in vivo* applications due to high background auto-fluorescence and low resolution images. Employing near infrared (NIR) fluorophores such as cyanine dyes can overcome this disadvantage.

Cyanine dyes can be synthesised using solution or solid-phase techniques with the use of solution phase chemistry allowing for larger scale and higher yielding reactions. Utilising a selection of functional groups and varying polymethine chain lengths a cyanine dye library with tuneable absorption and emission wavelengths was synthesised. This thesis gives the first detailed examples of how modifications on heptamethine cyanine dyes alter their cellular uptake and cellular toxicity. Furthermore, a NIR fluorescent microsphere is reported as well as NIR functionalised microspheres with the ability to be tracked within cells.

Additional lines of work involved the synthesis of a fluorescent sensor for the visualisation of bacteria. Aminopeptidases are present within the peptidoglycan cell wall of Gram negative bacteria and therefore can be targeted for real time detection of bacteria to aid in the detection of infectious diseases. A coumarin based probe is reported which detects aminopeptidase in gram negative bacteria *in vitro*.

Abbreviations

δ:	Chemical shift in ppm
τ:	Fluorescence lifetime
μw:	Microwave
A549:	Human adenocarcinomic alveolar basal epithelial cells
Ahx:	Aminohexanoic acid
AMC:	Aminomethyl coumarin
AU:	Arbitrary units
BLI:	Bioluminescence imaging
Boc:	Di-*tert*-butyl dicarbonate
BODIPY:	Boron-dipyrromethene
CT:	Computed tomography
Cy:	Cyanine
DCC:	Dicyclohexyl carbodiimide
Dde:	2-Acethyldimedone
DdeOH:	2-(1-hydroxyethylidene)-5,5-dimethylcyclohexane-1,3-dione
DIC:	*N*,*N'*-Diisopropylcarbodiimide
DIPEA:	*N*,*N*-Diisopropylethylamine
DMAP:	4-Dimethylaminopyridine
DMEM:	Dulbecco's modified Eagle medium
DMSO:	Dimethyl sulfoxide
d:	Doublet
dd:	Doublet of doublets
DVB:	Divinylbenzene
EDC:	1-Ethyl-3-(3-dimethylaminopropyl)carbodiimide
ELSD:	Evaporative light scattering detector
ESI:	Electrospray ionisation
FA:	Formic acid
FACS:	Fluorescence-activated cell sorting
FITC:	Fluorescein isothiocyanate

Fmoc:	Fluorenylmethoxycarbonyl
FMT:	Fluorescence-mediated tomography
FRET:	Fluorescence (Förster) resonance energy transfer
FRI:	Fluorescence reflectance Imaging
FTIR:	Fourier transform infrared spectroscopy
FTMS:	Fourier transform ion cyclotron resonance mass spectrometry
HEK293T:	Human embryonic kidney 293T cell line
HeLa:	Cervical cancer cell line
HOMO:	Highest occupied molecular orbital
HPLC:	High-performance liquid chromatography
HR:	High resolution
ICG:	Indocyanine green
ICP-OES:	Inductively coupled plasma – optical emission spectroscopy
IR:	Infrared
k_{nr}:	Non-radiative decay process
k_r:	Radiative decay process
m/z:	Mass to charge ratio
MAO:	Monoamine oxidase
MALDI-TOF:	Matrix-assisted laser desorption/ionization- time of flight
MMP:	Matrix metalloproteinase
mp:	Melting point
MRI:	Magnetic resonance imaging
MS:	Mass spectrometry
MTT:	3-(4, 5-dimethylthiazolyl-2)-2,5-diphenyltetrazolium bromide
NIR:	Near infrared
Ninhydrin:	2,2-Dihydroxyindane-1,3-dione
nm:	Nanometer
NMR:	Nuclear magnetic resonance
NP:	Nanoparticle
Oxyma:	Ethyl (hydroxyimino)cyanoacetate
PBS:	Phosphate-buffered saline
PC-3:	Human prostate cancer cell line

PEG:	Polyethyleneglycol
PeT:	Photo-induced electron transfer
PET:	Positron emission tomography
pH:	Potentia hydrogenii
ppm:	Parts *per* million
PS:	Polystyrene resin
q:	Quartet
RFU:	Relative fluorescent units
ROS:	Reactive oxygen species
RP-HPLC:	Reverse-phase high-performance liquid chromatography
rt:	Room temperature
s:	Singlet
SDS:	Sodium dodecyl sulfate
SPECT:	Single-photon emission computed tomography
t:	Triplet
tBu:	*tert*-Butyl
TEA:	Triethylamine
TFA:	Trifluoroacetic acid
TIS:	Triisopropylsilane
tlc:	Thin-layer chromatography
t_R:	Elution time of compound on HPLC
TX-100:	Triton X-100
UV:	Ultraviolet
V-50:	2,2´-Azobis-(2-amidinopropane) hydrochloride
VBA:	para-vinylboronic acid
VBAH:	para-vinylbenzylamino hydrochloride
λ:	Wavelength
λ_{em}:	Emission wavelength
λ_{ex}:	Excitation wavelength
Φ:	Quantum yield

Contents

Chapter 1

Near Infrared Fluorophores – A Future for Medical Imaging

1.1 Medical Imaging

Medical imaging is a broad term and covers imaging techniques that gain anatomic and functional information of a patient. Over the 20th century, techniques such as magnetic resonance imaging[1] (MRI), X-ray computed tomography[2] (X-ray-CT) and nuclear medicine (PET[3] and SPECT[4]) have been developed to generate contrast between the target of interest and the surrounding tissue. Even still, the development of new imaging modalities that are safer, cheaper, easy to use and offer increased image resolution are sought after.

Widely considered the future of medical imaging[5], molecular imaging techniques have been the focus of 21st century research. The development of clinical and optical imaging techniques over the past 100 years is described in Figure 1 and shows the immense technological advancements made since the first light microscope was developed.

Many phrases have been used to define molecular imaging, leading to a general consensus that molecular imaging is the "visualisation of *in vivo* biological processes at the molecular or cellular level using specific imaging probes" [6].

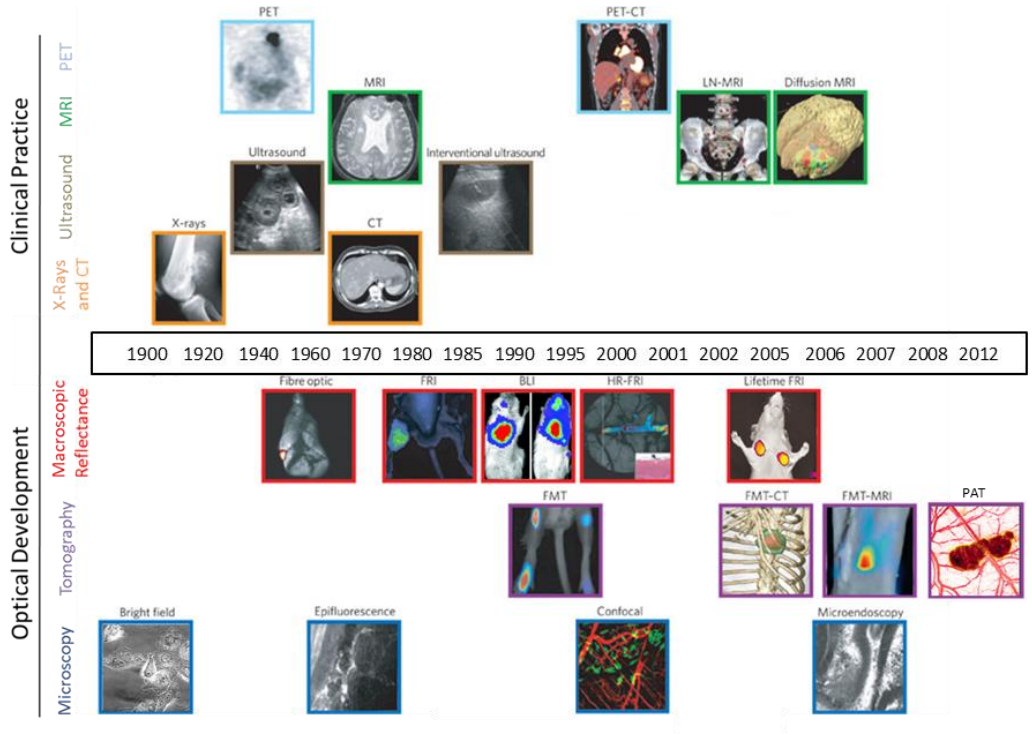

Figure 1: Imaging techniques used in: 1) clinical practice (above timeline) – imaging of bones (X-rays), soft tissue (ultrasound, MRI and CT). Tomographical 3D images (PET, CT and MRI). 2) Optical development (below timeline) - Imaging through microscopic, tomographic and macroscopic techniques. The timeline is approximate and not to scale. BLI, bioluminescence imaging; CT, computed tomography; FMT, fluorescence-mediated tomography; FRI, fluorescence reflectance imaging; HR-FRI, high-resolution FRI; LN-MRI, lymphotropic nanoparticle-enhanced MRI; MRI, magnetic resonance imaging; PET, positron-emission tomography; PAT, photoaucoustic tomography. Image adapted with permission from reference[7]. All individual image reference permissions obtained, see appendix 1. PET image[8]. Fibre optic image[9]. BLI image[10]. FRI image[11]. FMT-MRI image[12], PAT image[13] all references copyright (2005-2013).

The applications of molecular imaging are various, for example, Politi *et al* used MRI to monitoring tumour size variation after long term administration of a known anticancer drug, Erlotinib[14]. It was found that although the drug was initially successful at reducing the tumour size, intermittent drug administration failed to completely remove the tumour, while after 22 weeks, administration of the drug had no effect on the tumour. This was thought to be due to the up-regulation of growth factors unaffected by the drug.

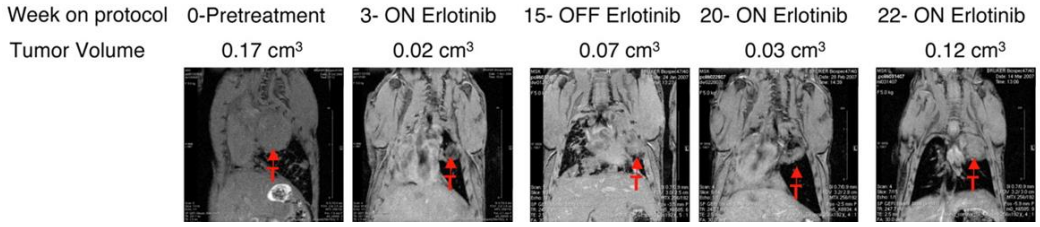

Figure 2: Tumour resistance to Erlotinib after intermittent treatment[14]. Mice were treated with Erlontinib (25 mg/kg/day) 5 days per week for 4 weeks after which treatment was interrupted for 4 weeks. Treatment cycle repeated three times. Images show development of drug resistance after 22 weeks due to tumour growth despite drug administration.

Molecular imaging has played a crucial role in oncology[15] but also in the detection cardiovascular disease[16] by targeting over-expression of specific enzymes or receptors. For example, Matrisian *et al* targeted the expression of matrix metalloproteinase (MMP) in a mouse model injected with cancer cells that either expressed or did not express MMP-7. MMP's are over expressed in cancer cells and are therefore a good target for tumour imaging[17]. Using a quenched cyanine molecule (Cy 5.5) linked to an MMP-7 cleavable peptide, fluorescence was detected on incubation with the MMP-7 expressing probe after un-quenching[18].

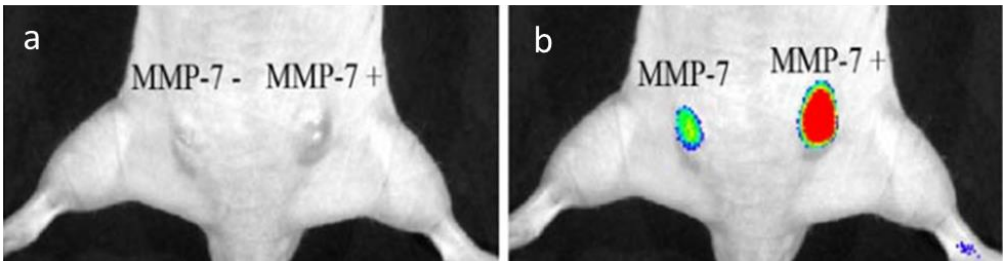

Figure 3: Detection of near infrared fluorescence of MMP specific imaging probe following subcutaneous injection of cancer cells expressing or not expressing MMP-7. a) Brightfield image of nude mouse 4 weeks post injection of cancer cells. b) Cyanine 5 detection 4 hours post injection of imaging probe. Red represents high fluorescent intensity. Image adapted and reproduced with permission from reference[18], copyright Society of of Nuclear Medicine and Molecular Imaging (2008).

A large increase in fluorescence signal was detected for the MMP-7 expressing probe indicating proteolytic activity.

Technological advancements[19] in medical and molecular imaging over the last 30 years have led to high resolution imaging modalities which are now used in tandem to give complimentary sets of information[12, 20]. For example, combination of the excellent soft tissue contrast properties of MRI and the high sensitivity of PET or SPECT to detect drug distribution can be applied[11, 21]. These advancements have also allowed medical imaging to be used in the field of drug discovery and development[11, 22] and drug resistance investigations[14].

Often, the decision of which imaging technique to apply can be difficult[23] as each technique has particular advantages and disadvantages. For example, MRI is easily used in clinical applications, however, the long imaging time, high cost and lack of patient compliance make it a difficult option for many. PET and SPECT offer images with unlimited depth penetration but require the use of radioactive materials which are costly and can raise safety concerns. Other techniques, such as CT and ultrasound allow high spacial resolution and are used clinically, but do not allow targeted specific imaging[22b]. Optical imaging is a highly sensitive technique which uses light to image target molecules in an affordable, safe, and quick to use manner. The main drawback for optical imaging is its low depth penetration making it difficult to use in clinical situations. Additionally, although FMT claims to generate quantitative data, these machines are often extremely specialised and not available to many research groups. To overcome the depth prenetration issue, investigations into near infrared (NIR) fluorophores as part of a molecular imaging probe are numerous and on-going[24] as a solution to increase the depth penetration of the technique. Table 1 summarises the main small animal imaging technologies and their respective advantages and disadvantages.

Technique	Advantages	Disadvantages	Resolution[I]	Depth	Time[II]	Quantitative	Multi-channel	Imaging agents	Cost[IV]
MRI	Clinical translation, high resolution and excellent tissue contrast	Cost and time	1 mm	No limit	Minutes to hours	Yes	No	Paramagnetic chelates	$$$
CT	Clinical translation and high resolution	No target specific imaging, radiation and poor tissue contrast	50 µm	No limit	Minutes	Yes	No	Iodinated molecules	$$
Ultrasound	Clinical translation and low cost	Limited targeted imaging and operator dependency	50 µm	Several cm	Seconds to minutes	Yes	No	Microbubbles	$$
PET	Clinical translation and high sensitivity	Cost and requires radiolabel	5-7 mm	No limit	Minutes to hours	Yes	No	^{18}F, ^{64}Cu or ^{11}C labelled compounds	>$$$
SPECT	Clinical translation	Limited resolution	8-10 mm	No limit	Minutes to hours	Yes	Possible	^{99m}Tc or ^{111}In labelled compounds	$$
FRI	High sensitivity	Limited clinical translation and low depth penetration	2-3 mm	<1 cm	Seconds to minutes	No	Yes	Fluorophores	$
FMT	High resolution 3D images	Low sensitivity to deep fluorophore	1 mm	<3 cm	Minutes to hours	Yes[III]	Yes	Near infrared fluorophores	$$
BLI	High-throughput	Limited imaging agents and cost	2-4 mm	Several cm	Minutes	Yes[III]	Yes	Luciferins	$$$
Confocal Microscopy	Sensitive and high resolution imaging	Limited clinical translation	1 µm	<400 µm	Seconds to hours	Yes[III]	Yes	Fluorophores	$$$

Table 1: Details of different pre-clinical imaging modalities and their properties. MRI, magnetic resonance imaging; CT, computed tomography; PET, positron-emission tomography; SPECT, single photon emission CT; FRI, fluorescence reflective imaging; FMT, fluorescence-mediated tomography; BLI, bioluminescence imaging. Image recreated and adapted with permission from reference[7] and reference[25], copyright (2008), Macmillan Publishers Ltd, Nature Medicine. [I]For high resolution, small animal imaging systems; [II]time for image acquisition; [III]Using specific instrumentation,[IV]purchase price of imaging system $ < US$ 100000, $$ US$ 100000-300000, $$$ >US$ 300000.

1.2 Optical Imaging Techniques

1.2.1 Fluorescence Reflective Imaging

A technique at the forefront of molecular imaging is fluorescence reflective imaging (FRI). FRI is a macroscopic imaging technique in which fluorescence can be captured non-invasively by shining light (excitation) on to the desired surface and collecting the emitted light, either on the same side as the excitation source (epi-illumination) or on the opposite side of the excitation source (trans-illumination), with the light (emission) collected by a highly sensitive camera using appropriate filters. Although useful, epi-illumination techniques do not allow quantitative measurements[26]. A modified version of this technique[27] was used by Weissleder[28] in the study of MMPs. This probe contained a self-quenched, modified cyanine dye attached to the cleavable peptide sequence GPLGVRGK which directed the probe in to the tumour region. On cleavage by MMP, the cyanine molecules were released resulting in an increase in fluorescence intensity (Figure 4).

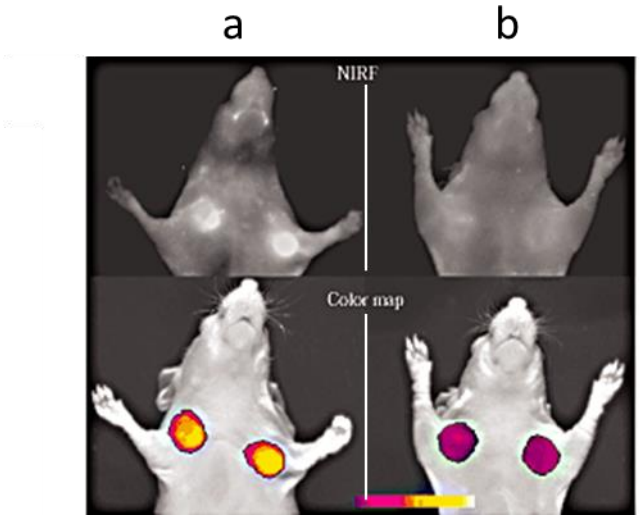

Figure 4: *In vivo* NIR fluorescence reflective imaging (modified) of tumour bearing mice. Column a) tumour bearing mice, Column b) tumour bearing mice, treated with MMP inhibitor. Top row shows raw image data acquired with λ_{ex} = 675 nm and λ_{em} =694 nm. Lower row shows colour-coded tumoural maps of MMP activity (yellow represents high fluorescent intensity). Reprinted and adapted with permission from reference[28], copyright (2001), Macmillan Publishers Ltd, Nature Medicine.

Mouse models, with and without a known MMP inhibitor (prinomastat) were imaged, showing a large fluorescent decrease for mice with the MMP inhibitor[28].

1.2.2 Fluorescence Molecular Tomography

Fluorescence molecular tomography gives 3-dimensional, high resolution images of *in vivo* fluorescence. By imaging through 360º's and combining the emission profiles through complex algorithms[29], FMT allows for quantification of the fluorescence signal making this modality superior to FRI. An excellent example of this tool was shown by Weissleder *et al*[30] on incubation of cyclophosphamide (a common anti-cancer drug) on cyclophosphamide resistant and non-resistant tumours. This study quantitatively determined the uptake of a tumour targeted probe modified with a fluorescent molecule (Annexin-Cy 5.5).

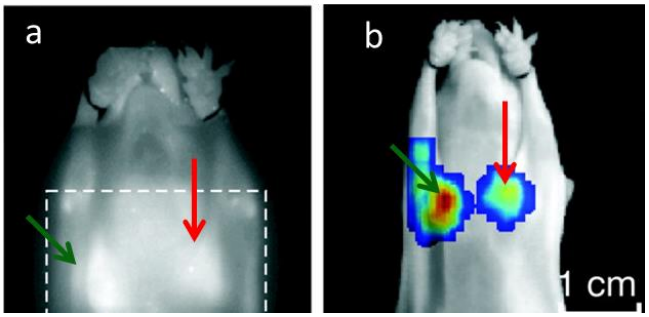

Figure 5: FMT analysis of Annexin-Cy 5.5 probe uptake by cyclophosphamide treated and non-treated tumours. a) Planar fluorescence image, cyclophosphamide resistant tumour (green arrow), non-resistant tumour (red arrow) b) FMT slice superimposed on planar image of cyclophosphamide resistant tumour (green arrow) and non-resistant tumour (red arrow). λ_{ex} = 670 nm, λ_{em} = 692 nm. Imaging probe accumulation noted in resistant tumour. Reprinted and adapted with permission from reference[30], copyright (2004), PNAS.

As expected, the drug resistant tumour accumulated more fluorescent probe due to its larger size[29].

1.2.3 Confocal Microscopy

For sub-cellular studies, confocal microscopy[26, 31] has seen applications across biology and medicine and it is used for live cellular imaging of fluorescent proteins[32], fluorescent nanoparticles[33] or cellular processes in real time to aid in disease diagnosis[34]. Based on a point source of light focussed upon a specimen it allows good resolution and 3D studies of individual cells over time[35]. For example, Bradley and co-workers[36] used confocal microscopy to show the real time intracellular deprotection of fluorescein using Pd^0. Furthermore, multiple wavelengths could be used to create a merged image of the full cell highlighting the nucleus, palladium catalyst and deprotected fluorescein.

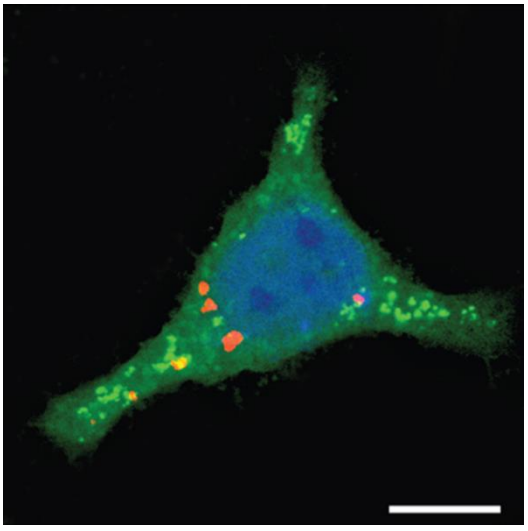

Figure 6: Merged confocal image of a single HeLa cell showing the nucleus (blue – Hoechst stained), Pd^0 microspheres (red – Texas red labelled) and deprotected rhodamine (green)[36]. Scale bar, 10 μm. Reprinted and adapted from reference[36], copyright 2011, Nature Publishing Group.

This was the first reported example of an intra-cellular Suzuki-Miyaura cross coupling reaction and highlights the capabilities of the confocal microscope.

1.3 Reporter Technologies and Probe Design

As highlighted by the example above, optical imaging requires a fluorescent imaging probe in order to generate the contrast required to visualise the target of interest. The concept and design of such molecular imaging probes require three features; 1) a targeting moiety specific to the imaging target. These can be DNA[37], antibodies or peptides[17], 2) a reporter molecule in order to generate a signal once the target has been reached, for example a PET radiolabel or fluorophore; 3) a carrier moiety to allow penetration into the cell if required, for example microspheres are often employed to aid in the cellular delivery of a cargo[33a].

Although all sections are equally important, this thesis will focus on the reporter molecules and their synthesis

1.3.1 Reporter Molecules

Reporter molecules can take many forms and must cause a change of a particular signal to be detected by the operator. For optical imaging, fluorophores are used and have advantages over other modalities as they are safe to use, can produce a long lived signal and can be tuned to give the desired reporting wavelength. Additionally, fluorophores can be manipulated to modify their emission or turn off the fluorescence completely. This has led to the synthesis of "smart" probes with the ability to "*turn on*" fluorescence in the presence of the target moiety.

One technique is to utilise the ability of a fluorophore or chromophore to quench its own emission or that of a neighbouring fluorescent molecule. This is often described as Förster resonance energy transfer (FRET) and describes the energy transfer between two chromophores[38]. Each fluorophore has a bathochromic shift between its absorption and emission spectra, termed the "Stokes shift".

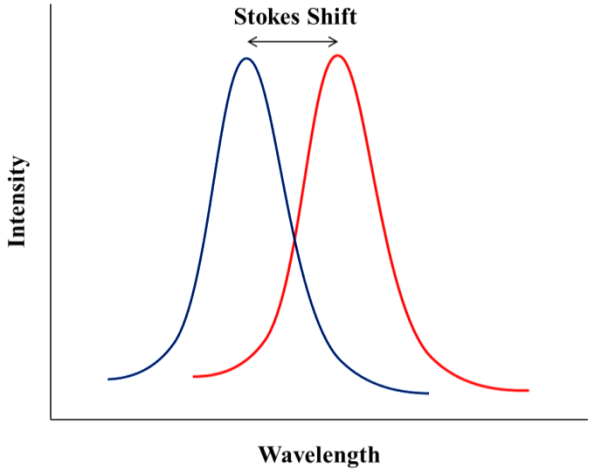

Figure 7: General absorption (blue) and emission (red) spectra showing Stokes shift.

A fluorophore with an extremely small Stokes shift, or in other words, a high overlap area between absorption and emission spectra, can quench its own fluorescence. FRET relies on the ability of one fluorophore (or quencher) to absorb the emitted fluorescence (acceptor) of the other fluorophore (donor). In order to be utilised in this manner the absorption profile of the acceptor, must overlap the emission profile of the donor. If the ability to quench is lost, fluorescence is regained. This technique forms the basis of many assays.

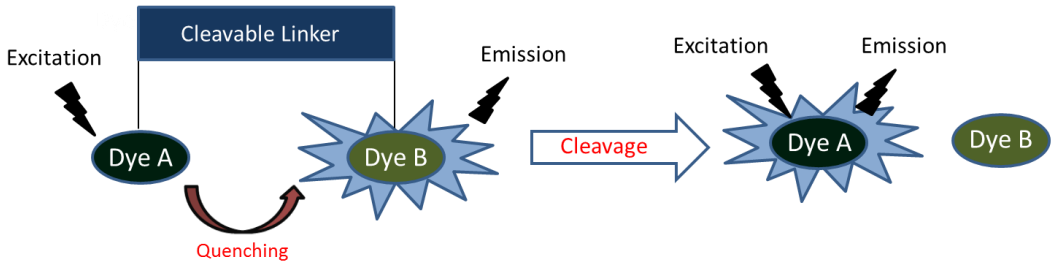

Figure 8: FRET quenching and subsequent emission on cleavage of the linker molecule.

Figure 8 shows a "*turn on*" system in more detail where the emission of Dye A is transferred to the acceptor Dye B. In the case of Dye B being a fluorophore, the emission wavelength of Dye B will be detected and in the case of Dye B being a quencher, no fluorescence will be observed. On cleavage of the linker, (for example a peptide substrate[39]) this energy transfer process is removed, allowing detection of

the fluorescence of Dye A. In this case, the probe design must take into account the distance between the fluorophores with a maximum distance of 10 nm[40]. Beyond this distance, fluorescence quenching drops exponentially but it is this limitation which allows FRET to be used as a molecular ruler with the ability to measure distances within biomolecules with high accuracy[41].

Another technique which utilises an electron donor/acceptor system is photoinduced electron transfer (PeT)[42]. In this instance, electron transfer from the fluorophore receptor to the fluorophore occurs on excitation of the fluorophore. This in turn prohibits the relaxation and fluorescence of the fluorophore. On receptor binding to the target analyte, electron transfer is no longer possible, resulting in a fluorescence *turn on* signal[42a].

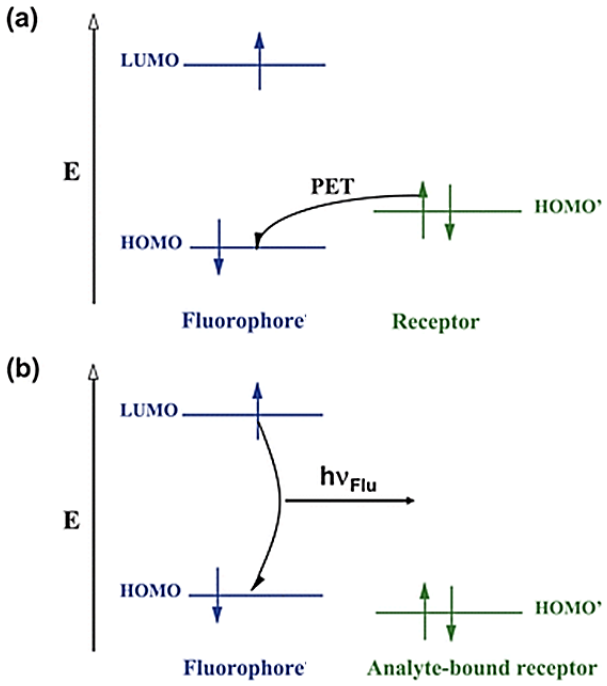

Figure 9: Relative energies of the frontier orbitals of fluorophore (blue) and fluorophore receptor (green). a) Analyte free, "off" conformation. b) receptor-analyte bound, "on" conformation. hυ represents emission of fluorophore. Reprinted and adapted with permission from reference[42a], copyright (2009) Royal Society of Chemistry.

Figure 9 shows the electron transfer between the receptor and fluorophore HOMO's in the "off" situation and no transfer in the "on" situation. This technique has been used in the detection of ions[43] and organic molecules[44] as well as cancer imaging[45]. For example, Tusa *et al* synthesised a fluorescent ion sensor with the ability to selectively detect potassium ions over sodium and calcium ions[46].

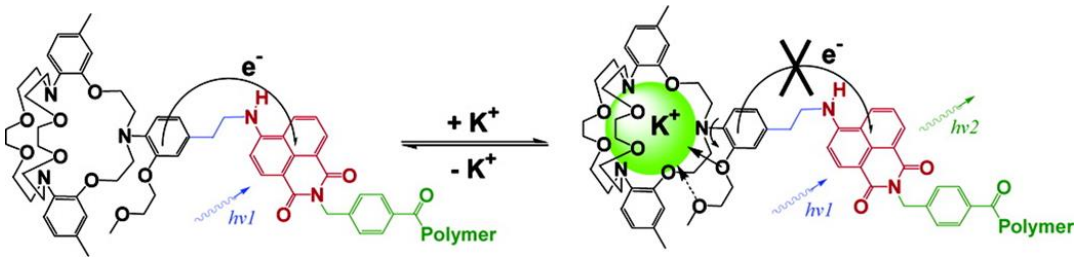

Figure 10: Tusa's Potassium ion sensor. While in the K^+ unbound state (left), no fluorescence emission is observed due to PeT. When K^+ binds (right), the PeT quenching is interrupted allowing fluorescence emission. λ_{ex} = 470 nm, λ_{em} = 540 nm. hυ1 represents excitation wavelength, hυ2 represents emission wavelength. Reprinted with permission from reference[46], copyright (2003) American Chemical Society.

This sensor was able to detect the presence of potassium ions at 2 mM allowing this probe to be used to measure the presence of extracellular potassium in serum or whole blood.

1.4 Fluorescence and Fluorophores

The choice of the fluorophore is an important decision and can determine the signal intensity of the reporting agent. Development of the optimum fluorophore allows better visualisation of the target.

1.4.1 Fluorescence Principle

Fluorescence[47] is described as the "spontaneous emission of radiation from an excited molecular entity with retention of spin multiplicity"[48]. Fluorescence is based on electron excitation from a ground electronic state to an excited electronic state. In this excited state, vibrational relaxation can occur, to the lowest vibrational energy

level of the lowest excited state. This relaxation occurs through several pathways and was first described by Alexsander Jablonski in 1933[49]. These pathways are namely, radiative emission (fluorescence) or non-radiative emission (heat)[50] and is represented in the Jablonski diagram (Figure 11). It is the loss of energy through heat (vibrational relaxation) that results in the emission wavelength being higher than the excitation wavelength and the generation of Stokes shift (see section 1.3). When studying fluorophores various factors are to be considered such as quantum yield (Φ), extinction coefficient (ε) and fluorescence lifetime (τ).

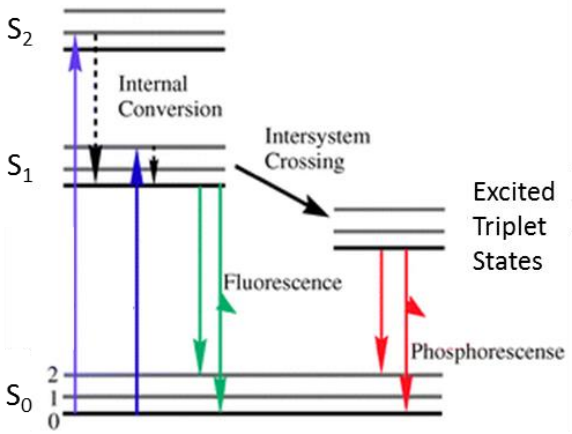

Figure 11: Jablonski diagram for an organic molecule. Lines: blue - light absorption (10^{-15} s), dashed black – vibrational relaxation and internal conversion (10^{-14} – 10^{-11} s), green – fluorescence (10^{-9} – 10^{-7} s), red – phosphorescence (10^{-3} – 10^{-2}), black – intersystem crossing (variable). Times indicate approximate speed of transition. Reprinted and adapted with permission from reference[51], copyright (2010), The Royal Society of Chemistry.

Quantum yield is arguably the most important factor relating to fluorophores and is described as a ratio between the number of photons absorbed, to the number of photons emitted. Although most fluorophores should have a quantum yield of at least 0.05 to be termed fluorescent, ideal fluorophores would have a value at 1.0 with 100% of photons being absorbed, re-emitting through fluorescence. Unfortunately, this is rare due to energy loss through heat or other relaxation pathways. Several factors must be taken into account when measuring a fluorescence quantum yield. These are mainly fluorophore concentration, pH and solvent system. Fluorophore concentration is a key factor with highly concentrated solutions resulting in self-quenching[52]. The quantum yield can also be described by the relative rates of

decay (radiative and non-radiative) pathways which deactivate the excited state (Equation 1).

$$\phi = \frac{k_r}{k_r + \sum k_{nr}}$$

Equation 1: Calculation of fluorescence quantum yield. k_r and k_{nr} correspond to the radiative and non-radiative decay processes respectively and Σk_{nr} describes the sum of the rate constants for the pathways that compete with photon emission, (e.g. collisional quenching, or inter system crossing).

Most simply, the quantum yield is calculated by comparing the sample under investigation with a reference sample of known quantum yield following procedures described by Demas [53] and Williams[54] and more recently by Brouwer[55]. In most cases, there are many options for the selection of a reference sample, however, for NIR fluorophores the scope is limited. An overview of the most common reference samples used in the literature is summarized in Table 2.

Compound	Solvent	Literature Quantum Yield	Appropriate Wavelength (nm)
ICG[55]	DMSO	0.11	650-800
Cresyl Violet[55]	Ethanol	0.56	600-650
Chlorophyll A[56]	Ether	0.32	600-750
Fluorescein[57]	0.1 M NaOH	0.95	500-600
Quinine Sulfate[52]	0.1 M H_2SO_4	0.54	400-600
Norharmane[58]	0.1 M H_2SO_4	0.58	400-550
Tryptophan[59]	Water, pH 7.2	0.14	300-380

Table 2: Typical quantum yield reference standards.

Experimentally, the fluorescence and absorbance of the reference is measured against the sample using the same conditions, i.e. same excitation wavelength, slit widths and gain.

1.4.2 Fluorescent Dyes

There are hundreds of fluorescent dyes with absorption and emission wavelengths ranging between 300-900 nm. The need for fluorescent dyes is high, and fortunately, the fluorophore tool box has never been as diverse as it is today. The ability to select a fluorophore with ideal photo-physical properties and reactive functional groups for a specific purpose is possible, although fluorescent dyes can be extremely expensive.

1.4.2.1 Commercial Dyes

Some of the most common fluorophores available are coumarin[60], fluorescein[61], rhodamine[62], squaraine[63], BODIPY[64] and cyanine[65] based molecules. Each molecule type has certain typical characteristics while due to the diverse modifications available, the variety and application of these molecules is high.

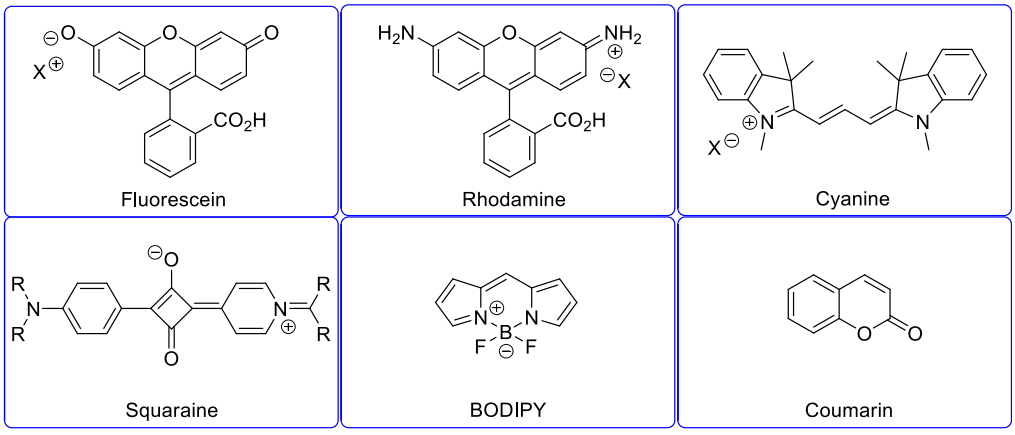

Figure 12: Structure of common commercially available fluorophores.

The applications of these dyes include research into solar cells[66], detection of metal ions[67], tumour detection[68] and reactive oxygen species detection[69] to name but a few.

Fluorophores are inherently highly conjugated molecules and therefore can often encounter solubility or aggregation issues when being utilised for biological applications. To overcome these problems, synthetic modifications often have to be made. For example, addition of sulfonates is a common route to increase aqueous solubility.

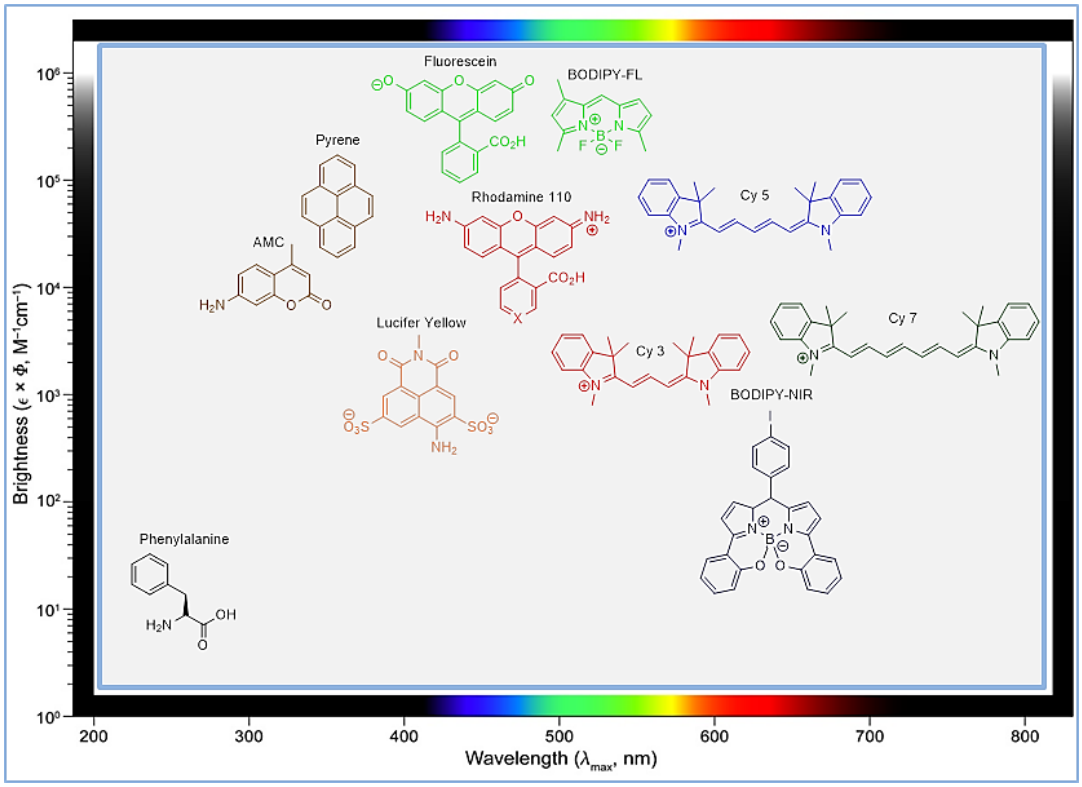

Figure 13: Common fluorophores. X-axis represents approximate absorption wavelengths, Y-axis represents approximate fluorescence intensity. AMC, aminomethyl coumarin; BODIPY, Boron-dipyrromethane; Cy, Cyanine. Reprinted and adapted with permission from reference[70], copyright (2008), American Chemical Society.

Ideally, fluorophores to be used for molecular imaging purposes should have the following characteristics; 1) absorption and emission maxima between 700-900 nm

to optimise depth penetration, 2) high quantum yield, 3) narrow absorption and emission bands, 4) high photo-stability, 5) non-toxic and 6) ability to be synthesised on a large scale. Currently, no fluorophores cover all of these requirements.

1.4.2.2 NIR Dyes

Fluorescence molecular imaging with the use of NIR imaging agents will provide new opportunities for diagnostic imaging[70]. Fluorophore excitation wavelengths are extremely important for a variety of reasons, for example, excitation in the ultraviolet (UV) region can cause tissue damage by crosslinking of DNA and therefore is unacceptable for clinical use[71]. Excitation in the blue/green region (< 495 nm) of the electromagnetic spectrum can be used for surface imaging applications, however, poor tissue penetration and tissue auto-fluorescence results in clinical limitations. Naturally occurring chromophores in biological tissue such as oxy- and deoxyhemoglobin, melanin, and fat absorb light below or above the NIR window. This is highlighted by the spectrum of naturally occurring endogenous fluorophores as shown in Figure 14.

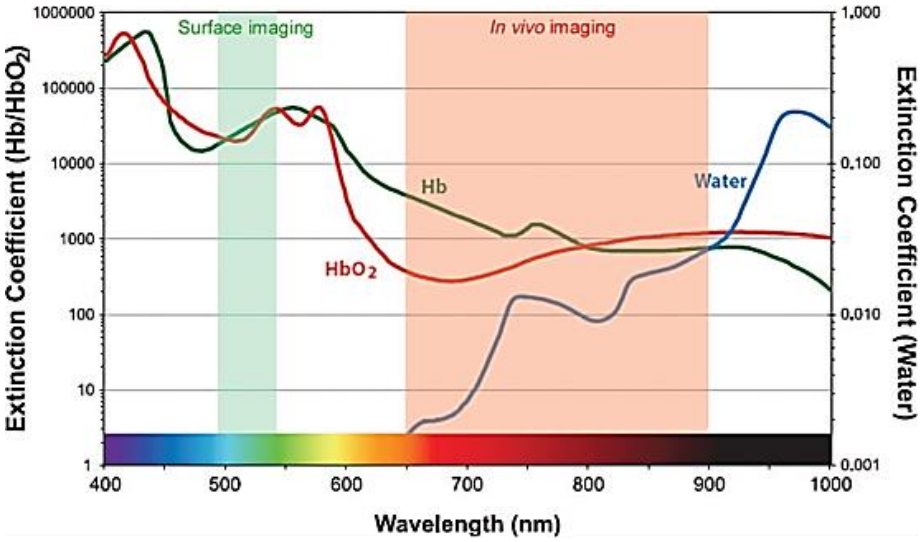

Figure 14: Extinction coefficients of water, oxyhemoglobin and deoxyhemoglobin over visible to near-infrared wavelengths. Reprinted with permission from reference[5], copyright (2010) American Chemical Society.

NIR fluorophores absorb and emit light in the near infrared window (700-900 nm) and therefore do not suffer from high background auto-fluorescence. Recent advances in this field[72] have seen the number of publications grow with fluorescent probes to detect DNA[73], degenerative disease[74] and cancer metastasis[75] common in the literature. For example, Bacskai *et* al targeted pathological deposits of amyloid-beta (Aβ) peptide in the brain, a key sign in the development of Alzheimer's disease. Synthesis of a NIR emitting smart probe with the ability to cross the blood brain barrier and to fluoresce intensely when bound to Aβ plaques allowed distinction between white matter, grey matter and Aβ deposits within the brain[74a].

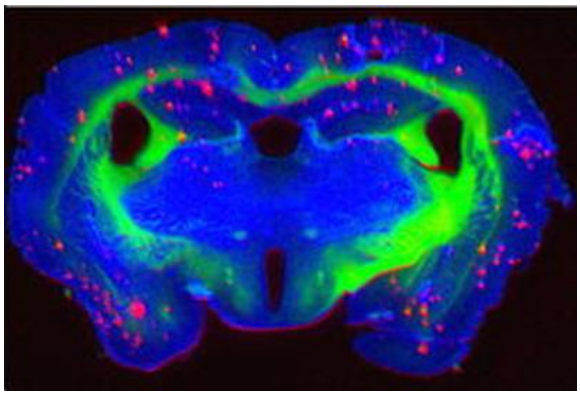

Figure 15: NIR emitting smart probe to detect the presence of Aβ plaques in mice brain. Tissues were incubated with NIR emitting probe and imaged with a fluorescence multispectral imaging system (Maestro). Red = Aβ plaques. Blue = grey matter. Green = white matter. λ_{ex} = 480 nm, λ_{em} = 525-720 nm. Image adapted from reference[74a], copyright European Journal of Nuclear Medicine (2007).

Similarly, Gremlich *et al* synthesised a NIR oxazine derivative with an analogous ability to cross the blood brain barrier and bind with high affinity to Aβ plaques. Semi-quantitative NIR imaging (modified fluorescence reflectance imaging) confirmed the specific interaction of the probe in the brain of mice over expressing amyloid plaques using an excitation wavelength of 670 nm[74b]. These *in* vivo studies using NIR fluorescent probes continue to advance the diagnosis of Alzheimer's disease, however, translation into humans may prove difficult in years to come.

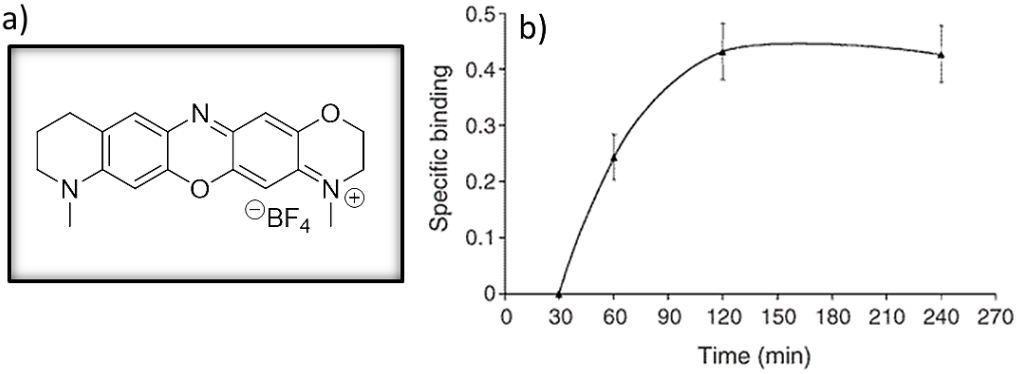

Figure 16: Specific binding of NIR fluorophore to Aβ plaques in the brain of mice over expressing amyloid deposits. a) Structure of NIR fluorophore, λ_{ex} = 650 nm, λ_{em} = 670 nm, quantum yield = 0.41. b) Specific binding of NIR fluorophore (0.1 mg/kg in saline solution) to Aβ plaques as a function of time. Calculated from fluorescent signal (APP23 transgenic mice), minus fluorescence signal (non-transgenic mice), divided by fluorescence signal (transgenic mice). Imaged reproduced from reference[74b], copyright Nature Publishing Group (2005).

1.4.2.3 Cyanine Dyes

Cyanine dyes, named after the Latin word *cyanos*, meaning blue, were discovered by accident in 1856 by Williams when he reacted *N*-amyl quinolinium iodide with *N*-amyl lepidinium iodide in ammonia[76]. Shortly afterwards in 1857, Von Babo independently discovered "one of the most beautiful substances in organic chemistry" by reacting quiniline with alkyl sulphates[77]. By 1863 a brilliant blue cyanine dye was available commercially and new analogues were being sought[76].

The structures of cyanine dyes vary in complexity. Generally, two heterocyclic "head groups" are connected by an odd (x) number of methine groups with x+1 electrons. This conjugated system results in a coloured, fluorescent molecule (Figure 17). Cyanine dyes can absorb and emit light between the visible to near-infra red region and these wavelengths can be tuned by modification of the polymethine chain. This tuneability, along with narrow absorption and emission bands resulted in cyanine dyes being used in a variety of applications, such as photography[78], solar cells[66b, 79], proteomics[80], photovoltaics[81] and more recently molecular imaging[82].

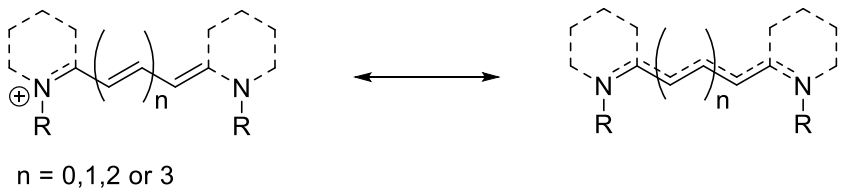

Figure 17: General structure of cyanine dyes with delocalised cation along polymethine chain.

Cyanine dyes are named depending on the number of carbon atoms in the polymethine chain with n = 0,1,2 or 3, the mono-, tri- (cyanine 3), penta (cyanine 5), or heptamethine (cyanine 7) cyanine's respectively. Cyanine dyes cover a large part of the electromagnetic spectrum (500-900 nm) with each vinylene increment in the polymethine chain corresponding with a bathochromic shift of approximately 100 nm. Due to the large variation in possible structures, cyanine dyes can have diverse quantum yields, extinction coefficients and Stokes shifts. Although cyanine quantum yields are generally lower than some other fluorophores such as fluorescein, the long NIR absorption and emission wavelengths of cy 5 and cy 7 result in brighter images when using light or confocal microscopes due to the decreased tissue absorption. Further, the addition of functional groups such as carboxylic acids can be achieved to allow conjugation to biomolecules for cellular or *in vivo* studies.

As described by Tung[83], NIR fluorophores generally suffer from problems such as low quantum yields, photo-instability and spectral broadening as the wavelength increases. Further, the hydrophobicity of cyanine dyes can cause aggregation with self-quenching becoming a problem[84].

Further studies into cyanine dyes may help overcome these issues with the synthesis and application of cyanine dyes being discussed in more detail in Chapters 2 and 3.

1.5 Aims of Thesis

The need for new imaging probes is growing with an ever increasing number of targets. For successful optical imaging probe design, the correct fluorophore must be selected. This thesis aims to synthesise a variety of cyanine dyes with differing functionalities to determine their effects on the photo-physical properties of the dyes. Detailed studies into the cellular uptake and toxicity of the new cyanine dyes will be discussed with a recent example of a cyanine dye as part of an imaging probe. Furthermore, the synthesis of an inherent NIR fluorescent microsphere and its cellular uptake will be investigated.

Finally, the synthesis of a coumarin based aminopeptidase probe will be reported with the specific detection of several Gram negative bacteria over Gram positive bacteria *in vitro*.

Chapter 2

Synthesis and *In Vitro* Studies of Cyanine Dyes

2.1 An Introduction to Cyanine Dyes

There is a pressing need for new fluorophores, with NIR cyanine dyes at the forefront of this demand. Many different synthetic routes to cyanine dyes have been reported as discussed in recent reviews by Mishra *et al*[84b, 85]. Most commonly, cyanine dyes are described as being symmetrical or non-symmetrical with respect to their indole head groups, with all cyanine dyes existing in the *trans* form with the two indole nitrogens in either a tertiary or quaternary form.

Cyanine dyes are fully conjugated planar molecules showing resonance stabilisation along the polymethine chain. Non-symmetrical cyanine dyes exhibit less planarity than the symmetrical analogues, causing a decrease in fluorescence intensity. As with all fluorophores, increasing the rigidity of the molecule is beneficial, leading to brighter colours and higher fluorescence intensities.

Although there are many examples, synthesis of tri- penta- and heptamethine cyanine dyes will be discussed herein.

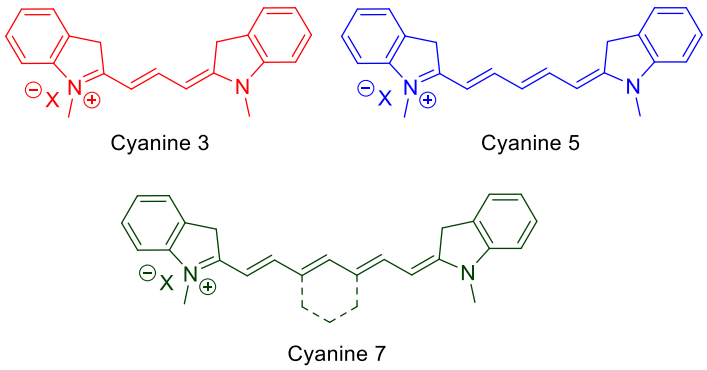

Figure 18: General structures of cyanine dyes. Colours represent approximate colour in solution. Approximate absorption and emission properties (nm): cyanine 3 λ_{abs} = 550, λ_{em} = 580, cyanine 5 λ_{abs} = 650, λ_{em} = 680, cyanine 7 λ_{abs} = 750, λ_{em} = 780. X = counter ion.

2.2 Synthesis of Symmetrical and Non-Symmetrical Cyanine Dyes

2.2.1 Tri-methine Cyanine Dyes

Symmetrical cyanine dyes were first synthesised using the "orthoester" method in which various quaternary indolium salts are reacted with orthoesters in the presence of a base[86] (Scheme 1).

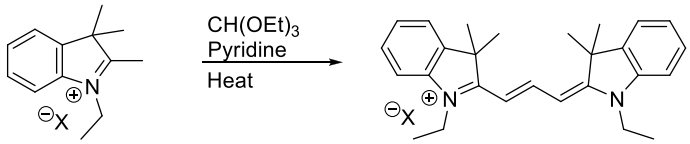

Scheme 1: Synthesis of symmetrical trimethine dyes[86].

Almeida *et* al used a similar route to synthesise a ratiometric pH sensor[87]. This one pot reaction involved a single step where the heterocyclic base was refluxed in excess alkylating agent using DMF as the solvent (Scheme 2).

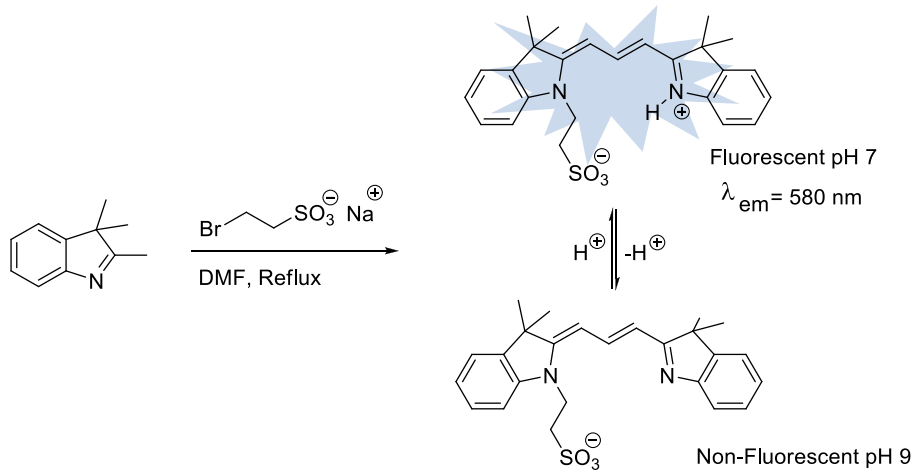

Scheme 2: Almeida's synthesis of pH sensitive probe[87].

This probe was able to detect pH changes between 6-8 (Scheme 2) with protonation of the tertiary nitrogen caused a detectable shift in colour and fluorescence[87].

Stepwise synthesis of an un-symmetrical cyanine 3 dye was carried out by Jung, who synthesised dyes for use in difference gel electrophoresis[88]. This procedure (detailed in Scheme 3) begins with the alkylation of trimethyl indole with propyl bromide, followed by condensation with diphenylformamidine in excess acetic anhydride. Alkylation of the indole with 1-bromohexanoic acid afforded the second indolium salt which, when reacted with acetanilidylvinyl indolium salt in ethanol gives the desired fluorophore.

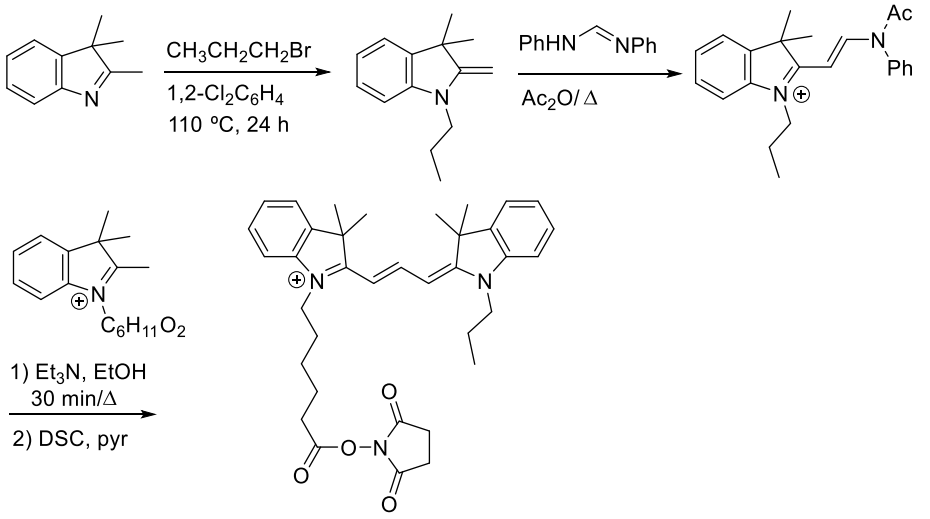

Scheme 3: Synthesis of trimethine dye by Jung[88a].

To avoid the synthesis of the unwanted symmetrical cyanine dye, Bradley *et al* synthesised a non-symmetrical cyanine 3 using solid-phase methods and microwave mediated synthesis[89] as described in detail in Chapter 3.

Cyanine 3 molecules are highly fluorescent but do not fall within the classic NIR window with absorption and emission wavelengths below 600 nm.

2.2.2 Pentamethine Cyanine Dyes

The synthesis of pentamethine cyanine dyes is widely reported in the literature. A detailed synthesis is described by Romieu and co-workers in which, symmetrical and non-symmetrical cyanine dyes were generated[90].

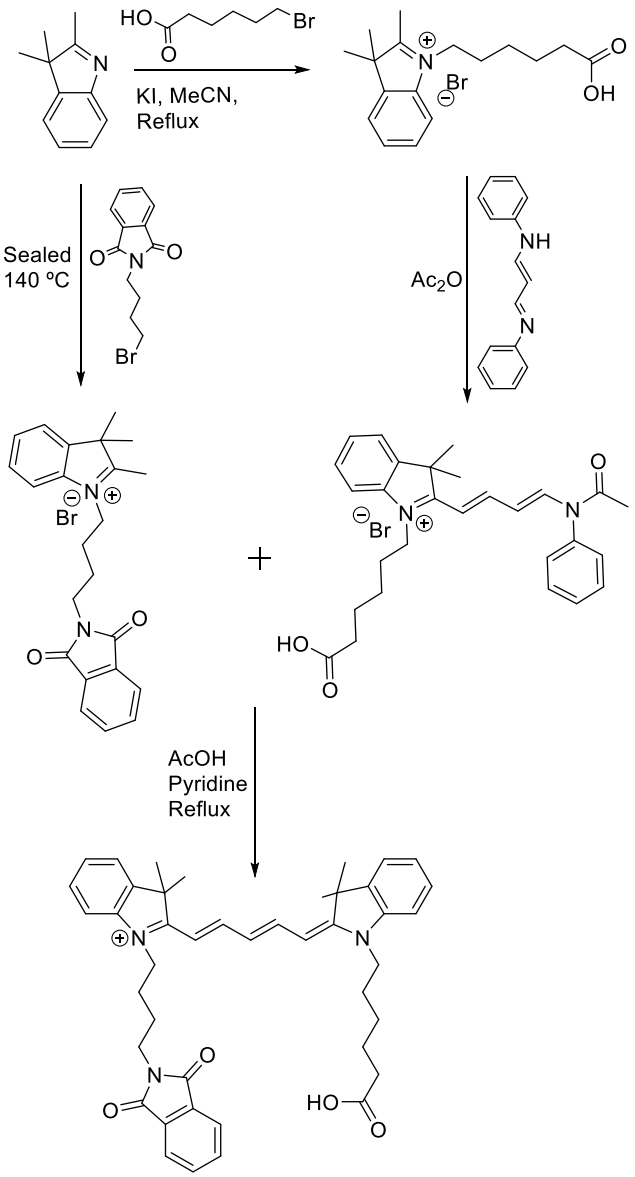

Scheme 4: Romieu synthesis of functionalised pentamethine dyes[90].

These molecules represented the first cyanine dyes with two orthogonal functional groups.

Wilson exploited the DNA binding nature of cyanine 5 dyes to synthesise anti-cancer therapeutics that bound to G-quadruplexes[91] (Scheme 5).

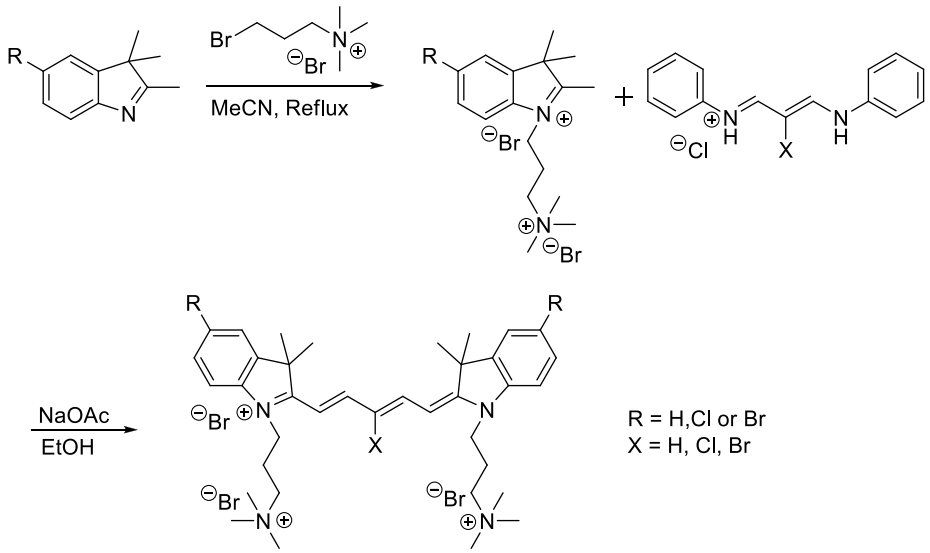

Scheme 5: Wilson's synthesis of a pentamethine DNA quadraplex binder[91a].

Cyanine dyes are known to bind to the minor groove of DNA duplexes[92] and the addition of further quaternary ammonium cations increased aqueous solubility and quadruplex affinity through electrostatic interactions[91a].

Another synthesis relating to DNA binding involved a condensation reaction between cyclopentane-1,3-diones with the quaternary salts of 2-methylbenzothiazolium at high temperatures. Yarmoluk *et al* utilised this method to synthesise a variety of pentamethine dyes (Scheme 6)[93].

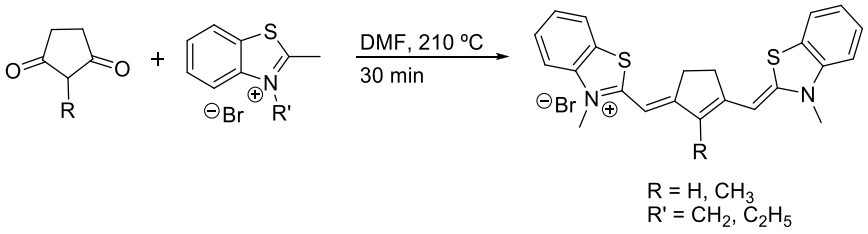

Scheme 6: Yarmoluk's synthesis of pentamethine dyes[93].

The resulting fluorophores showed that modification of the cyclopentene moiety had dramatic effects on DNA binding affinity. Once again, these solution phase syntheses

result in unwanted symmetrical cyanine dyes and require the purification of similar molecules[93].

2.2.3 Heptamethine Dyes

Heptamethine dyes have absorption and emission values above 750 nm and are therefore ideal candidates for use in molecular imaging. The most common synthesis of heptamethine cyanine dyes involves the introduction of a 6-membered hexene ring as part of the conjugated cyanine system. The 6-membered ring increases the rigidity of the molecule and decreases aggregation in solution, which results in an increase in fluorescence quantum yield. The reaction proceeds via a condensation of the Vilsmeier-Haack reagent and an activated indolium salt (Scheme 7)[94].

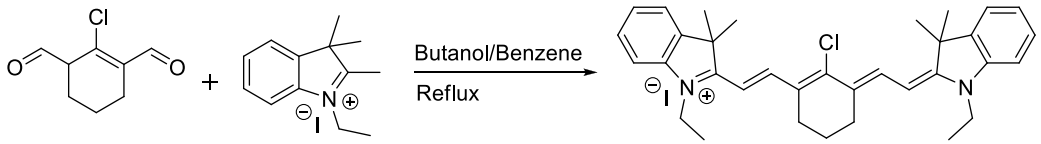

Scheme 7: Synthesis of heptamethine cyanine dyes[94].

The resulting heptamethine fluorophore has a labile chlorine group that can be substituted by a variety of nucleophiles leading to hundreds of possible derivatives[94b, 94c]. Interestingly, substitution of the chlorine atom can have a dramatic effect on the absorption and emission properties of the fluorophore[95] and will be discussed in detail later in this chapter.

Bradley and co-workers utilised solid-phase techniques to generate non-symmetrical cyanine 7, suitable for conjugation to bio-molecules[89].

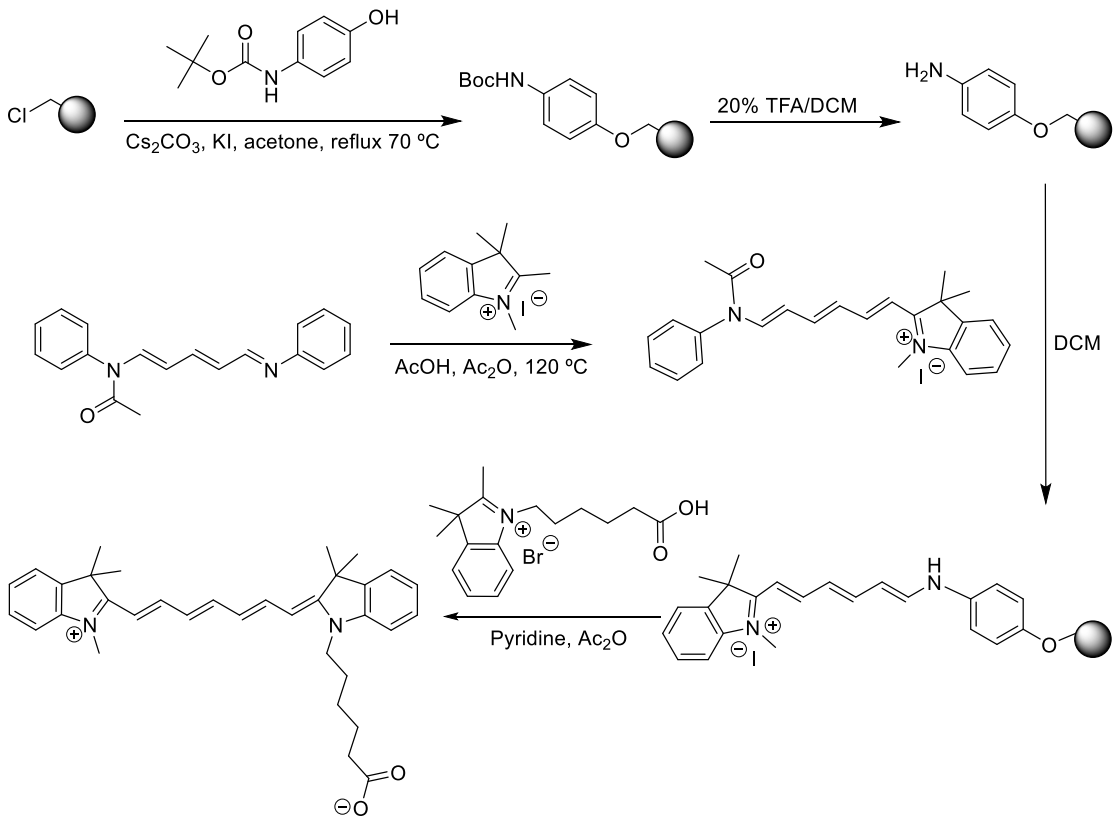

Scheme 8: Bradley's solid-phase synthesis of cyanine 7[89].

This efficient procedure requires no purification of the final dye and only requires room temperature reactions to yield the final product[89].

Commercially available heptamethine dyes include indocyanine green (ICG). Initially developed for photography by Kodak, ICG, which was approved by the food and drug administration (FDA) in 1958 has been utilised mainly in angiography and ophthalmology,[96] but has also found use in monitoring liver function[97].

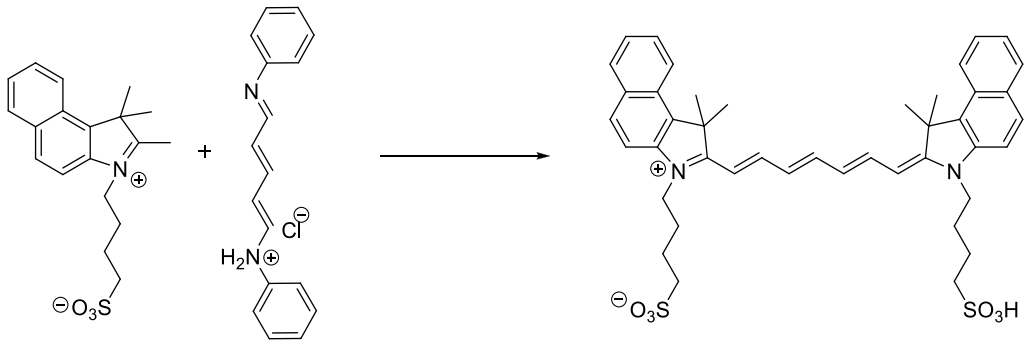

Scheme 9: Synthesis of indocyanine green.

The extensive use of ICG is highlighted by over 6000 publications describing its use[96a].

2.3 Further Applications of Cyanine Dyes

2.3.1 Reactive Oxygen Species

Reactive oxygen species[98] (ROS) are important for many biological functions such as signal transduction[99], blood pressure regulation[100] and platelet production[101], however, overproduction of ROS are linked with parthenogenesis of cardiovascular disease[102], carcinogenesis[103] and inflammation[104]. ROS are often difficult to measure quantitatively in biological systems[105] but due to the high sensitivity of fluorescent imaging, this technique may help overcome this[69b]. ROS can be in the form of radicals, for example, the radical species superoxide anion ($O_2^{\bullet-}$), hydroxyl radical ($OH^{\bullet}$), hydroperoxyl radical ($HO_2^{\bullet}$) or species such as hydrogen peroxide (H_2O_2) and singlet oxygen ($^1O_2$).

One example is the synthesis of non-fluorescent hydrocyanine dyes by Knight *et al*[69c]. As discussed, it is the extended conjugation system of fluorophores which accounts for the colourful and fluorescent properties. By temporarily disrupting this conjugation, it is possible to "turn-off" the fluorescence. This can be done using $NaBH_4$. On addition of the reducing agent, a colour change from green to yellow is immediately observed with a complete loss of fluorescence intensity.

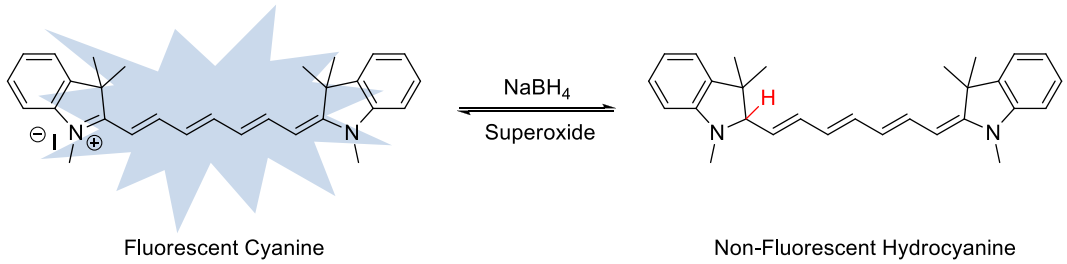

Scheme 10: Reduction and oxidation of cyanine 7.

In the presence of radicals, such as superoxide, a *turn on* fluorescence signal is observed allowing determination of the level of ROS species present. This is due to the oxidation of the cyanine molecule and restoration of the extended conjugation[69c].

Nagano *et al*[106] also reported detection of ROS in real time by linking two NIR cyanine dyes with different oxidation potentials initially resulting in static quenching of the fluorophores.

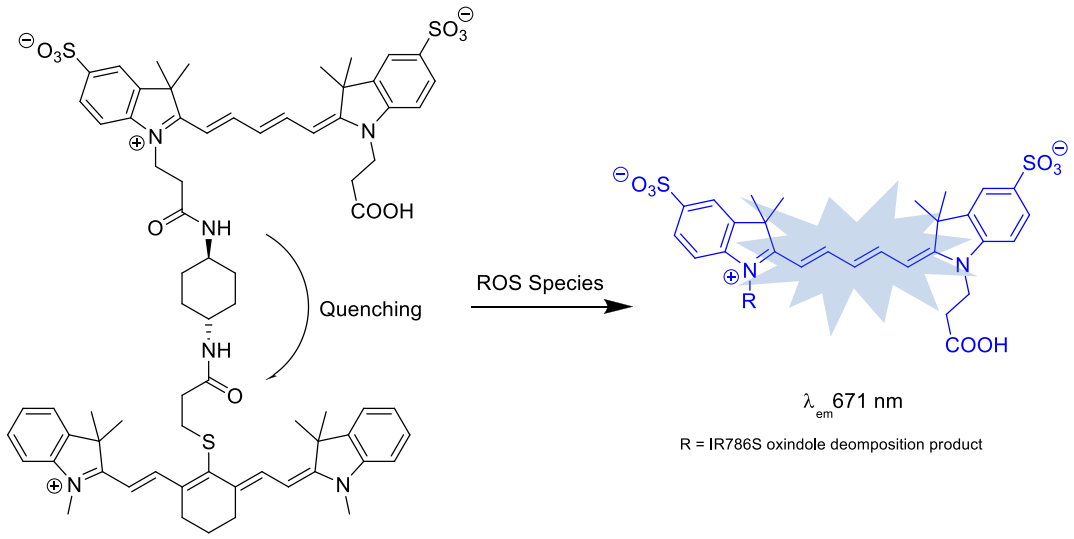

Scheme 11: Removal of quenching by ROS cleavage of imaging probe to generate the fluorescent cyanine molecule[106].

A *turn on* fluorescence signal was observed on oxidation of the more susceptible cyanine dye to the non-fluorescent oxindole by a variety of ROS such as the hydroxyl radical or superoxide. To analyse this probe in cells, HL60 cells were

incubated with the probe and after activation with phorbol mysritstate acetate (PMA, $O_2^{\cdot -}$ generation) or neutrophil activation (ROS generation) a fluorescent signal could be detected[106].

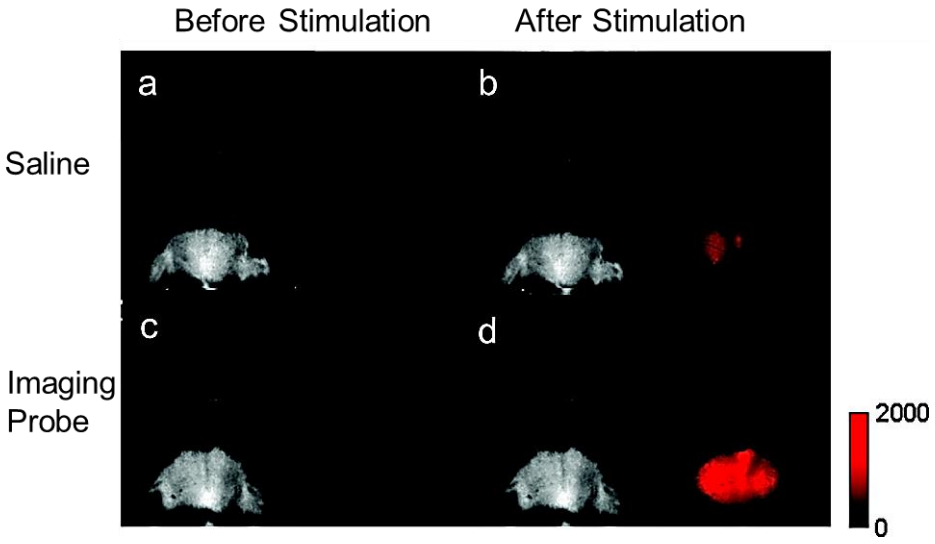

Figure 19: Comparison of the white light and fluorogenic images of a peritonitis mouse model before and after PMA activation. a) No probe before stimulation, b) no probe after stimulation, c) probe before stimulation, d) probe after stimulation. Red = fluorogenic image. λ_{ex} = 645 nm, λ_{em} = 668 nm. Reprinted and adapted with permission from reference[106], copyright (2010) American Chemical Society.

A mouse model of peritonitis also exhibited impressive oxidative stress detection showing the possibility of transfer to humans (Figure 19).

2.3.2 Other Small Molecules

There have been several published articles on the development of anion sensors[107] with the detection of cyanide[108] and fluoride[109] ions receiving considerable attention. Furthermore, sensors with the ability to detect thiol containing compounds such as cysteine[110], homocysteine[111] and most recently hydrogen sulfide[112] have also been published.

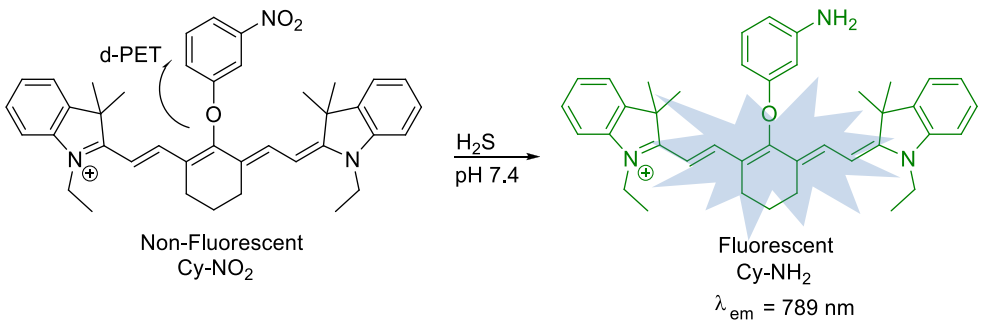

Scheme 12: NIR heptamethine sensor for hydrogen sulphide[112].

Zhang and co-workers developed a real time NIR sensor for H_2S by incorporating *m*-nitrophenol onto the heptamethine dye scaffold (Scheme 12), which as a result of PeT[113], quenched its fluorescence. Reduction of the nitro group by H_2S resulted in removal of the PeT process allowing fluorescence emission. Selectivity over reactive oxygen, nitrogen and sulfide species such as Na_2S was achieved[112].

2.3.3 Metal Ions

The fluorescent detection of toxic metal ions such as Hg^{2+} [114], Cu^{2+} [115], Cd^{2+} [116] and Pb^{2+} [67d] in biological systems have been investigated. Modification of the heptamethine scaffold by substitution of the labile chlorine atom, has led to the development of a ratiometric probes for the detection of metal ions, with Jiang developing a Ag^{+} sensor based on a heptamethine cyanine motif containing an adenine moiety[117].

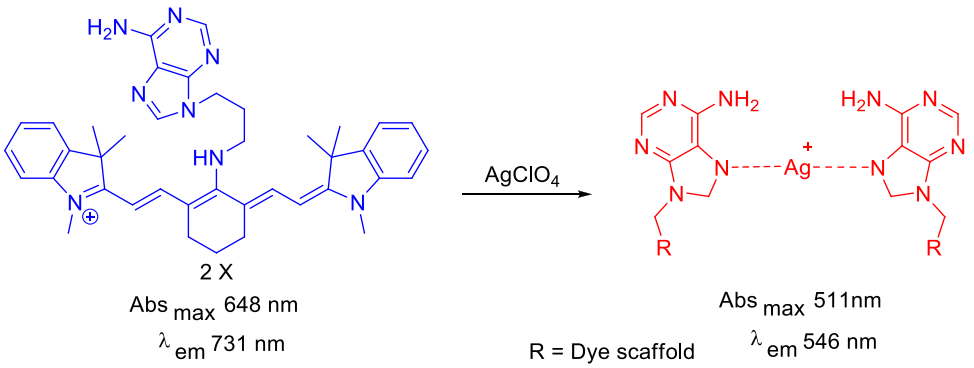

Scheme 13: Modified heptamethine cyanine dye for the detection of Ag^+ ions in water[117].

By modulation of the aggregation states[118] of the cyanine dye with increasing concentrations of Ag^+ ions, a fluorescence shift of 185 nm was observed. This sensor exhibited high selectivity over other metal ions such as copper and iron.

Naganoet *al*[108a] also synthesised a heptamethine fluorophore for the detection of Zn^{2+}.

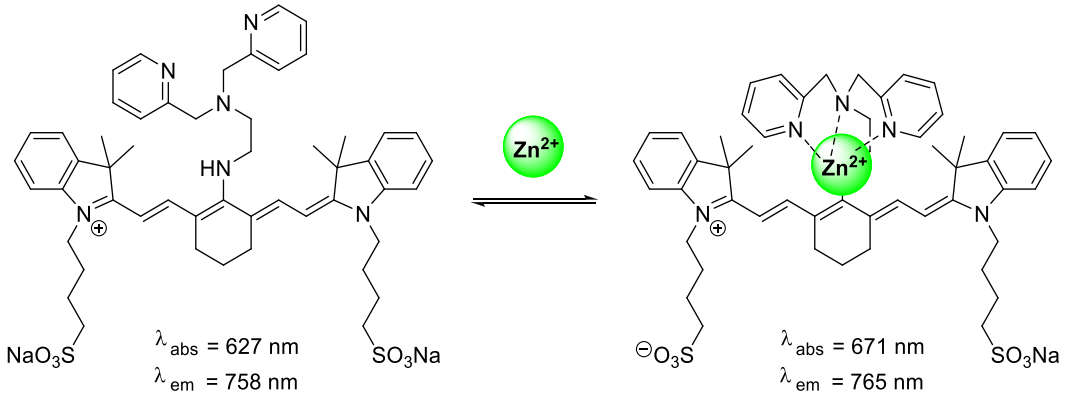

Scheme 14: Synthesis of ratiometric probe for Zn^{2+} ions[108a].

Addition of the dipicolylethylenediamine moiety as a metal chelator resulted in a change in electron donating ability of the amine. Zinc binding resulted in a detectable change in absorption and emission maxima as well as a colour change from blue to light green.

Modification of this sensor by Yoon provided a NIR fluorescent sensor for cyanide[119].

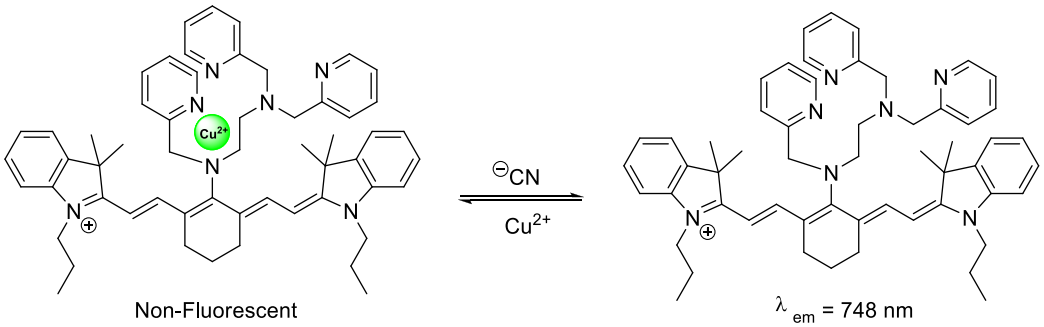

Scheme 15: Ratiometric fluorescent probe for Cu^{2+} and cyanide[119].

On binding copper ions, a complete reduction in fluorescence occurs. Addition of CN^- to the solution results in an increase in fluorescence at 748 nm[119].

2.4 Properties of Cyanine Dyes

2.4.1 Solubility and pH dependence

Cyanine dyes are hydrophobic organic molecules. This can often make synthesis and purification easy, however, limits their use in biological systems. To overcome this problem, the cyanine dye can be modified by the addition of polar functionalities, most commonly, the addition of sulfonates.

Cyanine dyes are susceptible to their environment and the absorption and emission wavelengths can vary depending on solvent polarity and pH. Extensive studies, to investigate the complex link between solvent and cyanine dye have been carried out leading to the conclusion that variation of polarity causes changes in the conformation between a charge distributed along the full molecule or fixed ionised and non-ionised segments. A study into the effect of pH led to the synthesis of a reversible pH sensor by Nagano[120].

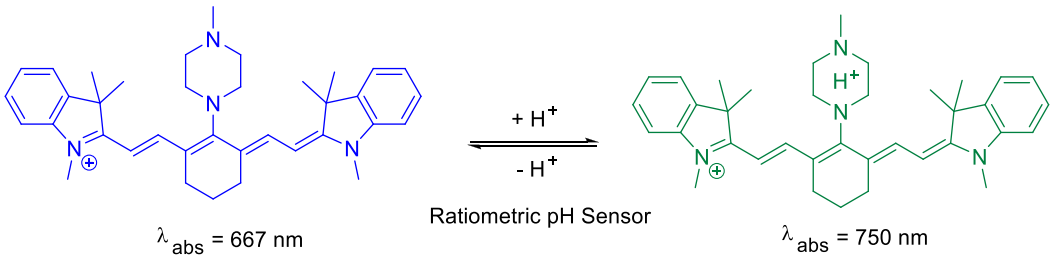

Scheme 16:Nagano's modified heptamethine cyanine dye to detect intracellular pH changes[120].

In this study, the heptamethine construct was modified with a 1-methyl piperizine moiety resulting in a ratiometric probe to measure pH between 4 and 12. Similar studies with the sulfonated analogue have also been carried out by Duan, confirming intracellular pH changes[121].

2.4.2 Photobleaching

Fluorophores are susceptible to photobleaching[122] which mainly occurs due to the presence of singlet oxygen. This effect is irreversible and is dependent on the intensity and duration of light exposure. Although detrimental, photobleaching can be used to study cell membrane diffusion and protein binding by using fluorescence recovery after photobleaching (FRAP) where non-oxidised fluorophores diffuse into the non-fluorescent area[123]. Modifications to the cyanine fluorophore can reduce the tendency to photobleach, such as fluorination. Armitage showed that poly fluorination of a modified cyanine dye resulted in reduced aggregation in solution, as well as being over 3 times less susceptible to photobleaching[124].

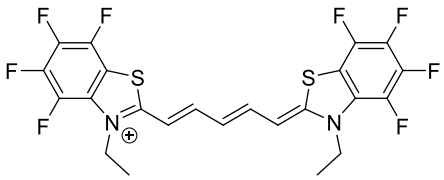

Figure 20: Structure of fluorinated cyanine dye with decreased sensitivity to photobleaching (compared to non-fluorinated derivative) after light irradiation[124].

2.5 Chapter Aims

The aim of this chapter was to synthesise a library of hepta- and penta-methine cyanine dyes, to analyse their respective photo-physical properties and determine their cellular uptake ability. Although there are increasing reports on these dye molecules, (with many coming out during the duration of the author's PhD) specific discussion into their cellular toxicity and cellular uptake is rarely mentioned. Additionally, the reactivity of heptamethine cyanine dyes in the *meso* position or susceptibility to nucleophilic attack is still not fully understood and investigation into this will help in the production of new molecular imaging probes for *in vivo* studies. Scheme 17 shows the proposed synthesis for the library.

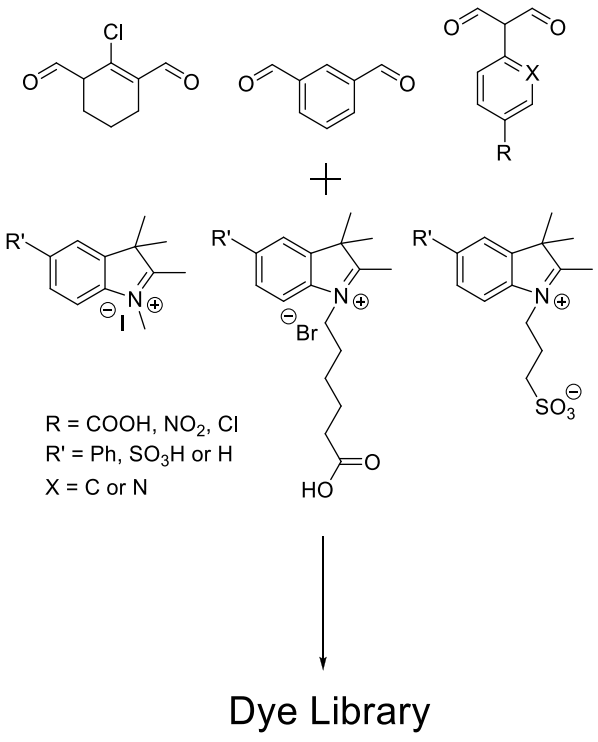

Scheme 17: Proposed cyanine dye library synthesis.

2.6 Results and Discussion

2.6.1 Synthesis of Indolium Salts

The synthesis of cyanine dyes requires two key intermediates. A conjugated carbon backbone and two indolium salts which act as "heads" or "capping groups". In order to synthesise a range of cyanine dyes, several indolium salts were synthesised.

The synthesis (Scheme 18) was high yielding and carried out using conventional heating, or microwave assisted heating which reduced reaction times significantly while maintaining good yields (Scheme 18).

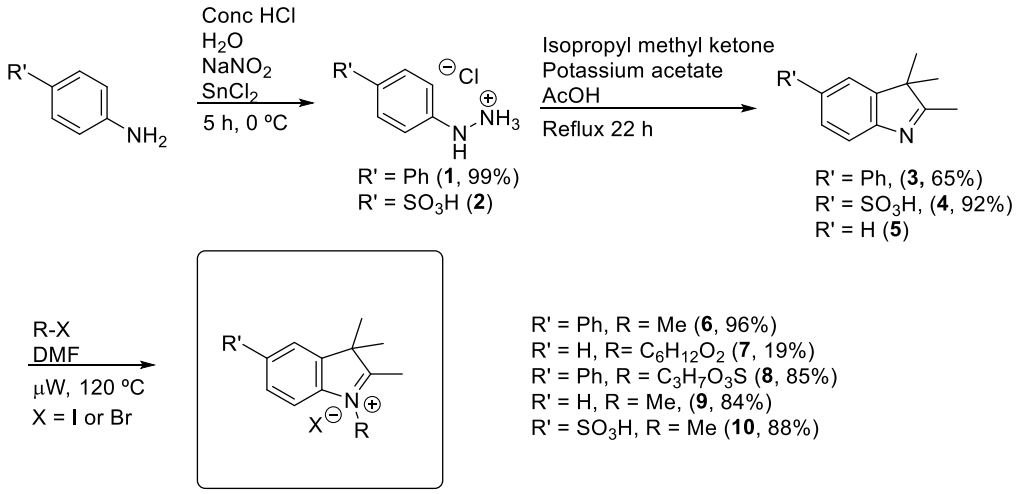

Scheme 18: Synthesis of indolium salts. Compound **2** was obtained from Dr Nicos Avlonitis, Edinburgh University. Compound **5** was commercially available.

The quinolinium derivative was synthesised via alkylation of quinoline.

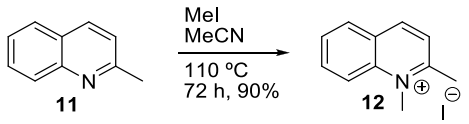

Scheme 19: Synthesis quinolinium salt.

2.6.2 Synthesis of a Cyanine Dye Library

In 1995 Patonay described the synthesis of heptamethine cyanine dyes utilising a bisaldehyde originally described by Reynolds in 1977[125] and an indolium salt. The bisaldehyde most commonly used is 2-chloro-1-formyl-3-hydroxymethylene cyclohexene (**13**). However, it is also possible to use isophthalaldehyde to generate different molecules with respect to optical properties. Although the synthesis generally results in symmetrical cyanine dyes, a labile chlorine atom on the backbone can be readily functionalised. It is possible to use other bisaldehydes to synthesise novel pentamethine cyanine dyes. Starting materials such as 2-(3-hydroxycarbonyl-6-pyridyl) malondialdehyde or the chloro or nitro derivatives combined with indolium salts would produce symmetrical cyanine 5 analogues with modifiable motifs to allow for bioconjugation or further functionalization.

2.6.3 Synthesis of Heptamethine Cyanine Dyes

Synthesis of the bis aldehyde (Scheme 20) was carried out by *in situ* formation of the formylating agent using DMF and phosphorous oxychloride.

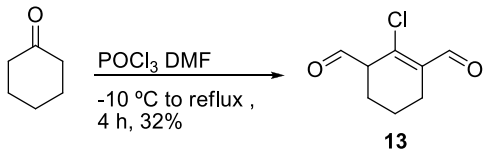

Scheme 20: Synthesis of the bis aldehyde in a Vilsmeier type reaction.

Synthesis of the NIR fluorophore (Scheme 21) was carried out using classical heating at 70-120 °C in a mixture of acetic acid and acetic anhydride with NaOAc as the base. These reactions were monitored by TLC or HPLC with purification carried out via column chromatography.

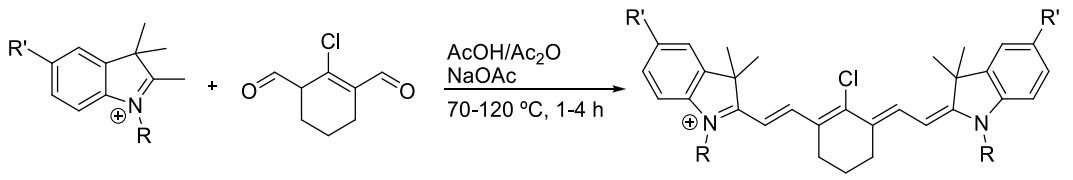

Scheme 21: Synthesis of a heptamethine cyanine dye.

The mechanism requires the deprotonation of the quaternary indole followed by condensation with the bisaldehyde moiety (Scheme 22).

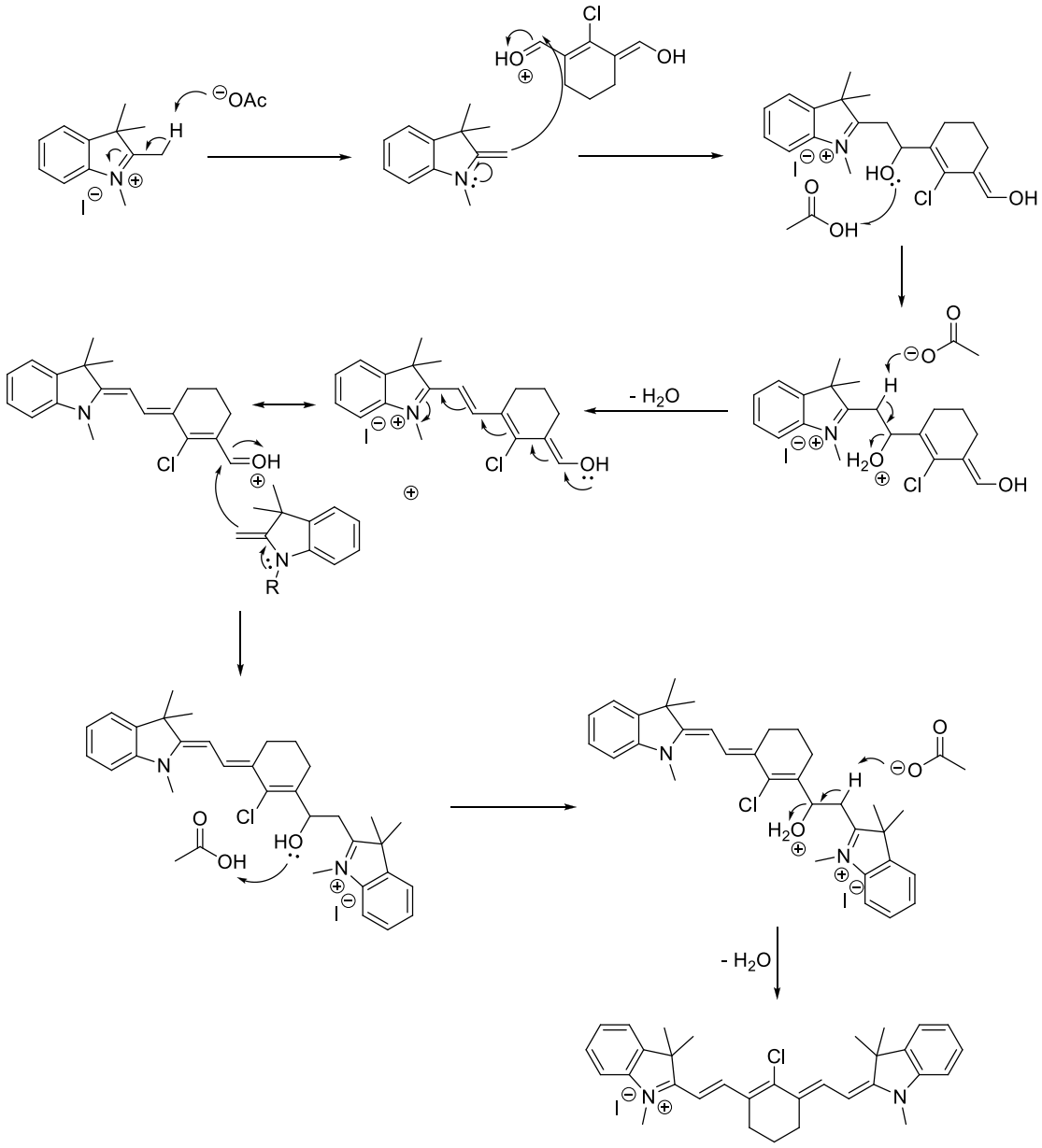

Scheme 22: Generation of heptamethine fluorophore with a labile chlorine group.

Substitution of the chlorine group by nucleophiles (Scheme 23) can be carried out to create a variety of fluorophores with different properties. Substitution of the chloro group with thiolates, phenolates or amines was attempted with a wide range of solvents explored although methanol or DMF gave the best results.

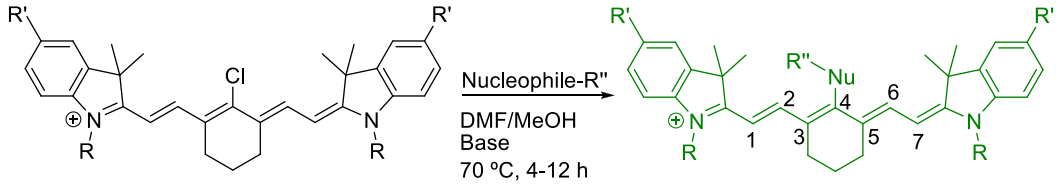

Scheme 23: Nucleophilic substitution to generate library.

The substitution reaction mechanism is not trivial and can occur via two pathways. The first and most obvious pathway is the addition of the nucleophile, followed by the elimination of the chlorine atom as shown in Scheme 24.

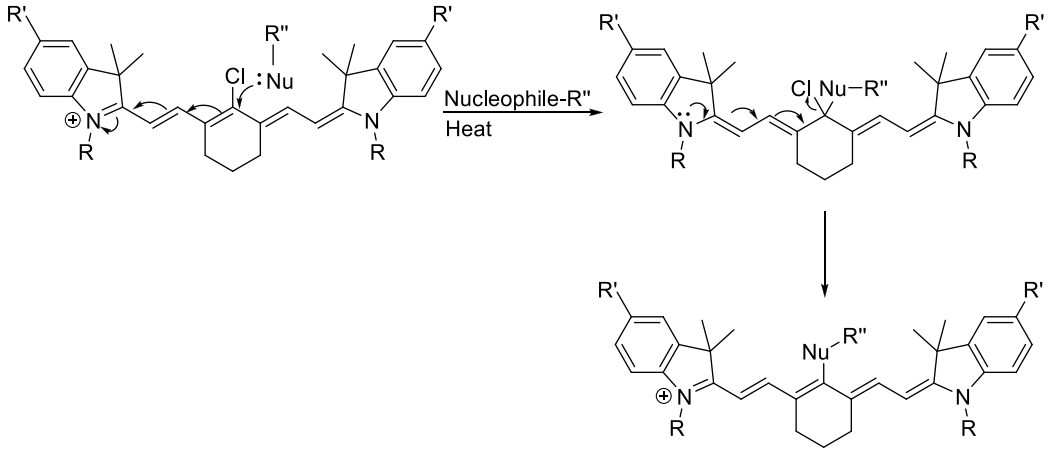

Scheme 24: Suggested addition-elimination mechanism.

A second suggested mechanism is the radical nucleophilic aromatic substitution reaction ($S_{RN}1$)[94c, 126]. This mechanism is supported by evidence obtained under certain reaction conditions. For example, when the reaction is attempted in the presence of molecular oxygen (a known free radical scavenger) the yields are reduced. Additionally, EPR spectroscopy was employed by Patonay which suggested the presence of radical intermediates[94c]. The first step of this radical substitution is

the single electron transfer (SET) from the nucleophile $Nu^{\ominus}$ to the conjugated π system of the fluorophore, generating the radical dye species. Dissociation of this species and reaction with the nucleophile $Nu^{\ominus}$ gives the radical Dye-Nu species, which acts as a one electron donor to re-initiate the reaction (Figure 21).

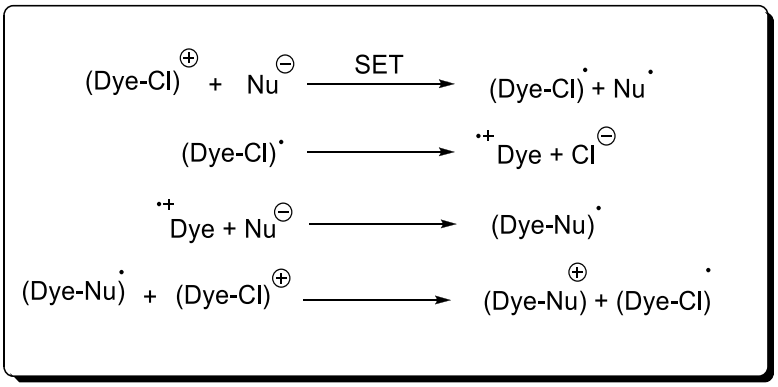

Figure 21: Propagation pathway for $S_{RN}1$ mechanism[94c].

Although there are differences between all the heptamethine dyes synthesised in terms of photo-physical properties, the heptamethine dyes absorb light in the NIR region as expected. Interestingly, amino-substituted heptamethine dyes showed a large hypsochromic shift and a decrease in photostability as previously described[127].

The heptamethine dyes synthesised, reaction yields and photo-physical properties are given in Table 3.

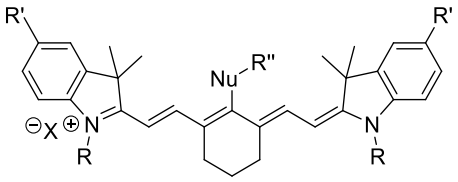

Figure 22: Structure of Cyanine Dye.

Dye	R	R'	R''	% Yield	Abs (λ_{Max})	Em (λ_{Max})	ε* ± 10 %	Φ_F ± 10 %
14	Me	H	Cl—R*	82	789	818	43500	0.160
15	$C_6H_{12}O_2$	H	Cl—R*	68	793	822	41000	0.145
16	$C_3H_7O_3S$	H	Cl—R*	30	797	825	68000	0.150
17	Me	Nap	Cl—R*	16	833	>850	85500	-
18	Me	SO_3H	Cl—R*	57	800	833	29000	0.110
19	Me	H	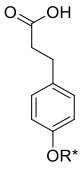	82	777	825	23000	0.100
20	Me	H	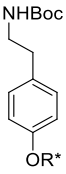	50	777	803	70000	0.430
21	Me	SO_3H	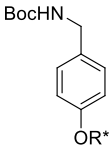	57	787	814	40000	0.280
22	Me	H	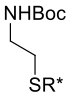	15	796	830	120000	0.190
23	Me	SO_3H	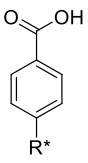	80	780	805	77500	0.360

24	Me	SO_3H	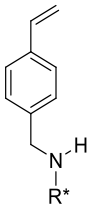	34	640	764	25500	0.030
25	Me	H	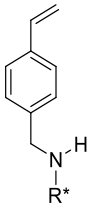	69	650	760	31000	0.026
26	Me	H	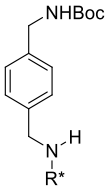	60	640	758	22000	0.034
27	Me	SO_3H	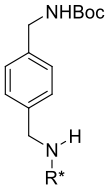	79	632	764	21000	0.051
28	Me	H	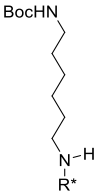	57	626	763	25000	0.036
29	Me	H	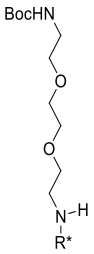	31	639	766	36000	0.078
30	Me	SO_3H	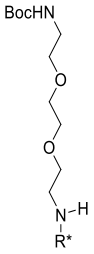	90	634	770	23000	0.035

31	Me	SO_3H	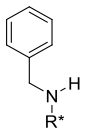	55	619	771	19000	0.040
32	Me	SO_3H		83	608	772	35500	0.061
33	Me	H		90	612	767	86500	0.093
34	Me	H	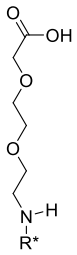	54	652	777	81000	0.100
35	Me	SO_3H	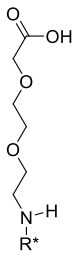	52	637	771	42000	0.110
36	Me	H		57	631	767	32000	0.078
37	Me	SO_3H		42	628	771	34000	0.082
38	Me	SO_3H	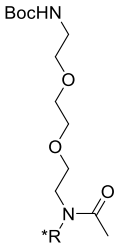	50	685	714	106000	0.590

39	Me	H	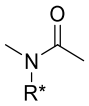	55	787	815	23500	0.160

Table 3: Structure, yield and photo-physical properties of heptamethine cyanine dyes. Absorption, emission, extinction coefficient and quantum yields were all measured in DMSO at 5µM. * -L Mol^{-1} cm^{-1}. R* = dye scaffold, Me = CH_3, Nap= phenyl moiety generating naphthalene ring.

2.6.3.1 Chloro Heptamethine Dyes (**14-18**)

The chloro-heptamethine derivatives **14-18** as described in Table 3 all had absorbance and emission values in the NIR region as expected. The benz[e]indolium analogue (**17**) had an emission maximum above 850 nm, and was out-with the limits of the fluorometer available due to the extended conjugation of the π system. Extinction coefficients of these derivatives varied with higher values for the sulfonated indole and benz[e]indolium modified structures (**17** and **18**). It is interesting to note that sulfonation at the R' position (**18**) over the R position (**16**) seems to lower the extinction coefficient substantially, whereas the quantum yield was only moderately lowered. Quantum yields of these 5 compounds (**14-18**) were higher than ICG (see Table 2), between 0.11-0.16 which was due to increased rigidity due to the cyclohexene ring in the centre of the molecule. Compounds **14-16** compare the effect of the alky chain on the indole moiety, showing a small increase in the extinction coefficient for the sulfonated derivative (**16**), although quantum yields were extremely similar leading to the conclusion that the alkyl chain does not affect the overall photo-physical properties of the fluorophores. Addition of polar sulfonate moieties does tend to red shift the absorbance and emission spectra (**14** and **15** compared to **16**) and is most likely due to the increased solubility of the molecule in DMSO, leading to decreased self-quenching.

All chloro derivatives except cyanine **15** exhibit symmetry in their NMR spectra with an example shown in Appendix 2.

2.6.3.2 Ether, Thio and Carbon Derivatives (**19-23**)

As water is known to supress the $S_{RN}1$ single electron transfer pathway[128] anhydrous solvents were used as a reaction medium to facilitate the substitution. Compounds **19** and **22** were successfully synthesised at room temperature using sodium hydride as the base. In order to use a milder base, chloro starting materials **14** and **18** were pre-incubated with K_2CO_3, however, this route required elevated temperatures (70 ºC, 40 min or 100 ºC, 30 min) to synthesise **20** and **21**. Synthesis of **23** employed the use of a Suzuki-Miyaura coupling reaction using $Pd(OAc)_2$ and PPh_3. The reaction required heating at 100 ºC for 15 hours to give the desired product in 80% yield.

Addition of functional groups with phenolates resulted in changes in the photo-physical properties. The absorbance wavelengths ranged from 777 to 796 nm while emission wavelengths between 803 and 830 nm characteristically remained in the NIR region. The emission wavelengths also increased with the addition of polar moieties (**20** vs **21**), however, they are generally blue shifted with respect to their chloro starting materials (**20** vs **14** and **21** vs **18**). Introduction of a carboxylic acid (**19**) or protected amine (**20**-**21**) into the scaffold have differing effects. The carboxylic acid introduction results in a decrease in extinction coefficient and quantum yield, possible due to the increased aggregation or dimer formation. The addition of *N*-Boc-tyramine (**20**) or *N*-[(4-hydroxyphenyl)methyl]-, 1,1-dimethylethyl ester (**21**) increases the quantum yield and extinction coefficients compared to the chloro starting materials (**14** and **18** respectively). This is most likely due to the decreased aggregation and therefore lower self-quenching. Substitution with a thiolate (**22**) gives a further bathochromic shift in absorbance to 796 nm. This molecule shows interesting properties with a high extinction coefficient (120000 L Mol^{-1} cm^{-1}), however, due to the possible instability *in vivo*, the sulphur derivatives were discontinued. Carbon-carbon bond formation allowed synthesis of **23** which has a high extinction coefficient (77500 L Mol^{-1} cm-1) and a high quantum yield (0.36) in DMSO[129]. Interestingly, repeating this reaction with the

non-sulfonated chloro heptamethine dye starting material (**14**) was unsuccessful, despite maintaining a high pH.

An example NMR spectrum of an ether derivative is shown in Appendix 3.

2.6.3.3 Amine Derivatives (**24-39**)

The synthesis of amine substituted heptamethine cyanine dyes is currently an extremely hot topic in the search for new ratiometric imaging probes. In order to further advance this field, a variety of amine substituted fluorophores were synthesised.

The reactivity of the amines was extremely dependant on the overall amine structure and on its ability to act as a single electron donor, while generally, triethylamine was required to allow the reaction to proceed. Optimisation of the purification conditions gave yields up to 90% yield. The methylamine derivatives (**33** and **34**) were synthesised using 2 M methylamine in MeOH. Care had to be taken not to add too many equivalents of the methylamine as the starting material decomposed.

As expected on heating the reagents at 70 ºC, a colour change from green to blue was observed allowing the conversion to the product to be followed by UV/Vis spectroscopy. The large hypsochromic shift is attributed to the electron donating ability of the nitrogen and the excited state intramolecular charge transfer as discussed in detail by Peng[95, 130]. Kiyose[108a] synthesised a variety of analogues to investigate the nature of the amine substituent on the absorption and emission profiles, concluding that decreasing the electron density on the amine, increased the absorption and emission wavelengths.

The absorbance values of amine derivatives **24-37** range between 612-652 nm with emission values between 758-777 nm. The smallest and largest Stokes shifts were 110 nm and 164 nm (in DMSO). These large shifts are extremely useful and may be exploited as part of a FRET or ratiometric probe. There are several trends amongst

these fluorophores. Firstly, sulfonation of the indole moiety results in a blue shift in the absorbance spectrum between 5-10 nm and a red shift in fluorescence maxima of 4-6 nm (for example **24** vs **25**, **26** vs **27** or **32** vs **33**). The resulting increase in Stokes shift is apparent. Further, the extinction coefficients of the sulfonated molecules are generally lower than the non-sulfonated counter parts while the quantum yields remain comparable to those found in the literature[108a, 131]. Derivitisation to novel PEGylated fluorophores revealed an increase in the quantum yield over the alkyl counter parts (**34** vs **36** and **35** vs **37**). The PEGylated derivatives had quantum yields of 0.10 (**34**) and 0.11 (**35**) and are similar to ICG. This increase can again be associated with solvent interaction, solubility and aggregation between the dye molecules.

Chang[127] found that the photo-stability of the amino substituted derivatives could be increased by modification of the amine moiety with an electron withdrawing group. This was due to the stabilization of the iminium intermediate that prevents the incorporation of the reactive oxygen species causing degradation[127]. For this reason, functionalization of the amine (**30** and **33**) was attempted to remove this instability. Interestingly, this reaction results in a shift in absorbance and emission wavelengths in to region of 750-800 nm.

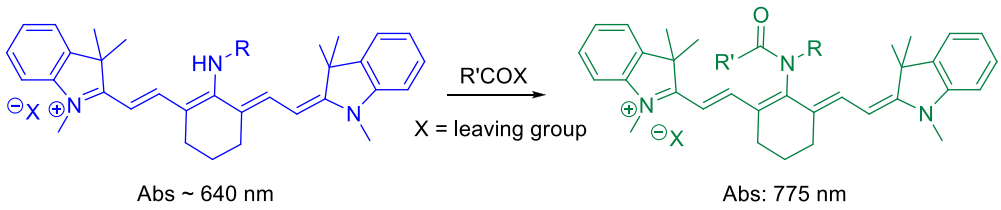

Scheme 25: Acylation of amino-modified heptamethine cyanine dyes.

This reaction was complex and was only successful in the presence of acetyl chloride. On addition of acetyl chloride to the amine derivatives **30** or **33** at 0 ºC, an instantaneous colour change occurs as the absorbance wavelength shifts into the red region. Derivitisation of **33** with acetyl chloride caused a large shift of absorption from 612 nm to 787 nm and emission from 767 nm to 815 nm. Although the Stokes shift of **39** is decreased to 28 nm (from 155 nm for compound **33**), there is a resulting

increase in quantum yield to 0.16. Acetylation of compound **30** to **38** resulted in a red shift of the absorbance (from 634 nm to 685 nm) but a large blue shift in emission spectra (from 770 nm to 714 nm). This reduction is Stokes shift to 29 nm, is accompanied by a large increase in quantum yield to 0.59 (from 0.035 for **30**). The changes in wavelength can be attributed to the removal of the photoactivating lone pair of the nitrogen[131], however, the increase in quantum yield is still not fully understood.

The general symmetry of the heptamethine dyes is conserved in the amine derivatives, while on acetylation of the amine (**38** and **39**) the symmetry is lost, likely due to the electron donation ability of the amine being substantially reduced. An example NMR spectrum is shown in Appendix 4.

2.6.3.4 Non-Fluorescent Derivatives

To develop additional novel fluorophores, isophthalaldehyde was selected as the cyanine backbone, in this case the reaction with the indolium salts gave a yellow or orange solid which was non-fluorescent.

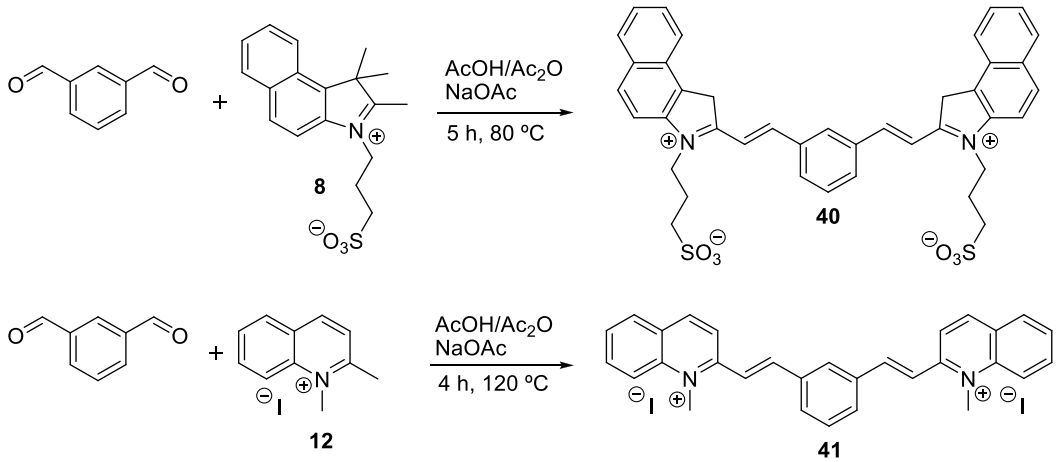

Scheme 26: Synthesis of non-fluorescent analogues.

As can be seen in Scheme 26, the 6π electron system will be conserved. The molecule is no longer fully conjugated, does not exhibit resonance along the

polymethine chain and is therefore rendered non-fluorescent. For this reason, these derivatives were discontinued.

2.6.3.5 UV/Vis Spectroscopy

The absorption wavelengths of selected substituted and non-substituted heptamethine cyanine dyes are in shown Figure 23.

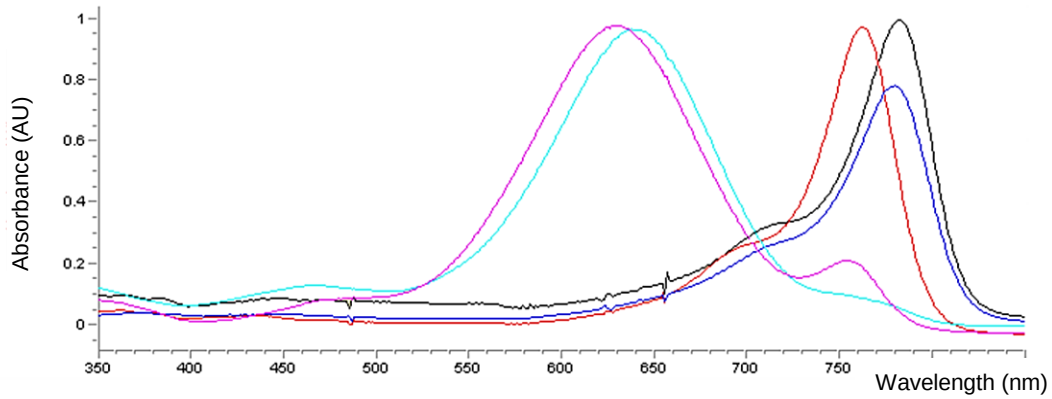

Figure 23: Absorbance spectrum of a selection of dyes. Black = chloro-substituted (**14**); Red = ether-substituted (**20**); Dark blue = sulfonated variant of ether substituted (**21**); Light blue = amino substituted (**26**); Pink = sulfonated variant of amino substituted (**27**).

This UV/Vis profiles show the difference between the amino, chloro, thio-ether or ether heptamethine derivatives with amino substitution resulting in a large blue shift.

2.6.4 Cell Penetration and Toxicity

Although there are many reports of cyanine dyes being used as molecular imaging probes *in vitro* and *in vivo*, the mechanism of uptake and localisation of the fluorophores are less well represented. The most comprehensive study was published in 2010 by Tong *et al*[132]. This report discusses the uptake of two common heptamethine cyanine dyes IR-783 and MHI-148 (Figure 24).

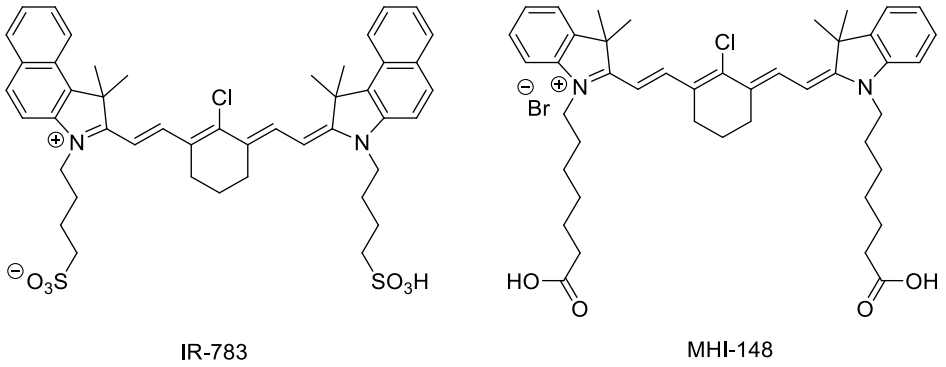

Figure 24: Commercial heptamethine cyanine dye IR783 and analogue MHI-148.

Tong[133] reported that these non-toxic fluorophores are specifically taken up by cancer cells over normal human cells. Additionally they discuss that the uptake mechanism is an active process carried out by a member of the OATP (organic anion transporting polypeptide) family. This was confirmed by blocking the dye uptake in the presence of an OATP competitive inhibitor, bromosulphthalein[132]. The localisation of heptamethine cyanine dyes within cells has resulted in some debate, with some suggesting accumulation in the mitochondria[134] while others suggest accumulation in the cytoplasm with binding to many types of intracellular proteins[112, 132, 135]. Within the molecular imaging community there are often discussions with regards to the "stickiness" of cyanine dyes, with binding throughout the cell. It was decided to investigate localisation of cyanine dyes within cancer cells while varying the functionality and overall aqueous solubility of the molecules. As mentioned, sulfonation is a common way to increase the aqueous solubility of cyanine dyes, with PEGylation of cyanine dyes yet to be investigated. The addition of the polar, uncharged PEG chain may affect cellular uptake due to limited interactions with the negatively charged cellular membrane. In order to assess the cell penetration ability of cyanine dyes, 4 modified heptamethine cyanine dyes were synthesised (Figure 25). Cyanine **60** was also used as a comparison.

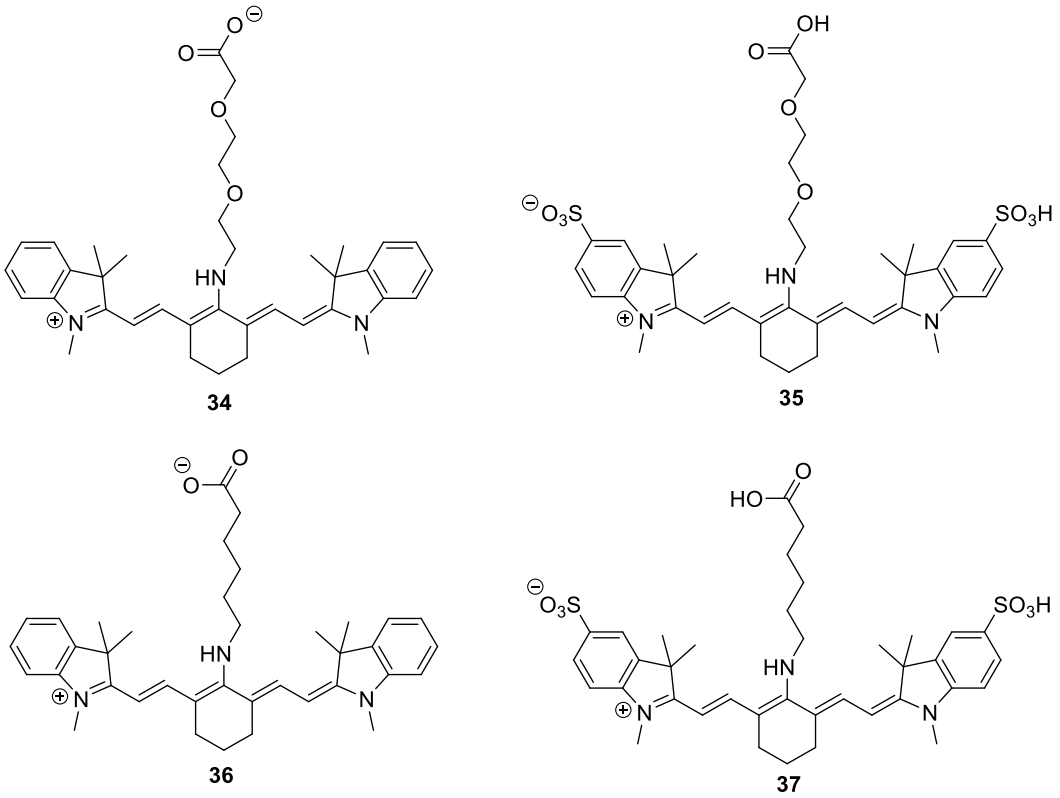

Figure 25: Structures of the 4 novel dyes for cellular uptake analysis.

Before carrying out any cellular work, the toxicity of these dyes was determined. In order to evaluate the toxicity potential, MTT[136] assays of compounds **34**-**37** and **60** were carried out using adenocarcinomic human alveolar basal epithelial (A549) cells and human prostate cancer (PC-3) cells.

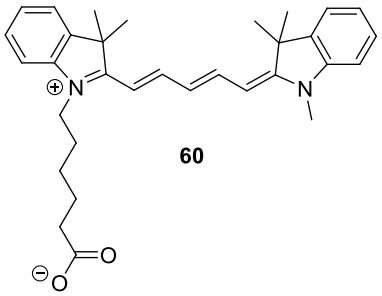

Figure 26: Cyanine 60.

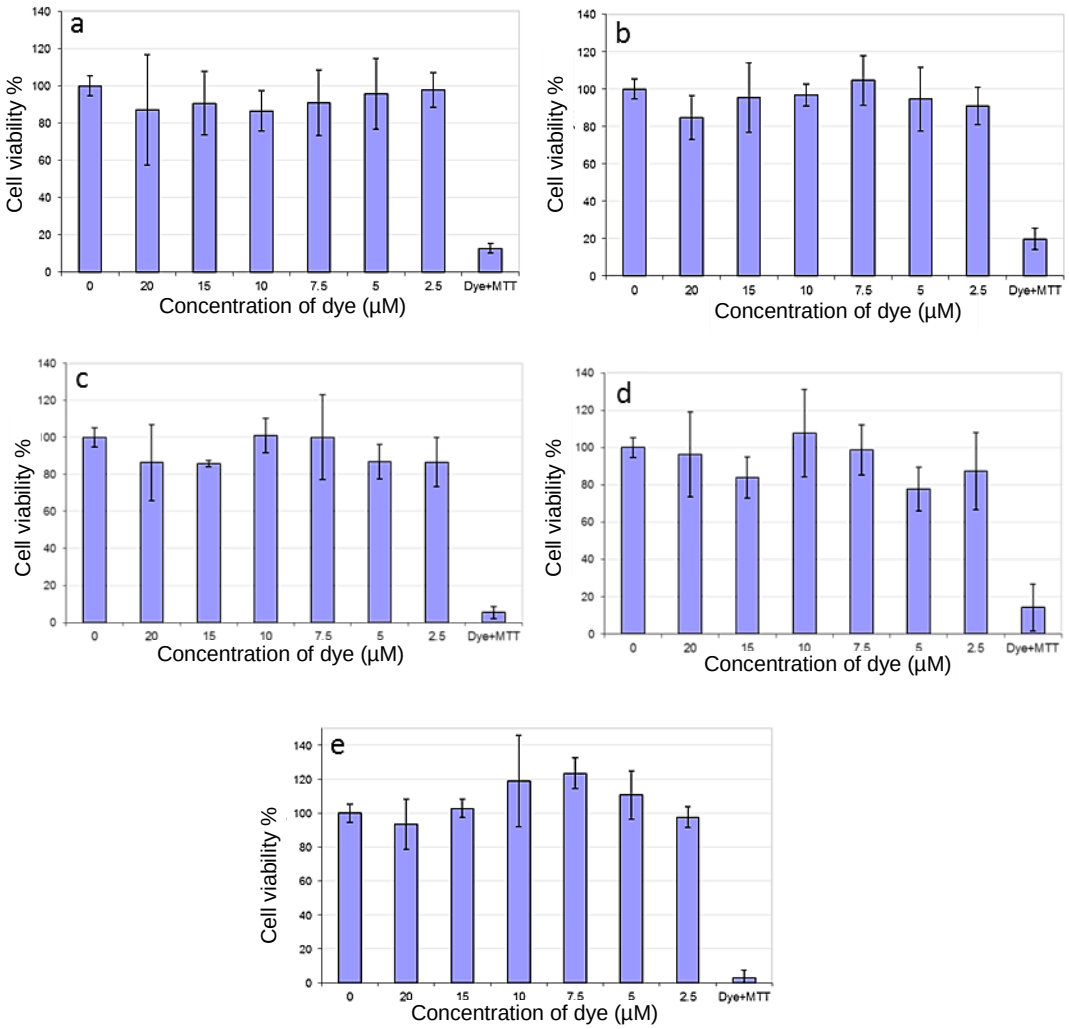

Figure 27: A549 cells incubated with 0, 2.5, 5, 7.5, 10, 15 and 20 µM dye for 24 hours prior to MTT analysis. a) **34**, b) **35**, c) **36**, d) **37**, e) Cyanine **60**. Dye + MTT used to confirm minor overlap between MTT absorption and cyanine dye absorption. (n = 4).

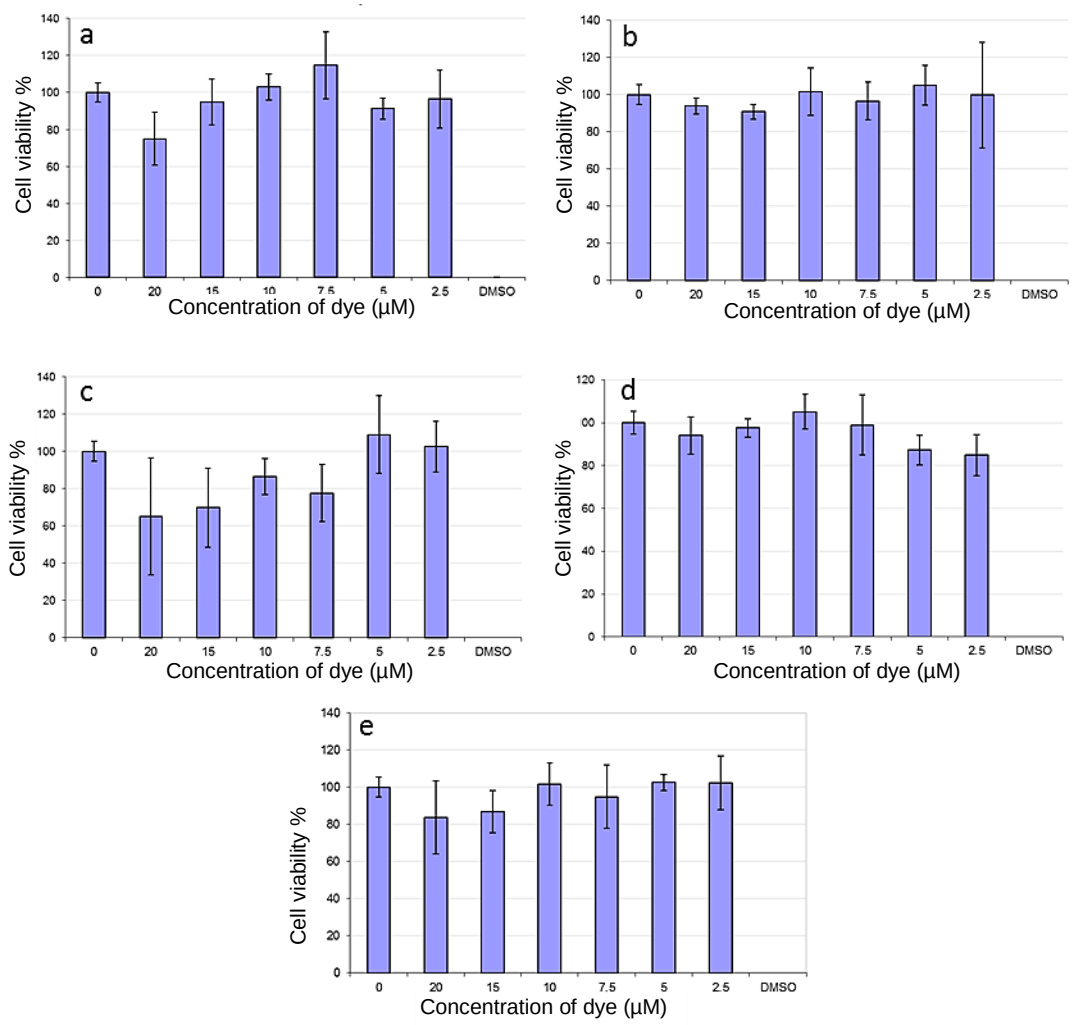

Figure 28: PC-3 cells incubated with 0, 2.5, 5, 7.5, 10, 15 and 20 µM dye for 24 hours prior to MTT analysis. a) **34**, b) **35**, c) **36**, d) **37**, e) Cyanine **60**. Dye + MTT used to confirm minor overlap between MTT absorption and cyanine dye absorption. (n = 3).

Analysis of the MTT assay data shows that all 5 heptamethine dyes were non-toxic up to 20 µM.

In order to determine cellular uptake of the cyanine dyes, flow cytometry[33a] was employed. This process begins by incubating cells with a fluorophore or molecule of interest for a given period. These cells were subsequently washed and analysed with flow cytometry (see Figure 29 for an example histogram).

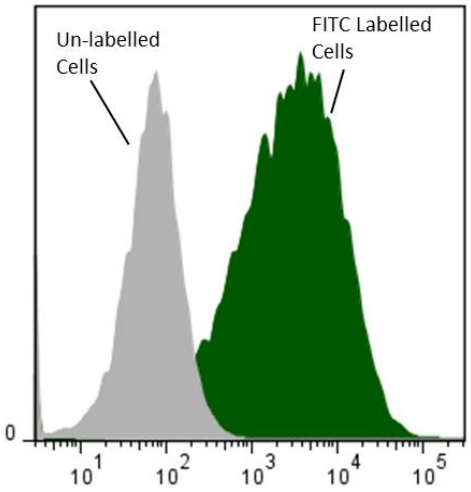

Figure 29: Example flow cytometry histogram of fluorescein labelled cells (green) and un-labelled cells (grey). Y-axis = cell count, X-axis = fluorescence intensity. λ_{ex} = 488 nm, λ_{em} = 515-545 nm. Data courtesy of Dr Sunay Chankeshwara.

From the histogram in Figure 29, the labelled cells have an approximate 100 fold increase in fluorescence. Although the literature is somewhat scarce regarding flow cytometry of cyanine dyes, some studies have been carried out using cyanine dyes to detect apoptosis in cells[137].

The cellular uptake of 4 selected amino-heptamethine cyanine dyes (**34**-**37**) and cyanine **60** were evaluated in A549 and PC-3 cells as shown in Figure 30 and Figure 31 respectively.

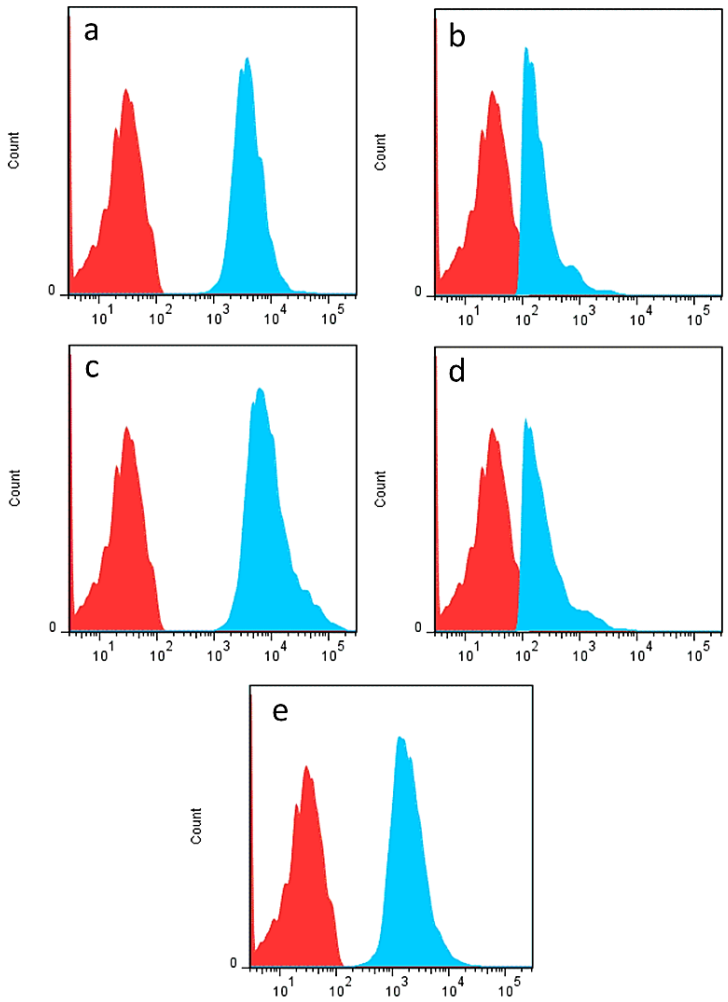

Figure 30: Flow cytometry histograms of A549 cells incubated with selected dyes at 10 μM for 2 hours. a) **34**, b) **35**, c) **36**, d) **37**, e) Cyanine **60**. X-axis represents fluorescence intensity, λ_{ex} = 633 nm, λ_{em} = 770-800 nm. Y-axis represents number of particles. Red = non-labelled cells, blue = labelled cells.

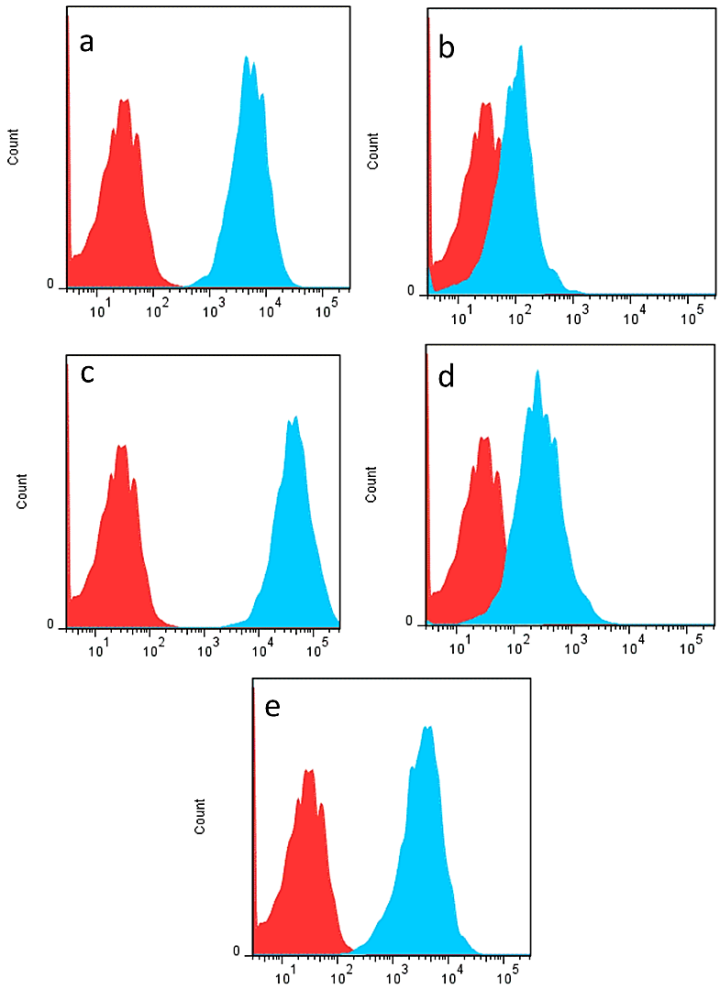

Figure 31: Flow cytometry histograms of PC-3 cells incubated with selected dyes at 10 µM for 2 hours. a) **34**, b) **35**, c) **36**, d) **37**, e) Cyanine **60**. X-axis represents fluorescence intensity, λ_{ex} = 633 nm, λ_{em} = 770-800 nm. Y-axis represents number of particles. Red = non-labelled cells, blue = labelled cells.

Both cell lines exhibited similar results with good cell penetration of all cyanine dyes. There was a distinct difference in uptake with regards to the sulfonated dyes compared to the non-sulfonated derivatives. The non-sulfonated molecules showed a 100-1000 fold increase in fluorescence where the sulfonated molecules only exhibited a 10 fold increase. Although these results were promising, they could not be taken as conclusive as the use of an extracellular quencher prior to analysis was not possible. Extracellular quenchers are usually employed to ensure that any fluorescence intensity measured using flow cytometry is due to intra-cellular excitation and not membrane bound dye. As there were no suitable quenchers available in the region of 650 nm, whether the dyes were inside the cell was still

uncertain. In order to determine the position cyanine dye accumulation, confocal microscopy studies were carried out. With confocal microscopy cells are imaged as a succession of slices (Z-slices) with only one "slice" in focus and being imaged at any one time. After the sample has been fully analysed, these individual images are combined to give a final 3-D image or video clip.

After incubation of the 5 selected cyanine dyes in A549 cells at 10 µM for 30 minutes, the cells were counter stained with Syto 82 (nuclei stain). The cells were then washed once with PBS and imaged directly. In order to obtain different images, different excitation wavelengths were used. To visualise the nuclei stain and cyanine dyes, a He-Ne laser was used and the sample excited at 543 nm (nuclei stain), and 633 nm (cyanine dye). The bright field image was used to visualise the cell membrane.

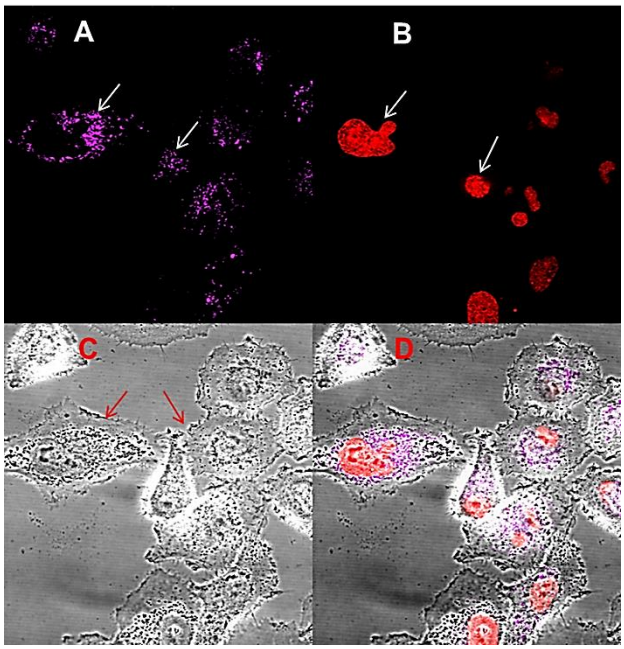

Figure 32: Confocal images of A549 cells labelled with cyanine 60 (10 µM) for 1 h. A) arrow shows localisation of cyanine **60** (λ_{ex} = 633, λ_{em} = 661-704 nm), B) nuclei staining with Syto 82 (λ_{ex} = 543 nm, λ_{em} = 554-587 nm), arrow shows localisation of Syto 82, C) brightfield image to visualise cell, arrow shows outer membrane, D) Merged image.

As we can see from the images in Figure 32, the localisation of cyanine **60** is similar to that obtained by the aforementioned imaging probes[112, 134b, 134c, 135]. The localisation is clearly in the cytoplasm, however, as the fluorescence seems to be punctate, one can assume that the dye has collected in the mitochondria. It is useful to note that the fluorophore is not trapped in the membrane, and does not pass into the nucleus as can be seen from the merged image (Figure 32, Image D). Analysis of the other cyanine dyes (Figure 33-Figure 36) show similar results, however, the fluorescence is more evenly spread out and can we can therefore suggest that they are bound non-specifically in the cytoplasm.

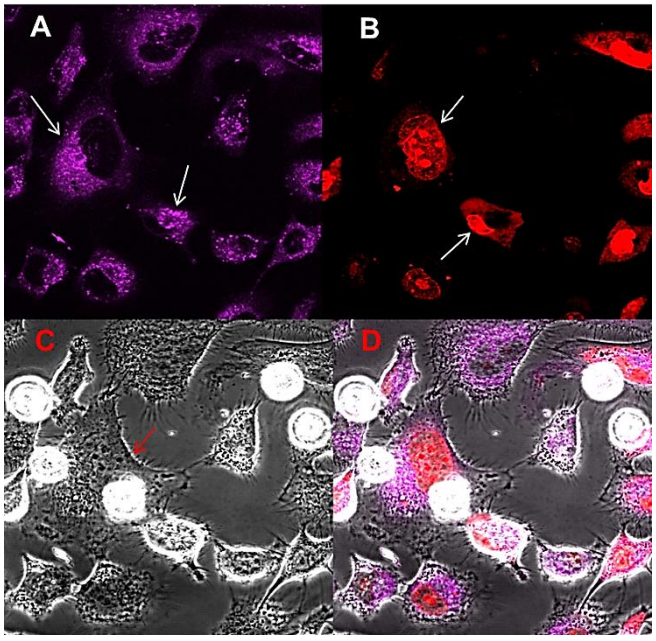

Figure 33: Confocal images of A549 cells labelled with 34 (10 μM) for 1 h. A) arrow shows localisation of **34** (λ_{ex} = 633, λ_{em} = 661-704 nm), B) Nuclei staining with Syto 82 (λ_{ex} = 543 nm, λ_{em} = 554-587 nm), arrow shows localisation of Syto 82 C) Brightfield image to visualise cell, arrow shows outer membrane, D) Merged image.

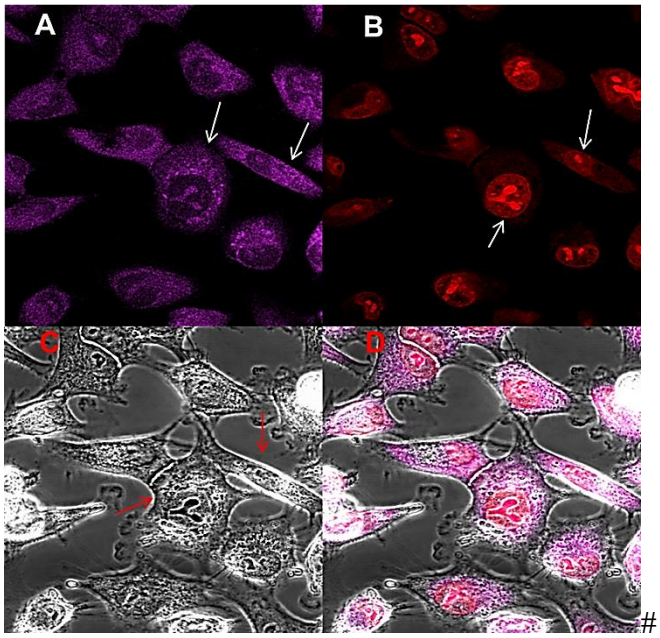

Figure 34: Confocal images of A549 cells labelled with 35 (10 μM) for 1 h. A) arrow shows localisation of **35** (λ_{ex} = 633, λ_{em} = 661-704 nm), B) nuclei staining with Syto 82 (λ_{ex} = 543 nm, λ_{em} = 554-587 nm), arrow shows localisation of Syto 82, C) brightfield image to visualise cell, arrow shows outer membrane, D) Merged image.

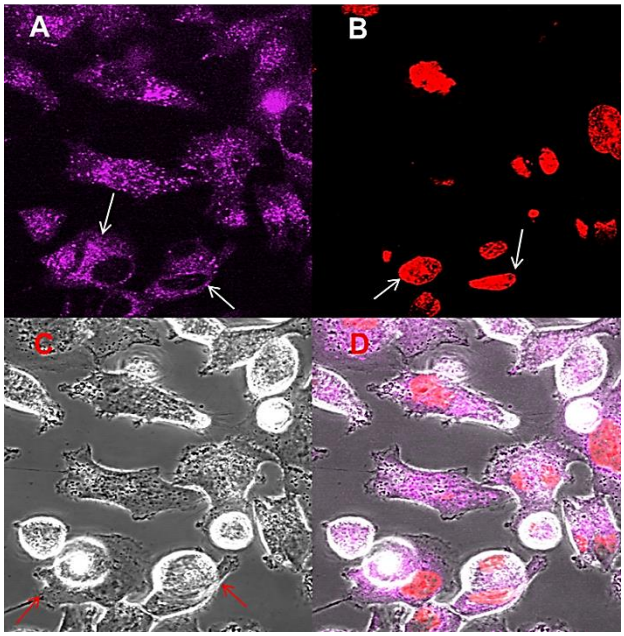

Figure 35: Confocal images of A549 cells labelled with 36 (10 μM) for 1 h. A) arrow shows localisation of **36** (λ_{ex} = 633, λ_{em} = 661-704 nm), B) nuclei staining with Syto 82 (λ_{ex} = 543 nm, λ_{em} = 554-587 nm), arrow shows localisation of Syto 82, C) brightfield image to visualise cell, arrow shows outer membrane, D) Merged image.

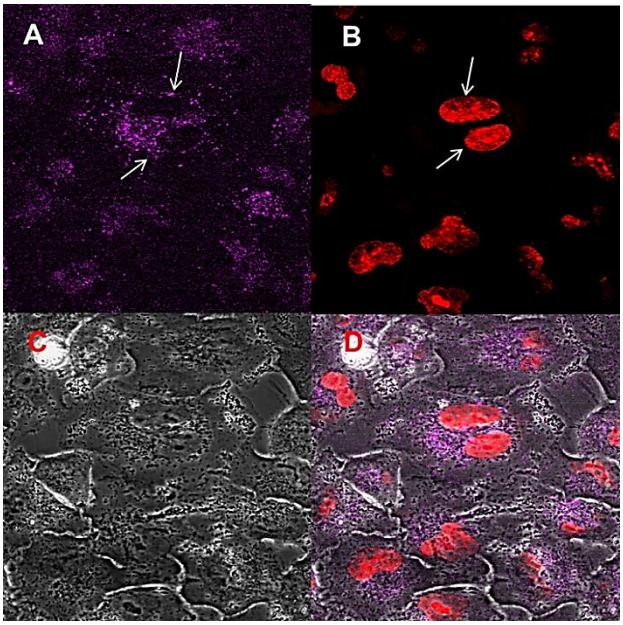

Figure 36: Confocal images of A549 cells labelled with 37 (10 μM) for 1 h. A) arrow shows localisation of **37** (λ_{ex} = 633 nm, λ_{em} = 661-704 nm), B) nuclei staining with Syto 82 (λ_{ex} = 543 nm,λ_{em} = 554-587 nm), arrow shows localisation of Syto 82, C) brightfield image to visualise cell, D) Merged image.

As expected, the sulfonated derivatives showed lower fluorescence intensity confirming the flow cytometry results. It was expected that PEGylation would have some effect on cellular uptake. However, this does not seem to be the case (compounds **34** and **35**). This can perhaps be explained due to the PEG chain being too small with only 3 ether linkages.

To further confirm these results a Z-stacking experiment was carried out using confocal microscopy to confirm cell penetration while staining the cytoplasm with Calcein to confirm cell localisation.

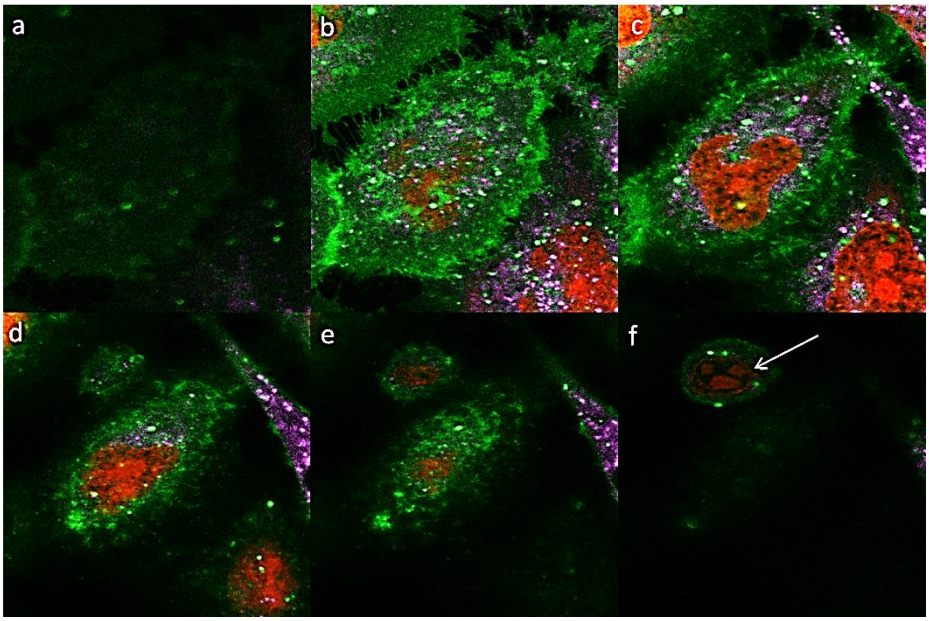

Figure 37: Z-stack confocal merged images of 34 (10 μM) in A549 cells. Pink – 34, λ_{ex} = 633 nm, λ_{em} = 651-704 nm. Red –Syto 82, λ_{ex} = 543 nm, λ_{em} = 576-619 nm. Green – Calcein, λ_{ex} = 488 nm, λ_{em} = 501-522 nm. 20 image slices taken penetrating through the cell. Images from a-f show increasing cell depth. Cell centre located approximately at image 9 a) Z-stack image 4/20, no cell visible b) Z-stack image 6\20 cell coming into focus with nuclei appearing. c) Z-stack image 8\20, full cell visible with cyanine dye and nuclei fluorescence. d) Z-stack image13\20, cell moving out of focus. e) Z-stack image13\20, cyanine particles no longer visible as cell moves out of focus. f) Z-stack image 18\20, initial cell out of focus with new cell appearing (white arrow).

From these results we can confirm that the cyanine dyes are taken up by mammalian cells and are not bound to the membrane. Structural modifications do not seem to have an effect although it can be said that cyanine **60** looks to be localised in the mitochondria more so than the others. The negative charge associated with the sulfonated derivatives is the most likely cause for the lower cellular uptake. As the cell membrane is negatively charged, the cyanine dye will be repelled to a larger extent than the non sulfonated analogue.

2.6.5 Towards the Synthesis of Molecular Imaging Probes

Studies relating to the *meso* substitution of cyanine dyes by nucleophiles has been discussed[126a] and has found to reduce the stability of the final fluorophore[138]. Research by Chang [127, 131] investigated the effects of amine substitution at the *meso*

position by analysing the decomposition products formed (Scheme 27) and found that reacting the amino-functionalised heptamethine dye with acetyl chloride, photostability was remarkably improved (Scheme 28)

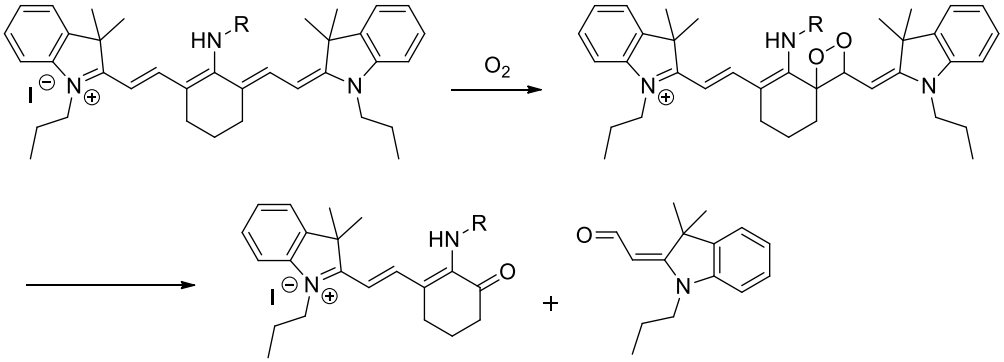

Scheme 27: **Decomposition of heptamethine cyanine dye by light irradiation.**

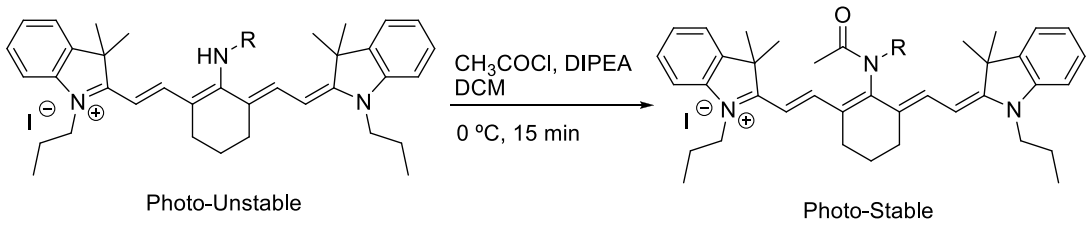

Scheme 28: **Increasing the photostability of heptamethine cyanine dyes.**

Interestingly, these studies do not discuss the differing fluorescence properties of the acylated and non-acylated amino modified heptamethine dyes. As discussed earlier in this chapter, amino substitution of heptamethine cyanine dyes causes a large blue shift in the absorption wavelength[139]. With this information in hand, the development of a new molecular probe was attempted following the concept detailed in Scheme 29.

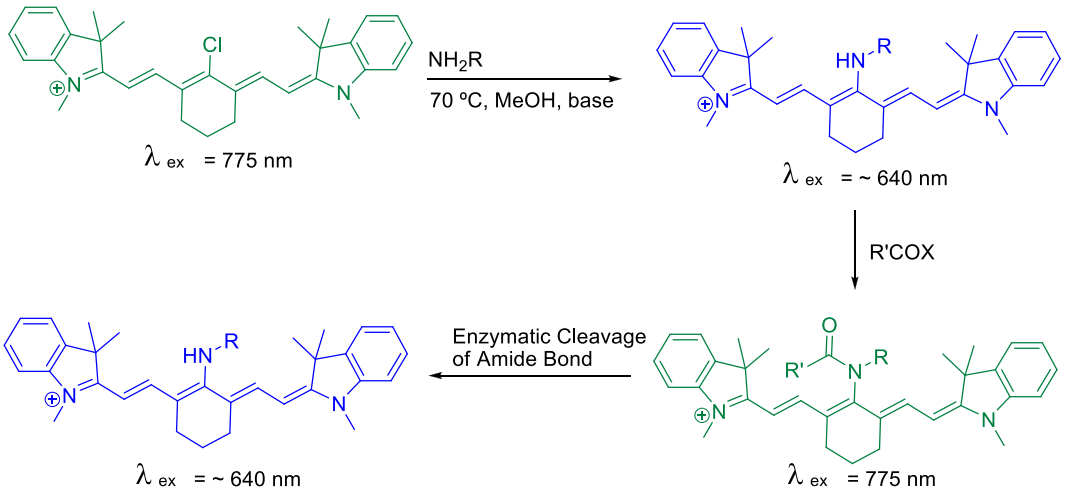

Scheme 29: Target synthesis of enzymatic cleavage ratiometric imaging probe.

In order to determine whether these amino-functionalised heptamethine scaffolds would be a substrate for enzymatic cleavage of an amide bond as shown, an aminomethyl-heptamethine molecule was synthesised by stirring chloro derivative **14** with 2 M methylamine in methanol for 4 hours at 70 °C generating compound **33**. Attempts to find milder conditions to acylate the secondary amine was tried using acetic anhydride and triethylamine, however, no product was formed. Amide bond formation using Fmoc protected amino acids was also attempted with a variety of coupling reagents including acid chloride formation, however, these were also unsuccessful. Successful acylation was found using the reported acetyl chloride in DIPEA to give compound **39** (Scheme 30). Taking insight from Nagano in their synthesis of a heptamethine esterase probe[140] and due to the presence of an acyl group it may be possible to develop an acylase probe.

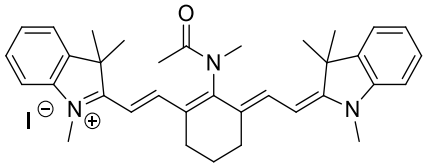

Scheme 30: Cyanine dye 39 Acylated aminomethyl heptamethine dye.

The optimum concentration (i.e. highest fluorescence intensity) of **39** was determined to carry out the *in vitro* studies. Several concentrations of molecule **39**

were dissolved in 50 mM ammonium bicarbonate buffer and their fluorescence intensities recorded.

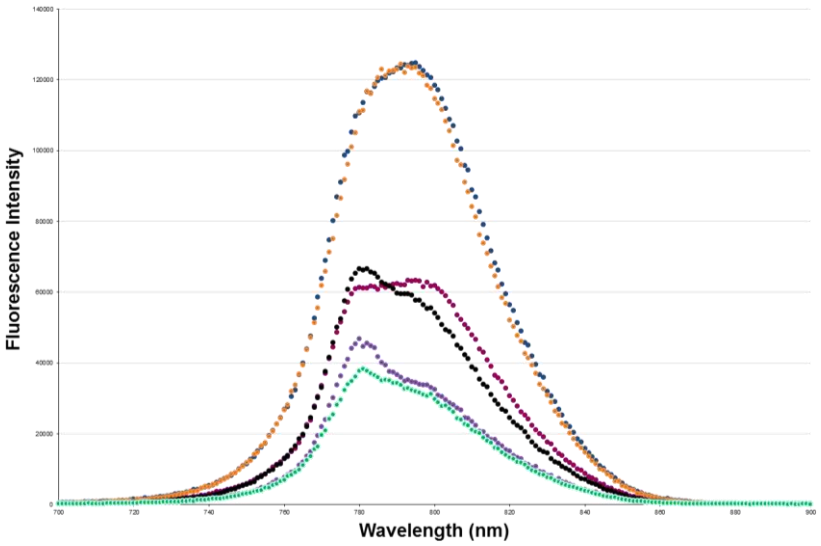

Figure 38: Investigation into the concentration effects on fluorescence of heptamethine dye 39. Dark pink – 97 µM, Blue – 48 µM, Orange – 24 µM, Black – 12 µM, Purple – 6 µM, Cyan – 3 µM. λ_{ex} = 700 nm, λ_{em} = 790 nm.

Figure 38 shows that higher concentrations result in self-quenching and lower overall fluorescence intensity. Sufficient dilution of the fluorophore was at a concentration of 24 µM and therefore this concentration was selected for our cleavage assay. To test the cleavage of the amide bond, 4 enzymes were selected: trypsin, chymotrypsin, acylase and pepsin. **39** was dissolved in 50 mM ammonium bicarbonate solution (pH 7.8) to give a final concentration of 24 µM. After incubation with a 1 mg/mL enzyme solution for 3-48 hours the solution was then measured for any change in fluorescence maxima, absorption maxima or HPLC ELSD shift.

Unfortunately, analysis revealed no fluorescence increase or HPLC shift, concluding that cleavage of the amide bond did not occur in the presence of any enzyme. This is most likely due to the large and rigid structure of the cyanine dye that is unable to fit into the active site of the enzymes selected. In order to address the steric hindrance of the probe, a "self-immolative" linker was selected in order to increase the distance between the reactive site and the fluorophore. A self-immolative linker is one in

which on initial reaction a protecting group is removed, therefore causing a subsequent elimination reaction to release the desired molecule. These linkers are commonly used when dealing with controlled release of drugs within delivery systems[141]. One such strategy was employed by Cohen[142] to develop a hydrogen peroxide activated MMP inhibitor. Modification of this strategy and application to heptamethine dyes was attempted (Scheme 31).

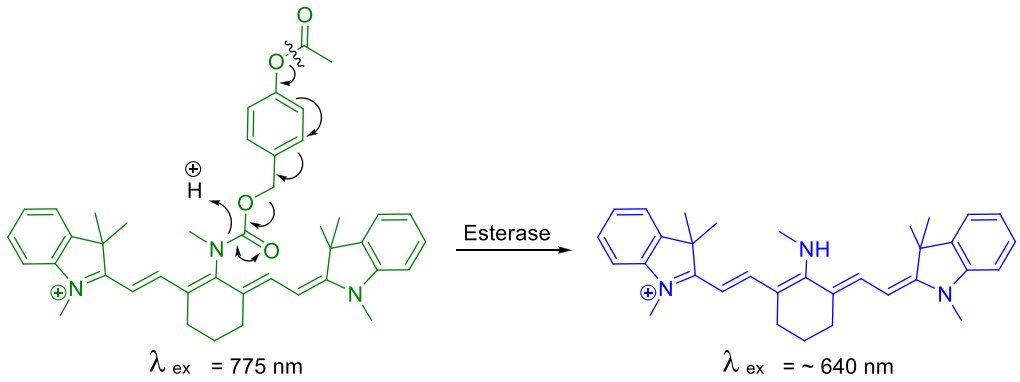

Scheme 31: Possible self-immolation of ratiometric acylase probe.

Functionalization of the heptamethine fluorophore with 4-hydroxymethyl phenyl boronic acid pinocol ester would allow development of a NIR hydrogen peroxide probe as described in (Scheme 32).

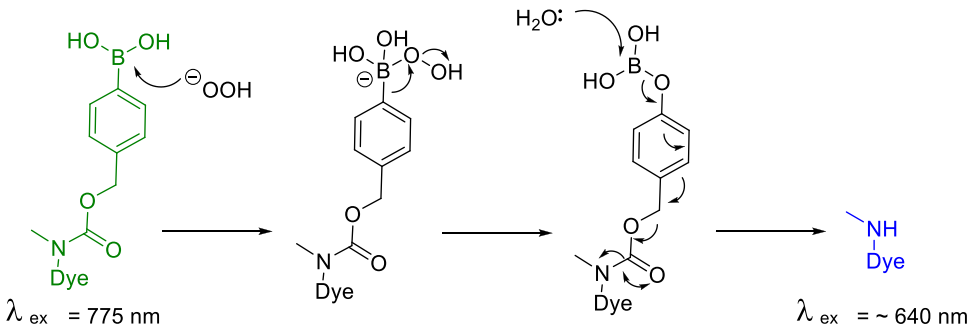

Scheme 32: H_2O_2 mediated 1-6 elimination.

2.6.5.1 Heptamethine Dye H_2O_2 Stability

Before further experiments were carried out, it was important to determine the stability of the heptamethine dye in the presence of H_2O_2.

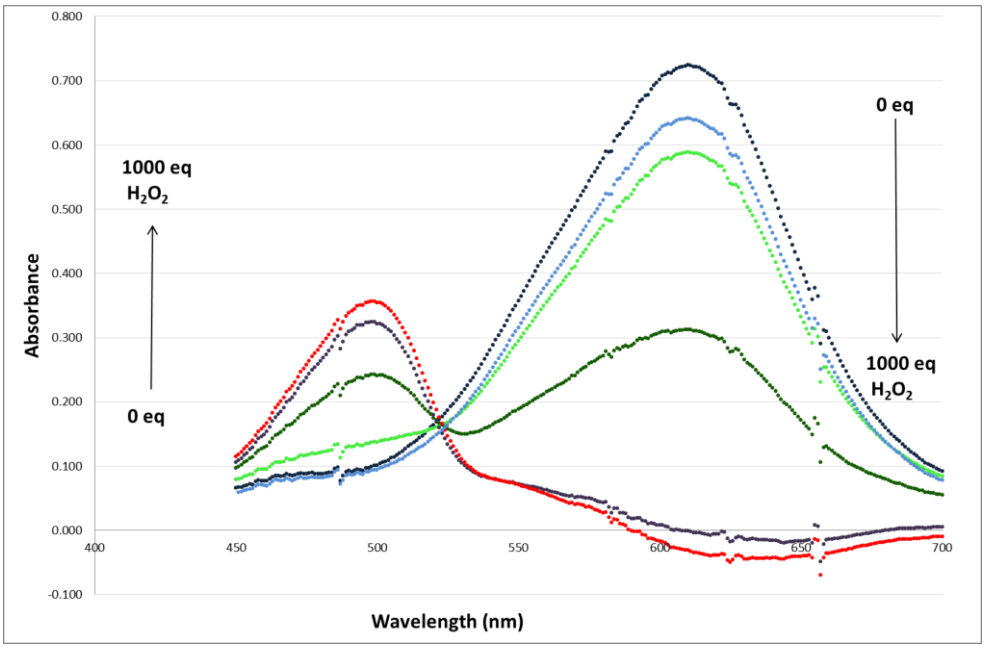

Figure 39: Absorption spectra of compound 33 (1 mL solution, 92 µM) with H_2O_2 - Dark blue – no H_2O_2. Light blue – 10 eq H_2O_2 (0.92 mM). Light green – 100 eq H_2O_2 (9.2 mM). Dark green – 250 eq H_2O_2 (23 mM). Purple – 500 eq H_2O_2 (46 mM). Red – 1000 eq H_2O_2 (92 mM).

Figure 39 shows that compound **33** was stable with up to 100 equivalents of H_2O_2 (9.2 mM) after 1 hour. This confirms that heptamethine dyes could potentially be used as an H_2O_2 sensor[142]. It is interesting to note that a new absorption peak occurs at 500 nm which is accompanied by a colour change from blue to pink (Figure 40). This pink solution supports the non-fluorescent degradation product described earlier in Scheme 27. Full decomposition of the fluorophore occurs with 500 equivalents (46 mM) of H_2O_2.

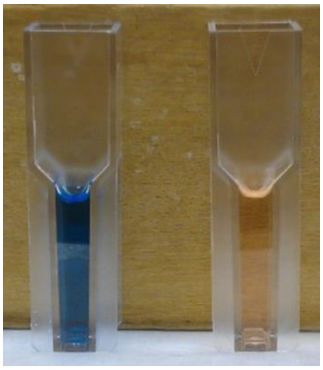

Figure 40: Compound 33 Left: without H_2O_2. Right: with H_2O_2.

Synthesis of the acylase probe linker moiety began from 4-hydroxybenzaldehyde. Protection of the phenol by treatment with acetic anhydride in pyridine at room temperature gave **49** with reduction of the aldehyde with sodium borohydride in ethanol gave the desired alcohol **50** (Scheme 33).

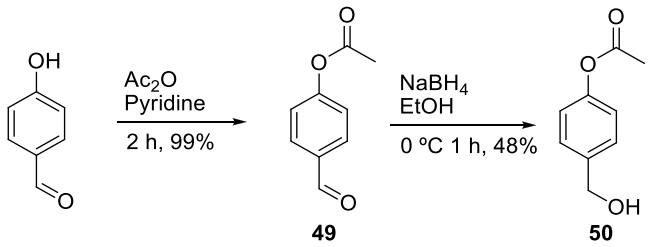

Scheme 33: Synthesis of acylase probe self-immolative linker.

Activation of alcohol **50** was initially attempted using triphosgene, however, no product was isolated. As an alternative, nitrophenyl chloroformate was reacted with the alcohol of **50** (Scheme 34) and commercially available hydroxymethyl phenyl boronic acid pinocol ester (**82**) (Scheme 35). Immediate column chromatography was carried out to yield the desired products (**51** and **53**). Confirmation that the carbamate underwent reaction with amines was modelled with benzylamine to give compounds **52** and **54**.

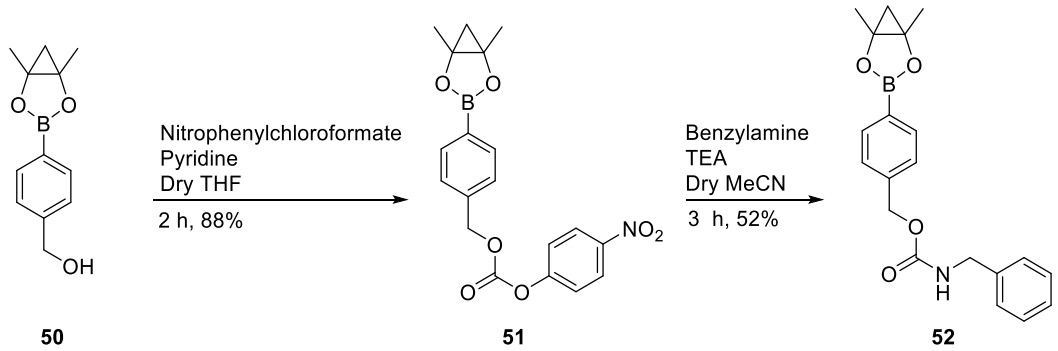

Scheme 34: Synthesis of activated carbonate and test reaction.

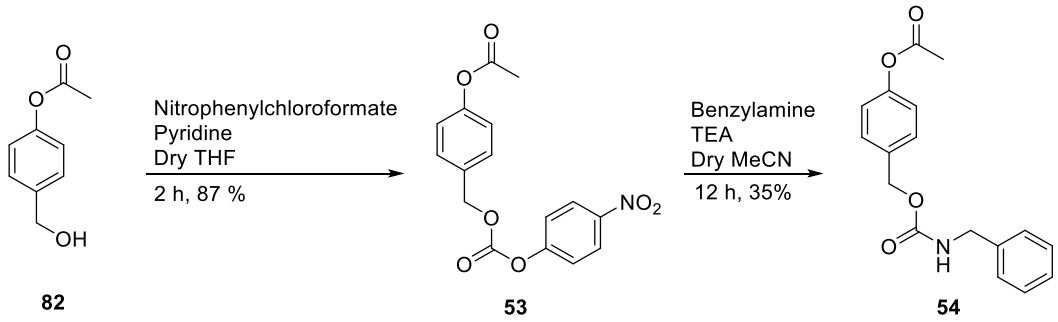

Scheme 35: Synthesis of activated carbonate and test reaction.

Activation using nitrophenyl chloroformate was carried out on a large scale (1 g) with the stable adduct kept at 4 °C for up to 3 months.

To complete the synthesis of the probes, carbamate bond formation was attempted. Initially, heptamethine dye **33** and compound **53** were dissolved in dry MeCN with potassium carbonate and heated under microwave irradiation for 30 minutes. As expected, the solution turned from blue to green, with a characteristic absorption band appearing at 780 nm. Additionally, the correct mass was found by LCMS, however, on purification, the compound could not be isolated. Several purification techniques including differing solvents were attempted with no positive results.

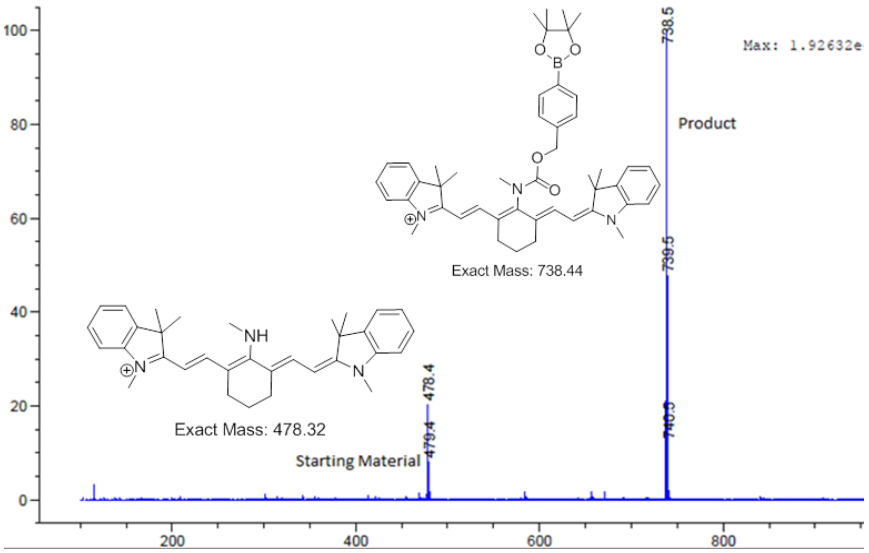

Figure 41: LCMS spectra of crude mixture of reactants showing presence of starting material (33) and the product.

In order to increase the yield of this reaction, several different organic bases, solvents and reaction conditions were attempted with no success.

2.6.5.2 Monoamine Oxidase Probe

Monoamine oxidases (MAO) exist in two distinct forms, MAO A and MAO B. MAOs catalyse the oxidation of a variety of neurotransmitters such as dopamine within the body[143] and are generally found in the mitochondria of most mammalian cells[144]. Up-regulation of MAO can result in several degenerative diseases such as Parkinson's or Alzheimer's and therefore, real-time detection of these enzymes has become of extreme importance in medicinal chemistry. Chang[145] reported a fluorescent probe for detection of MAO A and B. This sensor relied on a coumarin based fluorophore and will therefore suffer from high background auto-fluorescence in cells. The *turn on* fluorescence signal relies on the oxidation and β-elimination of an aminopropyl group attached to the fluorophore.

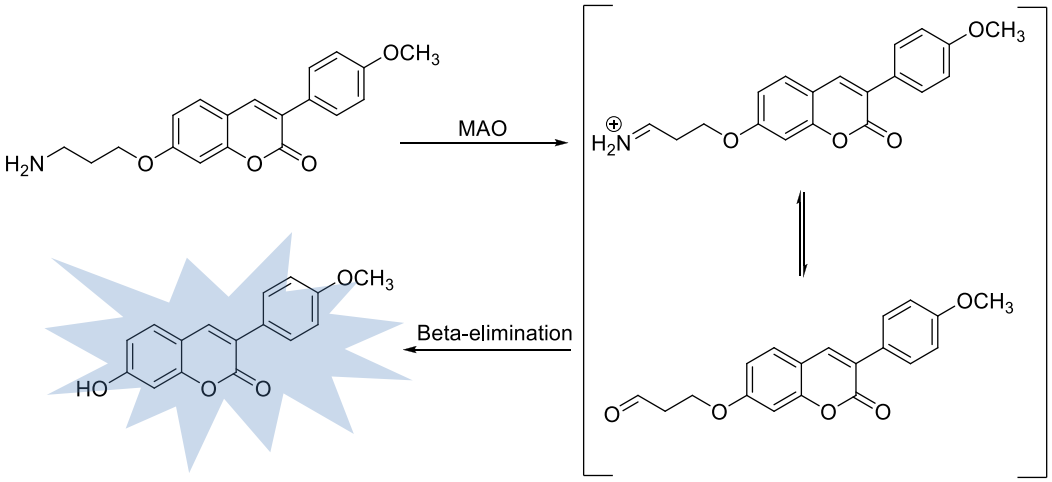

Scheme 36: Coumarin based MAO probe[145].

More recently, Qian[146] synthesised a similar coumarin based MAO probe, specific for MAO B. A novel, NIR MAO A or MAO B imaging probe would help in the battle against the degenerative neurological disorders mentioned above. To accomplish this, insight was taken from Yoon in the development of a NIR cyanine sensor for cysteine[110]. In this study, modulation of the π-conjugation system of *meso* substituted heptamethine cyanine dyes was utilised (Scheme 37).

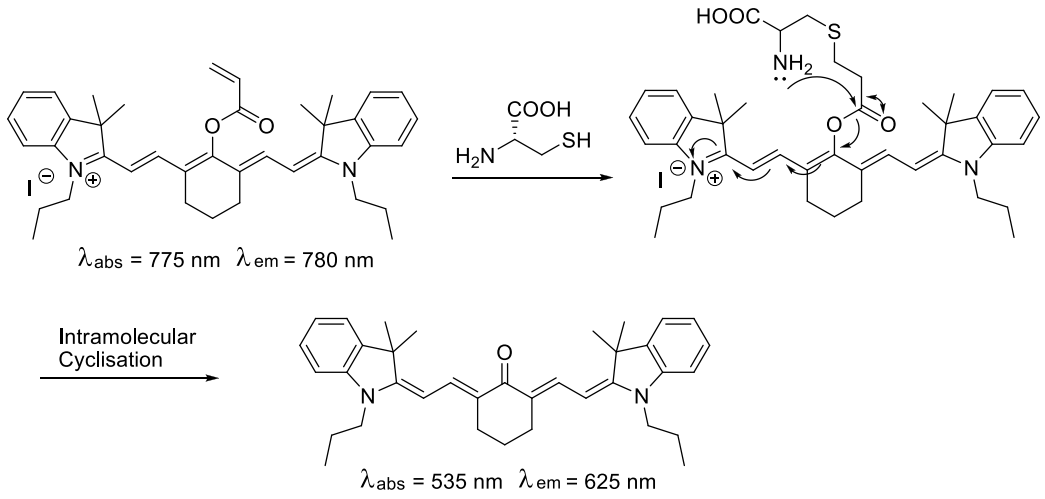

Scheme 37: Cysteine detection by intramolecular cyclisation[110].

A similar strategy could be employed to develop a NIR MAO probe (Scheme 38).

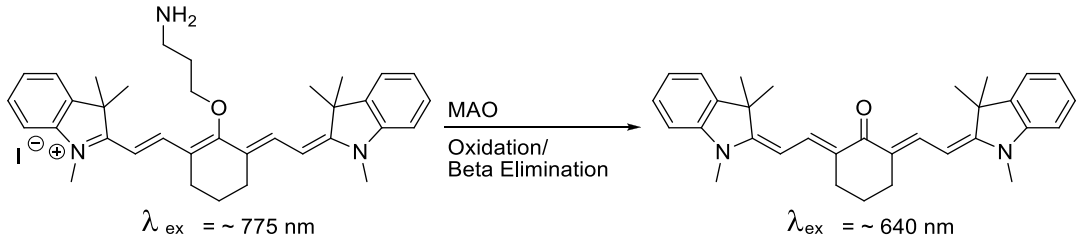

Scheme 38: Hypothetical NIR MAO heptamethine probe.

The first strategy employed to synthesise this MAO probe started from the synthesis of the 3-aminopropanol moiety. The amine was first protected with 2-acetyldimedone(4,4-dimethyl-2,6-dioxocyclohexylidene)ethyl (Dde-OH), a protecting group that can be removed under conditions suitable for the fluorophore. Protection of the amine was carried out in methanol with DIPEA, requiring a simple purification to obtain product **55**.

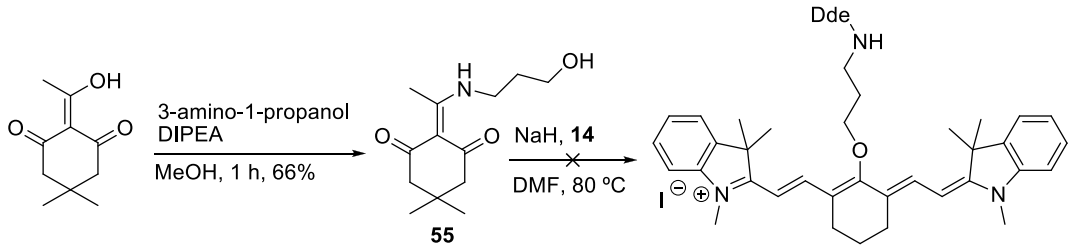

Scheme 39: Attempted synthesis of NIR MAO probe. Dde-OH courtesy of Aurelie Brunet, Edinburgh University.

As the literature has yet to show the $S_{RN}1$ mechanism by a hydroxy group on heptamethine dyes, NaH was chosen as a strong non-nucleophilic base, however, on reaction with heptamethine derivative **14** no product was found, only recovering the dye starting material (Scheme 39).

As shown by Yoon *et al*[110] it is possible to generate a free alcohol from heptamethine derivative **14** using sodium acetate in DMF shown in Scheme 37. Using this design, the amino-propanol moiety was modified and replaced with 1-bromo-3-proylamine with Dde-OH protection was carried out to produce **56** before attempted substitution of the bromine (Scheme 40).

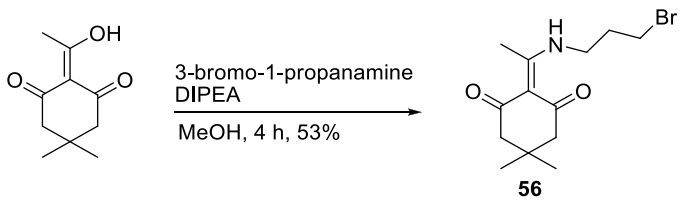

Scheme 40: Synthesis of DDE protected 3-bromo-1-propanamine.

Synthesis of the hydroxyl-heptamethine dye was successful to give **57.**

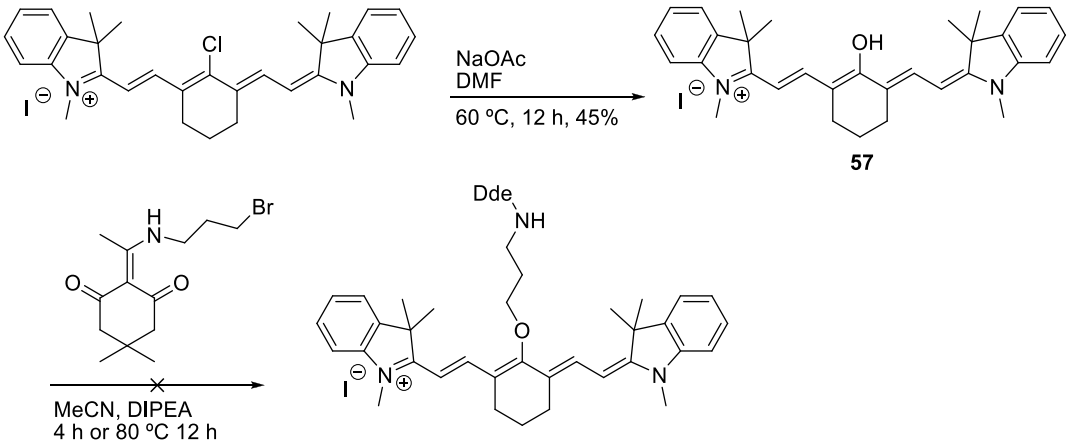

Scheme 41: Attempted synthesis of MAO probe from hydroxy-heptamethine dye.

Two attempts were made to synthesise the final MAO probe with neither proving successful. The difficulty in this reaction can be related to the basic conditions in which the hydroxy-heptamethine dye is likely to be in the ketone form and therefore cannot react.

2.6.6 Pentamethine Cyanine Dyes (**42-48**)

Pentamethine (cyanine 5 type) fluorophores absorb and emit around 630-680 nm. Although these wavelengths are similar to the amine substituted heptamethine dyes, these dyes do not suffer for the same instability problems as amino cyanines. The He-Ne laser[147] is a commonly used laser in confocal microscopy and has an excitation wavelength of 633 nm, ideal for cyanine 5 type fluorophores. Currently,

commercial cyanine 5 dyes are extremely expensive with prices reaching $860 for 1 mg[148].

Novel fluorophores are required and therefore synthesis of a new type of pentamethine dye using a similar approach as for heptamethine dyes was carried out (Scheme 42).

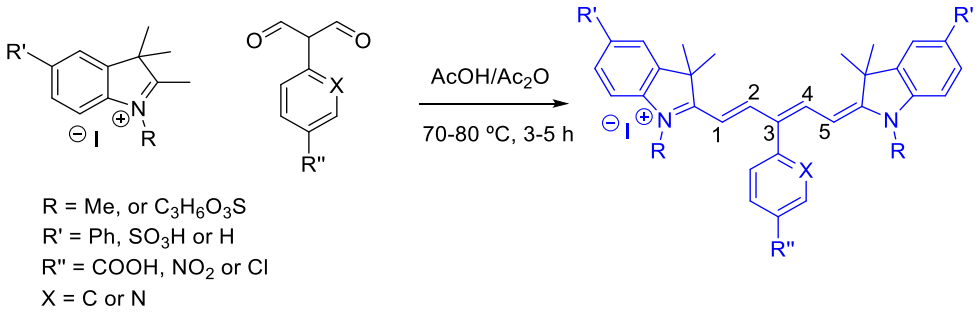

Scheme 42: Synthesis of novel pentamethine cyanine dyes.

The reaction was carried out on small (25 mg) or large (5 g) scale which purifications only becoming troublesome when using sulfonated indolium salts. This problem was overcome by developing a new silica based purification system using MeCN:IPA rather than DCM:MeOH as the solvent mixture during column chromatography.

Figure 42: 10 g Pentamethine Dye.

Table 4 gives the structures, yields and photo-physical properties of the pentamethine dyes synthesised.

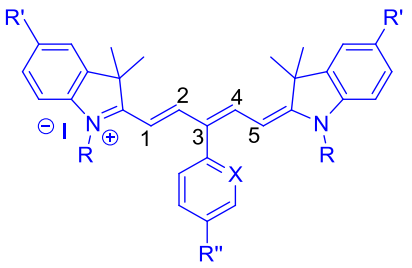

Figure 43: General structure of pentamethine dye.

Dye	R	R'	R''	X	Yield (%)	Abs (λ_{Max})	Em (λ_{Max})	ε* ± 10 %	Φ_F ± 10 %
42	Me	Ph	COOH	N	37	677	702	51500	0.250
43	Me	SO_3H	COOH	N	35	650	676	78500	0.220
44	$C_3H_6O_3S$	Ph	COOH	N	57	683	708	62000	0.220
45	$C_3H_6O_3S$	Ph	Cl	C	42	686	709	39500	0.210
46	$C_3H_6O_3S$	Ph	NO_2	C	67	684	710	81000	0.120
47	Me	SO_3H	NO_2	C	81	650	676	61000	0.070
48	Me	SO_3H	Cl	C	82	654	678	68500	0.290

Table 4: Structure, yield and photo-physical properties of pentamethine cyanine dyes. Absorption, emission, extinction coefficient and quantum yield all measured in DMSO. * = L Mol^{-1} cm^{-1}.

This new class of pentamethine cyanine dyes have an absorption maximum between 676 and 686 nm and an emission maximum between 676 and 710 nm. These deep blue coloured molecules have a small Stokes shift (24-26 nm) characteristic of cyanine dyes and are suitable for excitation with a He-Ne laser (633 nm). The reaction yields vary between 35-82 % with increasing yields due to the optimisation of the purification solvent system. In general, purification of the sulfonated analogues was laborious, with the addition of acetic acid to the eluent system needed to allow elution and limiting "streaking" of the dye.

The extinction coefficients of these dyes (**42-48**) range between 50000-81000 L Mol^{-1} cm^{-1} which is comparable fluorescein (ε = 69000 L Mol^{-1} cm^{-1} in aqueous solution[149]). Interestingly, the quantum yields are remarkably high for cyanine dyes in the region of 0.20-0.29, however, addition of a nitro group to the phenyl ring (**46** and **47**), caused this value to drop dramatically to 0.070 and 0.120. Modification of the indole ring provides some insight into the effect of the sulfonate group in the R position. In addition to increased aqueous solubility, a slight red shift was observed when compared to the methylated fluorophore (**42** vs **44**). The increased rigidity and planarity of the structure in the case of the benz[e]indolium fluorophores supports the increased quantum yield when compared to the indole derivative (**42** vs **43**). The ^{1}H NMR of all compounds showed symmetry down the centre of the molecule common to cyanine dyes.

Compounds **42-48** were suitable for further functionalisation via Suzuki-Miyaura coupling for the chloro derivatives[33a], nucleophilic substitutions or reduction of the nitro group to an amine[150]. Such modifications could be the generation of FRET probes by the addition of a cleavable sequence attached to an appropriate fluorophore such as cyanine 3.

An example NMR spectra is shown in appendix 5.

2.6.6.1 Photo-Stability of Pentamethine Cyanine Dyes

For most practical procedures the fluorophore is exposed to light and it was important to verify the stability of these new fluorophores. Compound **43** was dissolved in NMP (0.01% w/v) and was irradiated with UV light for 30 minutes with and without the addition of a photoinitiator 1-hydroxycyclohexyl phenyl ketone (Iragacure 184) (0.2% w/v) and the fluorescence intensity measured. The photointiator under UV light generates free radicals (Scheme 43) which destroys the conjugated system of the cyanine dye, resulting in a loss of fluorescence.

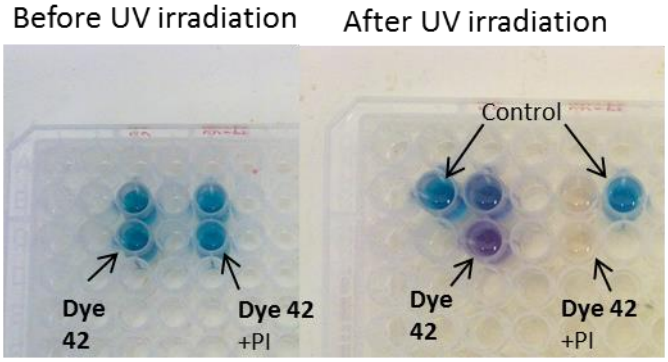

Figure 44: UV Irradiation of pentamethine dye 42 with and without the presence of photointiator. Left image: Before UV irradiation. Right image: After UV irradiation. Control is dye **42** alone at time 0.

Visually, it is apparent that after 30 minutes in the presence of the photoinitiator the cyanine dye has decomposed, which was confirmed using fluorescence spectroscopy.

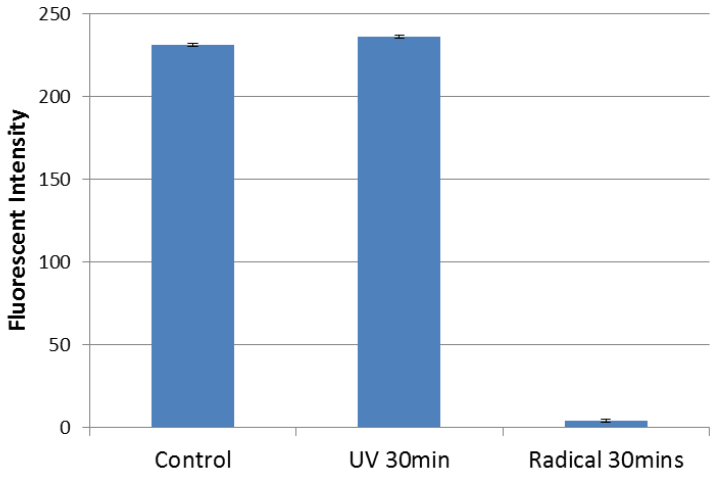

Figure 45: Pentamethine dye (42) stability to UV irradiation. Fluorescence intensity of cyanine **42** dye after irradiation with UV light, with and without the photoinitiator.

This data shows that without a photointiator, irradiation with intense UV light for 30 minutes does not cause photobleaching of the cyanine dye.

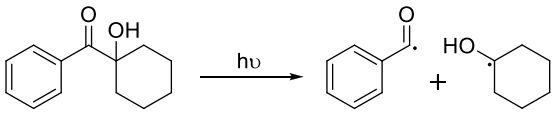

Scheme 43: Radical initiation of Iragacure 184 with UV irradiation.

2.7 Conclusion

The synthesis of cyanine dyes has become trivial with the ability to use solid or solution phase chemistry. More pressing issues are the modification of heptamethine cyanine dyes to develop molecular sensors and optical imaging agents. The synthesis of 26 heptamethine dyes with a broad range of absorption and emission wavelengths and a large Stoke's shift range has been carried out. Variation of the functional groups was found not to play a part in cellular toxicity or cellular uptake which may prove useful for qualification of new fluorescent molecules for use *in vivo*. These dyes can be further functionalised to generate *turn-on* fluorescent probes or imaging agents.

A new class of pentamethine cyanine dyes is also described with ideal absorption wavelengths for the He-Ne laser. These molecules can be further functionalised increasing their possibility for use in molecular imaging. Currently, collaborators at DestiNA Genomics and STMicroelectronics are attempting to utilise these new cyanine dyes as part of a microchip based system for the detection of substrates.

Chapter 3

Near Infrared Fluorescent Microspheres

3.1 Introduction to Nanoparticles

The need for new delivery systems and controlled release technologies for medical diagnostics is high with annual sales expected to exceed $133 billion by 2015[151]. Novel small molecules tend to have low solubility in aqueous media and often require delivery systems that are non-toxic[152]. Drug release from polymers dates back to 1960 when Folkman described the controlled release of drugs from silicone rubber[153]. Since then, polymeric particles including nano-materials have been used as drug delivery vehicles. Polymeric nanoparticles are becoming an increasingly viable option[154] due to their ease of synthesis[155] and their ability to easily encapsulate the molecule to be delivered[156]. Furthermore, biodegradable[157] micro- and nanoparticles do not require removal of the delivery device after cargo release.

Nanoparticles are becoming widely used in biological sciences due to their high cellular uptake[33a, 158], and low cellular toxicity[159]. One of the most important features of nanoparticles is their high surface area to volume ratio, resulting in a high number of functional groups present on the surface of the particle[160]. Functionalised particles below 200 nm are very reactive with these high surface area molecules often being used in catalysis[161]. One example of the use of nanoparticles is shown in the field of "theranostics"[162] in which both diagnosis and therapy can be administered simultaneously[163]. For example, Rossi[164] functionalised silica coated magnetic particles with methylene blue (a photodynamic therapy drug) and then further with an MRI contrast agent allowing simultaneous diagnosis and treatment of tumours.

The addition of fluorophores to nanoparticles has resulted in a number of applications, for example, Bradley functionalised microspheres with fluorescein imparting the ability to sense intracellular pH between 6 and 8[165]. Other applications include calcium sensing[166], gene silencing[167] and drug delivery[36]. So far, the fluorophores used absorb and emit light below the near infrared window and therefore novel NIR microspheres are sought after.

Although the addition of fluorophores to the outside of polymeric particles through covalent linkers have interesting applications, the synthesis of more exotic probes can be difficult. Furthermore, functionalisation can be problematic due to the large number of molecules on the particles surface. The ability to penetrate the particle core and produce inherent fluorescent nanoparticles may overcome this. Such synthesis of organic NIR inherent microspheres, with the ability to be further functionalised have to my knowledge, never been investigated and could provide a useful tool for the imaging of cellular process *in vivo*.

3.2 Inherent Near Infrared Nanoparticles (NIR-NPs)

There are multiple methods to synthesise microspheres including dispersion[168], emulsion[169] and emulsion free polymerisation[170] procedures. Emulsion free polymerisation uses charged monomer units such as 4-vinylbenzylamine hydrochloride[171] or acrylic acid. These monomers prevent particle aggregation and also introduce reactive functional groups at the particle surface which can be used for derivitisation.

Currently, to obtain inherent fluorescent particles the most common route is to use a solvent evaporation method[172] or a swelling and shrinking procedure to trap a fluorophores inside the particle of choice[173]. These techniques may give the desired fluorescent core, however, the encapsulated molecule may leak out of the particle[174]. For example, Yang *et al*[175] utilised the solvent evaporation method to generate several bovine serum albumin (BSA) containing microspheres to monitor

drug distribution in tropical fish. Utilising the fluorescence attribute of BSA and by varying the microsphere structure, the rate of BSA diffusion was monitored using confocal microscopy (λ_{ex} 488 nm)[175]. It is also possible to synthesise fluorescent particles by incorporating the fluorophore into the particle during synthesis as a monomer. some examples include Hostasol Yellow 3G[176] through emulsion polymerisation with an anionic surfactant (λ_{max} 450 nm, Figure 46), Europium based β-diketonate complexes[177] (λ_{max} 300-450 nm) or styrene containing fluorescein[158a] (λ_{max} 488 nm), however, these do not fall within the sought after near infra-red window.

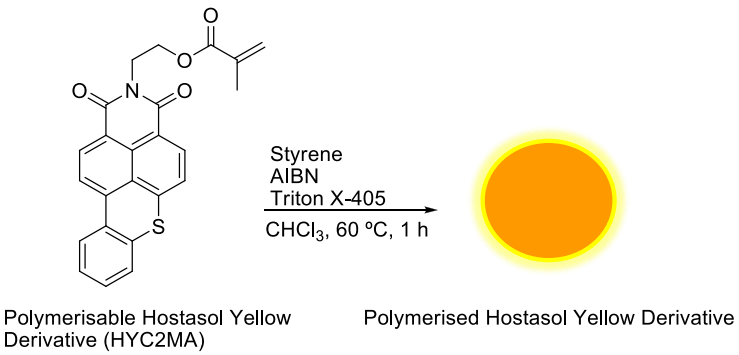

Figure 46: Emulsion polymerisation of Hostasol Yellow derivative (HYC2MA) in the presence of surfactant to give polymer particles with Styrene (30% wt), AIBN (1% wt) and Triton X-405 (25% wt). λ_{ex} = 450 nm, λ_{em} = 510 nm. Average particle size = 50 nm[177].

Gold or Fe_3O_4 based NIR absorbing particles have also been constructed with the ability to be coated with the desired functional group, for example, silica doped with a NIR fluorophore[178]. Many derivatives[179] exist including Ag-Au[180] or lanthanide based nanoparticles[181]. Nanoparticles such as these can provide a synergistic effect due to their ability to be used as contrast agents for MRI while having the photo-physical ability to convert NIR irradiation into heat, enabling proximity damage to tumour cells. Although useful, these particles contain unwanted metal components and suffer from *in vitro* and *in vivo* toxicity[182].

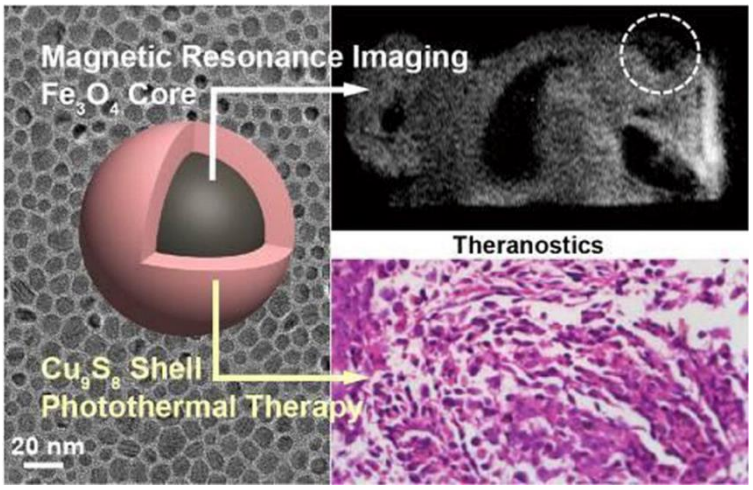

Figure 47: Dual imaging Fe_3O_4 based nanoparticles coated with Cu_9S_8 (left). Magnetic properties allow MRI imaging (top right) and NIR absorption allowing for thermal imaging (bottom right). Reprinted with permission from[179b], copyright (2013) American Chemical Society.

Similarly, quantum dots, most commonly constructed from cadmium and selenium have excellent photo-physical properties with tuneable absorption and emission wavelengths[183]. Quantum dots are commonly described as toxic to cells[184], however, more recent studies have suggested that this toxicity to cells may not be transferable to human or primate subjects[185].

3.3 Chapter Aims

Fluorescent microspheres most commonly include fluorophores with absorption and emission wavelengths below the NIR window. The use of nanoparticles which absorb and emit light in the NIR region will allow for increased *in vivo* applications. The synthesis of a NIR fluorescent particle with the ability for further modification was targeted with investigations into the particles' cellular uptake and toxicity explored.

Furthermore, the use of NIR fluorophores to track the localisation of microspheres within cells while covalently attached to polymeric nanoparticles is discussed, with an example of the delivery of a cargo into a cell demonstrated.

3.4 Results and Discussion

3.4.1 Synthesis of Polymerisable Cyanine Dyes

In order to synthesise near infrared organic fluorescent particles, a heptamethine dye was designed with a styrene moiety to allow polymerisation (Scheme 44). Starting from chloro-heptamethine cyanine dye (**14** or **18**) (see Chapter 2, Table 3), 4-aminomethyl styrene was attached by stirring at 100 ºC for 1 hour under microwave irradiation in the presence of a base. Purification gave the desired compounds in reasonable yields.

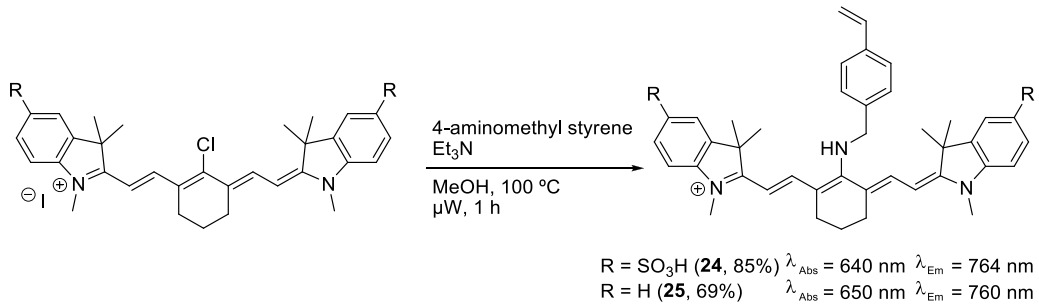

Scheme 44: Synthesis of styrene modified heptamethine dye.

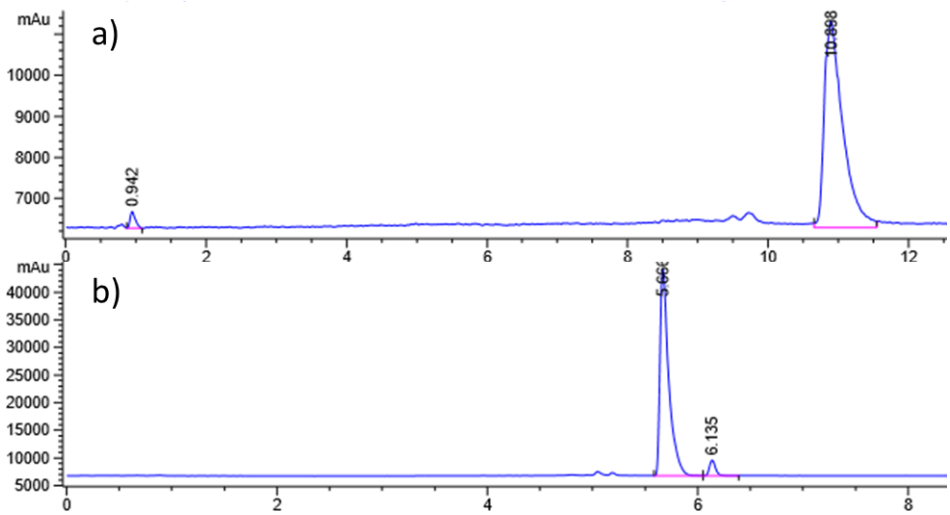

Figure 48: HPLC-ELSD traces of a) 24 (HPLC method 3) and b) 25 (HPLC method 2). x-axis represents retention time in minutes, y-axis represents signal intensity. (see chapter 6.1 for HPLC methods).

3.4.2 Synthesis of Inherent Near Infrared Nanoparticles

The synthesis of the near infrared nanoparticles (NIR-NP) was carried out using an emulsifier free polymerisation. Styrene, divinylbenzene (DVB, 2%), para-vinylbenzylamine hydrochloride (VBAH, 3%), heptamethine dye (**25**, 3%) and the water soluble initiator 2,2'-azobis(2-methylpropionamidine)dihydrochloride (V-50) were stirred in water at 80 ºC for 15 hours. The particles were collected by centrifugation and washed with DMF, MeOH and water until the supernatant was no longer coloured (Scheme 45).

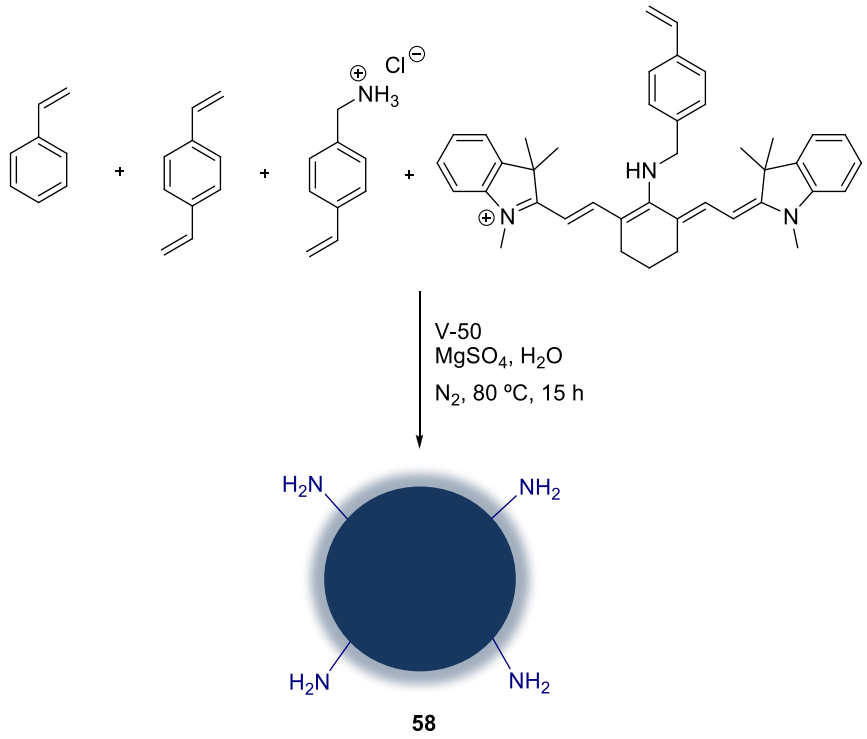

Scheme 45: Synthesis of NIR particles 58 and cartoon of fluorescent nanoparticle with free amines at surface.

Particles **58** were examined by flow cytometry and dynamic light scattering to confirm particle fluorescence and determine particle size respectively (Figure 49).

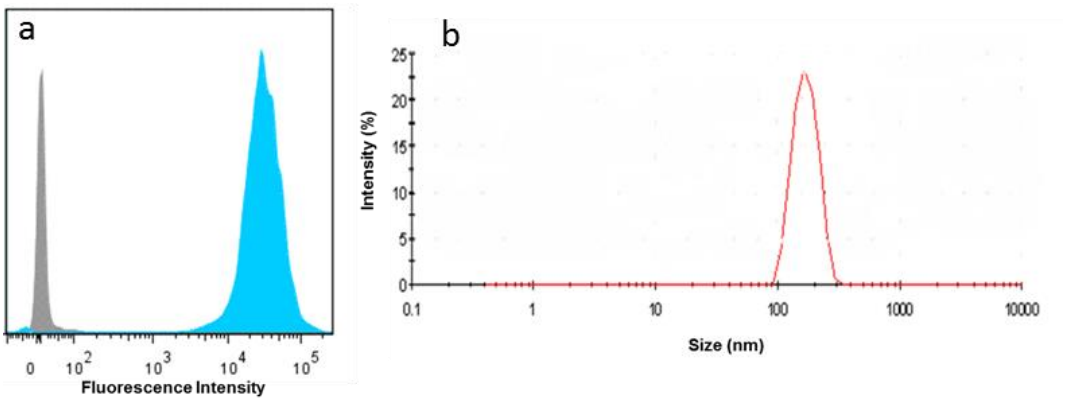

Figure 49: Analysis of NIR-NP 58 a) Flow cytometry histogram, λ_{ex} = 633 nm, λ_{em} = 785 nm, grey section – particles without cyanine dye monomer, blue section –particles with cyanine dye monomer. y-axis represents number of particles, x-axis represents fluorescence intensity b) Dynamic light scattering analysis, y-axis represents percentage of particles, x-axis represents particle size. Average particle size was 165 nm with a polydispersity index of 0.09.

NIR-NPs **58** were synthesised with an average hydrodynamic diameter of 165 nm and a polydispersity index of 0.09. Particle fluorescence was confirmed using flow cytometry showing an increase in fluorescence intensity over particles with no fluorophore by over 100 fold.

3.4.3 Cellular Toxicity and Uptake of Near Infrared Nanoparticles

In order to determine the toxicity of the NIR-NPs **58**, the MTT assay was utilised to determine cell viability. Incubation of particles **58** with HeLa cells for 24 hours confirmed internalisation did not cause cell death up to a concentration of 75 µg/mL (Figure 50).

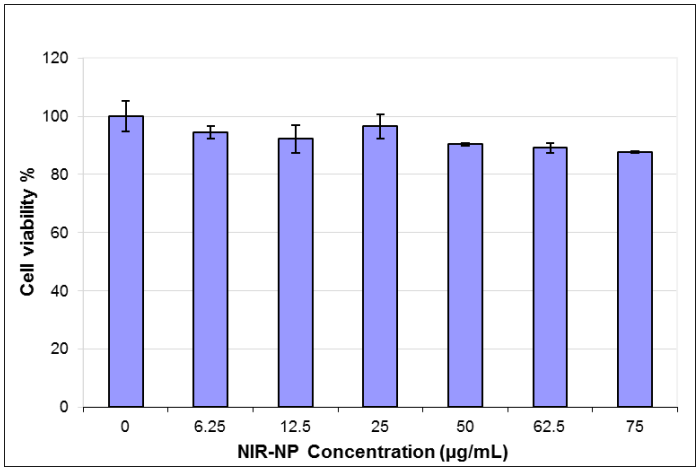

Figure 50: HeLa cells treated with 0 to 75 µg/mL of 58 for 24 hours prior to MTT analysis. DMSO represents no cells. (n = 3).

Confocal microscopy was carried out to show the location of the nanoparticles within the cell. A549 cells were selected and incubated with **58** (100 µL of 75 µg/mL in PBS pH 7.4) for one hour followed by washing once with PBS and live cell imaging. To determine the location of the particles the A549 cells were incubated with Syto 82 and Calcein for 30 minutes prior to imaging to stain the nucleus and cell cytosol respectively.

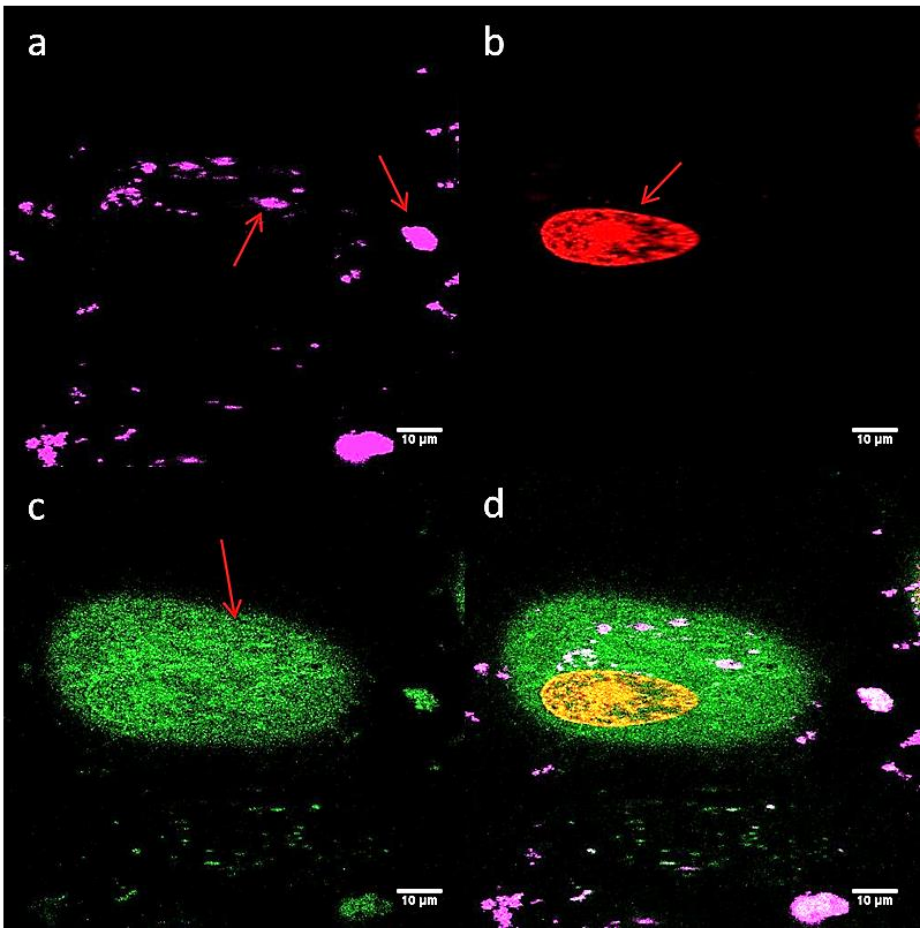

Figure 51: Confocal images of A549 cells incubated with 58 at 75 µg/mL for 1h. a) Microsphere uptake and cellular labelling with **58** (pink, λ_{ex} = 633, λ_{em} = 651-704 nm), arrow shows localisation of NIR-NP's throughout the cell, b) Nuclei staining with Syto 82 (red, λ_{ex} = 543 nm, λ_{em} = 576-619 nm), arrow shows localisation of Syto 82 within nucleus c) cytosol labelling with Calcein (green, λ_{ex} = 488 nm, λ_{em} = 501-522 nm) arrow shows outer membrane, d) Merged image. Arrows show aggregated microspheres localised within the cytoplasm.

The confocal images suggested cellular uptake of the microspheres into the cells, throughout the cytoplasm, although the microspheres appeared to have aggregated. A Z-stacking experiment was carried out to confirm cell penetration and cytoplasm location.

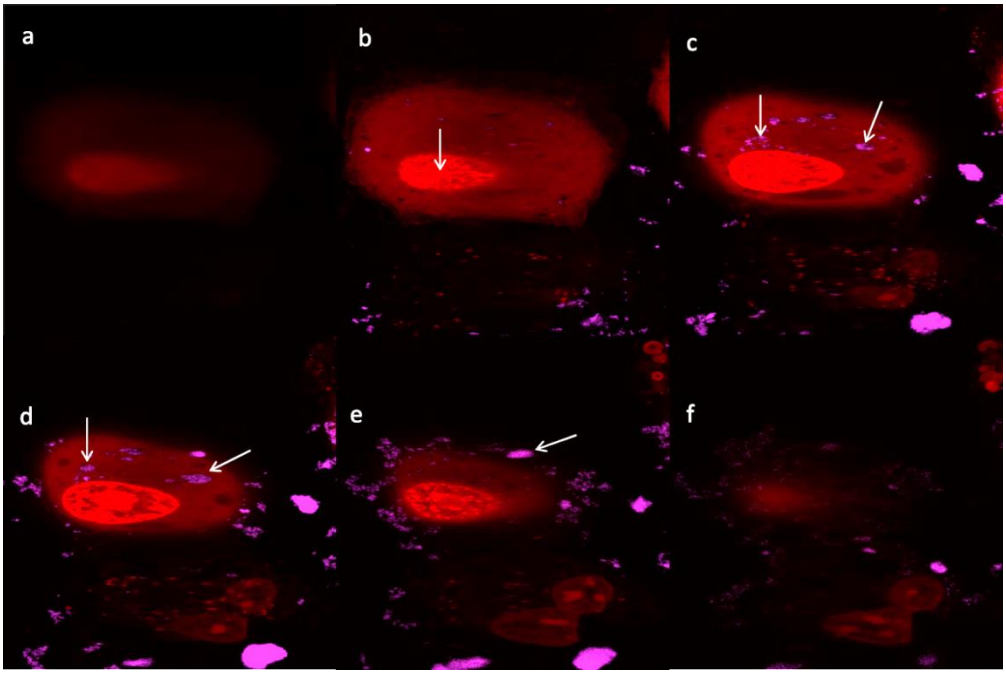

Figure 52: Z-stack confocal merged images of A549 cells incubated with 58 at 75 µg/mL for 1h. Pink – Particles **58,** λ_{ex} = 633 nm, λ_{em} = 651-704 nm. Red -Syto 82, λ_{ex} = 543 nm, λ_{em} = 576-619 nm. 38 image slices taken penetrating through the cell. Cell centre located at image 11 a) Z-stack image 2/38, no NIR-NP detection b) Z-stack image 5\38 arrow highlights nucleus, little NIR-NP detection c) Z-stack image 8\38, arrow shows emergence of NIR-NP's within the cell, d) Z-stack image 11\38, arrow shows localisation of NIR-NP's within the cell, e) Z-stack image 17\38, arrow shows localisation of NIR-NP's outside the cell, f) Z-stack image 24\38.

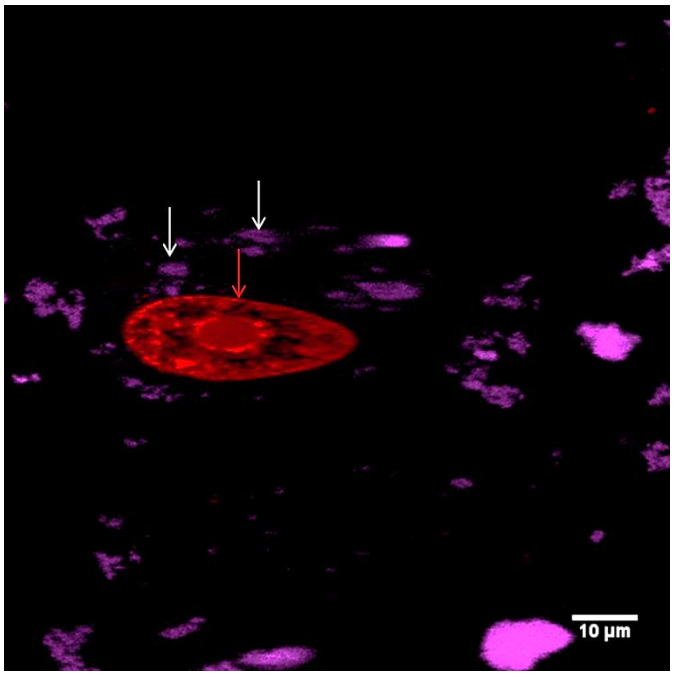

Figure 53: Zoom of Z-stack slice image 12/38 of A549 cells incubated with 58 at 75 µg/mL for 1 h. Pink – Particles **58,** λ_{ex} = 633 nm, λ_{em} = 651-704 nm. Red -Syto 82, λ_{ex} = 543 nm, λ_{em} = 576-619 nm. Red arrow shows nucleus, white arrows show fluorescent microspheres located inside the cell.

The NIR particles were visualised inside the cell and were not observed to penetrate the nucleus. Analysis of the Z-stack images confirmed cellular uptake and revealed attachment to the cellular membrane and aggregation of particles outside the cell. Aggregation of these particles may result in lower fluorescent intensity and therefore, the optimum concentration should be determined to limit this aggregation.

3.5 Functionalised Particles

3.5.1 Aim

Functionalisation of polymer particles is an effective tool to develop optical imaging probes. The ability to attach both a reporter molecule to track the particle, and a cargo moiety to be delivered can be difficult, however, polymer particles with orthogonal reactive functional groups at the particles surface may overcome this.

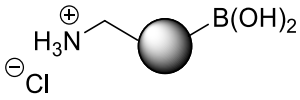

Figure 54: Targeted dual functionalised microspheres for attachment of cyanine dyes and cargos.

Orthogonal reactive groups allow the controlled addition of two individual components to a particle surface. Synthesis of a NIR fluorophore with a free carboxylic acid moiety would allow particle attachment with further orthogonal functionalization of the particle through a Suzuki-Miyaura coupling reaction allows a secondary cargo moiety to be attached. Development of a polymer particle for cellular uptake and a *turn on* fluorescent signal on activation was attempted by dual functionalization of the particles with cyanine **60** and quenched fluorescein.

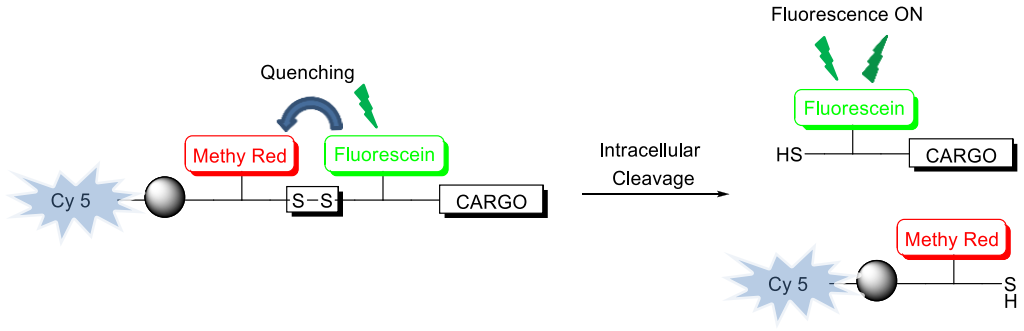

Figure 55: Hypothetical cellular delivery probe undergoing intracellular cleavage to release cargo and fluorescein moieties. Cyanine dye allows tracking of particle within cell at all times. Intracellular cleavage results in removal of fluorescence quenching and a "*turn on*" signal of fluorescein.

3.5.2 Solid-Phase Synthesis of Cyanine

3.5.2.1 Synthesis of Starting Materials

The synthesis of cyanine 3 and 5 dyes with free carboxylic acid moieties were attempted.

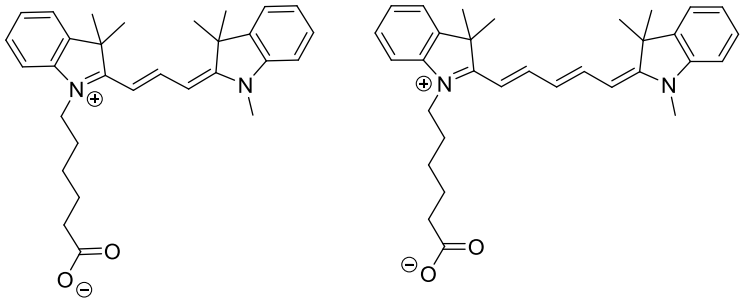

Cyanine 3 **59** Cyanine 5 **60**

Figure 56: Targeted cyanine dyes.

The initial synthetic steps were the same for both cyanine 3 and cyanine 5 and involved the preparation of N-*tert*-butoxycarbonyl protected 4-aminophenol (**61**) (Scheme 46).

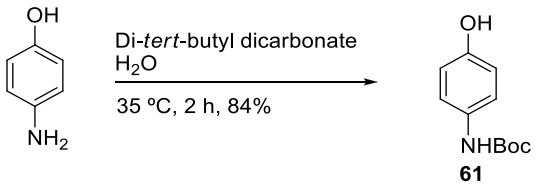

Scheme 46: Amine protection with Boc-anhydride.

Specific amine protection was achieved by using di-*tert*-butyl dicarbonate (Boc-anhydride), following the procedure by Chankeshwara *et al*[186] with the pure product precipitating.

To perform solid-phase synthesis, 1% divinyl benzene (DVB) cross-linked chloromethyl polystyrene resin (Merrifield resin, 2.0 mmol g^{-1}) was reacted with the protected amino phenol **61** (Scheme 47) while following the reaction using a colorimetric test[187].

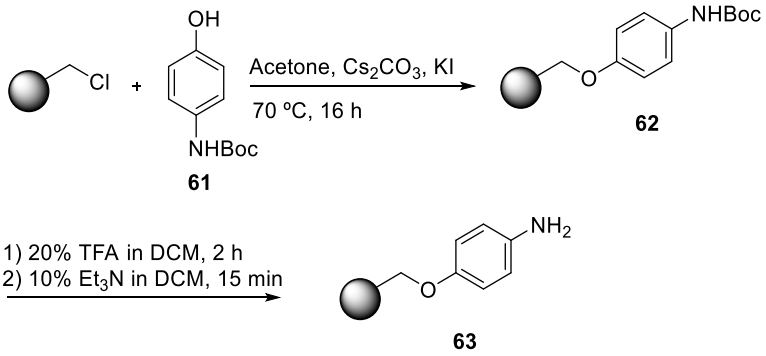

Scheme 47: Attachment of 61 and deprotection of the Boc group.

Boc deprotection of **62** in 20% TFA in DCM gave aniline **63** allowing dye synthesis to begin (Scheme 47).

3.5.2.2 Cyanine 3 Synthesis

The synthesis of cyanine 3 requires a three carbon polymethine chain and thus triethylorthoformate was selected for the synthesis of ethyl

4-hydroxyphenylimidoformate polystyrene (PS) (**64**) and 2-[(E)-2-(4-hydroxyanilino)ethenyl]-1,3,3-trimethyl-3*H*-indolium iodide PS (**65**) (Scheme 48).

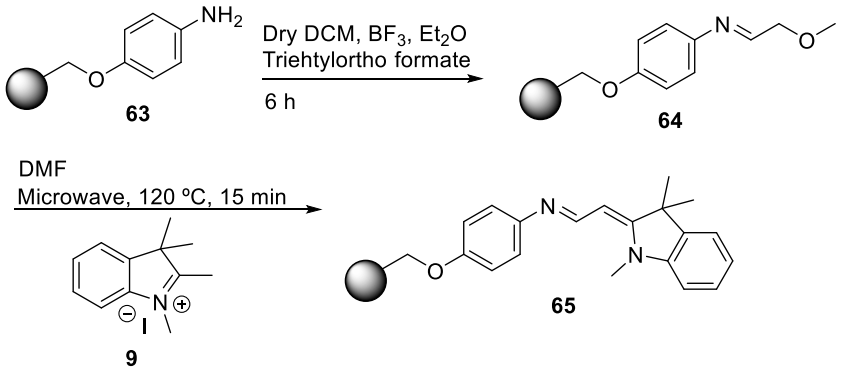

Scheme 48: Synthesis of ethyl 4-hydroxyphenylimidoformate PS.

Extensive washing was essential to remove any residual 1,2,3,3-tetramethyl-3*H*-indolium iodide (**9**) still present.

The final step of the reaction involved simultaneous cleavage of the dye and addition of the carboxypentyl carboxylic acid functionalised indole (Scheme 49).

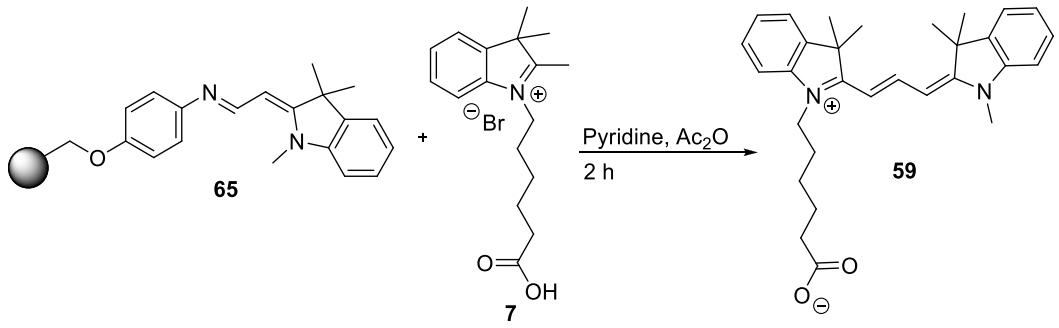

Scheme 49: Synthesis of cyanine 3.

Evaporation of the solvent and purification of the pink solid by column chromatography (a slow gradient of methanol in DCM) gave the pure product **59**. The column did suffer from some difficulties owing to the fact that the pure dye appeared to elute twice at different levels of polar solvent, most likely caused by the

carboxylic acid in the acid or carboxylate form. The symmetrical hemicyanine dye was also synthesised (Figure 57), however, due to its apolar nature, it was eluted before the un-symmetrical cyanine 3 (**59**). Although most of the product eluted at 15% MeOH in DCM, increasing the solvent polarity to 20% MeOH ensured maximum dye recovery. Dye synthesis was confirmed using proton and carbon NMR spectroscopy, specifically observing the presence of the aliphatic carbons on the carboxypentyl acid chain. The cyanine 3 molecule had a maximum absorption of 547 nm and a maximum emission of 570 nm in MeOH.

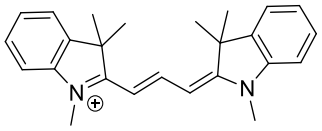

Figure 57: Undesired symmetrical cyanine dye.

3.5.2.3 Cyanine 5 Synthesis

The addition of the polymethine chain to obtain a chain length of 5 carbons was carried out using tetramethoxy propane (Scheme 50).

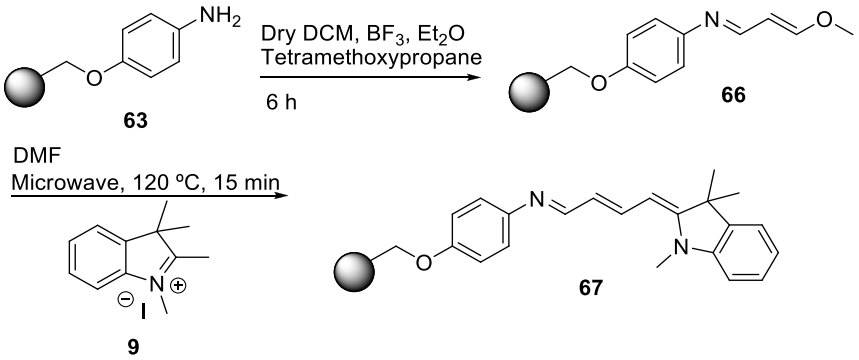

Scheme 50: Synthesis of 4-[(E,2E)-3-methoxy-2-propenylidene]amino}phenol PS.

Once again, extensive washing of the resin with DCM and MeOH was essential to reduce formation of the symmetrical dye. The final step of the reaction involved simultaneous cleavage of the dye and addition of the carboxypentyl carboxylic acid functionalised indole (Scheme 51).

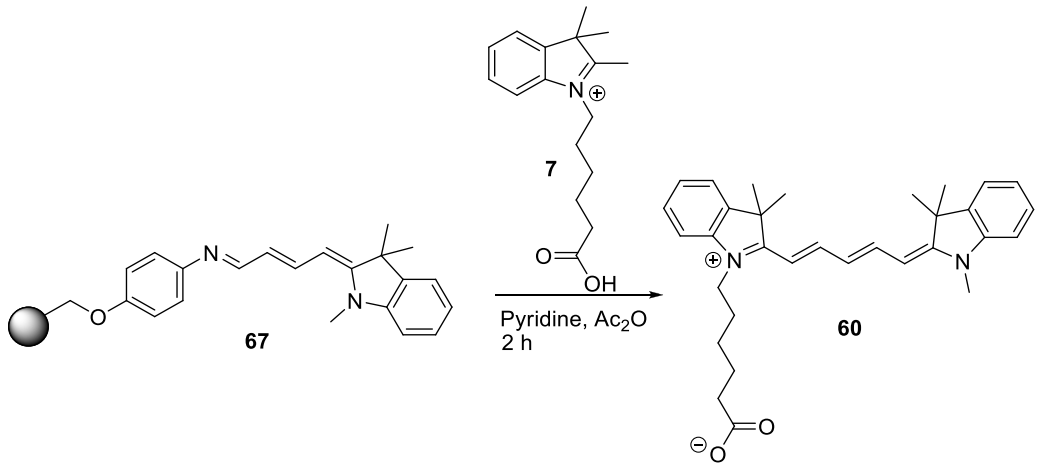

Scheme 51: Synthesis of cyanine 5.

The dark blue solid (**60**) was purified by column chromatography in a similar manner to cyanine 3, with only small quantities of the symmetrical by-product formed (Figure 58). The cyanine 5 molecule had a maximum absorption of 640 nm and a maximum emission of 665 nm in MeOH.

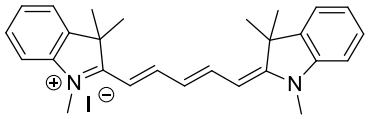

Figure 58: Undesired symmetrical cyanine 5 dye.

Although the unwanted symmetrical by-product was obtained, it was easy to separate, and has been shown to have uses in the detection of reactive oxygen species (ROS)[188].

As cyanine 5 dye has higher absorption and emission wavelength than cyanine 3 it is less affected by the auto-fluorescence of biological tissue and was therefore was attached to the polymeric particles for tracking within cells.

3.5.3 Synthesis of Functionalised Polymer Particles

In order to obtain amino-boronic acid particles of the required size (~200 nm), the particles were synthesised as discussed previously (Chapter 3 Section 3.4.2) by an emulsifier-free emulsion polymerisation[189] The addition of *para*-vinylbenzyl boronic acid (VBA) to the synthesis (Scheme 52) allowed for the synthesis of dual amino and boronic acid functionalised nanoparticles.

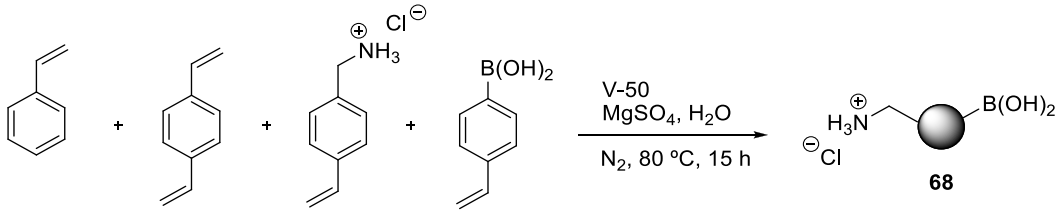

Scheme 52: Synthesis of dual functionalised nanoparticles.

The emulsifier free synthesis was attempted using styrene, DVB (3%), VBAH (3%) and VBA (3%) in water using the water soluble initiator V-50. These conditions gave particles **68** with an average hydrodynamic diameter of 230 nm and a PDI of 0.071. Increasing levels of VBA to 6 and 9 % resulted in increasing PDI's. This may be because of the acid-base interactions between VBAH and VBA disturbed VBAH-mediated micelle formation during polymerisation[169]. To measure the functionalization level of the particles, a ninhydrin test[190] was used to determine amine loading. To quantify the boronic acid loading, inductively coupled plasma – optical emission spectroscopy (ICP-OES[191]) was employed. Particles **68** exhibited an amine loading of 129 ± 15 µmol g^{-1} and boronic acid loading of 62 ± 1 µmol g^{-1}. After, the efficiency of the Pd-mediated cross-coupling reaction to an aryl halide was tested.

3.5.4 Palladium Mediated Suzuki-Miyaura Cross-Coupling

Palladium mediated cross-coupling on to the boronic acid functionalised particles **68** was attempted using 5-iodo fluorescein and different Pd salts under physiological

conditions (Scheme 53 and Table 5)[192]. Introduction of a fluorescent molecule to the particle surface allowed monitoring of the coupling reaction using flow cytometry and ICP-OES to monitor the decreasing boron content.

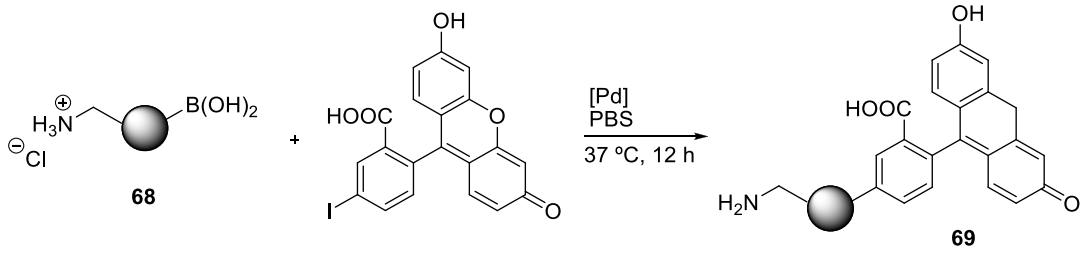

Scheme 53: Pd mediated particle conjugation.

Run	Catalyst/Conditions	Yield (%)
1	$PPh_3/Pd(OAc)_2$/PBS/37 ºC/24h	26
2	$Pd(dppf)Cl_2/Pd(OAc)_2$/PBS/37 ºC/24h	22
3	$Pd(OAc)_2/PPh_3/K_2CO_3$/ PBS/37 ºC/24h	24
4	$Pd(OAc)_2/PPh_3/Cs_2CO_3$/ PBS/37 ºC/24h	17
5	$Pd(OAc)_2$/*o*-Tol_3P/K_2CO_3/ PBS/37 ºC/24h	15
6	$Pd(PPh_3)_4/K_2CO_3$/ Glutathione/PBS/37 ºC/24h	24
7	$Pd(PPh_3)_4/K_2CO_3$/ PBS/microwave/60 °C/1h	23
8	$Pd(OAc)_2$/NaADHP/PBS/37 ºC/12h	38 ± 4 (n=3)

Table 5: Palladium mediated coupling conditions (Pd, 5 % with respect to iodo-fluorescein).

The coupling reaction was carried out using an excess of 5-iodofluorescin (40 µM, 50 eq) and a palladium catalyst concentration of 5% with respect to iodo-fluorescein. Analysis of the boron content of the fluorescein labelled particles showed the optimum reaction conditions were 37 °C using the water soluble catalyst complex ~2-amino-4,6-dihydroxypyrimidine-$Pd(OAC)_2$ in PBS (entry 8 in Table 5, compound **69**). ICP-OES analysis of the particles revealed a 40% reduction in boron content with flow cytometry showing a 500-fold increase in fluorescence compared to the initial dual functionalised particles. Control reactions carried out using

non-iodinated fluorescein and no catalyst showed no reaction took place as expected. The low reduction in boron content (40% reduction) was attributed to the boronic acid groups residing throughout the particles and as the surface moieties react, the internal boronic acid functionalities become less accessible[193].

3.5.5 Probe Synthesis

A molecule containing a disulphide linkage, iodo-fluorescein and a fluorescence quencher[194] (methyl red) that could be attached to the particle *via* the Pd mediated coupling as described above (Figure 55 and Scheme 54) was synthesised by Dr Frank Thielbeer. Reduction and cleavage of the disulphide linkage by reducing agents such as glutathione[195] results in release of the fluorescein-cargo moiety from the quencher, allowing the emission of fluorescein to be detected. A non-cleavable hydrocarbon chain was also used in place of the disulphide bridge to act as a control.

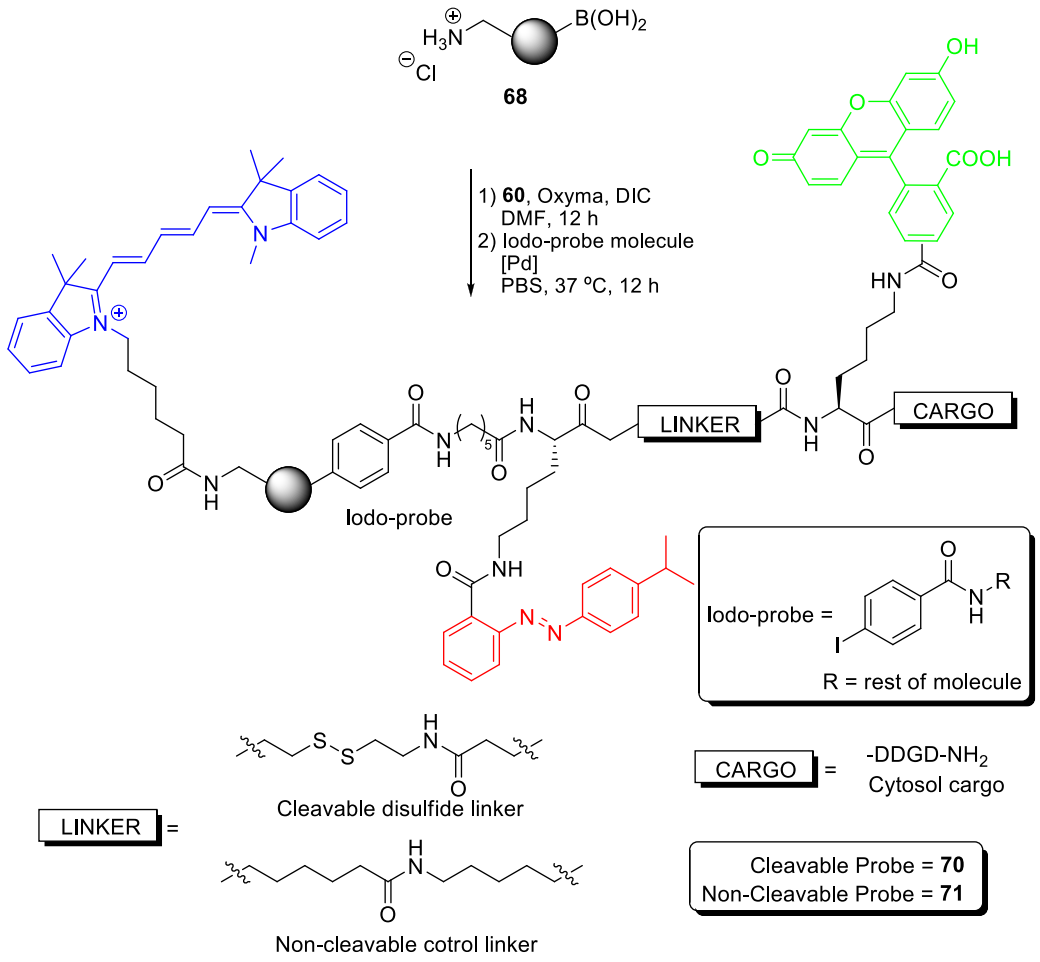

Scheme 54: Synthesis of dual functionalised particles. Cyanine **60** (blue), methyl red quencher (red), fluorescein (green). Quenched fluorescein section of probe courtesy of Dr Frank Thielbeer.

The particle was prepared by coupling cyanine **60** using ethyl 2-cyano-2-(hydroxyimino)acetate (Oxyma) and *N*,*N*-diisopropylcarbodiimide (DIC) in DMF. The iodo-fluorescein molecule was attached using Pd mediated chemistry as described above. To confirm coupling of the large molecule, ICP-OES was carried out, revealing a 23% drop in boron content. The cargo molecule was a short anionic peptide (DDGD-NH_2) to ensure the fluorescein would remain within the cell due to the negative charge of the cell membrane.

3.5.6 *In Vitro* Analysis of Dual Functionalised Particles

To determine cellular uptake, the particles were incubated with HEK293T and HeLa cells and the uptake monitored by flow cytometry detecting the cyanine **60**. Figure 59 confirms the ability of the disulphide linked probe particles and non-cleavable control particles to be taken up by cells.

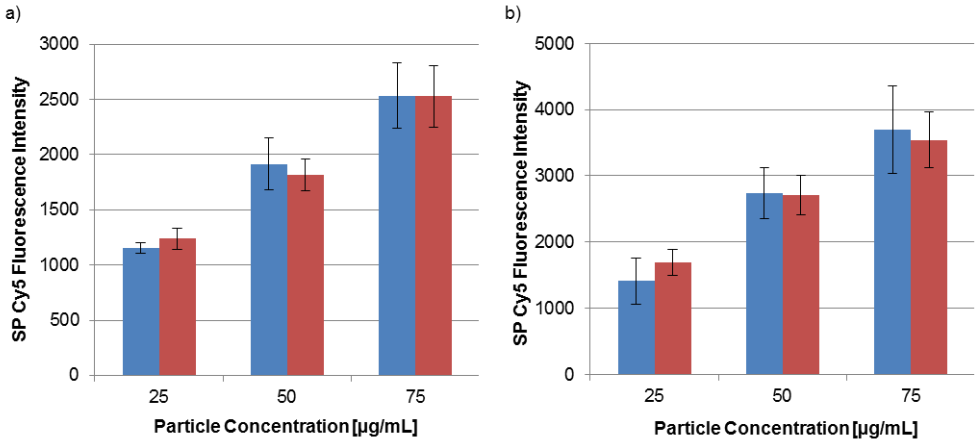

Figure 59: Cyanine 60 fluorescence intensity of a) HEK293T and b) HeLa cells following uptake of dual functionalised particles with cytosol cargo. Disulfide-linked cleavable probe (**70**, red), non-cleavable control particles (**71**, blue). Data courtesy of Dr Frank Thielbeer.

To determine the localisation of the probe, and confirm tracking of the nanoparticles with cyanine **60**, HEK293T cells were incubated with **70** and **71** for 48 hours and imaged using confocal microscopy. The nuclei and cytoplasm of HEK293T cells were stained with Hoechst 33342 and cell-tracker red.

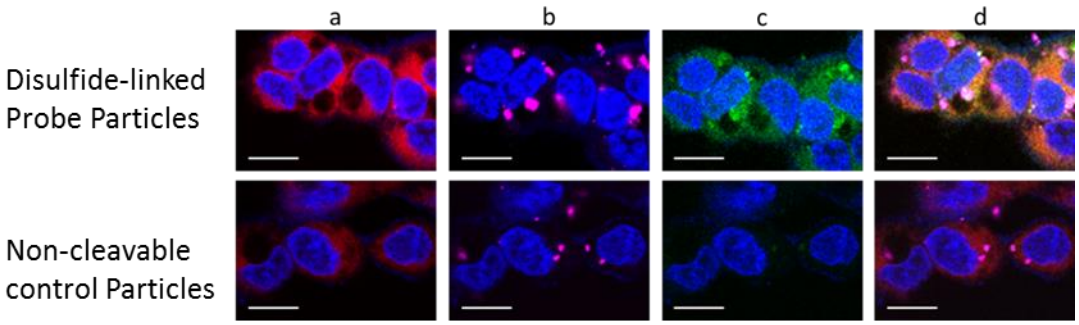

Figure 60: Confocal microscopy images of HEK293T cells following incubation with cytosol targeted disulphide linked cleavable probe 70 (50 mg mL^{-1}) and non-cleavable control 71 (50 mg mL^{-1}). a) nuclei stain Hoechst 33342 (blue, λ_{ex} = 404 nm, λ_{em} = 535-590 nm), cytoplasm stain cell tracker red CMTPX (red, λ_{ex} = 594 nm, λ_{em} = 575-615 nm); b) nucleus stain (blue), and particles labelled with cyanine **60** (pink, λ_{ex} = 633 nm, λ_{em} = 650-710 nm); c) nucleus stain (blue) and released fluorescein (green, λ_{ex} = 488 nm, λ_{em} = 480-520 nm); d) merged image. Scale bar: 50 µm Data courtesy of Dr Frank Thielbeer.

The images verified linker cleavage and cytosol localisation of the disulphide cleavable probe. The ability to track both the nanoparticle (cyanine **60** excitation - λ_{ex} 633 nm) and the cargo moiety (fluorescein - λ_{ex} 488 nm) was successful (Figure 60). As the cargo moiety was an anionic peptide, both segments of the probe remained in the cytoplasm. Additionally, the non-cleavable control particles showed only the microsphere (cyanine dye) fluorescence and confirmed that the fluorescein remained quenched.

3.6 Conclusion

A synthesis of NIR microspheres was developed and the beads characterised. *In vitro* experiments showed that the particles were non-toxic while confocal microscopy images, including z-stacking, confirmed cellular uptake and localisation within the cytoplasm, with no nuclear penetration observed. The particles were also found to aggregate, with binding to the cell membrane detected. The amine groups present on the surface of the microspheres allows for further derivitisation, with opportunities to track intra-cellular processes or help in the design of delivery vehicles. Addition of further functionalities may also be achieved by increasing the number of polymerisable starting materials, such as *para*-vinylbenzyl boronic acid to introduce a boronic acid group, suitable for Suzuki-Miyaura cross coupling. Currently, collaborators are working on the functionalisation of these beads with different chargd moieties to determine the effect on cellular uptake.

These studies also reported the successful synthesis of dual functionalised nanoparticles. Cyanine **60** was synthesised and attached to the microspheres through carbodiimide chemistry while dual functionalisation was achieved through the addition of a fluorescent reporting cargo moiety using a water soluble, optimised, Suzuki-Miyaura cross-coupling reaction. The quenched probe molecule could be taken up by cells while cleavage of the disulphide linker resulted in the removal of quenching. Non-cleavable control particles did not exhibit fluorescein fluorescence after cellular uptake. Tracking of the particles using cyanine 5 and the cargo moiety was carried out using confocal microscopy. This study provided the first example of employing a bio-orthogonal approach to dual functionalization of particles resulting in monitoring and controlled release within the cytoplasm. A cyanine 3 molecule (**59**) was also developed and could be used in a similar manner if the wavelengths are more preferable for the application.

Chapter 4

Development of a Sensor for Gram Negative Bacteria

4.1 Bacteria Introduction

Bacteria are unicellular micro-organisms which lack a membrane bound nucleus. Most commonly described as prokaryotes (Figure 61), bacteria can vary in size from the micro bacteria family of *thermodiscus* at 0.2 µm in diameter to the gigantobacteria of *thiomargarita namibiensis* which can reach a diameter of 750 µm[196]. Although these are immense size differences, in general the prokaryotic cell structure is much simpler than mammalian cells[197].

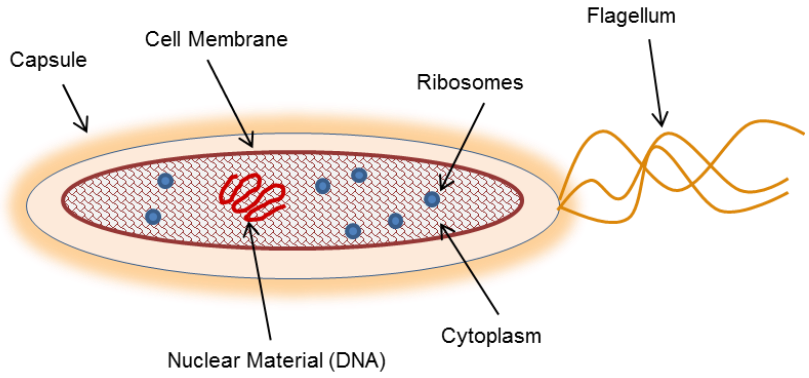

Figure 61: Cartoon representation of prokaryotic cell.

Although bacteria can be characterised by their morphology, for example rod, spherical or spiral, characterisation of bacteria is most commonly discussed by the cell wall structure present. First described by Gram in 1884 while developing a colorimetric test based on crystal violet[198], bacteria can be largely separated into

either a Gram positive or Gram negative status, although there are some notable exceptions, e.g. mycobacterium[199].

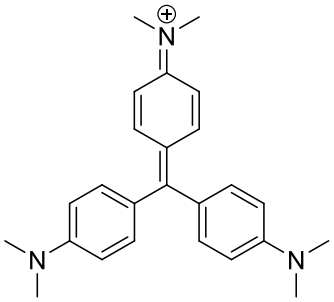

Figure 62: Crystal violet structure.

Gram positive bacteria, have a thick peptidoglycan cell wall which mainly consists of glycan strands which are cross-linked by alternating *N*-acetylglucosamine and *N*-acetymuramic acid sugar subunits linked together by covalent bonds[197]. This wall can retain crystal violet, staining the bacteria purple. Gram negative bacteria have the same cell wall, however, it is much thinner and therefore does not retain the stain as effectively, staining the bacteria pink[200]. Gram negative bacteria do however have an outer cell membrane containing phospholipids and lipopolysaccharides (LPS). This outer layer functions as an exclusion barrier, hindering the passage of large (> 600 Daltons) materials into the bacteria. This in turn results in increased resistance to antibiotics (Figure 63)[197].

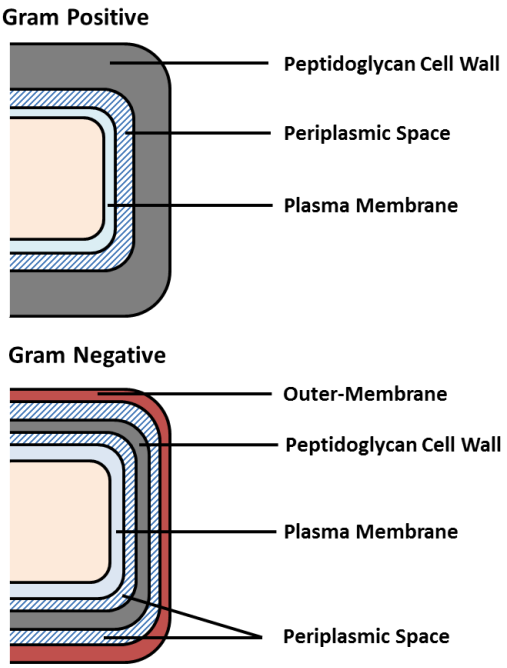

Figure 63: Structures of Gram positive and Gram negative bacterial cell wall.

Although the Gram stain test is popular, it can give false positives or negatives, can be time consuming and due to being a colorimetric test, can have low sensitivity[201]. Another issue is the occurrence of false negatives due to some Gram positive bacteria decolouring[202]. Additionally, Edlich suggested that various factors may cause a false decolourisation, these include the amount and mode of fixation of the sample[203]. For this reason other tests have been developed. For example, Gregerson[204] developed a KOH test to distinguish between Gram positive and Gram negative bacteria. This protocol requires the use of 3% KOH in order to dissolve the thin cell wall of Gram negative bacteria, resulting in a visible change in viscosity of the test solution. Gram positive bacteria are un-affected as 3% KOH cannot rupture the thicker cell wall. Although this seems reasonable, some studies have found discrepancies between the KOH and the Gram stain test[202, 205]. Cerny[206] developed a colorimetric test using the presence of aminopeptidases in the LPS membrane of Gram negative bacteria (Scheme 55).

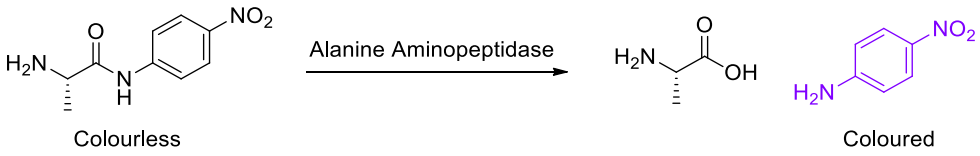

Scheme 55: Colorimetric detection of alanine-aminopeptidase.

This probe takes advantage of the cleavage of amide bonds by proteases, in this case, alanine aminopeptidase. L-alanine 4-nitroanalide is weakly coloured but hydrolysis of the amide results in the highly coloured 4-nitroalanine molecule[207].

Specific detection of bacterial infections in real time is lacking and it would be of great use to clinicians to accurately diagnose patient infections and personalise treatment. Diagnosis of respiratory problems such as lung infections most commonly require a bronchoalveolar lavage followed by colorimetric culture tests like those described above to determine the type of bacterial infection[208]. Advancing technologies in the field of imaging has led to development of a micro-endoscope which allows real time fluorescence imaging of the lungs[209]. Utilising this technology, development of a bed side imaging probe to specifically detect Gram negative bacteria *in vivo* to aid in the diagnosis of bacterial infections would be of great use[210].

4.1.1 Aminopeptidases

Aminopeptidases are enzymes that catalyse the cleavage of amino acids from the amino terminus of proteins and peptides. Although there are many different aminopeptidase enzymes, the periplasmic alanine aminopeptidase has received the most attention[207]. Most aminopeptidases are metalloproteinases and require one or two Zn^{2+} or Co^{2+} ions at the active site. Aminopeptidases are found throughout the cell, including in organelles such as the mitochondria[211] and can even be membrane bound[212]. Despite the differences in location and structure, all aminopeptidases are inhibited by bestatin[213].

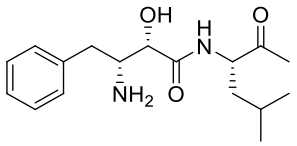

Figure 64: Bestatin.

Aminopeptidases are found in the cell membrane of Gram negative bacteria and are therefore a good target for developing simple and fast methods of detecting specific bacteria. During this work, the Cerny method has been adapted by others to generate more sensitive fluorescent sensor[214]. However, this research does not discuss live bacterial assays.

4.2 Chapter Aims

The ability to detect the presence of Gram negative bacteria in a specific and fast manner would be of great benefit to the medical community. Fluorescent imaging is a highly sensitive technique which can be used in real-time to provide a *turn on* response to a given target. This chapter aims to synthesise a coumarin based aminopeptidase probe, specific for Gram negative bacteria.

4.3 Results and Discussion

4.3.1 Synthesis of Aminopeptidase Probe

The first step in the synthesis of the coumarin based aminopeptidase probe was the high yielding carbamate formation between 3-aminophenol and ethyl chloroformate in ethyl acetate. This was followed by the Pechman reaction between carbamate **72** and diethyl acetyl succinate in 70% H_2SO_4. On reaction completion, addition of ice water caused the crude product to precipitate to give compound **73**. The next two steps were the hydrolysis of the ester with LiOH in water/ethanol under reflux, followed by hydrolysis of the carbamate with 10 M NaOH while also heating to reflux. After cooling and acidifying with 2 M H_2SO_4, the pure product (**74**)

precipitated in good yield. Temporary protection of the aniline was carried out using Fmoc-OSu. This reaction required the use of TMS-Cl (to temporarily protect thte carboxylic acid), followed by cooling and addition of Fmoc-OSu. Initially low yielding, this step was optimised by distillation of TMS-Cl prior to the reaction reducing the possible side reaction, giving quantitative yields (**75**) (Scheme 56).

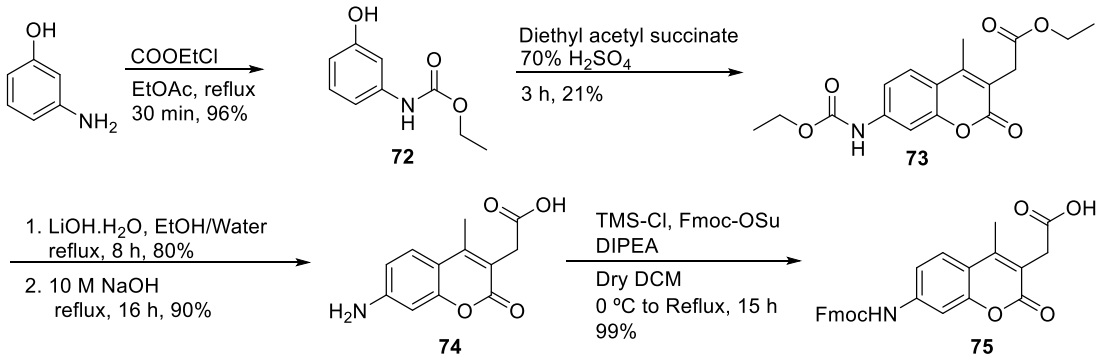

Scheme 56: Synthesis of Fmoc-Coum (76) with free carboxylic acid moiety.

To allow for the addition of the amino acid using solid phase techniques a polystyrene aminomethyl resin was chosen as the solid support due to ease of handling and low cost. Fmoc-Rink linker was first attached to the resin to allow for simple cleavage of the product on completion of the synthesis. Pre-swelling of the resin in DCM was required and the coupling was carried out using Oxyma and DIC to give compound **76** with qualitative measurement of the coupling efficiency monitored using the Kaiser Test[215]. After Fmoc deprotection of the solid supported coumarin (20% piperidine in DMF), Oxyma and DIC were again used to couple Fmoc-Ala-OH, however, the Kaiser test revealed that the coupling was inefficient which could be attributed to the low reactivity of the amine moiety. Following the recommendation by Ellman[216], (Dimethylamino)-*N*,*N*-dimethyl(3*H*-[1,2,3]triazolo[4,5-*b*]pyridin-3-yloxy)methaniminium hexafluorophosphate (HATU) with DIPEA was selected as the coupling reagent and proved successful to yield final compound **77** (Scheme 57).

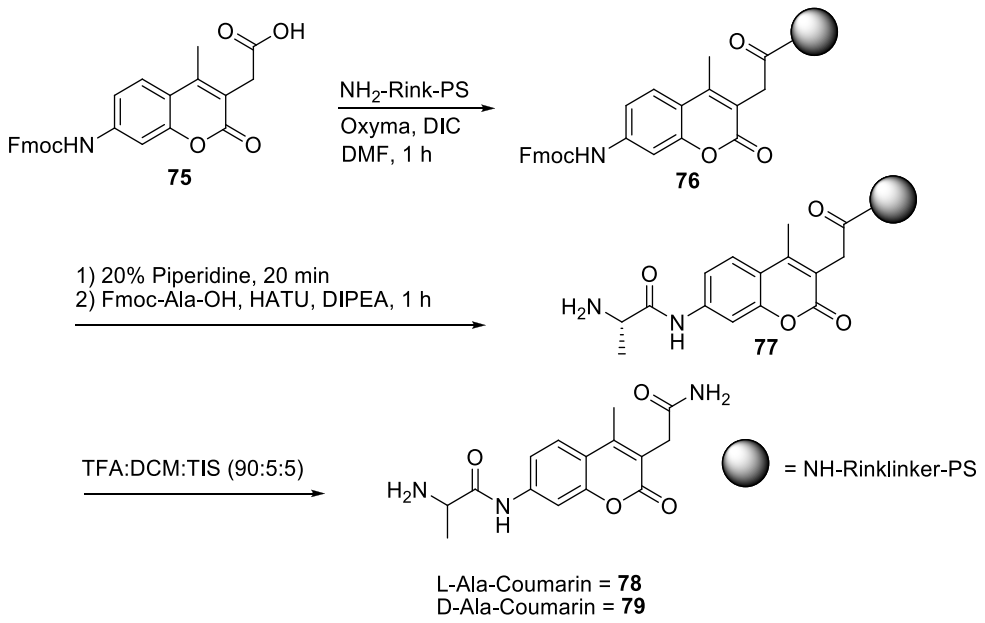

Scheme 57:Synthesis of aminopeptidase probe 78 and control probe 79.

The aminopeptidase probe **78** was cleaved from the resin using TFA:DCM:TIS (90:5:5) and purified by preparative HPLC. Synthesis of the D-Ala-Coumarin derivative **79** was carried out in the same manner using Fmoc-D-Ala-OH.

4.3.2 Absorption and Emission Properties

The absorption and emission properties of the coumarin, **78**, over the amino acid free coumarin **74** were analysed. Absorption wavelengths were similar at 312 nm and 322 nm for **72** and **78** respectively.

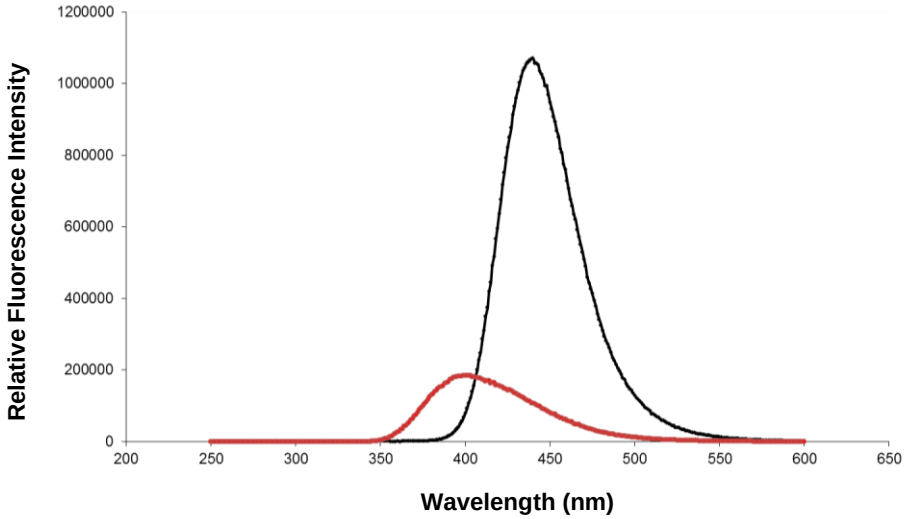

Figure 65: Fluorescence spectra of 74 (black, λ_{ex} = 312 nm) and 78 (red, λ_{ex} = 322 nm) in water at equivalent concentrations.

Figure **65** shows that upon addition of alanine to the coumarin, the fluorescence maxima is again only slightly shifted, however, as expected, the fluorescence was greatly reduced to approximately one fifth of the intensity.

4.3.3 Solvent Effects

As this project aimed to carry out biological studies of this probe, it was important to ascertain solvent effects on the fluorescence intensity of the coumarin probe. The phenomenon of solvatochromic effects is explained by the fact that a change in solvent can represent a change in polarity and dielectric constant. As explained by the Jablonkski diagram (Chapter 1, Figure 11), the fluorescence of a molecule is dependent on the ground and excited electronic states, which are altered by the presence of differing solvents[217].

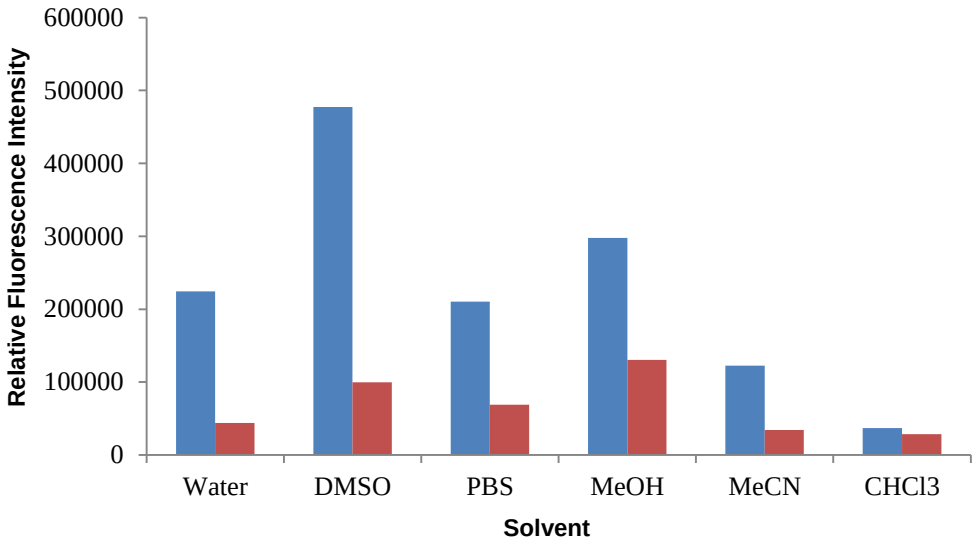

Figure 66: Solvent effects on fluorescence of 74 (blue, λ_{ex} = 400 nm) and 78 (red, λ_{ex} = 350 nm) at 165 µM.

Figure 66 shows the differing fluorescence intensities in 6 solvents of varying polarities. It is interesting to note that although DMSO and MeCN have similar polarities, their fluorescence maxima are extremely different. This may be due to the increased solubility of the coumarin molecule in DMSO. Compound **78** was only soluble in water after sonication and may account for the low but acceptable fluorescent intensity.

4.3.4 Bacterial Studies

Previous studies by Minyong[214a] report a *turn on* fluorescent coumarin based probe for aminopeptidase, however, they do not distinguish between Gram negative and Gram positive bacteria and rely on the presence of the aminopeptidase enzyme directly.

Before extensive bacterial studies were carried out, the *turn on* capabilities of **78** were investigated. For the fluorescence studies an excitation wavelength of 400 nm was selected to give optimum emission of the cleaved coumarin molecule. As the probe was expected to be selective for Gram negative bacteria, *Escherichia coli* was

selected for preliminary studies. The bacteria were sub-cultured and re-suspended in a hypo-tonic buffer to cause osmotic shock releasing periplasmic proteins such as aminopeptidase[218]. Probe **78** was then incubated with the bacteria at 37 ºC for 1 hour at varying concentrations.

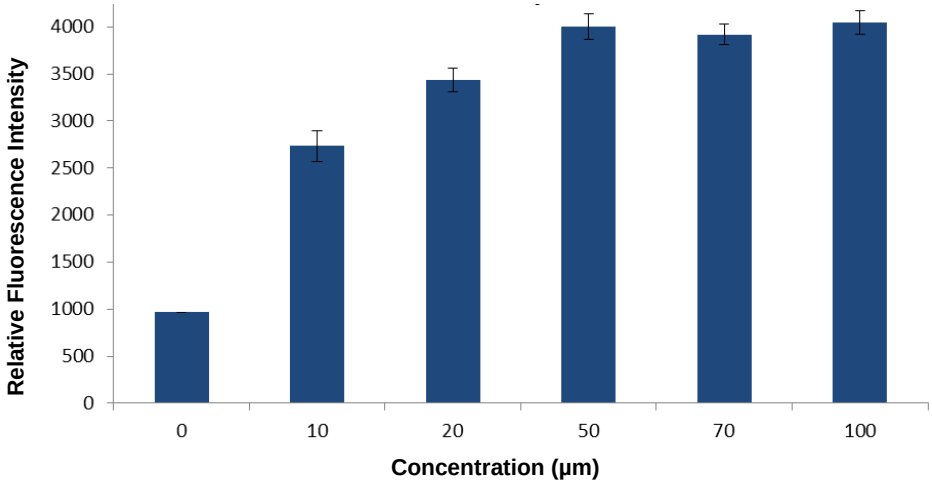

Figure 67: Concentration dependence of 78 with *Escherichia coli*. λ_{ex} = 400 nm.

From this study, it was found that 50 µM of probe **78** generated the maximum fluorescence increase over time. Furthermore, probe **78** shows an limit of detection below 20 µM which makes it the most sensitive aminopeptidase probe reported[214a, 214c].

To investigate the specific cleavage of **78**, six bacterial strains were selected, three Gram positive: *Staphylococcus aureus*, *Staphylococcus epidermis*, and *Enterococcus* and three Gram negative: *Escherichia coli*, *Pseudomonas aeruginosa* and *Klepsiella pneumonia*. To monitor the different effects of Gram negative and Gram positive bacteria, 50 µM of probe was incubated with 10 billion bacteria (OD = 1) of each bacterial strain and left to incubate for 30 minutes at 37 °C.

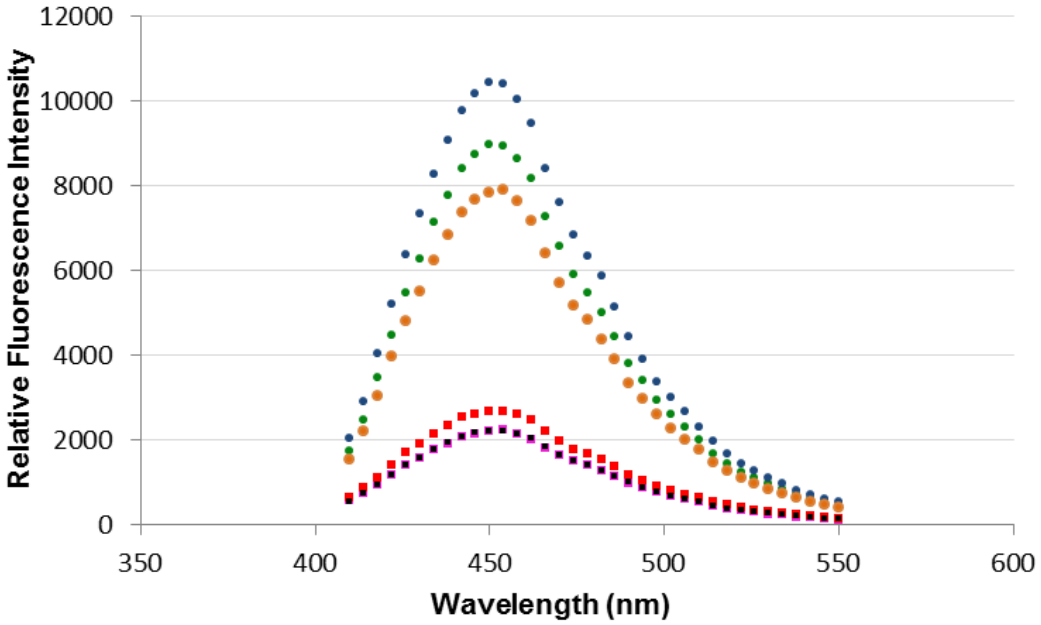

Figure 68: Cleavage of 78 (50 µM). *pseudomonas aeruginosa* (blue), *Escherichia coli* (green), *Klepsiella pneumonia* (orange), *Staphylococcus aureus* (red), *Staphylococcus epidermis* (black), *Enterococcus* (pink) for 30 minutes at 37 ºC. λ_{ex} = 400 nm. Circles represent Gram negative bacteria, squares represent Gram positive bacteria. Data shown is one set of data obtained. Experiment was carried out in duplicate on 3 different days giving similar results on all occasions.

As can be seen in Figure 68 incubation of **78** with Gram negative bacteria causes a large increase in the fluorescence intensity when compared with incubation with Gram positive bacteria confirming cleavage of the amide bond. A marked fluorescence signal is detected after 30 minutes with a maximum increase after 120 minutes.

To investigate inhibitor effects and confirm that it was the aminopeptidase enzyme responsible for the fluorescence increase, the Gram negative bacteria were also pre-incubated with the inhibitor bestatin for 30 minutes prior to incubation with the **78** (Figure 69).

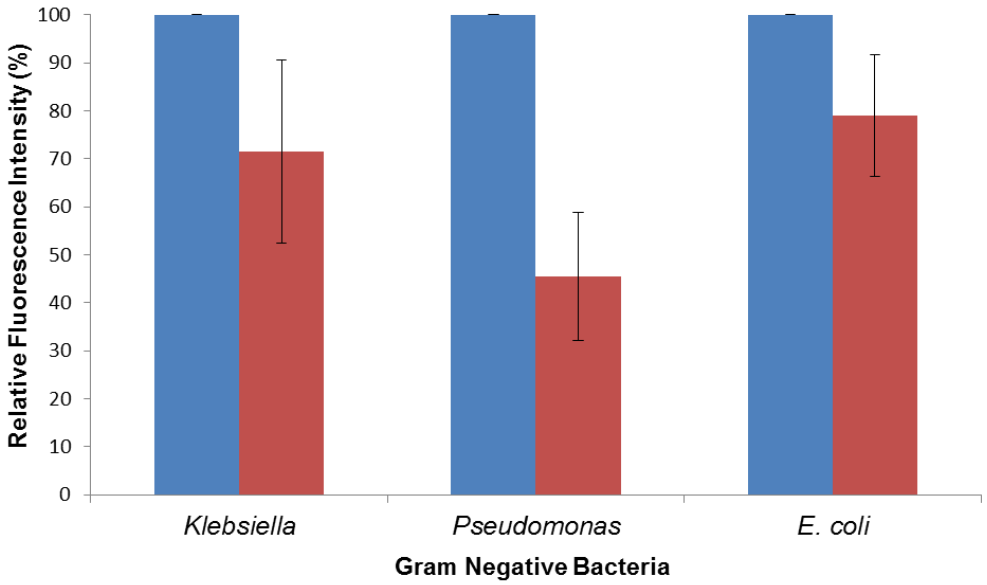

Figure 69: Probe 78 (50 µM) was incubated with Gram negative bacteria (blue), and Gram negative bacteria plus bestatin (40 nM) for 30 minutes at 37 ºC. λ_{ex} = 400 nm. Experiment carried out in duplicate on 2 different days.

On pre-incubation with bestatin there was a decrease of approximately 20-55% in fluorescence signal confirming that significant amide bond cleavage is due to the presence of aminopeptidase. As can be seen, the error values are quite large. This may be avoided in future by incubating with the recommended 60 nM concentration of bestatin.

To confirm these results, L-alanine was replaced with the D-alanine to generate control probe **79**. Control probe **79** was incubated with 3 Gram negative bacteria *Pseudomonas aeruginosa*, *Escherichia coli* and *Klepsiella pneumonia* at 50 µM at 37 °C for a longer period of 2 hours to further stress the experiment. The fluorescence intensity increase of **79** incubated with Gram negative bacteria compared to **79** without Gram negative bacteria is shown in Figure 70.

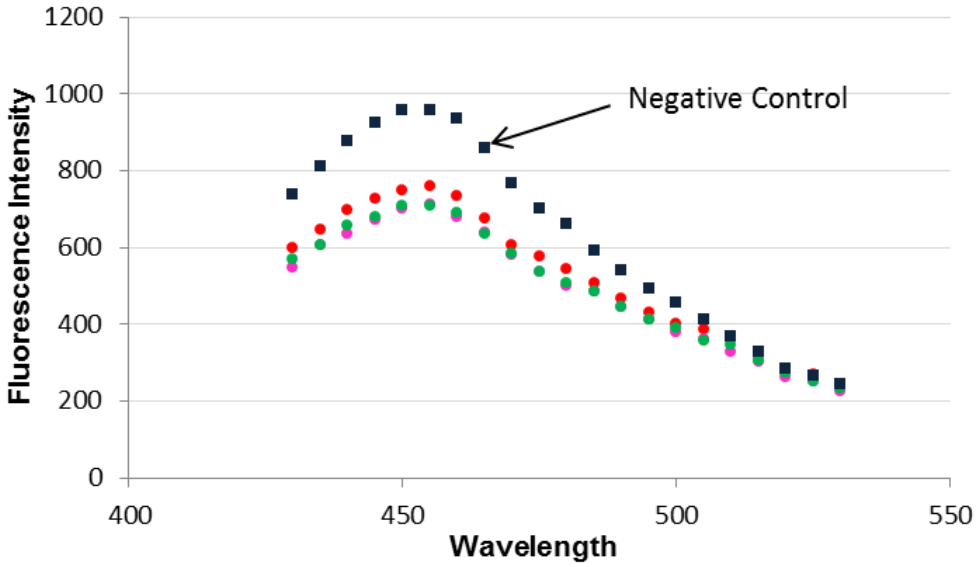

Figure 70: Effect of Gram negative bacteria on 79 (50 μM): control probe 79 only (black), *pseudomonas aeruginosa* (pink), *Escherichia coli* (red), *Klepsiella pneumonia* (green). λ_{ex} = 400 nm. One data set shown. Experiment carried out in duplicate with the same results on both occasions.

This data confirms that, as expected, cleavage of the amide bond does not occur on the control probe **79** and that the aminopeptidase enzyme is specific for the natural L amino acid.

4.3.5 Specificity of Aminopeptidase Probe

As the main target for this probe was to detect bacterial infection in the lungs, selectivity over other proteases must be achieved. During a bacterial infection the body attempts to defend itself by releasing proteases such as neutrophil elastase[219], an enzyme capable of degrading almost all extracellular matrix proteins. Even after the infection subsides an imbalance in the level of protease inhibitors within the body can cause neutrophil elastase to remain active, causing harm to the host[220]. Additionally, mammalian cells also contain enzymes that can break down or modify proteins. As our bacterial probe may be susceptible to these side processes, the specificity of probe **78** had to be determined.

To investigate, A549 epithelial cells, neutrophils and Gram negative bacteria were incubated with **78** and the fluorescence response recorded.

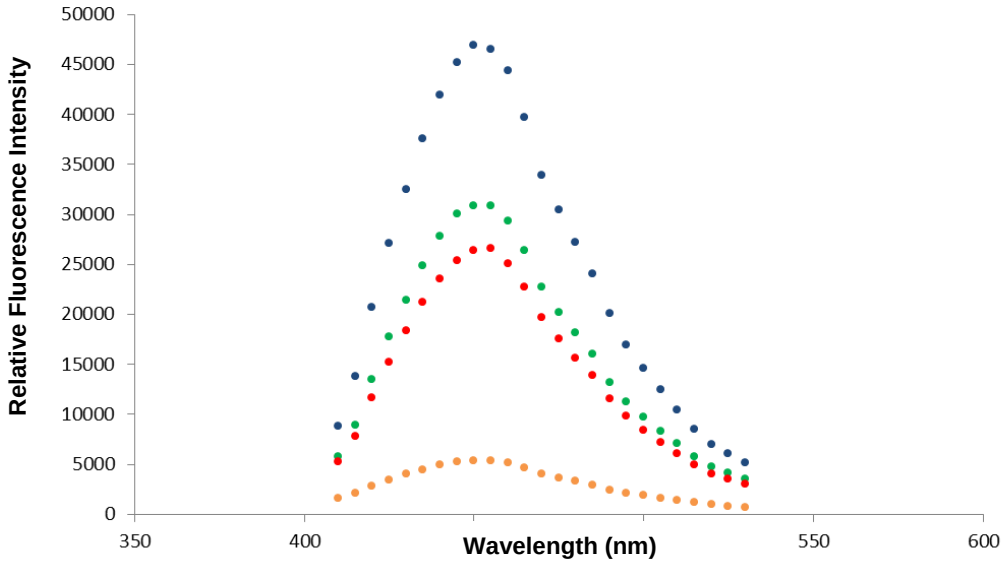

Figure 71: Incubation of 78 (50 μM) with Gram negative bacteria (green, 10 billion cells), neutrophils (blue, 100 million cells), epithelial cells (red, 100 million cells) for 30 minutes at 37 ºC. λ_{ex} = 400 nm. Probe 78 alone (orange).

Figure 71 shows the fluorescence response recorded on incubation of **78** (50 μM) for 1 hour at 37 ºC with *Escherichia coli*, neutrophils and mammalian epithelial cells. Unfortunately, the greatest fluorescence increase occurs in the presence of neutrophils. This is not surprising as neutrophils contain many proteases which could account for this high fluorescence increase.

To determine the number of neutrophils and epithelial cells required to generate a maximum response, the number of cells was varied and probe **78** (50 μM) incubated for 1 hour at 37 ºC (Figure 72).

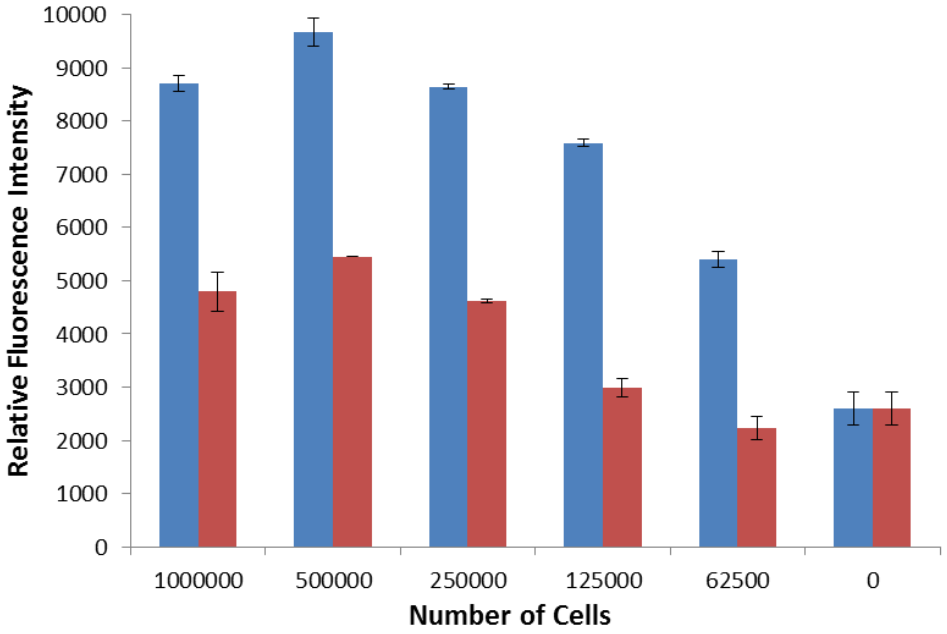

Figure 72: Fluorescence increase on incubation of (78) (50 μM) with varying numbers of neutrophils (blue) and epithelial cells (red). λ_{ex} = 400 nm. Experiment carried out in duplicate.

As expected, the cleavage by neutrophils exceeds that of epithelial cells and decreases on lowering the number of cells. In order to continue research into a bed side tool for bacterial infections, the specificity over other proteases must be improved and further work must be done to investigate the effect of neutrophils and other cells on the aminopeptidase probe *in vivo*. For example, Walling *et al* report that the specificity of aminopeptidases are dependant on the length of the peptide and the peptide sequence[221]. Additionally, the tripeptide Aspargine-Glycine-Arginine has shown to be specific for alanine aminopeptidase and may provide improved specificity.

4.5 Conclusion

The synthesis of an aminopeptidase probe has been carried out and has shown to produce a *turn on* fluorescence signal for Gram negative bacteria over Gram positive bacteria. Live bacterial cell assays showed a marked increase in fluorescence on probe incubation at concentrations below 20 μM while inhibition by bestatin resulted in a lower fluorescence increase. Synthesis of the D-amino acid analogue resulted in no *turn on* signal confirming the specificity for the natural L-amino acid. This probe can be adapted and modified to increase the specificity over neutrophils and epithelial cells, possibly by the introduction of more amino acids or more specifically, the NGR peptide sequence should be added onto the coumarin molecule. Further, modification to the fluorophore itself to increase the absorption and emission wavelengths will help in reducing the background signal. Modification to generate a hemi-cyanine-coumarin hybrid molecule will alter the photo-physical properties of this molecule and give the desirable increases in absorption and emission.

Chapter 5

Conclusions and Future Work

The aim of this thesis was to contribute to the field of optical imaging by synthesising a variety of NIR cyanine dyes and optical imaging agents for use as or part of *in vitro* and *in vivo* imaging probes.

Chapter 2 discusses the synthesis of novel heptamethine cyanine dyes with a broad range of absorption and emission wavelengths and a large Stoke's shift range. The photophysical properties of the dyes are reported, comparing the effects of differing functionalities. *In vitro* analysis of cellular toxicity and cellular uptake of a selection of these dyes showed no toxicity and localisation of the dyes within the cytoplasm of the cell. Investigations into the synthesis of novel ratiometric imaging probes were attempted, however, further studies into the reactivity of heptamethine dyes should be carried out to finalise the synthesis.

Chapter 2 also details the synthesis of a new class of pentamethine cyanine dyes with ideal absorption wavelengths for the He-Ne laser. These molecules are photostable and can be further functionalised increasing their possibility for use in molecular imaging. Currently, collaborators at DestiNA Genomics and STMicroelectronics are attempting to utilise these new cyanine dyes as part of a microchip based system for the detection of substrates with publications expected in the near future.

In chapter 3 a synthesis of novel inherent NIR microspheres was developed and the beads characterised. *In vitro* experiments confirmed that the particles were non-toxic while, using confocal microscopy, the ability to penetrate the cell membrane was shown. Further work should utilise the amine groups present on the surface of these

microspheres to carry out further derivitisation, with opportunities to track intra-cellular processes or help in the design of delivery vehicles. Collaborators are currently investigating the effects of introducing charged functionalities on cellular uptake. Addition of further functionalities may also be achieved by increasing the number of polymerisable starting materials, allowing bio-orthogonal reactions to be carried out.

Chapter 3 also reports the successful synthesis of dual functionalised nanoparticles. Dual functionalisation of the beads was carried out using carbodiimide chemistry to attach the NIR fluorophore and a water soluble, optimised, Suzuki-Miyaura cross-coupling reaction to attach a quenched fluorescein-cargo moiety. The quenched probe molecule could be taken up by cells while intracellular cleavage of the disulphide linker resulted in the removal of quenching. Tracking of the particles within cells using cyanine 5 and the fluorescein-cargo moiety was carried out using confocal microscopy. This study provided the first example of employing a bio-orthogonal approach to dual functionalization of particles resulting in monitoring and controlled release within the cytoplasm. This work could be adapted to effectively deliver other cargos into the cell.

Chapter 4 reports the synthesis of an aminopeptidase probe shown to produce a *turn on* fluorescence signal for Gram negative bacteria over Gram positive bacteria. Live bacterial cell assays showed a marked increase in fluorescence on probe incubation with Gram negative bacteria at concentrations below 20 μM while inhibition by bestatin resulted in a lower fluorescence increase. Synthesis of the D-amino acid analogue resulted in no *turn on* signal confirming the specificity for the natural L-amino acid. This aminopeptidase probe should be adapted and modified to increase the specificity over neutrophils and epithelial cells. One such method may be the introduction of more amino acids, inparticular the NGR trimer onto the coumarin molecule.

Chapter 6

Experimental

6.1 General Section

All solvents and reagents were obtained from commercial suppliers and used without purification, unless otherwise stated. Evaporation of solvents was performed at reduced pressure, using a Büchi rotary evaporator.

All solution phase reactions were stirred magnetically unless otherwise stated and followed to completion by thin layer chromatography (TLC) where appropriate using TLC aluminium sheets coated with silica gel 60 F_{254}. TLC visualisation was performed using short wave UV light (254 nm) and/or TLC staining solutions where stated. Reactions involving moisture sensitive reagents were performed under dry nitrogen and reactions involving light sensitive compounds were kept under aluminium foil at all times.

Flash column chromatography was carried out on silica gel 60 (mesh 0.040-0.063).

Solid-phase synthesis was carried out in polypropylene syringes equipped with polyethylene frits (mesh) and Teflon stopcocks.

^{1}H and ^{13}C spectroscopy were recorded on automated Bruker ARX-250, DPX-360, AV 400 or a AV 500 spectrometer in the deuterated solvents indicated at 298K. Chemical shifts are reported on the δ scale in ppm. Resonances were characterised as singlet (s), broad singlet (bs), doublet (d), doublet of doublet (dd), triplet (t) or multiplet (m) with coupling constants given in hertz (Hz).

FTIR spectra were obtained using neat compounds on a Fourier transform IR Bruker Tensor 27 spectrophotometer, with 16 scans, resolution $\pm$ 4 cm^{-1} fitted with a

Specac single reflection diamond attenuated total reflexion (ATR) Golden Gate accessory.

Melting points were determined using Gallenkamp melting point apparatus.

Microwave assisted heating was carried out by irradiating the reaction mixture in a Biotage Initiator at 2.45 GHz. Experiments were carried out in a sealed, heavy-walled Pyrex tubes. Microwave irradiation was conducted at a defined temperature, pressure and power during the reaction time.

UV/Vis Spectroscopy analyses were conducted on an Agilent 8453 spectrophotometer or a Bio Tek Synergy H1 plate reader.

Fluorescence spectra were recorded on a SPEX Fluoromax, using a 1 cm path length fused silica cuvettes or a BioTek Synergy H1 plate reader using Costar®, 96 well, flat bottom, clear well plates with readings made from the bottom and analysed using the Gen 5 (1.11) software.

Quantum yield measurement was carried out on a BioTek Synergy H1 plate reader using Costar® 96 well, flat bottom, clear plates with readings made from the bottom and analysed using the Gen 5 (1.11) software. Fluorophore absorption and emission (λ_{ex} 600 nm for cyanine 5 analogues, λ_{ex} 750 nm for cyanine 7 analogues) were analysed at a concentration of 5 µM in DMSO and compared to a 5 µM solution of ICG in DMSO. The equation to calculate the quantum yield is shown in Equation 2.

$$QY = QY_{ref} \cdot \frac{\eta^2}{\eta_{ref}^2} \cdot \frac{I}{A} \cdot \frac{A_{ref}}{I_{ref}}$$

Equation 2: Quantum yield calculation QY = quantum yield of the sample, QY_{ref} = quantum yield of the reference sample, η = refractive index of the solvent in which the sample is in η_{ref} = refractive index of the solvent in which the reference sample is in, I = integrated fluorescence of the sample, I_{ref} = integrated fluorescence of the reference, A = absorbance of the sample, A_{ref} = absorbance of the reference sample.

Analytical reverse-phase high-performance liquid chromatography (RP–HPLC) was performed on an Agilent Technologies 1100 modular HPLC system coupled to a Polymer Lab 100 ES Evaporative Scattering Detector (ELSD), with detection at 220, 254, 260, 282 and 495 nm. Column: Discovery® C18, 5 µM particle size, reverse-phase (5 cm x 50 mm) with a flow rate of 1 mL/min. Solvents used were HPLC grade.

Solution A: MeOH + 0.1% formic acid
Solution B: H_2O + 0.1% formic acid
Solution C: MeCN + 0.1% formic acid

Method 1: 5% to 95 % A in B over 3 min; Isocratic for 1 min; 95% to 5% A over 1 min; 1 min isocratic.
Method 2: 5 to 95 % A in B over 6 min; Isocratic for 3 min; 95 %to 5% A over 1 min; 2 min isocratic.
Method 3: 5% to 95 % A in B over 10 min; Isocratic for 4 min; 95% to 5% A over 1 min; 1 min isocratic.
Method 4: 5% to 95 % C in B over 3 min; Isocratic for 1 min; 95% to 5% C over 1 min; 1 min isocratic.
Method 5: 5 to 95 % C in B over 6 min; Isocratic for 3 min; 95 %to 5% C over 1 min; 2 min isocratic.
Method 6: 5% to 95 % C in B over 10 min; Isocratic for 4 min; 95% to 5% C over 1 min; 1 min isocratic.
Method 7: 5% to 95 % C in B over 11 min; Isocratic for 3 min; 95% to 5% C over 1 min; 1 min isocratic.

Semi-preparative RP–HPLC was performed on an HP1100 system equipped with a Phenomenex Prodigy C18 reverse-phase column (250 x 10 mm, 5 µm) with a flow rate of 2.5 mL/min eluting with 0.1% HCOOH in H_2O (A) and 0.1% HCOOH in CH_3CN (B), with a gradient of 5 to 95% B over 18 min and an initial isocratic period of 5 min and a final isocratic period of 2 min.

Electrospray ionization mass spectrometry (ESI–MS) analyses were carried out on an Agilent Technologies LC/MSD Series 1100 quadrupole mass spectrometer (QMS) in the ESI mode.

High Resolution Mass Spectra (HRMS) was obtained from the MS section of the University of Edinburgh performed on a Finnigan MAT 900 XLP high resolution double-focussing mass spectrometer.

Inductively coupled plasma – optical emission spectroscopy (ICP-OES) analysis were obtained from Dr Lorna Murray (Edinburgh University, School of Chemistry) on a Perkin Elmer Optima 5300 DV ICP-OES (detection limits: 0.0002-1000ppm).

Centrifugation was performed on an Eppendorf 5430R equipped with a fixed-angle rotor (Eppendorf, 45-24-11-HS).

Light Scattering: The hydrodynamic diameter was determined with a Malvern Zetasizer Nano-ZS. A suspension of particles 1 µL was diluted in 10% PBS (pH = 7.4, 8 g/L NaCl, 0.2 g/L KCl, 1.15 g/L Na_2HPO_4, 0.2 g/L KH_2PO_4) in water (1 mL), vortexed and transferred into a 4 mL polystyrene cuvette (FB55143, Fisher Scientific). The data were collected and analysed with the Dispersion Technology Software 4.20 (Malvern) giving histograms for the particles size as a number distribution.

6.2 General Coupling Reactions and Capping.

To the Fmoc-amino acid (3 eq) in DMF (0.10 M), Oxyma (3 eq) was added and allowed to stir for 5 min. DIC (3 eq) was added and stirred for a further 5 min. The coupling solution was then added to Fmoc-Rink amide-aminomethyl PS resin (0.10 g) pre-swelled in DCM and allowed to stir for 1 h. The resin was isolated by filtration, washed with DMF (3 × 10 mL), DCM (3 × 10 mL), and MeOH (3 × 10

mL). Capping was carried out using DMF, pyridine and Ac_2O (15:3:2) (2 mL, 2 x 10 min).

Coupling reactions were monitored by a qualitative ninhydrin test[215].

Coupling of 7-amino-4-methylcoumarin-3-acetic acid PS (**76**) was carried out using 2-(1*H*-7-azabenzotriazol-1-yl)-1,1,3,3-tetramethyl uroniumhexafluorophosphatemethanaminium (HATU, 5 eq) and DIPEA (10 eq) under microwave irradiation at 60 °C for 20 min.

Colourimetric test for the detection of the chloromethyl groups

A 75 mM solution of 4-(4-nitrobenzyl)pyridine in toluene with 5% of TEA (1 mL) was added to 2 mg of resin **4**. No colouration was observed (naked eye). The test was repeated on Merrifield resin. The resin turned pink.

Fmoc Deprotection

Fmoc deprotection was carried out by suspending the resin (0.10 g) in 20% piperidine in DMF (2 mL) for 10 min. The resin was filtered and a fresh solution of 20% piperidine in DMF (2 mL) was added and shaken for 10 min. The resin was then filtered and washed with DMF (3 x 10 mL) and DCM (3 x 10 mL).

TFA Cleavage

The resin (0.10 g), pre-swollen in DCM, was treated with the cleavage cocktail of (3 mL) for 3h. The solution was drained and the resin was washed with the cleavage cocktail. The crude material was concentrated under reduced pressure and re-dissolved in a minimum amount of cleavage cocktail (500 μL). Ice-cold ether (7.5 mL) was added and the precipitate was collected by centrifugation. The precipitate was washed further with cold ether (3 x 5 mL). Cleavage cocktails were either TFA/TIS/DCM (95:2.5:2.5), TFA/TIS/DCM (48:2:48) or TFA/phenol/H_2O/TIS (88:5:5:2).

Qualitative Ninhydrin Test[215]

This test was carried out after washing of the resin on a few beads. 3 drops of reagents A and 1 drop of reagent B are added to the beads and allowed to sit at 100 °C for 3 min. A blue solution indicated the presence of free amines, a yellow solution corresponds to protected amines, or no amines present.

Preparation of ninhydrin reagents A and B:

Reagent A, solution 1:

Reagent grade phenol (40.0 g, 0.43 mmol) was added to absolute ethanol (10 mL) and allowed to heat at 40 °C until the solution became clear. Amberlite mixed-bed resin MB-3 (4.0 g) was added, stirred for 45 min at room temperature and filtered.

Reagent A, solution 2:

KCN (65 mg, 1 mmol) was dissolved in water (100 mL). This solution (2 mL) was diluted with freshly distilled pyridine to 100 mL. Amberlite mixed-bed resin MB-3 (4 g) was added, stirred for 45 min and filtered. Solutions 1 and 2 were mixed to obtain reagent A.

Reagent B:

Ninhydrin (2.5 g, 14 mmol) was dissolved in absolute ethanol (50 mL) and stirred for 15 min at room temperature.

Cellular Studies

Cell culture experiments were carried out in a HERAsafe KS 18 class II negative-flow cabinet and in a HERAcell 150 incubator both from Heraeus.

General Cell Culture

Human embryonic kidney cells (HEK293T), human cervical cancer cells (HeLa), human prostate cancer cells (PC-3) and human adenocarcinomic alveolar basal epithelial cells (A549) were cultured in Dulbecco's modified eagle medium (DMEM) supplemented with 10% (v/v) heat inactivated fetal bovine serum, *L*-glutamine (4 mM) and antibiotics (100 units/mL penicillin and 100 units/L

streptomycin) at 37 °C and 5% CO_2. Cells were cultured in T-75 flasks until 80% confluency followed by removal of growth medium, washing with PBS (10 mL) and harvesting by trypsination (trypsin/EDTA, Gibco) (1 mL) at 37 ºC. Detached cells were collected in fresh growth media and an aliquot was reseeded to a flask for regrowth. Cell experiments were carried out with cells passaged between 4- and 20-times.

Cell Labeling

HEK293T, HeLa, PC-3 or A549 cells were plated in DMEM, supplemented with 10% (v / v) heat inactivated fetal bovine serum, L-glutamine (4 mM) and antibiotics (100 units/mL penicillin and 100 units/L streptomycin) in a 8, 24 or 96-well plate at a density of 20,000 cells per well and grown for 24 h at 37 °C and 5% CO_2. Thereafter, the probe of interest was added and incubated with the cells for 0.5-24 h. Cells were washed with PBS and either imaged live with confocal microscopy, fluorescent microscopy (microplate reader) or harvested with trypsin/EDTA and analysed. Commercial membrane or organelle stains used when stated and incubated with cells 30 min prior to analysis.

Stain Target	Commercial Name	Laser Excitation (nm)	Filter (nm)
Nucleus	Syto 82	543	554-587
Cytosol	Calcein	488	501-522
Nucleus	Hoechst 33342	404	535-590
Cytoplasm	Cell Tracker Red CMTPX	594	575-615

Table 6: Commercial membrane and organelle stains.

Flow Cytometry

A suspension of the material under investigation (1 µL, 20 µg, solid content 20 mg/mL) was diluted in 350 µL of water, vortexed and analysed using the appropriate filters according to the fluorophores under investigation using the BD FACSAria (Table 7). Results were analysed using FlowJo Version 7.6.3 software. Quantitative flow cytometric analysis was carried out at least in triplicate.

Laser Excitation (nm)	Filter (nm)	Fluorophore
375	450/20	DAPI/Hoechst blue
488	530/30	Fluorescein
561	670/14	Cyanine 5 and cyanine 5 analogues
633	780/60	Cyanine 7 analogues

Table 7: BD Biosciences FACSAria® system excitation wavelengths, filters and corresponding fluorophores.

Cellular Toxicity

Cell Viability Assay (MTT Assay): HEK293T,HeLa, PC-3 or A549 were plated in DMEM, supplemented with 10% (v/v) heat inactivated fetal bovine serum, L-glutamine (4 mM) and antibiotics (100 units/mL penicillin and 100 units/mL streptomycin) in a 96-well plate and allowed to grow for 24 h at 37 °C and 5% CO_2. Thereafter, the probe of interest was added at varying concentrations and allowed to incubate with the cells for 24 h. After incubation, cells were washed with PBS and then further incubated with 3-(4,5-dimethylthiazol-2-yl)-2,5-diphenyltetrazolium bromide (MTT) solution (7 mg MTT in 7 mL PBS and 3 mL phenol red free DMEM) for 4 h at 37 °C. 100 µL of solubilisation solution (10% triton-X 100 in acidic isopropanol (0.1 M HCl)) was added and the absorbance at 570 nm measured (Benchmark Biorad microplate reader) and results compared to untreated cells. Cell viability was calculated using Equation 3.

$$\% \text{ of cellular viability} = (Abs_{570exp} / Abs_{570\ cont}) \times 100$$

Equation 3:"$Abs_{570\ exp}$" is the absorbance at 570 nm of cells treated with compound of interest and "$Abs_{570\ cont}$"refers to absorbance at 570 nm of untreated cells.

Confocal Microscopy

Cells were fixed on to 8 well chambers and incubated (37 °C, 5% CO_2) for 24 h prior to incubation with the compounds of interest. After the incubation, cells were washed

twice with PBS and imaged directly using a Zeiss LSM 510 Meta microscope. Zeiss 510 meta software was used for digital image acquisition.

6.3 Synthesis of Starting Materials

1,2,3,3-tetramethyl-3*H*-indolium iodide (9)

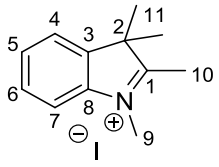

A mixture of 2,3,3-trimethyl-3*H*-indole **5** (40.0 mL, 0.25 mol) and methyl iodide (38.9 mL, 0.63 mol) in acetonitrile (150.0 mL) was heated under reflux for 3 days. The reaction mixture was cooled to room temperature and the solvent evaporated under vacuum. The residue obtained was washed with ether (50.0 mL) and ethanol (50.0 mL) to remove any starting material. The residue was dried *in vacuo* to give a pink solid (36.5g, 84%).

HPLC (method 2) t_r = 0.82min, Purity 100% (ELSD).
MS (ES): calculated for $C_{12}H_{16}N$ $[M]^+$ m/z 174.1. Found 174.1 (100%).
IR (υ): 1629 (C=N), 1197 (C-N) cm^{-1}.
^{1}H NMR (250 MHz, DMSO-d6) δ: 7.92-7.90 (m, 1H,**4**), 7.84-7.82 (m, 1H, **6**), 7.64-7.62 (m, 2H, **5,7**), 3.97 (s, 3H, **10**), 2.77 (s, 3H,**9**), 1.53 (s, 6H, **11**).
^{13}C NMR (62.9 MHz, DMSO-d6) δ: 196.0 (**1**), 142.0 (**3**), 141.5 (**8**), 129.3 (**6**), 129.8 (**5**), 123.2 (**4**), 115.1 (**7**), 53.9 (**2**), 34.6 (**9**), 21.63 (**10**), 13.7 (**11**).
All data in agreement with the literature[89].

1-(5-carboxypentyl)-2,3,3-trimethyl-3*H*-indolium bromide (7)

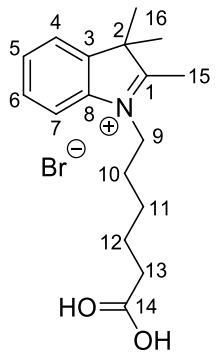

A mixture of 2,3,3-trimethyl-3*H*-indole **5** (12.1 mL, 75.4 mmol) and 6-bromohexanoic acid (30.0 g, 189.0 mmol) in acetonitrile (50.0 mL) was heated at 100 °C for 16 h. The solution was cooled to room temperature and the solvent evaporated under vacuum. The residue obtained was washed with ether and DCM until removal of starting material to give a pink solid (2.3 g, 19 %).

HPLC (method 2) t_r = 3.74 min, Purity 100% (ELSD).

MS (ES): calculated for $C_{17}H_{25}NO_2$ $[M+H]^+$ m/z (%) 275.2. Found 275.2 (100%).

IR (υ): 3302 (O-H), 1743 (C=O), 1699 (C=N), 1188 (C-N)cm^{-1}.

^{1}H NMR (500 MHz, DMSO-d6)*δ*: 7.96-7.98 (m, 1H,**4**), 7.83-7.85 (m, 1H, **6**), 7.61-7.63 (m, 2H **5,7**), 4.42-4.45 (m, 2H, **13**), 2.83 (s, 3H, **15**), 2.23 (t, 2H, *J*=7.3Hz, **9**), 1.82-1.84 (m, 2H, **10**), 1.56-1.58 (m, 2H, **12**), 1.53 (s, 6H, **16**),1.41-1.44 (m, 2H, **11**).

^{13}C NMR (125 MHz, DMSO-d6):*δ* 197.0 (**1**), 174.8 (**14**), 142.4 (**3**), 141.5 (**8**), 129.9 (**6**), 129.5 (**5**), 124.0 (**4**), 116.0 (**7**), 54.6 (**2**), 47.9 (**9**), 33.8 (**13**), 27.43 (**10**), 25.9 (**12**), 24.5 (**11**), 22.5 (**15**), 14.4 (**16**).

All data in agreement with the literature[89].

1,2,3,3-tetramethyl-3*H*-indolium-5-sulfonate (10)

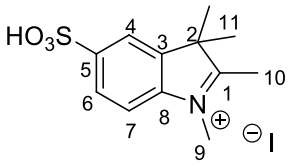

2,3,3-trimethyl-3*H*-indole-5-sulfonic acid **4** (18.0 g, 75.3 mmol) and methyl iodide (23.5 mL, 377.0 mmol) were dissolved in EtOH (280.0 mL) and heated under reflux for 72 h. The solvent was evaporated and the crude product washed with cold Et_2O (50.0 mL) and EtOH (50.0 mL) to yield a red solid (16.9 g, 88%).

HPLC (method 1) t_r = 0.8 min, Purity 70% (ELSD).
MS (ES): calculated for $C_{12}H_{16}INO_3S$ [M+I] m/z 381.0. Found 380.8 [M+I] (100%).
Mp. 260 °C decomposed.
IR (υ): 1628 (C=N), 1469 (S=O), 1197 (S=O), 1118 (C-N) 1032 (S-O) cm^{-1}.
^{1}H NMR (500 MHz, MeOD) *δ*: 8.00 (s, 1H, **4**), 7.85-7.75 (m, 2H, **6,7**), 4.10 (s, 3H, **10**), 2.77 (s, 3H, **9**), 1.63 (s, 6H, **11**).
^{13}C NMR (126 MHz, MeOD) δ: 173.80 (**1**), 146.97 (**5**), 143.08 (**3**), 141.74 (**8**), 126.89 (**6**), 120.65 (**4**), 114.86 (**7**), 54.59 (**2**), 34.26 (**9**), 20.98 (**10**), 19.36 (**11**).
All data in agreement with the literature[89].

1,1,2,3-tetramethyl-1*H*-benzo[e]indoliumiodide (6)

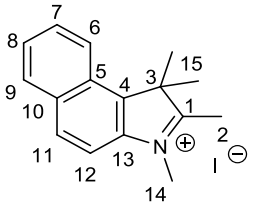

Trimethyl-benzindole **3** (1.7 g, 8.0 mmol) and MeI (3.0 mL, 48.0 mmol) were dissolved in MeCN (5.0 mL) and heated under microwave irradiation at 150 °C for

1 h. The crude product was cooled and washed with ether to give a yellow solid (1.7 g, 96%).

HPLC (method 2) t_r = 0.77 min, Purity 100% (ELSD).

MS (ES): calculated for $C_{16}H_{18}N$ [M] m/z 224.1. Found 224.2 [M] (100%).

Mp. 220°C.

IR (υ): 1638 (C=N), 1389 (C-N) cm^{-1}.

^{1}H NMR (500 MHz, MeOD) δ: 8.34 (dd, J = 8.5, 1.3 Hz, 1H, **9**), 8.26 (d, J = 8.9, 1.1 Hz, 1H, **6**), 8.18 (d, J = 8.3 Hz, 1H, **11**), 8.01 (d, J = 8.9 Hz, 1H, **12**), 7.83 (ddd, J = 8.4, 6.9, 1.3 Hz, 1H, **8**), 7.74 (ddd, J = 8.1, 6.9, 1.1 Hz, 1H, **7**), 4.20 (s, 3H, **2**), 2.93 (s, 3H, **14**), 1.86 (s, 6H, **15**).

^{13}C NMR (126 MHz, MeOD) δ: 196.03 (**1**), 139.40 (**13**), 136.85 (**4**), 133.88 (**11**), 130.89 (**8**), 129.66 (**7**), 128.27 (**9**), 127.62 (**5**), 127.19 (**10**), 123.01 (**6**), 112.18 (**12**), 55.75 (**3**), 34.43 (**14**), 20.75 (**2**), 12.94 (**15**).

All data in agreement with the literature[89, 222].

3-(1,1,2-trimethyl-1*H*-benzo[e]indolium-3-yl)propane-1-sulfonate (8)

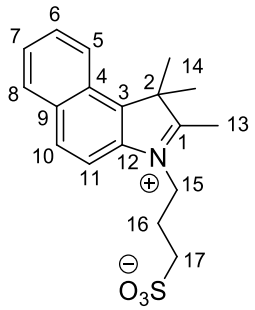

A solution of 1,3-propansultone **3** (0.7 g, 5.4 mmol) in 1,2-dichlorobenzene (10.0 mL) was added to 1,1,2-trimethylbenz(e)indole (1.0 g, 4.9 mmol) and allowed to stir at 120 °C for 18 h. The solvent was evaporated and the product crystallised from cold Et_2O to yield an orange solid (1.4 g, 85%).

HPLC (method 2) t_r = 5.0 min, Purity 100% (ELSD).

MS (ES): calculated for $C_{18}H_{20}NO_3S$ $[M-H]^-$ m/z 331.1. Found 330.1 (75%).

Mp. 262 °C.

IR (υ): 1633 (C=N), 1417 (S=O), 1217 (C-N), 1182 (S=O), 1034 (S-O) cm^{-1}.

^{1}H NMR (500 MHz, DMSO-d6) δ: 8.37 (d, J = 8.4 Hz, 1H, **5**), 8.30 (d, J = 8.9 Hz, 1H, **8**), 8.26 – 8.20 (m, 2H, **10,11**), 7.79 (t, J = 7.0 Hz, 1H, **6**), 7.73 (t, J = 7.1 Hz, 1H, **7**), 4.81 – 4.76 (m, 2H, **16**), 2.95 (s, 3H, **13**), 2.69 (t, J = 6.5 Hz, 2H, **17**), 2.23 (t, J = 7.3 Hz, 2H, **15**), 1.77 (s, 6H, **14**).

^{13}C NMR (126 MHz, DMSO-d6) δ: 196.88 (**1**), 139.11 (**12**), 137.47 (**3**), 133.51 (**10**), 131.17 (**7**), 130.23 (**6**), 128.83 (**8**), 127.73 (**4**), 127.66 (**9**), 123.85 (**5**), 113.82 (**11**), 55.95 (**2**), 47.87 (**15**), 47.32 (**16**), 24.42 (**14**), 22.13 (**17**), 14.10 (**13**).

1,2-dimethylquinolinium iodide (12)

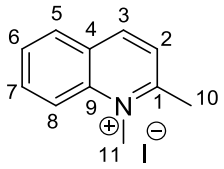

Quinalidine **11** (1.9 mL, 14.0 mmol) and iodomethane (4.4 mL, 7.0 mmol) were stirred in MeCN (20.0 mL) for 70 h under reflux. The solvent was then evaporated and the orange product crystallised from cold Et_2O (Iodate salt - 3.6 g, 90 %).

MS (ES): calculated for $C_{11}H_{12}N$ [M] m/z 158.1. Found 158.2 (100%).

Mp. 191 °C.

IR (υ): 1615 (C=N) 1225 (C-N) cm^{-1}.

^{1}H NMR (400 MHz, DMSO-d6) δ:9.10 (d, J = 8.6 Hz, 1H, **3**), 8.59 (dd, J = 9.0, 0.5 Hz, 1H, **5**), 8.40 (dd, J = 8.1, 1.4 Hz, 1H, **8**), 8.23 (ddd, J = 8.8, 7.0, 1.5 Hz, 1H, **7**), 8.12 (d, J = 8.6 Hz, 1H, **2**), 7.99 (ddd, J = 7.9, 7.2, 0.7 Hz, 1H, **6**), 4.45 (s, 3H, **11**), 3.08 (s, 3H, **10**).

^{13}C NMR (100 MHz, MeOD) δ:161.04 (**1**), 145.80 (**3**), 139.87 (**9**), 135.29 (**7**), 130.35 (**6**), 129.04 (**5**), 128.46 (**4**), 124.96 (**2**), 118.47 (**8**), 39.31 (**11**), 22.50 (**10**).

All data in agreement with the literature[223].

2-(1-(3-hydroxypropylamino)ethylidene)-5,5-dimethylcyclohexane-1,3-dione (55)

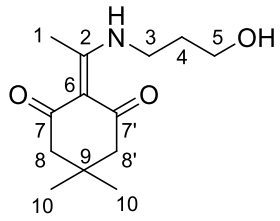

3-Amino-1-propanol (0.1 g, 1.3 mmol), Dde-OH (0.2 g, 1.5 mmol) and DIPEA (226.0 µL, 1.3 mmol) were dissolved in MeOH (2.0 mL) and allowed to stir at room temperature for 3 h. The solvent was evaporated and the crude product purified by column chromatography (99:1 DCM:MeOH) to yield a white solid (0.2 g, 70%).

HPLC (method 2) t_r = 5.9 min, Purity 100% (ELSD).

MS (ES): calculated for $C_{13}H_{20}NO_3$ $[M-H]^-$ m/z 240.2. Found 240.2 (55%).

MS (HRMS, ES) m/z calc $[M+Na]^+$ 262.14137. Found 262.14130.

Mp. 141 °C.

IR (υ): 3342 (O-H),1566 (C=O), 1351 (C-N) cm^{-1}.

^{1}H NMR (400 MHz, $CDCl_3$) δ: 3.82 (t, J = 5.9 Hz, 2H, **5**), 3.59 (dd, J = 12.3, 6.8 Hz, 2H, **3**), 2.61 (s, 3H, **1**), 2.39 (s, 4H, **8,8'**), 1.99 – 1.92 (m, 2H, **4**), 1.06 (s, 6H, **10**).

^{13}C NMR (100 MHz, $CDCl_3$) δ: 197.99 (**7**,**7'**), 173.80 (**2**), 107.94 (**6**), 59.34 (**5**), 52.83 (**8,8'**), 40.23 (**3**), 31.54 (**4**), 30.12 (**9**), 28.27 (**10,10'**), 17.92 (**1**).

2-(1-(3-bromopropylamino)ethylidene)-5,5-dimethylcyclohexane-1,3-dione (56)

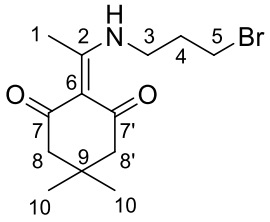

Dde-OH (0.15 g, 0.99 mmol) in MeCN (0.5 mL) and DIPEA (60.0 µL, 0.33 mmol) were stirred at room temperature for 10 min. 3-bromopropylamine (72 mg, 0.33 mmol) in MeCN (2.0 mL) was added dropwise over a period of 30 min and allowed to stir at room temperature for 4 h. The solvent was evaporated and the crude product was washed with 1 M HCl (20.0 mL) before purification by column chromatography (100% DCM) to yield a pale yellow solid (53 mg, 53%).

HPLC (method 2) t_r = 7.8 min, Purity 100% (ELSD).
MS (ES): calculated for $C_{13}H_{21}BrNO_2$ $[M+H]^+$ m/z 302.1. Found 302.1 (100%).
MS (HRMS, ES) m/z calc $[M+Na]^+$ 324.05696. Found 324.05770.
Mp. 61 °C.
IR (υ): 1567 (C=O), 1288 (C-N) cm^{-1}.
^{1}H NMR (500 MHz, $CDCl_3$) δ: 3.63 (dd, *J* = 12.3, 6.6 Hz, 2H, **3**), 3.52 (t, *J* = 6.2 Hz, 2H, **5**), 2.63 (s, 3H, **1**), 2.39 (s, 4H, **8,8'**), 2.24 (m, 2H, **4**), 1.06 (s, 6H,**10**).
^{13}C NMR (126 MHz, $CDCl_3$)δ: 198.09 (s, **7,7'**), 173.92 (s, **2**), 108.16 (s, **6**), 52.91 (s, **8,8'**), 41.40 (s, **3**), 31.72 (s, **4**), 30.11 (s, **5**), 29.63 (s, **9**), 28.42 (s, **10, 10'**), 17.93 (s, **1**).

***tert*-butyl 4-hydroxybenzylcarbamate (81)**

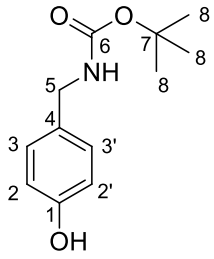

Di-tertbutyl-dicarbonate (1.95 g, 8.9 mmol) was dissolved in water (8.0 mL). 4-hydroxybenzylamine (1.0 g, 8.0 mmol) was added and stirred at 35 °C for 2 h. The organic layer was extracted with DCM (50.0 mL) and dried over sodium sulphate. This solution was filtered and evaporated to yield a white solid (1.95 g, 98%).

HPLC (method 2) t_r = 5.5 min, Purity 79% (ELSD).

MS (ES): calculated for $C_{12}H_{17}NNaO_3$ $[M+Na]^+$ m/z 246.1. Found 246.1 (100%).

Mp. 92 °C.

IR (υ):3342 (N-H), 3151 (O-H), 1670 (C=O), 1226 (C-N), 1158 (C-O) cm^{-1}.

^{1}H NMR (500 MHz, $CDCl_3$) *δ*: 7.11 (d, *J* = 8.4 Hz, 2H, **2,2'**), 6.76 (d, *J* = 8.3 Hz, 2H, **3,3'**), 5.29 (s, 1H, **NH**), 4.86 (s, 1H, **OH**), 4.22 (d, *J* = 3.4 Hz, 2H, **5**), 1.46 (s, 9H, **8**).

^{13}C NMR (126 MHz, $CDCl_3$) *δ*: 155.48 (**6**), 150.29 (**1**), 128.94 (**4**), 121.46 (**3,3'**), 115.51 (**2,2'**),44.22 (**7**), 28.45 (**5**), 27.71 (**8**).

All data in agreement with the literature[224].

4-formylphenyl acetate (49)

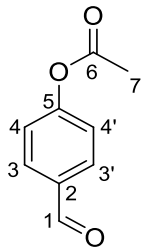

4-hydroxybenzaldehyde (5.0 g, 40.1 mmol) was dissolved in a mixture of acetic anhydride and pyridine (1:1, 20 mL) and stirred at room temperature for 2 h. The solvent was evaporated and the product was washed with 1 M NH_4HCO_3 (25.0 mL) and extracted with DCM (100.0 mL) to give a clear oil (6.6 g, 99%).

HPLC (method 5) t_r = 3.7 min, Purity 100% (ELSD).

IR (υ): 1758 (HC=O), 1183 (C=O), 1101 (C-O) cm^{-1}.

^{1}H NMR (500 MHz, CD_3CN) *δ*: 9.98 (s, 1H, **1**), 7.94 (d, *J* = 8.7 Hz, 2H, **3,3'**), 7.31 (d, *J* = 8.4 Hz, 2H, **4,4'**), 2.28 (s, 3H, **7**).

^{13}C NMR (126 MHz, CD_3CN) *δ*: 191.47 (**1**), 169.09 (**6**), 155.54 (**5**), 134.26 (**2**), 130.99 (**3,3'**), 122.72 (**4,4'**), 20.32 (**7**).

All data in agreement with the literature[225].

4-(hydroxymethyl)phenyl acetate (50)

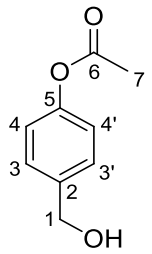

Aldehyde **49** (2.5 g, 15.3 mmol) was dissolved in ethanol (45.0 mL) and cooled to 0 °C. While stirring, $NaBH_4$ (0.23 g, 6.1 mmol) was added over a period of 1 h. After a further 1 h, 6 M aqueous HCl was added until the solution reached pH 2. The solvent was evaporated and the product extracted with DCM (60.0 mL). Volatiles were removed under reduced pressure and the desired product obtained as a viscous oil (1.2 g, 48%).

HPLC (method 2) t_r = 3.7 min, Purity 100% (ELSD).
MS (ES): calculated for $C_9H_{10}NaO_3$ $[M+Na]^+$ m/z 189.1. Found 189.2 (100%).
MS (HRMS, ES) m/z calc [M] 166.06245. Found 166.06316.
IR (υ): 3355 (O-H), 1164 (C=O), 1011 (C-O) cm^{-1}.
^{1}H NMR (500 MHz, CD_3CN) δ: 7.36 (d, J = 8.5 Hz, 2H, **3,3'**), 7.05 (d, J = 8.5 Hz, 2H, **4,4'**), 4.57 (s, 2H, **1**), 2.24 (s, 3H, **7**).
^{13}C NMR (126 MHz, CD_3CN) δ: 169.77 (**6**), 149.92 (**5**), 139.79 (**2**), 127.76 (**3,3'**), 121.62 (**4,4'**), 63.16 (**1**), 20.27 (**7**).

4-(((4-nitrophenoxy)carbonyloxy)methyl)phenyl acetate (53)

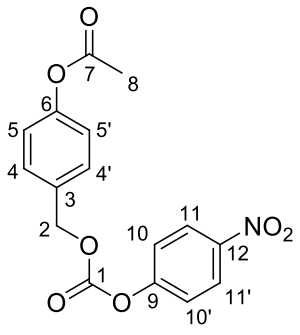

Alcohol **50** (0.1 g 0.60 mmol), pyridine (53.0 µL, 0.66 mmol), and nitrophenylchoroformate (0.13 g, 0.66 mmol) were dissolved in anhydrous THF (1.5 mL) and stirred at room temperature for 2 h. The solvent was evaporated and the residue was immediately purified by column chromatography (93:7 Hexane:EtOAc) to yield a white powder (0.17 g, 87%).

HPLC (method 2) t_r = 5.6 min, Purity 100% (ELSD).

MS (ES): calculated for $C_{16}H_{13}NNaO_7$ $[M+Na]^+$ m/z 354.1. Found 354.0 (100%).

MS (HRMS, ES) m/z calc [M] 331.06865. Found 331.06831.

Mp. 101 °C.

IR (υ):1757 (OOC=O), 1514 (N-O), 1337 (N-O), 1214 (C=O) 1189 (C-O), 1163 (C-O) cm^{-1}.

^{1}H NMR (500 MHz, CD_3CN) *δ*: 8.31 (d, *J* = 9.3 Hz, 2H, **11,11'**), 7.53 (d, *J* = 8.7 Hz, 2H, **4,4'**), 7.48 (d, *J* = 9.3 Hz, 2H, **10,10'**), 7.18 (d, *J* = 8.6 Hz, 2H, **5,5'**), 5.32 (s, 2H, **2**), 2.29 (s, 3H, **8**).

^{13}C NMR (126 MHz, CD_3CN) *δ*: 155.69 (**7**), 152.49 (**1**), 151.28 (**6**), 145.68 (**9**), 132.57 (**3**), 129.88 (**4,4'**), 129.31 (**12**) 125.33 (**11,11'**), 122.29 (**10,10'**), 122.18 (**5,5'**), 70.02 (**2**), 20.26 (**8**).

4-((benzylcarbamoyloxy)methyl)phenyl acetate (54)

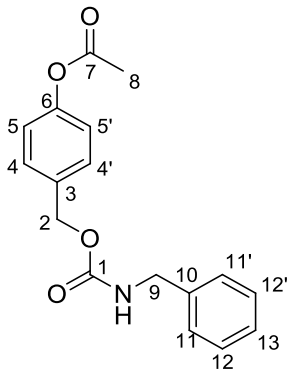

Nitrocompound **53** (50 mg, 0.15 mmol), benzylamine (25.0 µL, 0.23 mmol) and TEA (42.0 µL, 0.30 mmol) were dissolved in dry MeCN (0.5 mL) and stirred at room temperature for 2 h. The solvent was evaporated and the residue dissolved in DCM (1.0 mL), which was washed with 1 M aqueous HCl (5.0 mL) and 1 M aqueous NaOH (5.0 mL) and dried over sodium sulphate. The organic solvent was evaporated to yield the product (16 mg, 35%).

HPLC (method 1) t_r = 5.3 min, Purity 100% (ELSD).

MS (ES): calculated for $C_{17}H_{17}NNaO_4$ $[M+Na]^+$ m/z 322.1. Found 322.0 (100%).

MS (HRMS, ES) m/z calc [M] 299.11521. Found 299.11571.

Mp. 80 °C.

IR (υ): 3329 (N-H), 1687 (NC=O), 1218 (C=O), 1199 (C-O) cm^{-1}.

^{1}H NMR (500 MHz, CD_3CN) δ: 7.39 (d, J = 8.2 Hz, 2H, **4,4'**), 7.30 (m, 5H, **11,11',12,12',13**), 7.08 (d, J = 8.3 Hz, 2H, **5,5'**), 6.13 (s, 1H, **NH**), 5.07 (s, 2H, **2**), 4.28 (d, J = 6.3 Hz, 2H, **9**), 2.24 (s, 3H, **8**).

^{13}C NMR (126 MHz, CD_3CN) δ: 169.62 (**7**), 156.52 (**1**), 150.61 (**6**), 139.64 (**10**), 135.05 (**3**), 129.05 (**13**), 128.45 (**4,4'**), 127.17 (**12,12'**), 127.05 (**11,11'**), 121.91 (**5,5'**), 65.43 (**2**), 44.22 (**9**), 20.25 (**8**).

4-nitrophenyl 4-(4,4,5,5-tetramethyl-1,3,2-dioxaborolan-2-yl)benzyl carbonate (51)

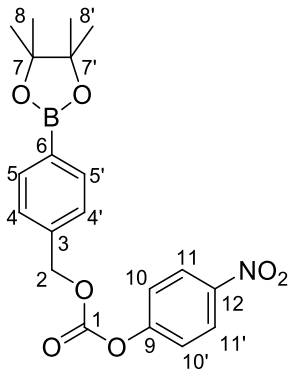

4-(hydroxymethyl) phenyl boronic acid pinocol ester (1.0 g, 4.3 mmol), nitrophenylchloroformate (0.94 g, 4.7 mmol) and pyridine (0.39 mL, 4.7 mmol) were dissolved in anhydrous THF (20.0 mL) and allowed to stir at room temperature for 2 h. The solvent was evaporated and the crude product was purified by column chromatography [eluting solvent: Hexane:EtOAc (93:7)] to yield a white powder (1.5 g, 88%).

HPLC (method 5) t_r = 6.6 min, Purity 100% (ELSD).

MS (ES): calculated for $C_{40}H_{44}B_2N_2NaO_{14}$ $[2M+Na]^+$ m/z 821.3. Found 821.3 (85%).

MS (HRMS, ES) m/z calc [M] 399.14838. Found 399.14911.

Mp. 108 °C.

IR (υ): 1753 (C=O), 1526 (N-O), 1358 (B-O), 1335 (N-O), 1255 (C-O), 1213 (C-O) cm^{-1}.

^{1}H NMR (500 MHz, CD_3CN) δ: 8.16 (d, J = 9.2 Hz, 2H, **4,4'**), 7.64 (d, J = 8.0 Hz, 2H, **11,11'**), 7.38 – 7.28 (m, 4H, **5,5',10,10'**), 5.19 (s, 2H, **2**), 1.21 (s, 12H, **8,8'**).

^{13}C NMR (126 MHz, CD_3CN) δ: 156.57 (**1**), 153.40 (**9**), 146.57 (**3**), 138.89 (**12**), 135.65 (**5,5'**), 128.51 (**11,11'**), 126.23 (**4,4'**), 123.18 (**10,10'**), 84.91 (**7,7'**), 71.30 (**2**), 25.09 (**8,8'**).

4-(4,4,5,5-tetramethyl-1,3,2-dioxaborolan-2-yl)benzyl benzylcarbamate (52)

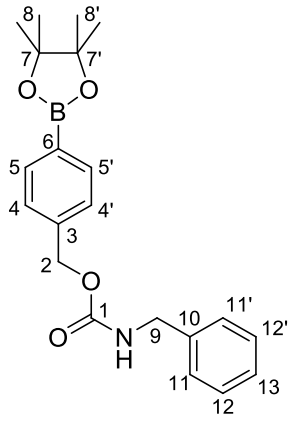

Nitrocompound **51** (50.0 mg, 0.13 mmol), benzylamine (20.6 µL, 0.19 mmol) and TEA (34.7 µL, 0.25 mmol) were dissolved in anhydrous MeCN and allowed to stir at room temperature for 3 h. The solvent was evaporated and the residue purified by column chromatography [eluting solvent: Hexane:EtOAc (90:10)] to yield a yellow oil (24 mg, 52%).

HPLC (method 5) t_r = 6.1 min, Purity 100% (ELSD).

MS (ES): calculated for $C_{21}H_{26}BNNaO_4$ $[M+Na]^+$ m/z 390.2. Found 390.2 (25%), 757.3 $[2M + Na]^+$(100%).

MS (HRMS, ES) m/z calc [M] 367.19494. Found 367.19494.

IR (υ): 3331 (N-H), 1698 (NC=O), 1357 (B-O), 1240 (C=O), 1141 (C-O) cm^{-1}.

^{1}H NMR (500 MHz, CD_3CN) δ: 7.70 (d, J = 7.7 Hz, 2H, **4,4'**), 7.39 – 7.23 (m, 7H, **5,5',11,11',12,12',13**), 6.19 (s, 1H, **NH**), 5.09 (s, 2H, **2**), 4.28 (d, J = 6.3 Hz, 2H, **9**), 1.32 (s, 12H, **8,8'**).

^{13}C NMR (126 MHz, CD_3CN) δ: 156.55 (**1**), 140.65 (**10**), 139.64 (**3**), 134.59 (**5,5'**), 128.45 (**12,12'**), 127.16 (**13**), 127.04 (**4,4'**), 126.88 (**11,11'**), 83.90 (**7,7'**), 65.80 (**2**), 44.22 (**9**), 24.20 (**8,8'**).

2-Chloro-1-formyl-3-hydroxymethylene cyclohexene (13)

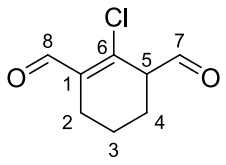

A mixture of DMF (40.0 mL) in DCM (40.0 mL) was cooled to -10 °C. A solution of phosphorousoxychloride (37.0 mL, 0.4 mol) in DCM (35.0 mL) was added dropwise over 15 min. Cyclohexanone (10.0 g, 0.1 mol) was added and the solution was refluxed for 3 h. The solution was cooled, poured onto 200 g of ice and left to stand overnight. The product was re-crystallised from acetone to yield a brown solid (2.7 g, 32%).

HPLC (method 2) t_r = 5.8 min, purity: 100% (ELSD).
MS (ES): calculated for $C_{16}H_{18}Cl_2NaO_4$ $[2M+Na]^+$ m/z 367.1. Found 367.2, (65%).
Mp: 129 °C.
^{1}H NMR (500 MHz, DMSO-d6) δ: 10.84 (s, 1H, **8**), 10.05 (s, 1H, **7**), 7.62 (s, 1H, **5**), 2.37 (m, 4H, **2,4**), 1.59 (m, 2H, **3**).
^{13}C NMR (126 MHz, DMSO-d6) δ: 189.73 (**8**), 149.93 (**7**), 127.82 (**6**), 112.41 (**1**), 61.96 (**5**), 31.08 (**3**), 24.19 (**2,4**).
Data in agreement with the literature[226].

6.4 Experimental for Chapter 2

6.4.1 Synthesis of Heptamethine Cyanine Dyes: Chloro Derivatives

2-(2-[2-Chloro-3-([1,3-dihydro-1,3,3-trimethyl-2*H*-indol-2-ylidene]ethylidene)-1-cyclohexen-1-yl]ethenyl)-1,3,3-trimethylindolium iodide (14)

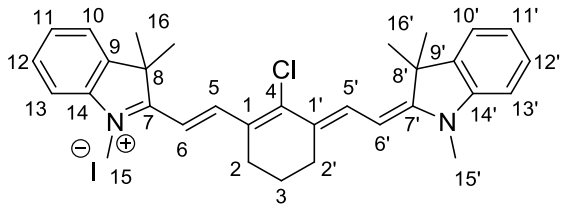

Indolium salt **9** (6.0 g, 34.8 mmol) and diadehyde **13** (2.0 g, 11.6 mmol) were stirred with NaOAc (5.7 g, 69.6 mmol) in a solution of acetic acid and acetic anhydride (1:1, 450.0 mL) for 4 h at 115 °C under N_2. The solvent was evaporated and the product extracted with DCM (150.0 mL) and dried over sodium sulphate. The crude product was purified by column chromatography [eluting solvent: DCM:MeOH (95:5)] to yield a green solid (4.2 g, 74%).

HPLC (method 2) t_r = 3.9 min, Purity: 100% (ELSD).
MS (ES): calculated for $C_{32}H_{36}ClN_2$ [M] m/z 483.3. Found 483.3 (100%).
MS (HRMS, ES) m/z calc [M] 483.25615. Found. 482.25685
λ_{abs}= 775 nm, λ_{em}= 795 nm (MeOH); λ_{abs}= 789 nm, λ_{em}= 718 nm (DMSO).
Mp: 245 °C.
^{1}H NMR (500 MHz, DMSO-d6) δ: 8.25 (d, *J* = 14.2 Hz, 2H, **5,5'**), 7.63 (d, *J* = 7.4 Hz, 2H, **10,10'**), 7.43-7.45 (m, 4H, **11,11',13,13'**), 7.38 – 7.23 (m, 2H, **12,12'**), 6.30 (d, *J* = 14.2 Hz, 2H,**6,6'**), 3.68 (s, 6H, **15,15'**), 2.71 (t, *J* = 6.0 Hz, 4H, **2,2'**), 1.92 – 1.79 (dt, J= 11.8, 6.3 Hz, 2H, **3**), 1.67 (s, 12H, **16,16'**).
^{13}C NMR (126 MHz, DMSO-d6) δ: 173.13 (**7,7'**), 148.21 (**5,5'**), 143.33 (**10,10'**), 143.05 (**12,12'**), 141.33 (**4**), 128.72 (**1,1'**), 126.52 (**9,9'**), 125.27 (**14,14'**), 122.98

(**13,13'**), 111.84 (**11,11'**), 101.77 (**6,6'**), 49.35 (**8,8'**), 31.90 (**15,15'**), 27.89 (**16,16'**), 26.34 (**2,2'**), 21.02 (**3**).

1-(5-carboxypentyl)-2-((E)-2-((E)-3-((E)-2-(1-(5-carboxypentyl)-3,3-dimethylindolin-2-ylidene)ethylidene)-2-chlorocyclohex-1-enyl)vinyl)-3,3-dimethyl-3*H*-indolium bromide (15)

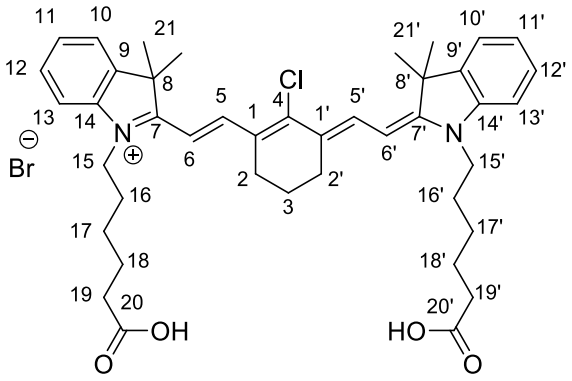

Indolium salt **7** (800 mg, 2.90 mmol), and dialdehyde **13** (130 mg, 0.73 mmol) were stirred with NaOAc (23.0 mg, 0.29 mmol) in acetic anhydride (37.5 mL) and stirred at 70 °C for 2 h under N_2. The reaction was allowed to cool and the resulting mixture was extracted with DCM (25.0 mL) and dried over sodium sulphate. The crude solid was purified by column chromatography [eluting solvent: DCM:MeOH (92:8)] to yield a green solid (67 mg, 68%).

HPLC (method 2) t_r = 7.5 min, Purity 100% (ELSD).
MS (ES): calculated for $C_{42}H_{52}ClN_2O_4$ [M] m/z 683.4. Found 683.3 (100%).
Mp. 219°C.
λ_{abs}= 780 nm, λ_{em}= 805 nm (MeOH); λ_{abs}= 793 nm, λ_{em}= 822 nm (DMSO).
IR (υ): 2924 (O-H), 1725 (C=O), 1545 (C=N), 1006 (C-N) cm^{-1}.
^{1}H NMR (500 MHz, MeOD) δ: 8.48 (d, J = 14.1 Hz, 1H, **5**), 8.46 (d, J = 14.1 Hz, 1H, **5'**), 7.55 (d, J = 7.5 Hz, 2H, **10,10'**), 7.46 (t, J = 8.2 Hz, 2H, **11,11'**), 7.36 (t, J = 7.4 Hz, 2H, **12,12'**), 7.32 (dt, J = 7.7, 2.8 Hz, 2H, **13,13'**), 6.33 (d, J = 14.1 Hz, 1H, **6**), 6.31 (d, J = 14.1 Hz, 1H, **6'**), 4.24 – 4.19 (m, 7.2 Hz, 4H, **15,15'**), 2.76 (t, J = 5.9

Hz, 4H, **2,2'**), 2.38 – 2.31 (m, 4H, **19,19'**), 2.00 – 1.97 (m, 2H, **3**), 1.93 – 1.89(m, 4H, **18,18'**), 1.76 (s, 12H, **21,21'**), 1.75 – 1.71 (m, 4H, **16,16'**), 1.56 – 1.48 (m, 4H, **17,17'**).

^{13}C NMR (126 MHz, MeOD) δ: 173.79 (**20,20'**), 173.01 (**7,7'**), 149.76 (**5**), 144.26 (**5'**), 144.04 (**10**), 142.25 (**10'**), 142.20 (**9**), 141.26 (**9'**), 141.20 (**14**), 128.54 (**14'**), 126.64 (**4**), 126.58 (**1**), 125.24 (**1'**), 125.15 (**12,12'**), 122.16 (**11,11'**), 110.96 (**13**),110.88 (**13'**), 101.07 (**6**), 100.87 (**6'**), 49.25 (**15,15'**), 43.73 (**9,9'**), 43.66 (**19,19'**), 33.36 (**16,16'**), 26.93 (**21,21'**), 26.74 (**18,18'**), 25.96 (**17,17'**), 24.37 (**2,2'**), 24.25 (**3**).

3-(2-((E)-2-((E)-2-chloro-3-((E)-2-(3,3-dimethyl-1-(3-sulfopropyl)indolin-2-ylidene)ethylidene)cyclohex-1-enyl)vinyl)-3,3-dimethyl-3*H*-indolium-1-yl)propane-1-sulfonate (16)

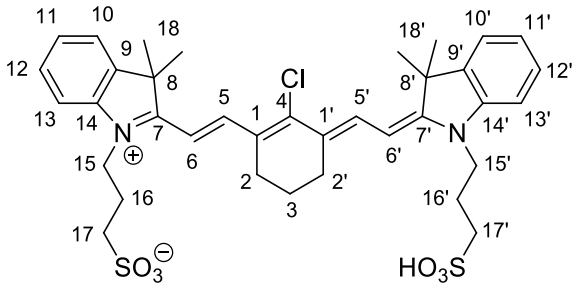

Indolium salt **8** (270.0 mg, 0.96 mmol), dialdehyde **13** (83.3 mg, 0.48 mmol) and NaOAc (80.0 mg, 0.96 mmol) were dissolved in a mixture of acetic acid and acetic anhydride (1:1, 27 mL) and stirred at 70 °C for 3 h under N_2. The solution was allowed to cool and the solvent evaporated. The crude product was purified by column chromatography [eluting solvent: DCM:MeOH (83:17)] to yield a green solid (100 mg, 30%).

HPLC (method 3) t_r = 7.18 min, Purity 95% (ELSD).
MS (ES): calculated for $C_{36}H_{42}ClN_2O_6S_2$ $[M– H]^-$ m/z 697.2. Found 697.0 (100%).
MS (HRMS, ES) m/z calc [M + 2 Na] 743.19627. Found. 743.19790.

Mp. 191°C.

λ_{abs}= 780 nm, λ_{em}= 811 nm (MeOH); λ_{abs}= 797 nm, λ_{em}= 825 nm (DMSO).

IR (υ): 1544 (C=N), 1452 (S=O), 1220 (C-N), 1101 (S=O), 1028 (S-O) cm^{-1}.

^{1}H NMR (500 MHz, MeOD) δ: 8.45 (d, J = 14.1 Hz, 2H, **5,5'**), 7.53 (d, J = 7.4 Hz, 2H, **10,10'**), 7.45 – 7.43 (m, 4H, **11,11', 13,13'**), 7.34 – 7.26 (m, 2H, **12,12'**), 6.47 (d, J = 14.1 Hz, 2H, **6,6'**), 4.44 – 4.37 (m, 4H, **15,15'**), 3.01 (t, J = 6.8 Hz, 4H, **2,2'**), 2.79 (t, J = 6.0 Hz, 4H, **17,17'**), 2.34 – 2.24 (m, 4H, **16,16'**), 2.00 – 1.96 (m, 2H, **3**), 1.75 (s, 12H, **18,18'**).

^{13}C NMR (126 MHz, MeOD) δ: 172.77 (**7,7'**), 150.17 (**5,5'**), 144.44 (**9,9'**), 142.1 (**14,14'**) 141.34 (**4**), 128.71 (**1,1'**), 127.24 (**10,10'**), 124.95 (**12,12'**), 122.12 (**11,11'**), 110.94 (**13,13'**), 101.52 (**6,6'**), 49.23 (**15,15'**), 48.50 (**8,8'**) 42.61 (**16,16'**), 26.75 (**18,18'**), 26.11 (**17,17'**), 22.73 (**2, 2'**), 20.45 (**3**).

2-[2-[2-chloro-3-[2-(1,3-dihydro-1,1,3-trimethyl-2*H*-benz[*e*]indol-2-ylidene)ethylidene]-1-cyclohexen-1-yl]ethenyl]-1,1,3-trimethylbenzeindolium iodide (17)

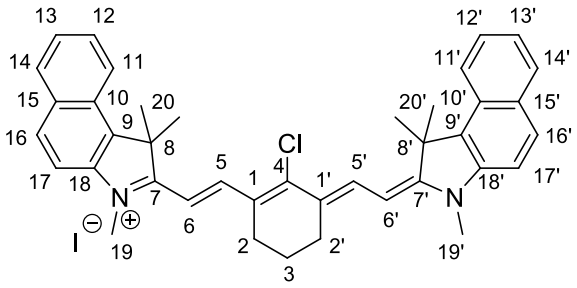

Benz[e]indolium salt **6** (0.26 g, 1.16 mmol), dialdehyde **13** (0.10 g, 0.58 mmol) and NaOAc (0.10 g, 1.16 mmol) were dissolved in a mixture of acetic acid and acetic anhydride (1:1, 20.0 mL) and allowed to stir at 70 °C for 3 h under N_2. The solvent was evaporated and the crude product purified by column chromatography [eluting solvent: DCM:MeOH (94:6)] to yield a green solid (53 mg, 16%).

HPLC (method 2) t_r = 5.36 min, Purity 76% (ELSD), 24% isolated as iodide salt.

MS (ES): calculated for $C_{40}H_{40}ClN_2$ [M] m/z 583.3. Found 583.3 (100%).

Mp.190 °C.

MS (HRMS, ES) m/z calc [M] 583.28745. Found. 583.28800.

λ_{abs}= 812 nm, λ_{em}= 837 nm (MeOH); λ_{abs}= 833 nm, λ_{em}= >850 nm (DMSO).

IR (υ): 1542 (C=N), 1334 (C-N) cm^{-1}.

^{1}H NMR (500 MHz, MeOD) δ: 8.57 (d, J = 13.8 Hz, 2H, **5,5'**), 8.29 (d, J = 8.5 Hz, 2H, **16,16'**), 8.07 -8.01 (m, 4H, **11,11',17,17'**), 7.69 – 7.62 (m, 4H, **12,12',13,13'**), 7.51 (t, J = 8.2 Hz, 2H, **14,14'**), 6.33 (d, J = 13.8 Hz, 2H, **6,6'**), 3.81 (s, 6H, **19,19'**), 2.82-2.76? (m, 4H, **2,2'**), 2.04 (s, 12H, **20,20'**), 2.02 – 2.01 (m, 2H, **3**).

^{13}C NMR (126 MHz, MeOD) δ: 174.82 (**7,7'**), 149.02 (**5,5'**), 143.11 (**9,9'**), 140.34 (**14,14'**), 133.66 (**4**), 132.18 (**1,1'**), 130.43 (**16,16'**), 129.76 (**13,13'**), 127.96 (**12,12'**), 127.43 (**14,14'**), 124.81 (**15,15'**), 122.03 (**10,10'**), 112.10 (**11,11'**), 110.63 (**17,17'**), 100.62 (**6,6'**), 53.50 (**9,9'**), 51.04 (**19,19'**), 30.72 (**20,20'**), 26.40 (**2,2'**), 20.78 (**3**).

2-((E)-2-((E)-2-chloro-3-((E)-2-(1,3,3-trimethyl-5-sulfoindolin-2-ylidene)ethylidene)cyclohex-1-enyl)vinyl)-1,3,3-trimethyl-3*H*-indolium-5-sulfonate (18)

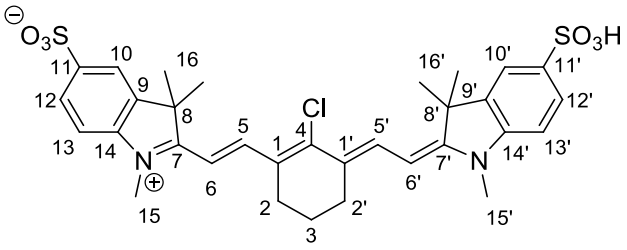

Sulfonated indole **10** (6.7 g, 22.0 mmol), dialdehyde **13** (0.95 g, 5.4 mmol) and NaOAc (0.89 g, 10.8 mmol) were dissolved in a mixture of acetic acid and acetic anhydride (1:1, 285.0 mL) and allowed to stir at 70 °C for 2 h under N_2. The solvent was evaporated and the crude product purified by column chromatography [eluting solvent: DCM:MeOH (80:20)] to yield a green solid (2.0 g, 57%).

HPLC (method 2) t_r = 5.7 min, Purity 99% (ELSD).

MS (ES): calculated for $C_{32}H_{34}ClN_2O_6S_2$ $[M– H]^-$ m/z 641.2. Found 640.9 (100%).

MS (HRMS, ES) m/z calc $[M+H]^+$ 643.16979. Found. 643.16970.

Mp. 170 °C.

IR (υ): 1557 (C=N), 1436 (S=O), 1167 (C-N), 1055 (S=O), 1032 (S-O) cm^{-1}.

λ_{abs}= 783 nm, λ_{em}= 800 nm (MeOH); λ_{abs}= 800 nm, λ_{em}= 833 nm (DMSO).

^{1}H NMR (500 MHz, MeOD) δ: 8.49 (d, J = 14.2 Hz, 2H, **5,5'**), 7.95 (d, J = 1.5 Hz, 2H, **10,10'**), 7.92 (dd, J = 8.3, 1.6 Hz, 2H, **12,12'**), 7.39 (d, J = 8.3 Hz, 2H, **13,13'**), 6.35 (d, J = 14.1 Hz, 2H, **6,6'**), 3.72 (s, 6H, **15,15'**), 2.77 (t, J = 6.1 Hz, 4H, **2,2'**), 2.02 – 1.96 (m, 2H, **3**), 1.79 (s, 12H, **16,16'**).

^{13}C NMR (126 MHz, MeOD) δ: 179.05 (**7,7'**), 175.32 (**5,5'**), 151.64 (**9,9'**), 145.75 (**14,14'**), 143.58 (**4**), 142.44 (**11,11'**), 129.01 (**1,1'**), 128.14 (**12,12'**), 121.34 (**10,10'**), 111.61 (**13,13'**), 103.19 (**6,6'**), 50.54 (**8,8'**) 31.97 (**15,15'**), 28.12(**16,16'**), 27.32 (**2,2'**), 23.32 (**3**).

6.4.2 Synthesis of Heptamethine Cyanine Dyes: Carbon, Oxygen and Sulfur Derivatives

3*H*-Indolium,2-[2-[2-[4-(2-carboxyethyl)phenoxy]-3-[2-(1,3-dihydro-3,3-dimethyl-1-propyl-2*H*-indol-2-ylidene)ethylidene]-1-cyclohexen-1-yl]ethenyl]-3,3-dimethyl-1-propyl-iodide (19)

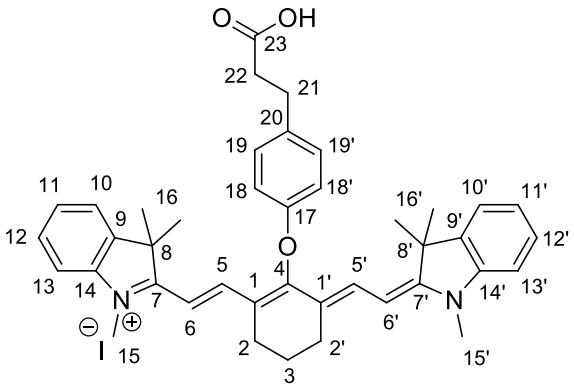

3-(p-Hydroxyphenyl) propionic acid (160.0 mg, 1.0 mmol) was dissolved in anhydrous DMF (7.0 mL) under N_2. NaH (77.0 mg, 1.93 mmol) was added and the

mixture was stirred for 15 min at room temperature. Chloro dye **14** (50.0 mg, 0.1 mmol) was added and the reaction allowed to stir for 3 h at room temperature. The reaction was quenched with water (0.5 mL) and the crude product was purified by column chromatography [eluting solvent: DCM:MeOH (92:8)] to yield a green solid (78 mg, 82%).

HPLC (method 3) t_r = 9.5 min, Purity 75% (ELSD). 13% isolated as iodide salt.

MS (ES): calculated for $C_{41}H_{45}N_2O_3$ [M] m/z 613.3. Found 613.3 (100%).

Mp: 210 °C.

λ_{abs}= 750 nm, λ_{em}= 775 nm (MeOH); λ_{abs}= 777 nm, λ_{em}= 797 nm (DMSO).

^{1}H NMR (500 MHz, MeOD) δ:8.01 (d, *J* = 14.3 Hz, 2H, **5,5'**), 7.44 – 7.34 (m, 4H,**10,10',13,13'**), 7.27 (t, *J* = 8.5 Hz, 4H, **12,12',19,19'**), 7.23 (t, *J* = 7.1 Hz, 2H, **11,11'**), 7.05 (d, *J* = 8.7 Hz, 2H, **18,18'**), 6.14 (d, *J* = 14.2 Hz, 2H, **6,6'**), 3.60 (s, 6H, **15,15'**), 2.87 (t, *J* = 7.4 Hz, 2H, **22**), 2.76 (t, *J* = 6.1 Hz, 4H, **2,2'**), 2.53 (t, *J* = 7.5 Hz, 2H, **21**), 2.06 (dt, *J* = 12.9, 6.6 Hz, 2H, **3**), 1.36 (s, 12H, **16,16'**).

^{13}C NMR (126 MHz, MeOD) δ: 176.89 (**23**), 173.92 (**7,7'**), 165.35(**17**), 159.97 (**5,5'**), 144.09(**10,10'**), 143.30(**4**), 142.24 (**9,9'**), 136.60 (**14,14'**), 131.01 (**20**), 129.59 (**1,1'**), 125.93 (**19,19'**), 123.17 (**12,12'**), 122.95 (**11,11'**), 115.52 (**18,18'**), 111.49(**13,13'**), 100.77 (**6,6'**), 54.63 (**8,8'**), 37.38 (**22**), 31.29 (**21**), 31.15 (**15,15'**), 27.77 (**16,16'**), 25.04 (**2,2'**), 22.19 (**3**).

3*H*-Indolium,2-[2-[3-[2-(1,3-dihydro-1,3,3-trimethyl-2*H*-indol-2-ylidene)ethylidene]-2-[4-[2-[[(1,1-dimethylethoxy)carbonyl]amino]ethyl] phenoxy]-1-cyclohexen-1-yl]ethenyl]-1,3,3-trimethyl iodide (20)

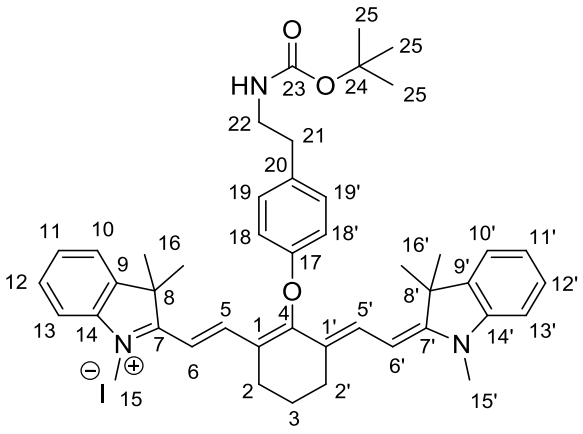

N-Boc-tyramine (420.0 mg, 1.7 mmol) was dissolved in anhydrous MeCN (7.0 mL) under N_2. K_2CO_3 (260.0 mg, 1.8 mmol) was added and the mixture was stirred for 60 min at room temperature. Chloro dye **14** (170 mg, 0.35 mmol) was added and allowed to stir for 30 min at 100 °C under microwave irradiation. The solvent was evaporated and the crude product was purified by column chromatography [eluting solvent: DCM:MeOH (94:6)] to yield a green solid (120 mg, 50%).

HPLC (method 2) t_r = 7.2 min, Purity 100% (ELSD).
MS (ES): calculated for $C_{45}H_{54}N_3O_3$ [M] m/z 684.4. Found 684.4 [M] (100%).
MS (HRMS, ES) m/z calc [M] 684.41597. Found. 684.41640.
Mp. 149 °C.
IR (υ): 1697 (C=O), 1504 (C=N), 1248 (C-O), 1212 (C-N), 1151 (OC-O) cm^{-1}.
λ_{abs}= 762 nm, λ_{em}= 781 nm (MeOH); λ_{abs}= 777 nm, λ_{em}= 803 nm (DMSO).
^{1}H NMR (400 MHz, $CDCl_3$) δ: 7.90 (d, *J* = 14.2 Hz, 2H, **5,5'**), 7.37 (td, *J* = 7.9, 1.2 Hz, 2H, **11,11'**), 7.26 (d, *J* = 6.7 Hz, 2H, **13,13'**), 7.23 – 7.17 (m, 4H, **12,12', 19,19'**), 7.13 (d, *J* = 8.0 Hz, 2H, **10,10'**), 7.01 (d, *J* = 8.6 Hz, 2H, **18,18'**), 6.12 (d, *J* = 14.2 Hz, 2H, **6,6'**), 4.54 (s, 1H, **NH**), 3.69 (s, 6H, **15,15'**), 3.29 (dd, *J* = 13.0, 6.4 Hz, 2H, **22**), 2.82 – 2.74 (m, 6H, **21, 2,2'**), 2.09 – 2.04 (m, 2H, **3**), 1.39 (s, 9H, **25**), 1.36 (s, 12H, **16,16'**).
^{13}C NMR (100 MHz, MeOD) δ: 174.03 (**7,7'**), 165.40 (**23**), 159.99 (**17**), 144.21 (**5,5'**), 143.31 (**4**), 142.32 (**9,9'**), 134.79 (**20**), 131.64 (**14,14'**), 129.68 (**1,1'**), 126.06 (**19,19'**), 123.24 (**12,12'**), 123.19 (**11,11'**), 115.81 (**10,10'**), 111.70 (**18,18'**), 101.05 (**13,13'**), 79.96 (**6,6'**), 54.84 (**24**), 50.10 (**8,8'**), 43.15 (**22**), 36.09 (**21**), 31.69 (**15,15'**), 28.75 (**16,16'**), 28.12 (**25**), 25.27 (**2,2'**), 22.41 (**3**).

2-((E)-2-((E)-2-(4-((*tert*-butoxycarbonylamino)methyl)phenoxy)-3-((E)-2-(1,3,3-trimethyl-5-sulfoindolin-2-ylidene)ethylidene)cyclohex-1-enyl)vinyl)-1,3,3-trimethyl-3*H*-indolium-5-sulfonate (21)

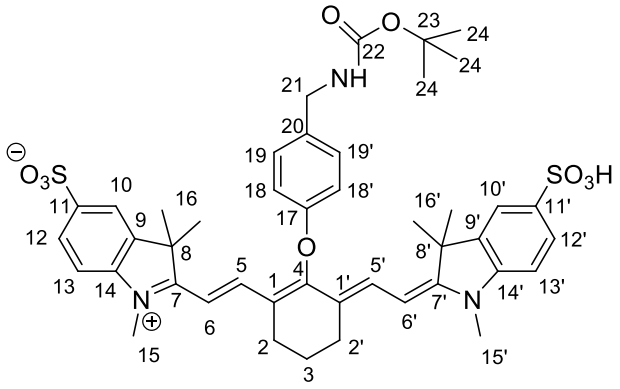

N-[(4-hydroxyphenyl)methyl]-, 1,1-dimethylethyl ester **81** (87.0 mg, 0.39 mmol) and K_2CO_3 (65.0 mg, 0.47 mmol) were stirred under N_2 for 60 min at room temperature in anhydrous DMF. Sulfonated chloro dye **18** (50.0 mg, 0.78 mmol) was added and the mixture stirred at 70 °C for 40 min under microwave irradiation. The crude product was purified by column chromatography [eluting solvent: DCM:MeOH (84:16)] to yield a green solid (22 mg, 34%).

HPLC (method 2) t_r = 6.2 min, Purity 97 % (ELSD).

MS (ES): calculated for $C_{44}H_{51}N_3O_9S_2$ [M] m/z 829.3. Found 829.0 (100%).

MS (HRMS, ES) m/z calc $[M+H]^+$ 830.31395. Found. 830.31100.

Mp. 186 °C.

IR (υ): 1694 (C=O), 1560 (C=N), 1483 (S=O), 1212 (C-O), 1162 (C-N), 1093 (OC-O), 1054 (S=O), 1003 (S-O) cm^{-1}.

λ_{abs}= 768 nm, λ_{em}= 788 nm (MeOH); λ_{abs}= 787 nm, λ_{em}= 814 nm (DMSO).

^{1}H NMR (500 MHz, MeOD) δ: 8.02 (d, *J* = 14.2 Hz, 2H, **5,5'**), 7.86 (dd, *J* = 8.3, 1.7 Hz, 2H, **12,12'**), 7.80 (d, *J* = 1.5 Hz, 2H, **10,10'**), 7.34 (d, *J* = 8.8 Hz, 2H, **19,19'**), 7.29 (d, *J* = 8.3 Hz, 2H, **18,18'**), 7.12-7.08 (m, 2H, **13,13'**), 6.19 (d, *J* = 14.2 Hz, 2H, **6,6'**), 4.16 (s, 2H, **21**), 3.62 (s, 6H, **15,15'**), 2.77 (t, *J* = 5.9 Hz, 4H, **2,2'**), 2.09 – 2.01 (m, 2H, **3**), 1.41 (s, 9H, **24**), 1.39 (s, 12H, **16,16'**).

^{13}C NMR (126 MHz, MeOH) δ: 173.30 (**7,7'**), 164.51 (**22**), 159.06 (**17**), 144.20 (**5,5'**), 142.33 (**9,9'**), 141.83 (**4**), 140.87 (**14,14'**), 129.09 (**11,11'**), 128.15 (**20**), 126.62 (**19,19'**), 122.80 (**18,18'**), 119.80 (**12,12'**), 114.74 (**1,1'**), 114.38 (**10,10'**), 109.86 (**13,13'**), 100.43 (**6,6'**), 78.81 (**23**), 42.86 (**8,8'**), 30.5(**21**), 27.42 (**24**), 27.07 (**2,2'**), 26.65 (**16,16'**), 23.82 (**15,15'**), 20.99 (**3**).

3*H*-Indolium,2-[2-[3-[2-[1,3-dihydro-1,3,3-trimethyl-]-2*H*-indol-2-ylidene]ethylidene]-2-[[2-[[(1,1-dimethylethoxy)carbonyl]amino]ethyl]thio]-1-cyclopenten-1-yl]ethenyl]-1,3,3-trimethyl iodide (22)

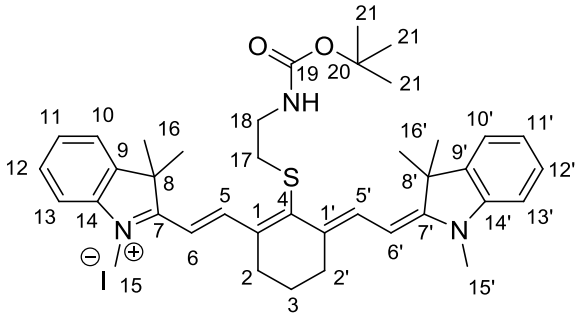

2-(Boc-amino) ethanethiol (92.0 mg, 0.52 mmol) was dissolved in anhydrous DMF (3.5 mL) under N_2. NaH (40.0 mg, 1.7 mmol) was added and the mixture was stirred for 15 min at room temperature. Chloro compound **14** (25.0 mg, 0.52 mmol) was added and allowed to stir for 3 h at room temperature. The solvent was evaporated and the crude product was purified by column chromatography [eluting solvent: DCM:MeOH (94:6)] to yield a green solid (5 mg, 15%).

HPLC (method 2) t_r = 7.2 min, Purity 100% (ELSD).
MS (ES): calculated for $C_{39}H_{50}N_3O_2S$ [M] m/z 624.4. Found 624.1 (100%).
λ_{abs}= 780 nm, λ_{em}= 802nm (MeOH); λ_{abs}= 796 nm, λ_{em}= 830 nm (DMSO).
^{1}H NMR (500 MHz, MeOD) δ: 8.91 (d, J = 14.2 Hz, 2H, **5,5'**), 7.51 (d, J = 7.4 Hz, 2H, **10,10'**), 7.42 (t, J = 7.2 Hz, 2H, **12,12'**), 7.32 – 7.25 (m, 4H, **11,11',13,13'**), 6.28 (d, J = 14.2 Hz, 2H, **6,6'**), 3.66 (s, 6H, **15,15'**), 3.27 – 3.21 (m, 2H, **18**), 2.91 (t, J = 7.2 Hz, 2H, **17**), 2.70 (t, J = 6.1 Hz, 4H, **2,2'**), 1.99 – 1.91 (m, 2H, **3**), 1.77 (s, 12H, **16,16'**), 1.38 (s, 9H, **21**).

^{13}C NMR (126 MHz, MeOD) δ: 173.15 (**7,7'**), 156.38 (**19**), 145.68 (**9,9'**), 143.04 (**14,14'**), 140.95 (**5,5'**), 133.27 (**1,1'**), 128.40 (**4**), 125.11 (**12,12'**), 124.84 (**11,11'**), 121.94 (**10,10'**), 110.37 (**13,13'**), 100.81 (**6,6'**), 78.90 (**20**), 53.40 (**8,8'**), 49.01 (**18**), 48.22 (**17**), 30.19 (**15,15'**), 29.26 (**16,16'**), 27.33 (**21**), 26.90 (**2,2'**), 25.83 (**3**).

2-(2-[2-hydroxy-3-([1,3-dihydro-1,3,3-trimethyl-2*H*-indol-2-ylidene]ethylidene)-1-cyclohexen-1-yl]ethenyl)-1,3,3-trimethylindolium iodide (57)

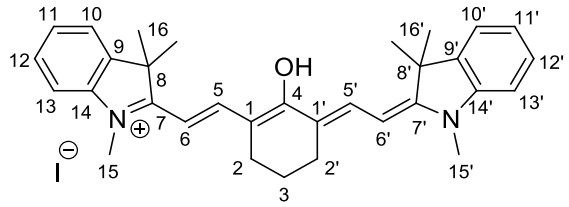

Chloro dye **14** (100.0 mg, 0.21 mmol) and NaOAc (52.0 mg, 0.63 mmol) were dissolved in DMF (5.0 mL) and stirred for 12 h at room temperature under N_2. The reaction was quenched with water (0.5 mL) and the solvent evaporated. The crude product was purified by column chromatography [eluting solvent: DCM:MeOH (95:5)] to yield a green solid (61 mg, 45%).

HPLC (method 7) t_r = 12.3 min, Purity 94% (ELSD).
MS (ES): calculated for $C_{32}H_{37}N_2O$ [M] m/z 465.3. Found 465.4 (100%).
MS (HRMS, ES) m/z calc [M] 465.29004. Found 465.28900.
^{1}H NMR (500 MHz, $CDCl_3$) δ: 8.20 (d, J = 13.1 Hz, 2H, **5,5'**), 7.24 – 7.18 (m, J = 7.8 Hz, 4H, **12,12',13,13'**), 6.93 (t, J = 7.3 Hz, 2H, **11,11'**), 6.72 (d, J = 7.6 Hz, 2H, **10,10'**), 5.44 (d, J = 13.2 Hz, 2H, **6,6'**), 3.24 (s, 6H, **15,15'**), 2.65 (t, J = 5.0 Hz, 4H, **2,2'**), 1.94 – 1.85 (m, 2H, **3**), 1.70 (s, 12H, **16,16'**).
^{13}C NMR (126 MHz, $CDCl_3$) δ: 186.50 (**7,7'**), 163.20 (**4**), 144.64 (**5,5'**), 139.64 (**9,9'**), 132.71 (**14,14'**), 127.65 (**1,1'**), 126.89 (**12,12'**), 121.75 (**11,11'**), 120.49 (**10,10'**), 106.43 (**13,13'**), 92.55 (**6,6'**), 46.45 (**8,8'**), 29.30 (**2,2'**), 28.72 (**16,16'**), 25.88 (**15,15'**), 22.57 (**3**).

The substitution of Cl to OH was confirmed by observing a colour change from green to red by increasing the pH.

2-((E)-2-((E)-2-(4-carboxyphenyl)-3-((E)-2-(1,3,3-trimethyl-5-sulfoindolin-2-ylidene)ethylidene)cyclohex-1-enyl)vinyl)-1,3,3-trimethyl-3*H*-indolium-5-sulfonate (23)

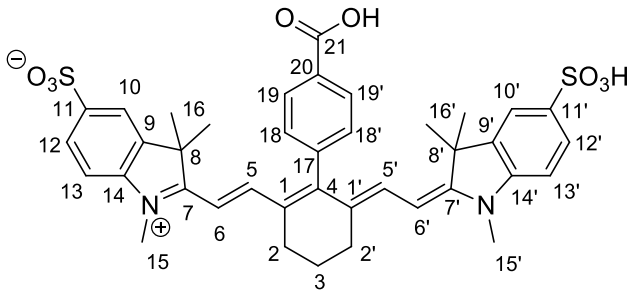

Sulfonated chloro dye **18** (500.0 mg, 7.8 mmol), 4-carboxyphenylboronic acid (230.0 mg, 1.4 mmol), $Pd(OAc)_2$ (12.6 mg, 0.17 mmol) and triphenylphosphine (44.1 mg, 0.17 mmol) were dissolved in H_2O (10.0 mL) and stirred at under reflux for 15 h. The solvent was evaporated and the green residue was purified by column chromatography [eluting solvent: DCM:MeOH:AcOH (86:13:1)] to yield a green solid (100 mg, 18%). Starting material was recovered (80%).

HPLC (method 2) t_r = 6.8 min, Purity 100% (ELSD).

MS (ES): calculated for $C_{39}H_{39}N_2O_8S_2$ $[M-H]^-$ m/z 728.2. Found 727.4(100%).

MS (HRMS, ES) m/z calc $[M-H]^-$ 727.21533. Found 727.21810.

Mp. 265 °C.

IR (υ): 3380 (O-H), 1704 (C=O), 1547 (C=N), 1339 (S=O), 1184 (C-O), 1163 (C-N), 1092 (S=O), 1009, (S-O) cm^{-1}.

λ_{abs}= 780 nm, λ_{em}= 805 nm (DMSO).

^{1}H NMR (500 MHz, MeOD) δ: 8.24 (d, *J* = 8.0 Hz, 2H, **5,5'**), 7.80 (dd, *J* = 8.3, 1.6 Hz, 2H**, 12,12'**), 7.72 (d, *J* = 1.6 Hz, 2H, **10,10'**), 7.26 (m, 4H, **19,19',18,18'**), 7.21

(d, *J* = 8.4 Hz, 2H, **13,13'**), 6.21 (d, *J* = 14.1 Hz, 2H, **6,6'**), 3.56 (s, 6H, **15,15'**), 2.74 (t, *J* = 6.0 Hz, 4H, **2,2'**), 2.10 – 2.02 (m, 2H, **3**), 1.18 (s, 12H, **16,16'**).

^{13}C NMR (126 MHz, MeOD)δ: 176.83 (**7,7'**), 172.88 (**21**), 162.67 (**17**), 148.30 (**4**), 144.25 (**5,5'**), 141.55 (**9,9'**), 141.19 (**14,14'**), 140.55 (**11,11'**), 136.71 (**19,19'**), 132.12 (**17**), 129.52 (**12,12',10,10'**), 128.94 (**18,18'**), 126.62 (**13,13'**), 119.74 (**20**), 109.67 (**1,1'**), 100.47 (**6,6'**), 48.36 (**8,8'**), 30.26 (**15,15'**), 24.26 (**2,2'**), 21.32 (**16,16'**), 21.09 (**3**).

The surprisingly low coupling constant for the *trans* system was also observed by Achilefu in the synthesis of similar molecules[129].

6.4.3 Synthesis of Heptamethine Cyanine Dyes: Amino Derivatives

1,3,3-trimethyl-2-((E)-2-((E)-3-((E)-2-(1,3,3-trimethyl-5-sulfoindolin-2-ylidene)ethylidene)-2-(4-vinylbenzylamino)cyclohex-1-enyl)vinyl)-3*H*-indolium-5-sulfonate (24)

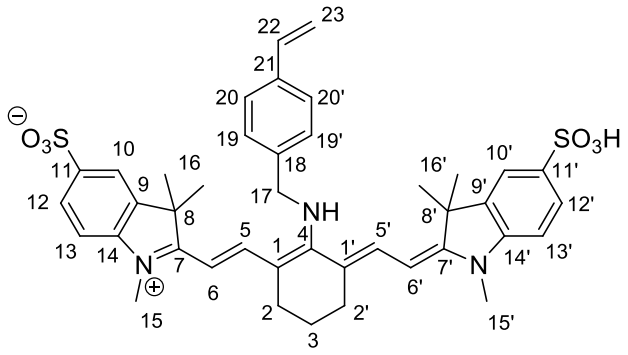

Sulfonated chloro dye **18** (72.0 mg, 0.11 mmol), 4-aminomethyl styrene (30.0 mg, 0.23 mmol) and TEA (31.0 µL, 0.23 mmol) were dissolved in MeOH (2.0 mL) and stirred at 100 °C for 1 h under microwave irradiation in a sealed vial. The solvent was evaporated and the residue purified by column chromatography [eluting solvent: DCM:MeOH (85:15)] to yield a blue solid (71 mg, 85%).

HPLC (method 3) t_r = 10.9 min, Purity 90 % (ELSD).

MS (ES): calculated for $C_{41}H_{44}N_3O_6S_2$ $[M-H]^-$ m/z 738.3 Found. 738.5 (35%), 368.8 $[M-2H]^{2-}$ (40%).

MS (HRMS, ES) m/z calc. 740.28226. Found 740.28248.

Mp. 226 °C decomposed.

IR (υ): 1524 (C=N), 1480 (S=O), 1168 (S=O), 1109 (C-N), 1020 (S-O) cm^{-1}.

λ_{abs}= 635 nm λ_{em}= 738 nm (MeOH), λ_{abs}= 640 nm, λ_{em}= 764 nm (DMSO).

^{1}H NMR (500 MHz, MeOD) δ: 7.79 (dd, *J* = 8.3, 1.4 Hz, 2H, **12,12'**), 7.72 (d, J = 1.5 Hz, 2H, **10,10'**), 7.68 (d, *J* = 12.8 Hz, 2H, **5,5'**), 7.57 (d, *J* = 8.0 Hz, 2H, **19,19'**), 7.38 (d, *J* = 8.0 Hz, 2H,**20,20'**), 7.09 (d, *J* = 8.3 Hz,2H**13,13'**), 6.83 (dd, *J* = 17.6, 11.0 Hz, 1H, **22**), 5.87 (m, 2H, **23**), 5.33 (d, *J* = 10.9 Hz, 2H, **6,6'**), 4.94 (s, 2H, **17**), 3.44 (s, 6H, **15,15'**), 2.62 (t, *J* = 6.1 Hz, 4H, **2,2'**), 1.92-1.88 (dt, m, 2H, **3**), 1.47 (s, 12H, **16,16'**).

^{13}C NMR (126 MHz, MeOD) δ: 170.44 (**7,7'**), 147.03 (**5,5'**), 141.64 (**4**), 141.30 (**9,9'**), 140.95 (**14,14'**), 139.67 (**18**), 139.39 (**21**), 138.05 (**22**), 129.52 (**11,11'**), 128.78 (**12,12'**), 128.27 (**20,20,19,19'**), 123.64 (**1,1'**), 121.37 (**10,10'**), 115.50 (**13,13'**), 109.66 (**23**), 97.34 (**6,6'**), 55.23 (**8,8'**), 29.13 (**16,16'**), 28.99 (**17**), 28.65 (**2,2'**), 26.64 (**15,15'**), 23.32 (**3**).

1,3,3-trimethyl-2-((E)-2-((E)-3-((E)-2-(1,3,3-trimethylindolin-2-ylidene)ethylidene)-2-(4-vinylbenzylamino)cyclohex-1-enyl)vinyl)-3*H*-indolium iodide (25)

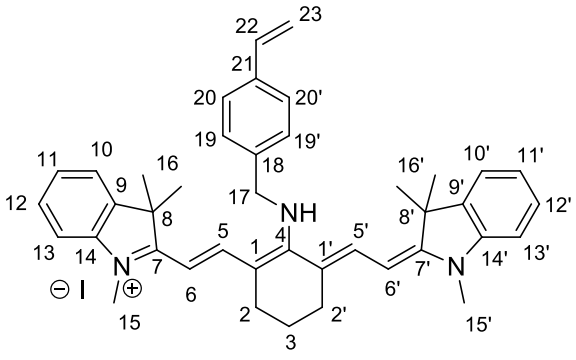

Chloro compound **14** (0.20 g, 0.41 mmol), 4-aminomethylstyrene (0.14 g, 1.04 mmol) and TEA (176.0 µL, 1.24 mmol) were dissolved in MeOH (4 mL) and stirred at 100 °C for 90 min under microwave irradiation. The solvent was evaporated and the residue purified by column chromatography [eluting solvent: DCM] to yield a blue solid (0.17 g, 69%).

HPLC (method 2) t_r = 5.7 Purity 95% (ELSD).

MS (ES): calculated for $C_{41}H_{46}N_3$ [M] m/z 580.4. Found 580.4 (100%).

MS (HRMS, ES) m/z calc 581.37645. Found 581.37694.

Mp. 138 °C.

IR (υ): 1562 (C=N), 1453 (S=O), 1165 (S=O), 1100 (C-N), 1069 (S-O) cm^{-1}.

λ_{abs}= 650 nm, λ_{em}= 760 nm (DMSO).

^{1}H NMR (500 MHz, CD_3CN) *δ*: 7.64 (d, *J* = 13.2 Hz, 2H, **5,5'**), 7.55 (d, *J* = 8.1 Hz, 2H, **20,20'**), 7.39 (d, *J* = 8.1 Hz, 2H, **10,10'**), 7.36 – 7.33 (m, 4H, **12,12',19,19'**), 7.10-7.13 (m, 2H, **11,11'**), 7.06 (d, *J* = 7.8 Hz, 2H, **13,13'**), 6.85 (dd, *J* = 17.7, 10.9 Hz, 1H, **22**), 5.89 (d, *J* = 17.7 Hz, 1H, **6 or 6'**), 5.80 (d, *J* = 13.2 Hz, 2H, **23**), 5.34 (d, *J* = 11.6 Hz, 1H, **6 or 6'**), 4.85 (s, 2H, **17**), 3.41 (s, 6H, **15,15'**), 2.56 (t, *J* = 6.3 Hz, 4H, **2,2'**), 1.88 – 1.81 (m, 2H, **3**), 1.47 (s, 12H, **16,16'**).

^{13}C NMR (126 MHz, CD_3CN) *δ*: 169.31 (**7,7'**), 168.22 (**5,5'**), 143.78 (**4**), 140.17 (**9,9'**), 139.59 (**14,14'**), 138.25 (**18**), 137.55 (**21**), 136.35 (**22**), 128.68 (**12,12'**), 128.22 (**19,19'**), 126.95 (**20,20'**), 122.92 (**11,11'**), 121.84 (**10,10'**), 120.79 (**13,13'**), 114.11 (**23**), 109.08 (**1,1'**), 95.20 (**6,6'**), 53.74 (**8,8'**), 47.56 (**17**), 30.18 (**2,2'**), 27.56 (**16,16'**), 24.72 (**15,15'**), 21.59 (**3**).

2-((E)-2-((E)-2-(4-((*tert*-butoxycarbonylamino)methyl)benzylamino)-3-((E)-2-(1,3,3-trimethylindolin-2-ylidene)ethylidene)cyclohex-1-enyl)vinyl)-1,3,3-trimethyl-3*H*-indolium iodide (26)

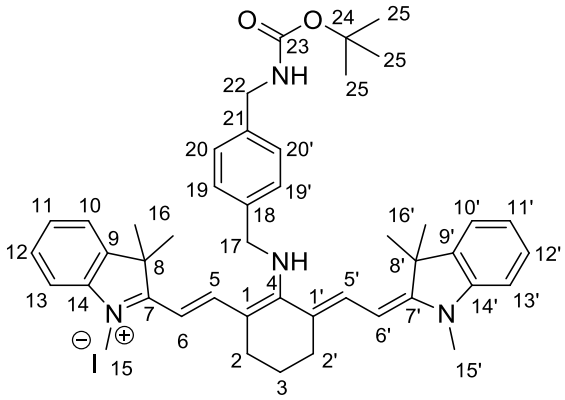

1-(*N*-boc-aminomethyl)-4-(aminomethyl) benzene (0.15 g, 0.62 mmol), TEA (86.0 µL, 0.62 mmol) and chloro dye **14** (0.15 g, 0.31 mmol) were dissolved in MeOH (2.5 mL) and stirred at 70 °C for 4 h. The solvent was evaporated and the crude product was purified by column chromatography [eluting solvent: DCM:MeOH (99:1)] to yield a blue solid (0.13 g, 60%).

HPLC (method 1) t_r = 4.6 min, Purity 100% (ELSD).

MS (ES): calculated for $C_{45}H_{55}N_4O_2$ [M] m/z 683.4. Found 683.4 (100%).

MS (HRMS, ES) m/z calc. 684.43978. Found 684.43945.

Mp. 198 °C.

IR (υ): 3332 (N-H), 3238 (N-H), 1683 (C=O), 1512 (C=N), 1250 (C-O), 1162 (C-N) cm^{-1}.

λ_{abs}= 642 nm, λ_{em}= 737 nm (MeOH); λ_{abs}= 640 nm, λ_{em}= 758 nm (DMSO).

^{1}H NMR (500 MHz, MeOD) δ: 7.74 (d, J = 13.0 Hz, 2H, **5,5'**), 7.46 -7.39 (m, 6H, **20,20',19,19',12,12'**), 7.34 (d, J = 7.6 Hz, 2H, **10,10'**), 7.15 -7.10 (m, 4H, **11,11',13,13'**), 5.86 (d, J = 13.1 Hz, 2H, **6,6'**), 4.92 (bs, 2H, **17**), 4.36 (bs, 2H, **22**), 3.47 (s, 6H, **15,15'**), 2.63 (t, J = 6.0 Hz, 4H, **2,2'**), 1.96 – 1.89 (m, 2H, **3**), 1.50 (s, 21H, **16,16',25**).

^{13}C NMR (126 MHz, MeOD) δ: 169.07 (**7,7'**), 168.78 (**23**), 157.16 (**5,5'**), 143.53 (**4**), 140.09 (**9,9'**), 139.67 (**14,14'**), 137.06 (**21**), 127.99 (**18**), 127.80 (**20,20'**), 127.60 (**19,19'**), 125.82 (**1,1'**), 122.68 (**12,12'**), 121.76 (**11,11'**), 120.69 (**10,10'**), 108.61 (**13,13'**), 94.88 (**6,6'**), 78.81 (**24**), 53.56 (**8,8'**), 46.66 (**17**), 43.37 (**22**), 29.36 (**15,15'**), 27.53 (**16,16'**), 27.43 (**25**), 24.73 (**2,2'**), 21.68 (**3**).

2-((E)-2-((E)-2-(4-((*tert*-butoxycarbonylamino)methyl)benzylamino)-3-((E)-2-(1,3,3-trimethyl-5-sulfoindolin-2-ylidene)ethylidene)cyclohex-1-enyl)vinyl)-1,3,3-trimethyl-3*H*-indolium-5-sulfonate (27)

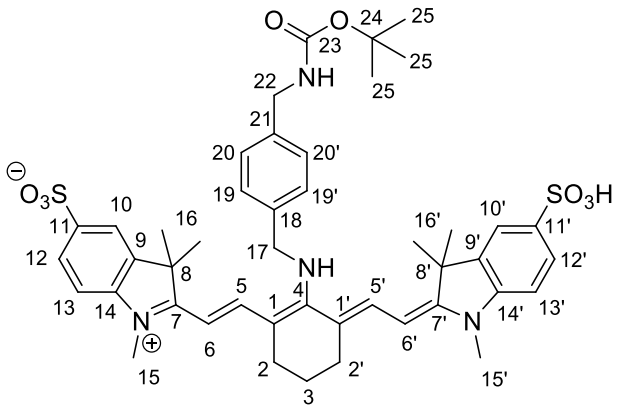

Sulfonated chloro dye **18** (0.15 g, 0.23 mmol), 1-(*N*-boc-aminomethyl)-4-(aminomethyl) benzene (0.16 g, 0.69 mmol) and TEA (95.0 µL, 0.69 mmol) were dissolved in MeOH and stirred at 70 °C for 4 h under N_2. The solvent was evaporated and the residue purified by column chromatography [eluting solvent: DCM:MeOH (80:20)] to yield a blue solid (0.15 g, 79%).

HPLC (method 2) t_r = 6.6 min, Purity 100% (ELSD).

MS (ES): calculated for $C_{45}H_{54}N_4O_8S_2$ [M] m/z 842.3. Found 842.3 (100%).

Mp. 220 °C decomposed.

IR (υ): 1523 (C=O), 1479 (C=N), 1397 (S=O) 1166 (C-O), 1062 (S=O), 1018 (S-O) cm^{-1}.

λ_{abs}= 630 nm, λ_{em}= 740 nm (MeOH), λ_{abs}= 632 nm, λ_{em}= 764 nm (DMSO).

^{1}H NMR (500 MHz, MeOD) δ: 7.81 (dd, J = 8.3, 1.7 Hz, 2H, **12,12'**), 7.77 (s, 2H, **10,10'**), 7.71 (d, J = 13.0 Hz, 2H, **5,5'**), 7.43-7.35 (m, 4H, **19,19',20,20'**), 7.09 (d, J = 8.3 Hz, 2H, **13,13'**), 5.86 (d, J = 12.8 Hz, 2H, **6,6'**), 4.93 (s, 2H, **17**), 4.31 (s, 2H, **22**), 3.44 (s, 6H, **15,15'**), 2.62 (t, J = 6.3 Hz, 4H, **2,2'**), 1.94 – 1.87 (m, 2H, **3**), 1.51 (s, 12H, **15,15'**), 1.46 (s, 9H, **25**).

^{13}C NMR (126 MHz, MeOD) δ: 170.17 (**7,7'**), 168.60 (**23**), 145.09 (**5,5'**), 140.22 (**4**), 139.51 (**9,9'**), 138.91 (**14,14'**), 138.76 (**21**), 136.56 (**18**), 127.68 (**11,11'**), 127.34 (**12,12'**), 126.42 9 (**1,1'**), 121.59 (**20,20'**), 119.64 (**19,19'**), 113.32 (**10,10'**), 107.71 (**13,13'**), 95.33 (**6,6'**), 78.88 (**24**), 53.22 (**8,8'**), 33.51 (**17**), 31.68 (**22**), 29.36 (**15,15'**), 27.52 (**25**), 27.25 (**16,16'**), 24.81 (**2,2**), 22.38 (**3**).

2-((E)-2-((E)-2-(6-(*tert*-butoxycarbonylamino)hexylamino)-3-((E)-2-(1,3,3-trimethylindolin-2-ylidene)ethylidene)cyclohex-1-enyl)vinyl)-1,3,3-trimethyl-3*H*-indolium iodide (28)

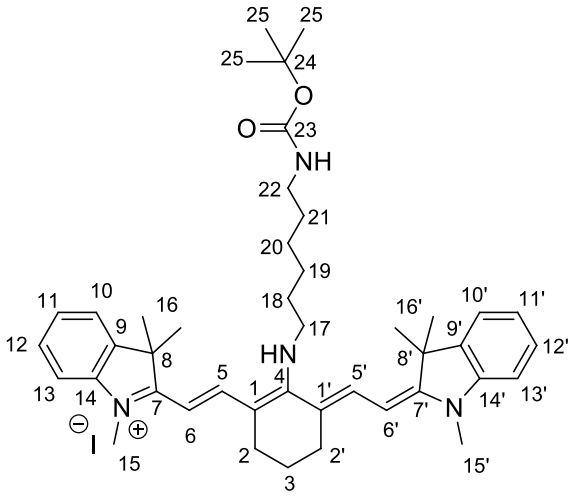

Chloro compound **14** (100.0 mg, 0.21 mmol), *N*-1-boc-1,6-diaminohexane (130.0 mg, 0.62 mmol) and TEA (86.0 µL, 0.62 mmol) were dissolved in MeOH (2.5 mL) and stirred for 4 h at 70 °C. The solvent was evaporated and the crude product was purified by column chromatography [eluting solvent: DCM:MeOH (99:1)] to yield a blue solid (80 mg, 57%).

HPLC (method 2) t_r = 7.2 min, Purity 100% (ELSD).

MS (ES): calculated for $C_{43}H_{59}N_4O_2$ [M] m/z 663.5. Found 663.4 (100%).

MS (HRMS, ES) m/z calc 664.47108. Found 664.47111.

Mp. 136 °C.

IR (υ): 1690 (C=O), 1523 (C=N), 1165 (C-O), 1100 (C-N) cm^{-1}.

λ_{abs}= 622 nm, λ_{em}= 750 nm (MeOH); λ_{abs}= 626 nm, λ_{em}= 763 nm (DMSO).

^{1}H NMR (500 MHz, MeOD) *δ*: 7.79 (d, *J* = 13.0 Hz, 2H, **5,5'**), 7.40 (d, *J* = 7.3 Hz, 2H, **10,10'**), 7.35-7.31 (m, 2H, **12,12'**), 7.13-7.08 (m, 4H, **11,11',13,13'**), 5.81 (d, *J* = 12.9 Hz, 2H, **6,6'**), 3.80 (t, *J* = 6.7 Hz, 2H, **17**), 3.46 (s, 6H, **15,15'**), 3.06 (t, *J* = 6.9 Hz, 2H, **22**), 2.58 (t, *J* = 6.2 Hz, 4H, **2,2'**), 1.88 – 1.81 (m, 4H, **3,18**), 1.68 (s, 12H, **16,16'**), 1.56-1,46 (m, 6H, **19,20,21**), 1.42 (s, 9H, **25**).

^{13}C NMR (126 MHz, MeOD) *δ*: 169.74 (**7,7'**), 168.47 (**23**), 157.18 (**5,5'**), 143.65 (**4**), 139.78 (**9,9'**), 138.84 (**14,14'**), 128.02 (**12,12'**), 122.51 (**11,11'**), 121.63 (**10,10'**), 120.31 (**1,1'**), 108.41 (**13,13'**), 94.18 (**6,6'**), 78.43 (**24**), 50.24 (**8,8'**), 39.81 (**17**), 31.13 (**22**), 29.65 (**18**), 29.36 (**19**), 29.08 (**21**), 27.70 (**16,16'**), 27.42 (**25**), 26.28 (**2,2'**), 26.17 (**20**), 24.59 (**15,15'**), 21.58 (**3**).

2-((E)-2-((E)-2-(2,2-dimethyl-4-oxo-3,8,11-trioxa-5-azatridecan-13-ylamino)-3-((E)-2-(1,3,3-trimethylindolin-2-ylidene)ethylidene)cyclohex-1-enyl)vinyl)-1,3,3-trimethyl-3*H*-indolium iodide (29)

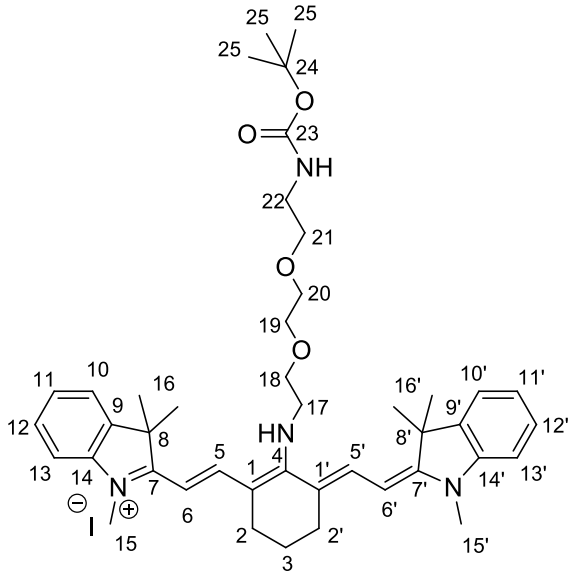

Chloro dye **14** (75.0 mg, 0.16 mmol), ***N***-[2-[2-(2-aminoethoxy)ethoxy]ethyl]-,1,1-dimethylethyl ester (116.0 mg, 0.47 mmol) and TEA (64.0 µL, 0.47 mmol) were dissolved in MeOH (2.0 mL) and stirred for 4 h at 70 °C. The solvent was evaporated and the crude product was purified by column chromatography [eluting solvent: DCM:MeOH (95:5)] to yield a blue solid (34 mg, 31%).

HPLC (method 2) t_r = 7.1 min, Purity 100% (ELSD).

MS (ES): calculated for $C_{43}H_{59}N_3O_4$ [M] m/z 695.5. Found 695.2 (100%).

MS (HRMS, ES) m/z calc 696.46091. Found 696.46036.

Mp. 125 °C.

IR (υ): 1724 (C=O), 1562 (C=N), 1166 (OC-O), 1094 (C-O), 1041 (C-N) cm^{-1}.

λ_{abs}= 635 nm, λ_{em}= 750 nm (MeOH); λ_{abs}= 639 nm, λ_{em}= 766 nm (DMSO).

^{1}H NMR (400 MHz, MeOD) δ: 7.87 (d, *J* = 13.1 Hz, 2H, **5,5'**), 7.41 (d, *J* = 7.2 Hz, 2H, **10,10'**), 7.34 (td, *J* = 7.8, 1.0 Hz, 2H, **12,12'**), 7.12 (m, 4H, **11,11',13,13'**), 5.84 (d, *J* = 13.1 Hz, 2H, **6,6'**), 3.94 (t, *J* = 4.7 Hz, 2H, **21**), 3.82 (t, 5.9 Hz, 2H, **20**), 3.71

– 3.66 (m, 6H, **17,18,19**), 3.64-3.63 (m, 2H, **22**), 3.49 (s, 6H, **15,15'**), 2.58 (t, *J* = 6.3 Hz, 4H, **2,2'**), 1.91 – 1.82 (m, 2H, **3**), 1.70 (s, 12H, **16,16'**), 1.46 (s, 9H, **25**).
^{13}C NMR (100 MHz, MeOD) *δ*: 168.99 (**7,7'**), 143.63 (**23**), 139.92 (**5,5'**), 139.49 (**4**), 128.04 (**9,9'**), 122.72 (**14,14'**), 121.66 (**12,12'**), 120.56 (**11,11'**), 108.59 (**10,10'**), 94.66 (**13,13'**), 78.70 (**1,1'**), 70.21 (**6,6'**), 69.99 (**24**), 69.94 (**22**), 69.90 (**19**), 69.74 (**18**), 60.83 (**20**), 49.74 (**8,8'**), 39.84 (**21**), 39.03 (**17**), 31.68 (**2,2'**), 29.36 (**15,15'**), 27.74 (**25**), 27.39 (**16,16'**), 24.47 (**3**).

2-((E)-2-((E)-2-(2,2-dimethyl-4-oxo-3,8,11-trioxa-5-azatridecan-13-ylamino)-3-((E)-2-(1,3,3-trimethyl-5-sulfoindolin-2-ylidene)ethylidene)cyclohex-1-enyl)vinyl)-1,3,3-trimethyl-3*H*-indolium-5-sulfonate (30)

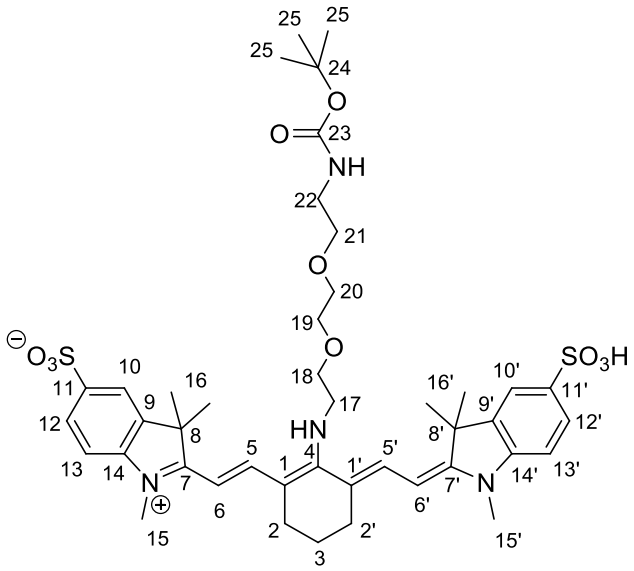

Sulfonated chloro dye **18** (0.15 g, 0.23 mmol), ***N***-[2-[2-(2-aminoethoxy)ethoxy]ethyl]-,1,1-dimethylethyl ester (0.17 g, 0.7 mmol) and TEA (97.0 µL, 0.7 mmol) were dissolved in MeOH (3 mL) and stirred for 4 h at 70 °C. The solvent was evaporated and the crude product was purified by column chromatography [eluting solvent: DCM:MeOH (82:18)] to yield a blue solid (0.18 g, 90%).

HPLC (method 2) t_r =6.0 min, Purity 95% (ELSD).

MS (ES): calculated for $C_{43}H_{57}N_4O_{10}S_2$ $[M-H]^-$ m/z 853.4. Found 853.0 (20%), 426.1 $[M -2H]^{2-}$ (100%).

MS (HRMS, ES) m/z calc 855.36671. Found 855.36642.

Mp. 103 °C.

IR (υ): 1704 (C=O) 1530 (C=N), 1475 (S=O), 1206 (S=O), 1170 (OC-O), 1105 (C-O), 1064 (C-N), 1020 (S-O) cm^{-1}.

λ_{abs}= 634 nm, λ_{em}= 770 nm (DMSO).

^{1}H NMR (500 MHz, MeOH) δ: 7.90 (d, *J* = 1.6 Hz, 2H, **10,10'**), 7.88 – 7.86 (m, 4H, **5,5',12,12'**), 7.18 (d, *J* = 8.2 Hz, 2H, **13,13'**), 5.94 (d, *J* = 12.7 Hz, 2H, **6,6'**), 4.05 (t, *J* = 4.8 Hz, 2H, **21**), 3.91 (t, *J* = 4.8 Hz, 2H, **20**), 3.79 (dt, *J* = 8.7, 3.6 Hz, 6H, **17,18,19**), 3.59 (t, *J* = 5.8 Hz, 2H, **22**), 3.55 (s, 6H, **15,15'**), 2.67 (t, *J* = 6.3 Hz, 4H, **2,2'**), 1.98 – 1.92 (m, 2H, **3**), 1.78 (s, 12H, **16,16'**), 1.48 (s, 9H, **25**).

2-((E)-2-((E)-2-(*N*-(2,2-dimethyl-4-oxo-3,8,11-trioxa-5-azatridecan-13-yl)acetamido)-3-((E)-2-(1,3,3-trimethyl-5-sulfoindolin-2-ylidene)ethylidene)cyclohex-1-enyl)vinyl)-1,3,3-trimethyl-3*H*-indolium-5-sulfonate (38)

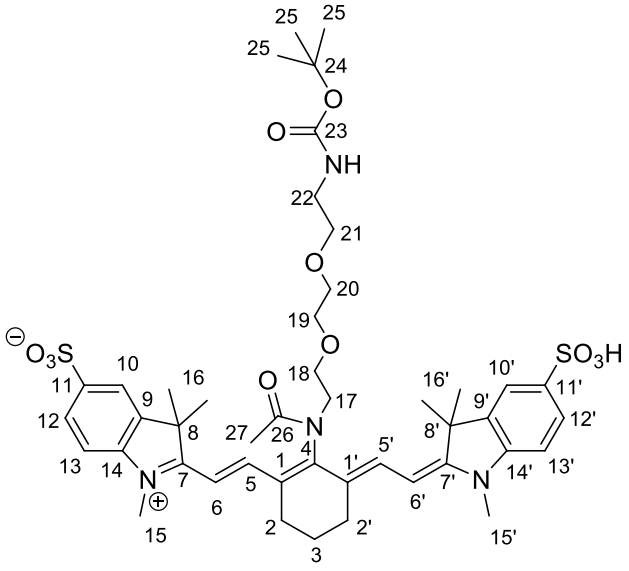

Amino dye **30** (50.0 mg, 0.6 mmol) was dissolved in anhydrous MeCN (1.0 mL) and cooled to 0 °C. While stirring, acetyl chloride (6.2 µL, 0.7 mmol) was added and left to stir for 30 min at room temperature. The solvent was evaporated and the residue purified by column chromatography [eluting solvent: DCM:MeOH (85:15)] to yield a green solid (26 mg, 50%).

HPLC (method 2) t_r =7.4 min, Purity 100% (ELSD).
MS (ES): calculated for $C_{45}H_{59}N_4O_{11}S_2$ $[M-H]^-$ m/z 895.4. Found 895.9 (100%).
λ_{abs}= 685 nm, λ_{em}= 714 nm (DMSO).
^{1}H NMR (500 MHz, D_2O) δ: 7.86 (s, 2H, **10, 10'**), 7.76 (d, *J* = 8.4 Hz, 2H, **12,12'**), 7.43 (d, *J* = 13.8 Hz, 2H, **5,5'**), 7.09 (d, *J* = 8.4 Hz, 2H, **13,13'**), 6.18 (d, *J* = 14.0 Hz, 2H, **6,6'**), 3.88 (t, 5.7 Hz, 2H, **18**), 3.49 (s, 3H, **27**), 3.42 (m, 8H, **2,2',19,20**), 3.22 (quartet, J = 7.28, 4H, **17,22**) 3.13 (t, *J* = 5.0 Hz, 2H, **21**), 2.44 (m, 2H, **3**), 1.59 (s, 6H, **16 or 16'**), 1.41 (s, 6H, **16 or 16'**), 1.27 (s, 9H, **25**).
^{13}C NMR (126 MHz, D_2O) δ: 173.44 (**26**), 173.19 (**7,7'**), 157.90 (**23**), 144.40 (**11**, **11'**), 141.29 (**14,14',9,9'**), 139.41 (**5,5'**), 128.79 (**4**), 126.90 (**1,1'**), 119.60 (**10,10',12,12'**), 111.11 (**13,13'**), 102.46 (**6,6'**), 99.46 (**24**), 96.92 (**8,8'**) 69.39 (**18**), 67.73 (**21**), 48.71 (**19,20**), 46.66 (**17**), 31.13 (**2,2'**), 27.64 (**22**), 27.55 (**27**), 27.03 (**16,16'**), 26.80 (**15,15'**), 24.46 **(25**), 20.89 (**3**).

2-((E)-2-((E)-2-(benzylamino)-3-((E)-2-(1,3,3-trimethyl-5-sulfoindolin-2-ylidene)ethylidene)cyclohex-1-enyl)vinyl)-1,3,3-trimethyl-3*H*-indolium-5-sulfonate (31)

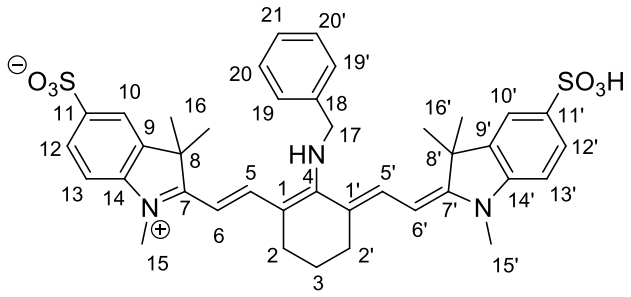

Sulfonated chloro dye **18** (100.0 mg, 0.16 mmol), benzylamine (51.0 µL, 0.47 mmol) and TEA (64.0 µL, 0.47 mmol) were dissolved in MeOH (1.5 mL) and stirred at 70 °C for 4 h. The solvent was evaporated and the residue purified by column chromatography [eluting solvent: DCM:MeOH (87:13)] to yield a blue solid (61 mg, 55%).

HPLC (method 1) t_r = 6.8 min, Purity 83% (ELSD).

MS (ES): calculated for $C_{39}H_{43}N_3O_6S_2$ $[M-H]^-$ m/z 712.3. Found 712.3 (40%), 355.6 $[M - 2H]^{2-}$ (100%).

Mp. 260 °C decomposed.

IR (υ): 1538 (C=N), 1475 (S=O), 1170 (S=O), 1115 (C-N), 1024 (S-O) cm^{-1}.

λ_{abs}= 685 nm, λ_{em}= 714 nm (DMSO).

^{1}H NMR (500 MHz, MeOD) δ: 7.80 (dd, *J* = 8.3, 1.5 Hz, 2H, **12,12'**), 7.74 (s, 2H, **10,10'**), 7.71 (d, *J* = 12.9 Hz, 2H, **5,5'**), 7.52-7.40 (m, 5H,**19,19',20,20',21**), 7.08 (d, *J* = 8.3 Hz, 2H, **13,13'**), 5.86 (d, *J* = 12.9 Hz, 2H, **6,6'**), 4.96 (s, 2H, **17**), 3.44 (s, 6H, **15,15'**), 2.63 (t, *J* = 6.2 Hz, 4H, **2,2'**), 1.92-1.88 (m, 2H, **3**), 1.49 (s, 12H, **16,16'**).

^{13}C NMR (126 MHz, MeOD) δ: 168.70 (**7,7'**), 145.14 (**5,5'**), 139.52 (**4**), 139.05 (**9,9'**), 137.92 (**14,14'**), 129.17 (**11,11', 12,12'**), 128.00 (**18**), 127.30 (**19,19',10,10'**), 126.39 (**21**), 121.52 (**20,20'**), 119.56 (**13,13'**), 107.70 (**1,1'**), 95.29 (**6,6'**), 53.57 (**8,8'**), 29.34 (**17**), 27.21 (**16,16'**), 24.73 (**15,15'**), 21.53 (**2,2'**), 21.44 (**3**).

1,3,3-trimethyl-2-((E)-2-((E)-2-(methylamino)-3-((E)-2-(1,3,3-trimethyl-5-sulfoindolin-2-ylidene)ethylidene)cyclohex-1-enyl)vinyl)-3*H*-indolium-5-sulfonate (32)

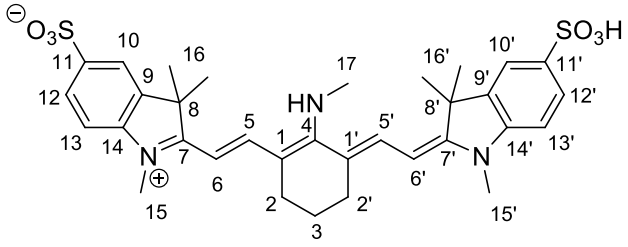

Sulfonated chloro dye **18** (25.0 mg, 0.4 mmol) and 2 M methylamine in MeOH (10.0 µL, 35 mmol) were dissolved in MeOH (0.25 mL) and stirred at 70 °C for 4 h. The solvent was evaporated and the residue purified by column chromatography [eluting solvent: DCM:MeOH (85:15)] to yield a blue solid (21 mg, 83%).

HPLC (method 2) t_r = 7.6 min, Purity 100% (ELSD).
MS (ES): calculated for $C_{33}H_{38}N_3O_6S_2$ $[M-H]^-$ m/z 636.2. Found 636.1 (70%).
MS (HRMS, ES) m/z calc $[M-H]^-$ 636.22075. Found 636.22490.
Mp. 177 °C.
IR (υ): 1523 (C=N), 1482 (S=O), 1271 (S=O), 1098 (C-N), 1018 (S-O) cm^{-1}.
λ_{abs}= 608 nm, λ_{em}= 772 nm (DMSO).
^{1}H NMR (500 MHz, MeOD) *δ*: 7.78 (dd, *J* = 8.2, 1.6 Hz, 2H, **12,12'**), 7.75 (d, *J* = 1.3 Hz, 2H, **10,10'**), 7.64 (d, *J* = 12.5 Hz, 2H, **5,5'**), 7.03 (d, *J* = 8.3 Hz, 2H, **13,13'**), 5.73 (d, *J* = 12.6 Hz, 2H, **6,6'**), 3.47 (s, 3H, **17**), 3.39 (s, 6H, **15,15'**), 2.60 (t, *J* = 6.3 Hz, 4H, **2,2'**), 1.87 – 1.82 (m, 2H, **3**), 1.67 (s, 12H, **16,16'**).
^{13}C NMR (126 MHz, MeOD)*δ*: 171.59 (**7,7'**), 167.13 (**5,5'**), 158.23 (**4**), 145.33 (**9,9'**), 138.99 (**14,14'**), 136.30 (**11,11'**), 135.05 (**12,12'**), 126.37 (**10,10'**), 119.56(**13,13'**), 107.22 (**1,1'**), 94.12 (**6,6'**), 35.98 (**8,8'**), 28.83 (**17**), 27.50 (**16,16'**), 25.65 (**15,15'**), 23.97 (**2,2'**), 20.93 (**3**).

1,3,3-trimethyl-2-((E)-2-((E)-2-(methylamino)-3-((E)-2-(1,3,3-trimethylindolin-2-ylidene)ethylidene)cyclohex-1-enyl)vinyl)-3*H*-indolium iodide (33)

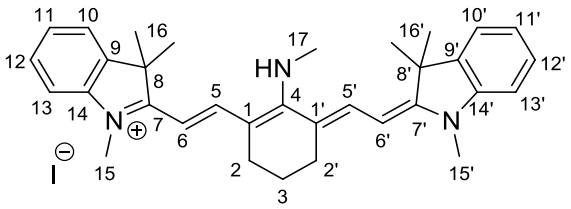

Chloro dye **14** (80.0 mg, 0.17 mmol) and 2 M methylamine in MeOH (50.0 µL, 175 mmol) were dissolved in MeOH (1.0 mL) and stirred at 70 °C for 4 h. The solvent

was evaporated and the residue washed with water (20.0 mL) to yield a blue solid (71 mg, 90%).

HPLC (method 2) t_r = 6.8 min, Purity 100% (ELSD).

MS (ES): calculated for $C_{33}H_{40}N_3$ [M] m/z 478.3. Found 478.3 (100%).

MS (HRMS, ES) m/z calc [M] 478.32168. Found 478.32100.

Mp. 208 °C.

IR (υ): 1525 (C=N), 1097 (C-N) cm^{-1}.

λ_{abs}= 612 nm, λ_{em}= 767 nm (DMSO).

^{1}H NMR (500 MHz, MeOD) *δ*: 7.71 (d, *J* = 12.7 Hz, 2H, **5,5'**), 7.36 (d, *J* = 7.3 Hz, 2H, **10,10'**), 7.31 (t, *J* = 7.6 Hz, 2H, **12,12'**), 7.10 – 7.03 (m, 4H, **11,11',13,13'**), 5.72 (d, *J* = 12.7 Hz, 2H, **6,6'**), 3.47 (s, 3H, **17**), 3.42 (s, 6H, **15,15'**), 2.60 (t, *J* = 5.9 Hz, 4H, **2,2'**), 1.90 – 1.83 (m, 2H, **3**), 1.67 (s, 12H, **16,16'**).

^{13}C NMR (126 MHz, MeOD) *δ*: 170.62 (**7,7'**), 167.60 (**5,5'**), 143.74 (**14,14'**), 139.71 (**4**), 136.91 (**9,9'**), 131.12 (**12,12'**), 128.69 (**1,1'**), 127.93 (**10,10'**), 122.19 (**11,11'**), 121.51 (**13,13'**), 119.64 (**6,6'**), 93.41 (**8,8'**), 36.14 (**17**), 27.59 (**15,15'**), 25.52 (**2,2'**), 21.12 (**16,16'**), 18.36 (**3**).

All data in agreement with the literature[227].

1,3,3-trimethyl-2-((E)-2-((E)-2-(*N*-methylacetamido)-3-((E)-2-(1,3,3-trimethylindolin-2-ylidene)ethylidene)cyclohex-1-enyl)vinyl)-3*H*-indolium iodide (39)

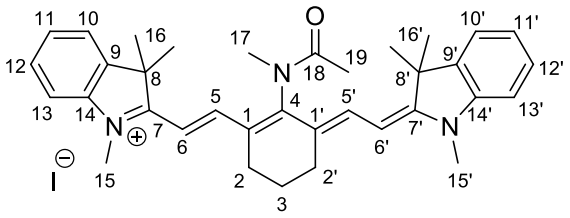

Amino dye **33** (20.0 mg, 0.042 mmol) was dissolved in anhydrous DCM (2.0 mL), the flask cooled to 0 °C and purged with N_2. DIPEA (90.0 µL, 0.5 mmol) and acetyl chloride (9.2 µL, 0.084 mmol) were added and the reaction allowed to stir at room temperature for 30 min. The solvent was evaporated and the green solid was purified by column chromatography [eluting solvent: DCM:MeOH (95:5)] to afford the desired product as a green solid (12 mg, 55%).

HPLC (method 2) t_r = 6.3 min, Purity 100% (ELSD).

MS (ES): calculated for $C_{35}H_{42}N_3O$ [M] m/z 520.3. Found 520.3 (100%).

MS (HRMS, ES) m/z calc [M] 520.33224. Found 520.33021.

Mp. 185 °C.

IR (υ): 1667 (C=O), 1547 (C=N), 1257 (C-O), 1008 (C-N) cm^{-1}.

λ_{abs}= 787 nm, λ_{em}= 815 nm (DMSO).

^{1}H NMR (500 MHz, MeOD) δ: 7.97 (d, J = 13.8 Hz, 2H, **5,5'**), 7.517.49(m, 2H, **10,10'**), 7.43 (td, J=7.5, 0.8 Hz, 2H, **12,12'**), 7.31-7.29 (m, 2H, **13,13'**), 7.27 (td, J = 7.5, 0.8 Hz, 2H, **11,11'**), 6.25 (d, J = 13.7 Hz, 2H, **6,6'**), 3.70 (s, 3H, **19**), 3.65 (s, 6H, **15,15'**), 2.80 (s, 3H, **17**), 2.68-2.66 (m, 4H, **2,2'**), 1.98 – 1.94 (m, 2H, **3**), 1.70 (s, 12H, **16,16'**).

^{13}C NMR (126 MHz, MeOD) δ: 173.17 (**18**), 172.26 (**7 or 7'**), 171.13 (**7 or 7'**), 155.07 (**4**), 151.43 (**5 or 5'**), 143.03 (**5 or 5'**), 142.87 (**14 or 14'**), 142.31 (**14 or 14'**), 141.01 (**9 or 9'**), 140.95 (**9 or 9'**), 131.80 (**12 or 12'**), 128.52 (**12 or 12'**), 128.35 (**1**

or 1'), 126.29 (**1 or 1'**), 125.25 (**11 or 11'**), 124.65 (**11 or 11'**), 122.02 (**10 or 10'**), 121.88 (**10 or 10'**), 110.77 (**13 or 13'**), 110.25 (**13 or 13'**), 101.37 (**6 or 6'**), 100.45 (**6 or 6'**), 53.40 (**8 or 8'**), 48.77 (**8 or 8 '**), 36.18 (**15 or 15'**), 35.46 (**15 or 15'**), 30.44 (**17**), 30.16 (**2 or 2'**), 27.08 (**2 or 2'**), 26.89 (**16 or 16'**), 25.25 (**16 or 16'**), 25.11 (**3**), 24.12 (**19**).

All data in agreement with the literature[227].

2-((E)-2-((E)-2-(2-(2-(carboxymethoxy)ethoxy)ethylamino)-3-((E)-2-(1,3,3-trimethylindolin-2-ylidene)ethylidene)cyclohex-1-enyl)vinyl)-1,3,3-trimethyl-3*H*-indolium iodide (34)

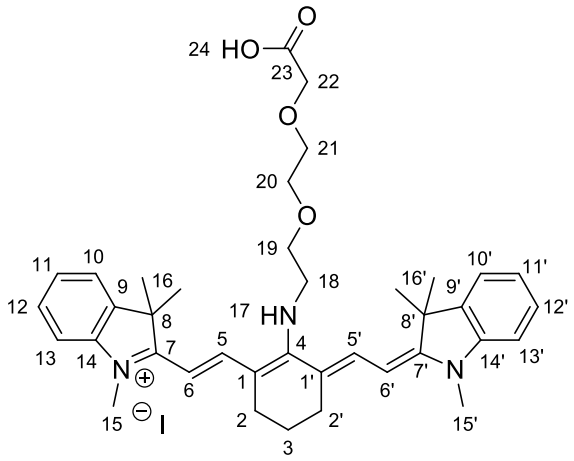

Chloro dye **14** (25.0 mg, 0.05 mmol), [2-(2-aminoethoxy)ethoxy]acetic acid (25.3 mg, 0.15 mmol) and TEA (0.5 mmol, 67 µL) were dissolved in MeOH (1.0 mL) and stirred at 70 °C for 4 h. The solvent was evaporated and the residue purified by column chromatography (94:5:1 DCM:MeOH:AcOH) to yield a blue solid (17 mg, 54%).

HPLC (method 2) t_r = 6.8 min, Purity 100% (ELSD).

MS (ES): calculated for $C_{38}H_{48}N_3O_4$ [M] m/z 610.4. Found 610.3 (100%).

MS (HRMS, ES) m/z calc $[M+H]^+$ 611.37176. Found 611.37163.

Mp. 241 °C decomposed.

IR (υ): 3337 (O-H), 1566 (C=N), 1167 (CO-O), 1097 (C-O), 1044 (C-N) cm^{-1}.

λ_{abs}= 652 nm, λ_{em}= 777 nm (DMSO).

^{1}H NMR (500 MHz, MeOD) δ: 7.86 (d, *J* = 13.0 Hz, 2H, **5,5'**), 7.40 (d, *J* = 7.3 Hz, 2H, **10,10'**), 7.34 (td, *J* = 11.2, 4.2 Hz, 2H, **12,12'**), 7.13-7.08 (m, 4H, **11,11',13,13'**), 5.83 (d, *J* = 13.1 Hz, 2H, **6,6'**), 3.97 (s, 2H, **22**), 3.93 (t, *J* = 4.7 Hz, 2H, **21**), 3.83 – 3.74 (m, 6H, **18,19,20**), 3.47 (s, 6H, **15,15'**), 2.57 (t, *J* = 6.3 Hz, 4H, **2,2'**), 1.91 – 1.84 (m, 2H, **3**), 1.69 (s, 12H, **16,16'**).

^{13}C NMR (126 MHz, MeOD) δ: 169.82 (**7,7'**), 168.92 (**23**), 143.64 (**5,5'**), 139.91 (**4**), 139.49 (**9,9'**), 127.99 (**14,14'**), 122.64 (**12,12'**), 121.65 (**10,10'**), 120.54 (**11,11'**), 108.49 (**13,13'**), 94.51 (**1,1'**), 70.07 (**6,6'**), 69.95 (**22**), 69.85 (**20,21**), 49.73(**19),** 48.23 (**8,8')**, 46.49 (**18**), 29.34 (**2,2'**), 27.67**(15,15'**), 24.43 (**16,16'**), 21.60 (**3**).

2-((E)-2-((E)-2-(2-(2-(carboxymethoxy)ethoxy)ethylamino)-3-((E)-2-(1,3,3-trimethyl-5-sulfoindolin-2-ylidene)ethylidene)cyclohex-1-enyl)vinyl)-1,3,3-trimethyl-3*H*-indolium-5-sulfonate (35)

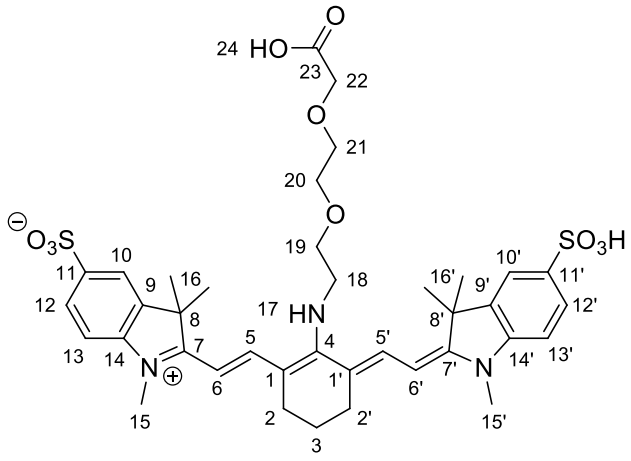

Sulfonated chloro dye **18** (50.0 mg, 0.78 mmol), [2-(2-aminoethoxy)ethoxy]acetic acid (38.0 mg, 0.23 mmol) and TEA (9.4 mmol, 130 µL) were dissolved in MeOH

(1.5 mL) and stirred at 70 °C for 4 h. The solvent was evaporated and the residue purified by preparative HPLC to yield a blue solid (31 mg, 52%).

HPLC (method 2) t_r = 5.7 min, Purity 100% (ELSD).

MS (ES): calculated for $C_{38}H_{46}N_3O_{10}S_2$ $[M-H]^-$ m/z 768.3. Found 768.1 (100%).

MS (HRMS, ES) m/z calc $[M+H]^+$ 770.27757. Found 770.27678.

Mp. 201 °C decomposed.

IR (υ): 1728 (C=O), 1521 (C=N), 1481 (S=O), 1290 (S=O), 1205 (OC-O), 1164 (C-O), 1095 (C-N), 1016 (S-O) cm^{-1}.

λ_{abs}= 637 nm, λ_{em}= 771 nm (DMSO).

^{1}H NMR (500 MHz, MeOD) *δ*: 7.82-7.78 (m, 6H, **5,5',10, 10',12,12'**), 7.09 (d, *J* = 8.4 Hz, 2H, **13,13'**), 5.85 (d, *J* = 12.4 Hz, 2H, **6,6'**), 3.98 (t, J = 5.0 Hz, 2H, **19**), 3.84 (t, J = 5.0 Hz, 2H, **18**), 3.78 (s, 2H, **22**), 3.47 (s, 4H, **20,21**), 3.37 (s, 6H, **15,15'**), 2.63-2.55 (m, 4H, **2,2'**), 1.90-1.85 (dt, *J* = 12.9, 6.5Hz, 2H, **3**), 1.70 (s, 12H, **16,16'**).

^{13}C NMR (126 MHz, MeOD) *δ*: 172.39(**23**), 168.49 (**7,7'**), 145.24 (**5,5'**), 139.71(**4**), 138.97 (**9,9'**), 138.91(**14,14'**), 126.47(**11,11'**), 121.49 (**12,12'**), 119.70 (**10,10'**), 119.69 (**13,13'**), 107.67 (**1,1'**), 70.54(**6,6'**), 70.42 (**20**), 69.98(**19**), 69.89(**21**), 69.71 (**22**), 67.73 (**8,8'**), 67.63 (**18**), 49.70 (**15,15'**), 27.58 (**16,16'**), 24.51 (**2,2'**), 21.39 (**3**).

HSQC with DEPT editing (500 MHz, MeOD)

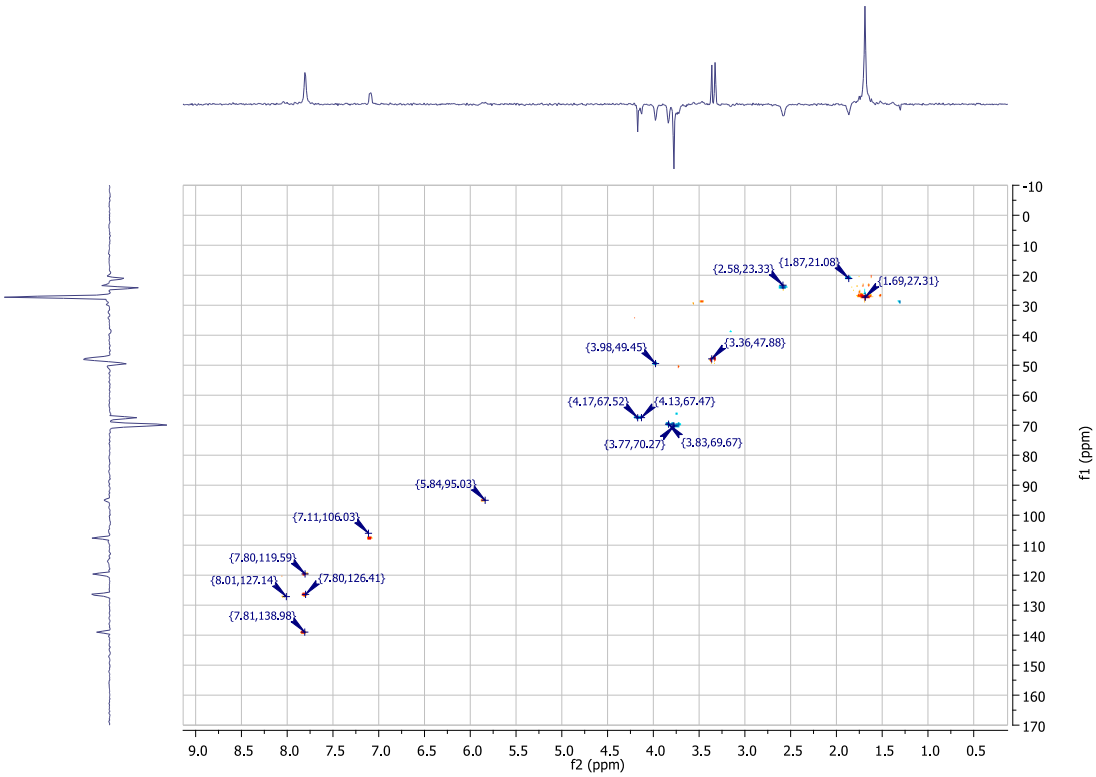

Confirmation of 6 aromatic protons, 7 CH_2 groups and 2 groups of methyls.

2-((E)-2-((E)-2-(5-carboxypentylamino)-3-((E)-2-(1,3,3-trimethylindolin-2-ylidene)ethylidene)cyclohex-1-enyl)vinyl)-1,3,3-trimethyl-3*H*-indolium iodide (36)

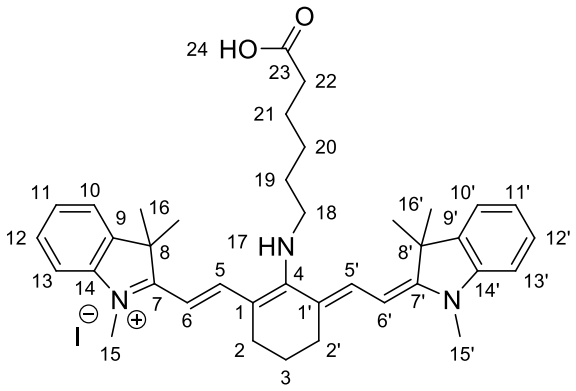

Chloro dye **14** (25.0 mg, 0.05 mmol), 6-aminocaproic acid (20.3 mg, 0.16mmol) and TEA (0.5 mmol, 67 µL) were dissolved in MeOH (1.0 mL) and stirred at 70 °C for 4 h. The solvent was evaporated and the residue purified by column chromatography (95:4:1 DCM:MeOH:AcOH) to yield a blue solid (17 mg, 57%).

HPLC (method 2) t_r = 6.7 min, Purity 100% (ELSD).

MS (ES): calculated for $C_{38}H_{48}N_3O_2$ [M] m/z 578.4. Found 578.2 (100%).

MS (HRMS, ES) m/z calc $[M+H]^+$ 579.38193. Found 579.38173.

Mp. 141 °C.

IR (υ): 1722 (C=O), 1526 (C=N), 1158 (OC-O), 1101 (C-N) cm^{-1}.

λ_{abs}= 631 nm, λ_{em}= 767 nm (DMSO).

^{1}H NMR (500 MHz, MeOD) δ 7.77 (d, *J* = 12.9 Hz, 2H,**5,5'**), 7.37 (d, *J* = 7.2 Hz, 2H, **10,10'**), 7.31 (td, 2H, 7.8, 0.8 Hz, **12,12'**), 7.06-7.10 (m, 4H, **11,11',13,13'**), 5.78 (d, *J* = 13.0 Hz, **6,6',** 2H), 3.78 (t, *J* = 6.8 Hz, 2H, **18**), 3.44 (s, 6H, **15**), 2.55 (t, *J* = 6.3 Hz, 4H, **2,2'**), 2.30 (t, *J* = 7.3 Hz, 2H, **22**), 1.88 – 1.79 (m, 4H, **19,21**), 1.68 (m, 2H, **3**), 1.67 (s,12H, **16,16'**), 1.51 – 1.44 (m, 2H, **20**).

^{13}CNMR (126 MHz, MeOD)*δ*: 169.82 (**7,7'**), 168.92 (**23**), 143.64 (**5,5'**), 139.91 (**4**), 139.49 (**9,9'**), 127.99 (**14,14'**), 122.64 (**12,12'**), 121.65 (**11,11'**), 120.54 (**10,10'**),

108.49 (**13,13'**), 94.51 (**1,1'**), 70.07 (**6,6'**), 69.95 (**18**), 69.85 (**20,21**), 49.73 (**22**), 48.23 (**8,8'**), 46.49 (**19**), 29.35 (**2,2'**), 27.67 (**16,16'**), 24.43 (**15,15'**), 21.60 (**3**).

2-((E)-2-((E)-2-(5-carboxypentylamino)-3-((E)-2-(1,3,3-trimethyl-5-sulfoindolin-2-ylidene)ethylidene)cyclohex-1-enyl)vinyl)-1,3,3-trimethyl-3*H*-indolium-5-sulfonate (37)

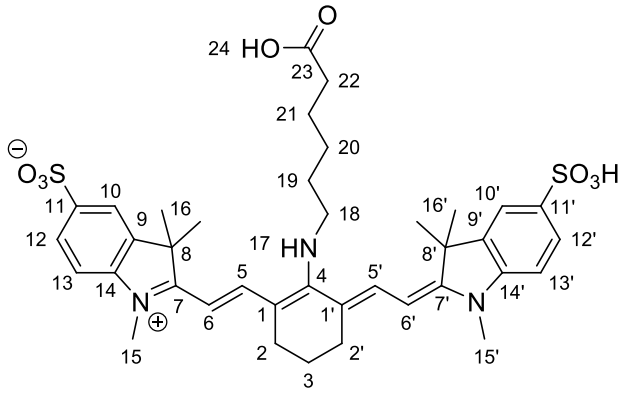

Sulfonated chloro dye **18** (50.0 mg, 0.78 mmol), 6-aminocaproic acid (31.0 mg, 0.24 mmol) and TEA (109.0 µL, 7.8 mmol) were dissolved in MeOH (1.5 mL) and stirred at 70 °C for 4 h. The solvent was evaporated and the residue purified by preparative HPLC to yield a blue solid (24 mg, 42%).

HPLC (method 2) t_r = 6.5 min, Purity 100% (ELSD).

MS (ES): calculated for $C_{38}H_{46}N_3O_8S_2$ m/z 736.3. Found 735.7 (25%), 367.6 $[M-2H]^{2-}$ (100%).

MS (HRMS, ES) m/z calc $[M+H]^+$ 738.28774. Found 738.28807.

Mp. 220 ºC decomposed.

IR (υ): 1714 (C=O), 1528 (C=N), 1437 (S=O), 1291 (S=O), 1167 (OC-O), 1113 (C-O), 1063 (C-N), 1020 (S-O) cm^{-1}.

λ_{abs}= 628 nm, λ_{em}= 771 nm (DMSO).

^{1}H NMR (500 MHz, MeOD) δ: 7.83 – 7.79 (m, 4H, **12**, **12',10,10'**), 7.74 (d, J = 12.7 Hz, 2H, **5,5'**), 7.08 (d, J = 8.3 Hz, 2H, **13,13'**), 5.83 (d, J = 12.9 Hz, 2H, **6,6'**), 3.83 (t, J = 6.8 Hz, 2H, **18**), 3.45 (s, 6H, **15,15'**), 2.59 (t, J = 6.3 Hz, 4H, **2,2'**), 2.29 (t, J = 7.4 Hz, 2H, **22**), 1.89-1.84(m, 4H, **19,21**), 1.73 (m, 2H, **3**), 1.70 (s, 12H, **16,16'**), 1.54-1.46 (m, 2H, **20**).

^{13}C NMR (126 MHz, MeOD)δ: 170.92 (**7,7'**), 168.01 (**23**), 145.22 (**5,5'**), 139.63 (**4**), 139.25 (**9,9'**), 138.28 (**14,14'**), 126.44 (**11,11'**), 121.34 (**12,12'**), 119.61 (**10,10'**), 107.54 (**13,13'**), 94.76 (**1,1'**), 93.63 (**6,6'**), 50.14 (**8,8'**), 35.49 (**18**), 30.59 (**22**), 29.35 (**2,2'**), 27.58 (**15,15'**), 27.52 (**19**), 26.39 (**21**), 25.09 (**16,16'**), 24.70 (**20**), 21.34 (**3**).

HSQC with DEPT editing (500 MHz, MeOD)

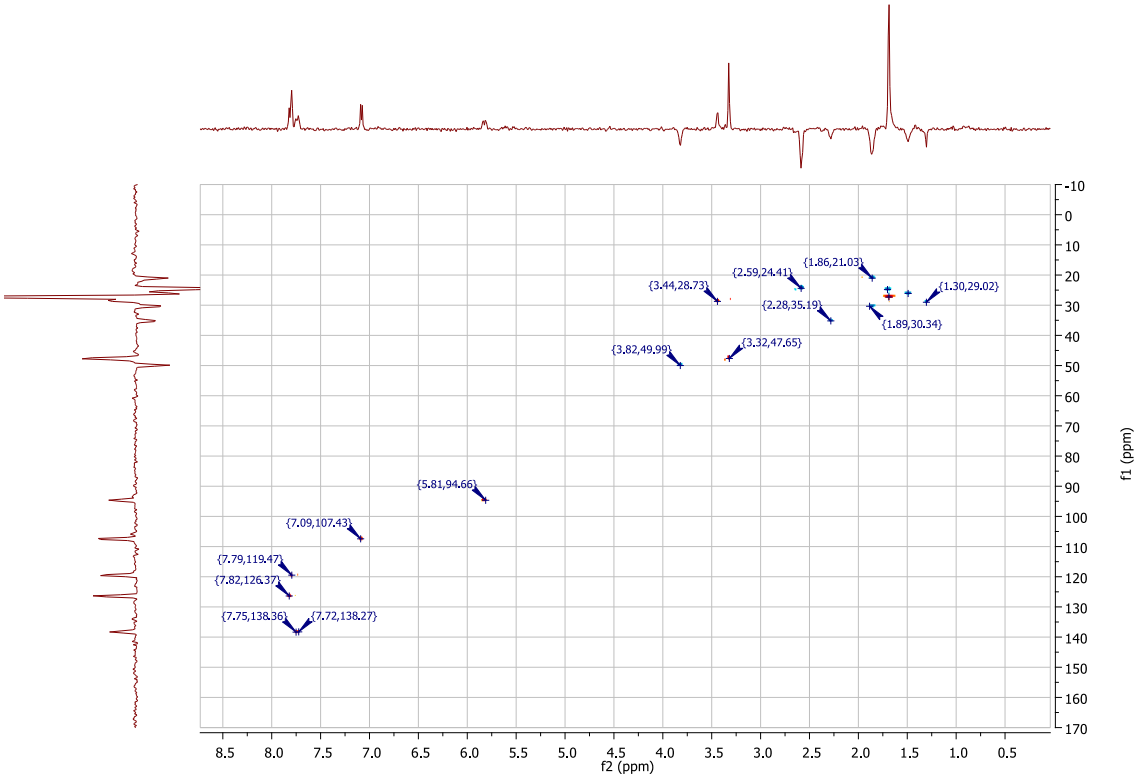

Confirmation of 6 aromatic protons, 7 CH_2 groups and 2 groups of methyls. 1 CH_2 present under methyl peak at 1.7 ppm.

6.4.4 Non-Fluorescent Analogues

3,3'-(2,2'-(1E,1'E)-2,2'-(1,3-phenylene)bis(ethene-2,1-diyl)bis(1,1-dimethyl-1*H*-benzo[e]indoleium-3,2-diyl))dipropane-1-sulfonate (40)

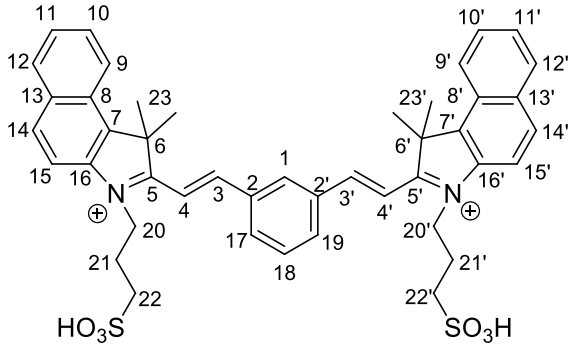

Sulfonated benz[e]indole **8** (154.0 mg, 0.47 mmol), isophthalaldehyde (25.0 mg, 1.9 mmol) and NaOAc (152.0 mg, 1.9 mmol) were dissolved in a mixture of AcOH and Ac_2O (1:1, 5 mL) and left to stir for 5 h at 80 °C. The solvent was evaporated and the product purified by preparative HPLC to yield a yellow sold (64 mg, 45%)

HPLC (method 2) t_r = 5.0 min, Purity 100% (ELSD).
MS (ES): calculated for $C_{44}H_{47}N_2O_6S_2$ $[M+H]^+$ m/z 763.3. Found 763.3 (80%).
MS (HRMS, ES) m/z calc. [M] 762.27918. Found 762.27873.
Mp. 210 °C.
IR (υ): 1592 (C=N), 1463 (S=O), 1200 (S=O), 1162 (C-N), 1037 (S-O) cm^{-1}.
^{1}H NMR (500 MHz, MeOD) δ: 8.74 (d, *J* = 16.4 Hz, 2H, **3,3'**), 8.51 (d, *J* = 8.4 Hz, 2H, **9,9'**), 8.34 (dd, *J* = 7.8, 1.2 Hz, 2H, **12,12'**), 8.30-8.24 (m, 5H, **1,4,4',15,15'**), 8.20 (d, *J* = 8.2 Hz, 2H, **14,14'**), 8.15 (d, *J* = 8.9 Hz, 2H, **17,19**), 7.85 (td, *J* = 7.2, 1.0 Hz, 2H, **10,10'**), 7.80 (t, *J* = 7.7 Hz, 1H, **18**), 7.76 (td, *J* = 7.6, 1.0 Hz, 2H, **11,11'**), 5.20 (t, J = 7.5 Hz, 4H, **20,20'**), 3.19 (t, J=5.0 Hz, 4H,**22,22'**), 2.61 – 2.52 (m, 4H, **21,21'**), 2.22 (s, 12H, **23,23'**).
^{13}C NMR (126 MHz, MeOD) δ: 183.38 (**5,5'**), 152.47 (**3,3'**), 139.66 (**7,7'**), 138.18 (**16,16'**), 135.75 (**2,2'**), 134.86 (**14,14'**), 134.16 (**8,8'**), 131.48 (**13,13'**), 130.70

(**17,19**), 130.19 (**1**), 129.95 (**18**), 128.26 (**12,12'**), 127.43 (**11,11'**), 127.30 (**10,10'**), 123.00 (**9,9'**), 113.43 (**4,4'**), 112.39 (**15,15'**), 54.48 (**6,6**), 45.87 (**22,22'**), 25.14 (**20,20'**), 24.84 (**23,23'**), 24.43 (**21,21'**).

2,2'-(1E,1'E)-2,2'-(1,3-phenylene)bis(ethene-2,1-diyl)bis(1-methylquinolinium) (41)

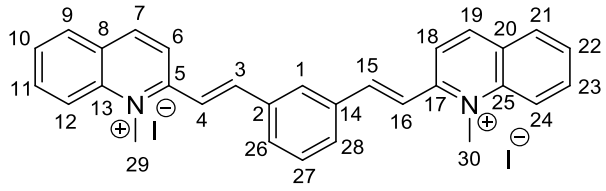

Quinolinium salt **12** (0.80 g, 2.8 mmol), NaOAc (0.54 g, 6.6 mmol) and isophthalaldehyde (0.15 g, 1.1 mmol) were dissolved in a mixture of acetic acid and acetic anhydride (1:1, 15.0 mL) for 4 h at 120 °C in a sealed vial. The solvent was evaporated and the crude product was purified by column chromatography [eluting solvent: Hexane:EtOAc (90:10)] to yield an orange solid (0.13 g, 28 %).

HPLC (method 2) t_r= 4.1 min, Purity 95% (31 % isolated as iodide salt) (ELSD).

Mp. 244 °C decomposed.

IR (υ): 1605 (C=N), 1193 (C-N) cm^{-1}.

^{1}H NMR (500 MHz, DMSO-d6) δ: 9.17 (d, J = 8.9 Hz, 2H, **7,19**), 8.63 (m, 4H, **9,12,21,24**), 8.42 (dd, J = 8.0, 0.9 Hz, 2H, **3,15**), 8.29 – 8.22 (m, 4H,**4,6,16,18**), 8.17 – 8.14 (m, 3H, **26,27,28**), 8.11 (s, 1H, **1**), 8.01 (t, J = 7.6 Hz, 2H, **11,23**), 7.75 (t, J = 7.7 Hz, 2H, **10,22**), 4.65 (s, 6H, **29,30**).

^{13}C NMR (126 MHz, DMSO-d6) δ: 156.48 (**5,17**), 146.12 (**13,25**), 145.16 (**2,14**), 139.75 (**7,19**), 136.21 (**3,15**), 135.64 (**26,28**), 131.92 9 (**11,23**), 130.65 (**8,20**), 130.43(**1**), 129.89 (**27**), 129.75 (**9,21**), 128.56 (**10,22**), 121.89 (**12,24**), 121.27 (**4,16**), 119.96 (**6,18**), 23.51 (**29,30**).

6.4.5 Novel Pentamethine Cyanine Dyes

2-((1E,3Z,5E)-3-(5-carboxypyridin-2-yl)-5-(1,1,3-trimethyl-1*H*-benzo[e]indol-2(3H)-ylidene)penta-1,3-dienyl)-1,1,3-trimethyl-1*H*-benzo[e]indolium iodide (42)

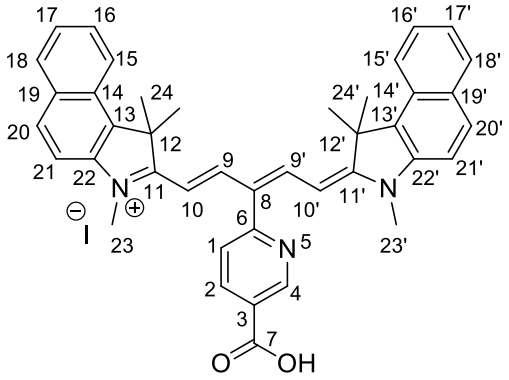

Benz[e]indolinium salt **6** (0.22 g, 1.0 mmol), 2-(5-carboxypyridin-2-yl)malondialdehyde (0.098 g, 0.5 mmol) and NaOAc (0.6 g, 7.2 mmol) were dissolved in a mixture of acetic acid and acetic anhydride (1:1, 20.0 mL) and stirred at 70 °C for 3 h under N_2. The solvent was evaporated and the product extracted with DCM (25.0 mL). The crude product was washed with EtOAc (20.0 mL) and Et_2O (20.0 mL) and dried under vacuum to yield a blue solid (0.11 g, 37%).

HPLC (method 2) t_r = 4.2 min, Purity 100% (ELSD).
MS (ES): calculated for $C_{41}H_{38}N_3O_2$ [M] m/z 604.3. Found 604.3 (100%).
MS (HRMS, ES) m/z calc $[M+H]^+$ 605.30368Found 605.30313.
Mp. 255 °C decomposed
λ_{abs}= 670 nm, λ_{em}= 690 nm (MeOH); λ_{abs}= 677 nm, λ_{em}= 702 nm (DMSO).
IR (υ): 3384 (O-H), 1587 (C=O),1523 (C=N), 1190 (C-O), 1103 (C-N) cm^{-1}.
^{1}H NMR (500 MHz, MeOD) δ: 9.37 (d, *J* = 1.8, 1H, **4**),8.61 (dd, *J* = 7.9, 2.0 Hz, 1H, **2**), 8.53 (d, *J* = 13.1 Hz, 2H, **9,9'**), 8.29 (d, *J* = 8.5 Hz, 2H, **20,20'**), 8.02 (t, *J* = 8.5 Hz, 4H, **15,15',18,18'**), 7.72 (d, *J* = 8.0, 1H, **1**), 7.70-7.67 (m, 2H, **17,17'**), 7.60 (d, *J* = 8.8 Hz, 2H, **21,21'**), 7.54 – 7.50 (m, 2H, **16,16'**), 5.88 (d, *J* = 10.5 Hz, 2H, **10,10'**), 3.55 (s, 6H, **23,23'**), 2.09 (s, 12H, **24,24'**).

^{13}C NMR (126 MHz, MeOD) δ: 175.99 (**11,11'**), 157.48 (**7**), 150.94 (**6**), 140.04 (**9,9'**), 138.73 (**4**), 133.86 (**22,22',13,13'**), 132.24 (**2**), 130.30 (**20,20'**), 129.73 (**17,17'**), 128.9 (**3),** 127.91 (**16,16'**), 127.42 (**18,18'**), 124.88 (**19,19',14,14'**), 122.03 (**15,15'**), 116.07 (**8**), 111.02 (**1**), 110.64 (**21,21'**), 99.97 (**10,10'**), 51.23 (**12,12'**), 30.59 (**23,23'**), 27.39 (**24**), 26.03 (**24'**).

2-((1E,3Z,5E)-3-(5-carboxypyridin-2-yl)-5-(1,3,3-trimethyl-5-sulfoindolin-2-ylidene)penta-1,3-dienyl)-1,3,3-trimethyl-3*H*-indolium-5-sulfonate (43)

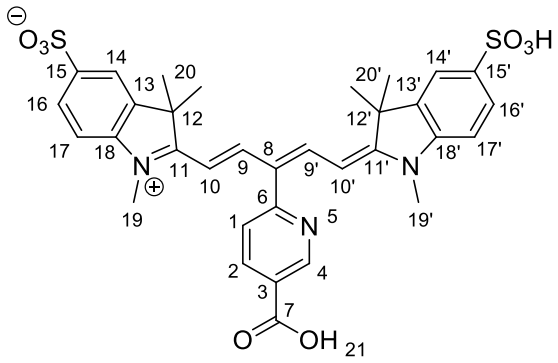

Sulfonated indolium salt **10** (4.85 g, 19.4 mmol), 2-(5-carboxypyridin-2-yl)malondialdehyde (1.50 g, 7.7 mmol) and NaOAc (4.45 g, 543 mmol) were dissolved in a mixture of acetic acid and acetic anhydride (1:1, 300.0 mL) and stirred at 70 °C for 5 h under N_2. The solvent was evaporated crude product was crystallised with EtOAc and washed with Et_2O. The compound was purified by column chromatography [eluting solvent: DCM:MeOH (80:20)] to yield a blue solid (1.8 g, 35%).

HPLC (method 2) t_r = 4.4 min, Purity 92% (ELSD).

MS (ES): calculated for $C_{33}H_{32}N_3O_8S_2$ m/z 662.2. Found 661.6 (100%).

MS (HRMS, ES), m/z calc $[M+H]^+$ 664.17819. Found 664.17836.

Mp. 160 °C.

IR (υ): 3421 (O-H), 1505 (C=N), 1473 (S=O), 1198 (S=O), 1105 (C-N), 1027 (S-O) cm^{-1}.

λ_{abs}= 640 nm, λ_{em}= 661nm (MeOH); λ_{abs}= 650 nm, λ_{em}= 676 nm (DMSO).

^{1}H NMR (500 MHz, MeOD) δ: 9.29 (d, J = 1.75 Hz, 1H, **4**), 8.51 (dd, *J* = 7.9, 2.0, 1H, **2**), 8.47 (d, *J* = 14.3 Hz, 2H, **9,9'**), 7.94 (d, J = 1.5 Hz, 2H, **14,14'**), 7.90 (dd, *J* = 8.3, 1.2 Hz, 2H, **16,16'**), 7.59 (d, *J* = 7.9 Hz, 1H, **1**), 7.34 (d, *J* = 8.3 Hz, 2H, **17,17'**), 5.85 (d, *J* = 14.0 Hz, 2H, **10,10'**), 3.44 (s, 6H, **19,19'**), 1.84 (s, 12H, **20,20'**).

^{13}C NMR (126 MHz, MeOD) δ: 176.78 (**11,11'**), 172.26 (**7**), 152.21 (**6**), 145.39 (**4**), 143.77 (**13,13'**), 142.63 (**18,18'**), 139.84 (**9,9'**), 139.68 (**2**), 134.36 (**15,15'**), 128.00 (**16,16'**), 126.78 (**3**), 122.29 (**17,17'**), 121.24 (**14,14'**), 111.74 (**8**), 102.70 (**1**), 58.32(**10,10'**), 31.69 (**12,12'**), 27.55 (**19,19'**), 25.56 (**20,20'**).

3-(2-((1E,3Z,5E)-3-(5-carboxypyridin-2-yl)-5-(1,1-dimethyl-3-(3-sulfopropyl)-1*H*-benzo[e]indol-2(3H)-ylidene)penta-1,3-dienyl)-1,1-dimethyl-1*H*-benzo[e]indolium-3-yl)propane-1-sulfonate (44)

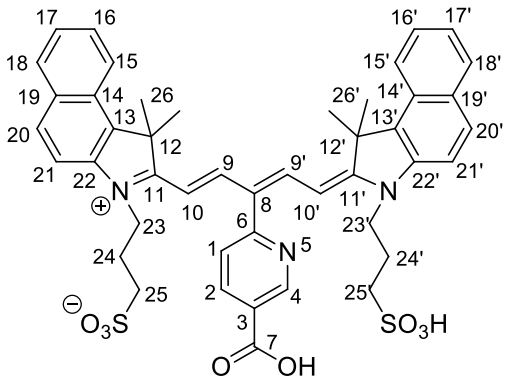

Sulfonated benz[e]indole **8** (280.0 mg, 0.85 mmol), 2-(3-hydroxycarbonyl-6-pyridyl)malondialdehyde (75.0 mg, 0.39 mmol) and NaOAc (190.0 mg, 2.35 mmol) were dissolved in a mixture of AcOH and Ac_2O (1:1, 8 mL) and left to stir for 5 h at 80 °C. The solvent was evaporated and the product purified by preparative HPLC to yield a blue solid (0.18 g, 57 %).

HPLC (method 2) t_r = 0.7 min, Purity 100% (ELSD).

MS (ES): calculated for $C_{45}H_{46}N_3O_8S_2$ $[M+H]^+$ m/z 820.3. Found 820.3 (20%), 818.3.

MS (HRMS, ES) m/z calc. $[M+H]^+$ 820.27209. Found 820.27133.

Mp. 229 °C.

IR (υ): 1597 (C=N), 1485 (S=O), 1235 (S=O), 1143 (C-O), 1124 (C-N), 934 (S-O) cm^{-1}.

λ_{abs}= 683 nm, λ_{em}= 708 nm (DMSO).

^{1}H NMR (500 MHz, MeOD) *δ*:9.37 (m, 1H, **4**), 8.69 (d, *J* = 14.2 Hz, 2H, **9,9'**), 8.61 (m, 2H, **20,20**), 8.28 (d, J = 8.3 Hz, 2H, **21,21'**), 8.05-7.99 (m, 4H, **15,15',18,18'**), 7.74 (d, J = 8.9 Hz, 1H, **1**), 7.71 – 7.65 (m, 2H, **17,17'**), 7.54-7.49 (m, 2H, **16,16'**), 5.86 (m, 2H, **10,10'**), 4.46 – 4.17 (m, 4H, **23,23'**), 2.96-2.87 (m, 4H, **25,25'**), 2.23-2.21 (m, 4H, **24,24'**), 2.04 (s, 12H, **26,26'**).

^{13}C NMR (126 MHz, MeOD)*δ*: 168.84 (**11,11'**), 139.61 (**7**), 134.83 (**6**), 133.78 (**9,9'**), 132.21 (**4**), 130.40 (**13,13', 22,22'**), 129.66 (**2**), 129.42 (**20,20'**), 128.09 (**3**), 127.33 (**16,16',18,18'**), 125.64 (**17,17'**), 124.86 (**19,19',14,14'**), 122.16 (**21,21'**), 110.86 (**10,10'**), 110.72 (**15,15'**) 101.18 (**8**), 100.03 (**1**), 51.49 (**12,12'**), 46.30 (**23,23'**), 26.01 (**26,26'**), 22.96 (**24,24'**), 7.77 (**25,25'**).

3-(2-((1E,3Z,5E)-3-(4-chlorophenyl)-5-(1,1-dimethyl-3-(3-sulfopropyl)-1*H*-benzo[e]indol-2(3H)-ylidene)penta-1,3-dienyl)-1,1-dimethyl-1*H*-benzo[e]indolium-3-yl)propane-1-sulfonate (45)

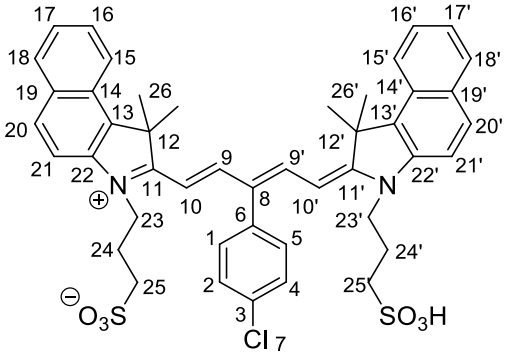

Sulfonated benz[e]indole **8** (230.0 mg, 0.68 mmol), 2-(4-chlorophenyl)malondialdehyde (50.0 mg, 0.27 mmol) and NaOAc (0.15 g, 1.65

mmol) were dissolved in a mixture of AcOH and Ac_2O (1:1, 5 mL) and left to stir for 5 h at 80 °C. The solvent was evaporated and the product purified by preparative HPLC to yield a blue solid (91 mg, 42 %).

HPLC (method 2) t_r = 4.8 min, Purity 87% (ELSD).

MS (ES): calculated for $C_{45}H_{44}ClN_2O_6S_2$ $[M-H]^-$ m/z 807.2. Found 807.2 (100%).

MS (HRMS, ES) m/z calc. $[M+H]^+$ 809.24804. Found 809.24714.

Mp. 201 °C decomposed.

IR (υ): 3422 (O-H), 1566 (C=N), 1410 (S=O), 1190 (S=O), 1042 (C-N), 1011 (S-O) cm^{-1}.

λ_{abs}= 686 nm, λ_{em}= 709 nm (DMSO).

^{1}H NMR (500 MHz, MeOD) *δ*: 8.66 (d, *J* = 14.0 Hz, 2H, **9,9'**), 8.29 (d, *J* = 8.5 Hz, 2H, **20,20'**), 8.05 – 7.99 (m, 4H, **15,15', 21,21'**), 7.71 (m, 4H, **2,4,18,18'**), 7.67 (td, *J* =8.0, 1.5 Hz, 2H, **17,17'**), 7.51 (t, *J* = 7.5 Hz, 2H, **16,16'**), 7.42 (d, *J* = 8.2 Hz, 2H, **1,5**), 5.83 (d, *J* = 13.0 Hz, 2H, **10,10'**), 4.28 (t, *J* = 8.75 Hz, 4H, **23,23'**), 2.91 (t, *J* = 6.4 Hz, 4H, **25,25'**), 2.25 (m, 4H, **24,24'**), 2.03 (s, 12H, **26,26'**).

^{13}C NMR (126 MHz, MeOD)*δ*: 178.05 (**11,11'**), 140.80 (**9,9'**), 135.08 (**13,13'**), 134.88 (**22,22'**) 133.40 (**6**), 133.14 (**3**), 131.69 (**20,20'**), 130.94 (**8**), 130.69 (**19,19',14,14'**), 129.35 (**17,17',16,16'**), 128.66 (**21,21'**), 126.13 (**1,2,4,5**), 123.36 (**18,18'**), 111.97 (**15,15'**), 101.74 (**10,10'**), 64.34 (**12,12'**), 52.57 (**23,23'**), 27.31 (**25,25'**), 25.50 (**24,24'**), 22.50 (**26,26'**).

3-(2-((1E,3Z,5E)-5-(1,1-dimethyl-3-(3-sulfopropyl)-1*H*-benzo[e]indol-2(3H)-ylidene)-3-(4-nitrophenyl)penta-1,3-dienyl)-1,1-dimethyl-1*H*-benzo[e]indolium-3-yl)propane-1-sulfonate (46)

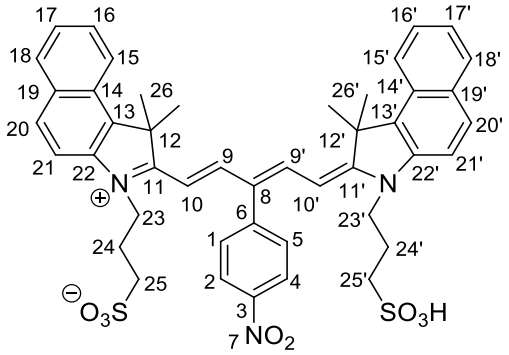

Sulfonated benz[e]indole **8** (107.0 mg, 0.32 mmol), 2-(4-nitrophenyl)malondialdehyde (25.0 mg, 0.13 mmol) and NaOAc (107.0 mg, 1.3 mmol) were dissolved in a mixture of AcOH and Ac_2O (1:1, 5.0 mL) and left to stir for 5 h at 80 °C. The solvent was evaporated and the product purified by column chromatography [eluting solvent: CH_3CN:iPrOH(60:40)] to yield a blue solid (71 mg, 67 %).

HPLC (method 2) t_r = 5.5 min, Purity 100% (ELSD).

MS (ES): calculated for $C_{45}H_{44}N_3O_8S_2$ $[M-H]^-$ m/z 819.3. Found 818.2 (90%).

MS (HRMS, ES) m/z calc. $[M+H]^+$ 820.27209. Found 820.27198.

Mp. 207 °C.

IR (υ): 1518 (N=H), 1479 (N=O), 1454 (S=O) 1345 (N-O), 1141 (S=O), 1092 (C-N), 1010 (S-O) cm^{-1}.

λ_{abs}= 684 nm, λ_{em}= 710 nm (DMSO).

^{1}H NMR (500 MHz, MeOD) δ: 8.62 (d, *J* = 14.3 Hz, 2H, **9,9'**), 8.50 (d, *J* = 8.6 Hz, 2H, **20,20'**), 8.23 (d, *J* = 8.5 Hz, 2H, **21,21'**), 7.95 (m, 4H, **16,16',17,17'**), 7.65 – 7.60 (m, 6H, **1,2,4,5,15,15'**), 7.45 (td, *J* = 7.3, 0.5 Hz, 2H, **18,18'**), 5.74 (d, *J* = 13.3 Hz, 2H, **10,10'**), 4.22 (t, *J* = 8.1 Hz, 4H, **23,23'**), 2.83 (t, *J* = 6.8 Hz, 4H, **25,25'**), 2.21 – 2.14 (m, 4H, **24,24'**), 1.96 (s, 12H, **26,26'**).

^{13}C NMR (126 MHz, MeOD) δ: 175.05 (**11,11'**), 152.07 (**9,9'**), 147.70 (**13,13'**), 139.54 (**22,22'**), 133.76 (**6**), 132.19 (**20,20'**), 131.59 (**3**), 130.40 (**8**), 129.66 (**14,14'**), 128.53 (**19,19'**), 128.08 (**16,16',17,17'**), 127.82 (**14,14'**), 127.35 (**21,21'**), 124.88 (**2,4**), 124.42 (**1,5**), 122.14 (**18,18'**), 110.78 (**15,15'**), 100.10 (**10,10'**), 51.45 (**12,12'**), 43.15 (**23,23'**), 25.97 (**26,26'**), 23.01 (**25,25'**), 22.63 (**24,24'**).

1,3,3-trimethyl-2-((1E,3Z,5E)-3-(4-nitrophenyl)-5-(1,3,3-trimethyl-5-sulfoindolin-2-ylidene)penta-1,3-dienyl)-3*H*-indolium-5-sulfonate (47)

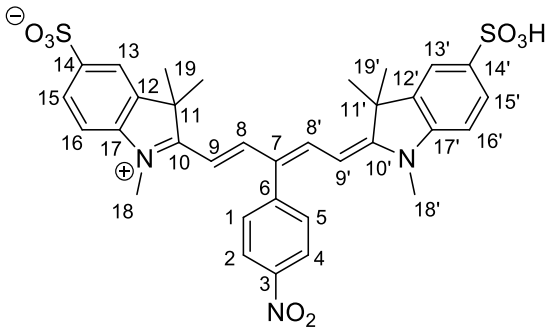

Sulfonated indolium salt **10** (124.0 mg, 0.33 mmol), 2-(4-nitrophenyl) malondialdehyde (25.0 mg, 0.13 mmol) and NaOAc (107.0 mg, 1.3 mmol) were dissolved in a mixture of acetic acid and acetic anhydride (1:1, 5 mL) and stirred at 80 °C for 5 h. The solvent was evaporated and the crude product purified by column chromatography [eluting solvent: CH_3CN:iPrOH (75:25)] to yield a blue solid (68 mg, 81%).

HPLC (method 1) t_r = 4.9 min Purity 99% (ELSD).

MS (ES): calculated for $C_{33}H_{32}N_3O_8S_2$ $[M-H]^-$ m/z 662.2. Found 662.3 (100%).

MS (HRMS, ES) m/z calc. $[M+H]^+$ 664.17819. Found 664.17851.

Mp. 235 °C decomposed.

IR (υ): 1574 (N=H), 1496 (N=O), 1458 (S=O), 1350 (N-O), 1191 (S=O), 1096 (C-N), 1016 (S-O) cm^{-1}.

λ_{abs}= 650 nm, λ_{em}= 676 nm (DMSO).

^{1}H NMR (500 MHz, MeOD) δ: 8.48-8.43 (m, 4H, **8,8', 1, 5**), 7.92 (s, 2H, **13,13'**), 7.87 (d, *J* = 8.2 Hz, 2H, **2,4**), 7.62 (d, *J* = 8.3 Hz, 2H, **15,15'**), 7.31 (d, *J* = 8.3 Hz,

2H, **16,16'**), 5.73 (d, *J* = 14.1 Hz, 2H, **9,9'**), 3.40 (s, 6H, **18,18'**), 1.81 (s, 12H, **19,19'**).

^{13}C NMR (126 MHz, MeOD) *δ*: 178.52 (**10,10'**), 176.57 (**3**), 164.44 (**14,14'**), 154.46 (**8,8'**), 149.02 (**6**), 145.22 (**17,17'**), 143.73 (**12,12'**), 142.48 (**2,4**), 132.69 (**13,13'**), 127.89 (**1,5**), 125.51 (**15,15'**), 121.16 (**7**), 111.62 (**16,16'**), 102.53 (**9,9'**), 50.53 (**11,11'**), 31.57 (**18,18'**), 27.37 (**19,19'**).

2-((1E,3Z,5E)-3-(4-chlorophenyl)-5-(1,3,3-trimethyl-5-sulfoindolin-2-ylidene)penta-1,3-dienyl)-1,3,3-trimethyl-3*H*-indolium-5-sulfonate (48)

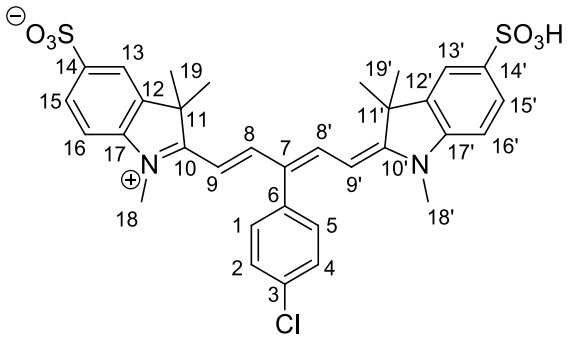

Sulfonated indole **10** (130.0 mg, 0.34 mmol), 2-(4-chlorophenyl) malondialdehyde (25.0 mg, 0.14 mmol) and NaOAc (112.0 mg, 1.4 mmol) were dissolved in a mixture of acetic acid and acetic anhydride (1:1, 5 mL) and stirred at 80 °C for 5 h. The solvent was evaporated and the crude product purified by column chromatography [eluting solvent: CH_3CN:iPrOH (77:23)] to yield a blue solid (73 mg, 82%).

HPLC (method 6) t_r = 5.3 min, Purity 94% (ELSD).

MS (ES): calculated for $C_{33}H_{32}ClN_2O_6S_2$ $[M-H]^-$ m/z 651.2. Found 651.2 (30%).

MS (HRMS, ES) m/z calc. $[M+H]^+$ 653.15414. Found 653.15322.

Mp. 230 °C decomposed.

IR (υ): 1573 (C=N), 1497 (S=O), 1188 (S=O), 1097 (C-N), 1016 (S-O) cm^{-1}.

λ_{abs}= 654 nm, λ_{em}= 678 nm (DMSO).

^{1}H NMR (400 MHz, MeOD) *δ*: 8.41 (d, *J* = 14.1 Hz, 2H, **8,8'**), 7.91 (m, 2H, **15,15'**), 7.88 (d, *J* = 1.7 Hz, 1H, **13 or 13'**), 7.86 (d, *J* = 1.7 Hz, 1H, **13 or 13'**), 7.61 (d, *J* =

8.5 Hz, 2H, **16,16'**), 7.31-7.37 (m, 4H, **1,2,4,5**), 5.76 (d, *J* = 14.1 Hz, 2H, **9,9'**), 3.40 (s, 6H, **18,18'**), 1.79 (s, 12H, **19,19'**).

^{13}C NMR (100 MHz, MeOD) δ: 178.91 (**10,10'**), 174.91(**8,8'**), 153.69 (**3**), 144.03 9 (**14,14'**), 142.24 (**17,17'**), 141.13 (**12,12'**), 133.87 (**6**), 131.59 (**2,4**), 130.51 (**13,13'**), 129.35 (**1,5**), 126.62 (**15,15'**), 119.87 (**7**), 110.22 (**16,16'**), 101.56 (**9,9'**), 49.27 (**11,11'**), 26.16 (**18,18'**), 22.75 (**19,19'**).

6.5 Experimental for Chapter 3

6.5.1 NIR Inherent Heptamethine Nanoparticles

General procedure for the synthesis of nanoparticles (58)

Styrene (122.0 µL, 1 mmol, freshly washed with 4 x 25% NaOH and 4 x brine), divinylbenzene (3.1 µL, 22.0 µmol freshly washed with 4 x 25% NaOH and 4 x brine), 4-vinylbenzylamine hydrochloride (5.9 mg, 35.0 µM), compound **25** (22.5 mg, 35.0 µM), 2,2-azobis (2-methylpropionamidine) dihydrochloride (V-50) (1.6 mg, 6 µmol) and $MgSO_4$ (0.4 mg, 3.0 µmol) were added to N_2 purged water (2.0 mL). The reaction mixture was stirred at 80 °C for 15 h. After cooling to room temperature, the particles were collected by centrifugation (15 min at 30000 g, eppendorf 5430R) and washed with DMF (6 x 2 mL), MeOH (8 x 2 mL) and water (6 x 2 mL). The particles were stored in water at a solid content of 20 mg ml^{-1}.

6.5.2 Solid-Phase Cyanine 3 Synthesis

(4-hydroxyphenyl)carbamic acid *tert*-butyl ester PS[89] (62)

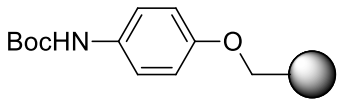

A mixture of (4-hydroxyphenyl)carbamic acid *tert*-butyl ester **61** (6.3 g, 30 mmol), Cs_2CO_3 (9.8 g, 30 mmol), KI (0.17 g, 1 mmol) and 1% DVB cross-linked chloromethyl polystyrene (2 mmol g^{-1}) (5.0 g, 10 mmol) in acetone (45.0 mL) was

heated at 70 °C for 16 h. The resin was isolated by filtration, washed with water (4 × 100.0 mL), DMF (4 × 50.0 mL), DCM (3 × 50.0 mL), Et_2O (3 × 50.0 mL) and dried overnight *in vacuo* at 40 °C to give the product as a beige resin.

IR (neat) 1717 (C=O), 1510 (N-H), 1156 (C-O) cm^{-1}.
All data in agreement with the literature[89].

4-aminophenol PS[89] (63)

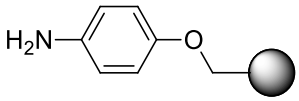

Resin **62** (5.0 g, 7.5 mmol) was shaken at room temperature with a 20% solution of TFA in DCM (75.0 mL) for 2 h, filtered and washed with DCM (50.0 mL). The resin was then shaken with a 10% solution of TEA in DCM (75.0 mL) for 15 min, filtered, washed with DCM (50.0 mL) and dried overnight *in vacuo* at 40 °C to give a product as a beige resin.

IR (υ) 3023 (N-H) 1601 (N-H), 1217 (C-O) cm^{-1}.
All data in agreement with the literature[89].

Ethyl 4-hydroxyphenylimidoformate PS[89] (64)

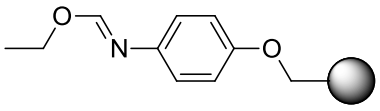

To resin **63** (6.0 g, 9.9 mmol) was added a solution of triethylorthoformate (25.0 mL, 150.0 mmol) and a solution of $BF_3 \cdot OEt_2$ (1.9 mL, 15 mmol) in dry DCM (50.0 mL) and the solution stirred at room temperature for 6 h. Dry DIPEA (3.5 mL, 20.0 mmol) was added and the mixture stirred for 5 min. The resin was isolated by

filtration, washed with DCM (3 x 20 mL), and dried *in vacuo* to give the product as a brown resin.

IR (υ) 1630 (N=N), 1219 (C-O) cm^{-1}.
All data in agreement with the literature[89].

2-[(E)-2-(4-hydroxyanilino)ethenyl]-1,3,3-trimethyl-3*H*-indolium iodide PS[89] (65)

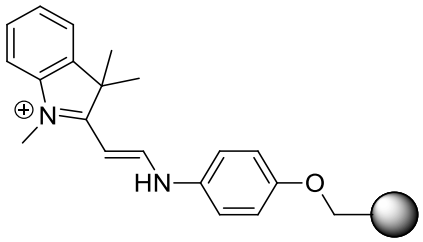

To resin **64** (1.0 g, 1.53 mmol) and indolium salt **9** (2.3 g, 7.65 mmol) was added DMF (8.0 mL) and the mixture stirred at 120 °C for 15 min under microwave irradiation. After cooling, the resin was isolated by filtration, washed with DMF (3 × 10.0 mL) and DCM (3 × 10.0 mL), and dried *in vacuo* to give the product as an orange resin.

IR (υ) 3023 (N-H), 1684 (C=N), 1227 (C-N), 1004 (C-O) cm^{-1}.
All data in agreement with the literature[89].

6-((E)-3,3-dimethyl-2-((E)-3-(1,3,3-trimethyl-3*H*-indolium-2-yl)allylidene)indolin-1-yl)hexanoate (59)

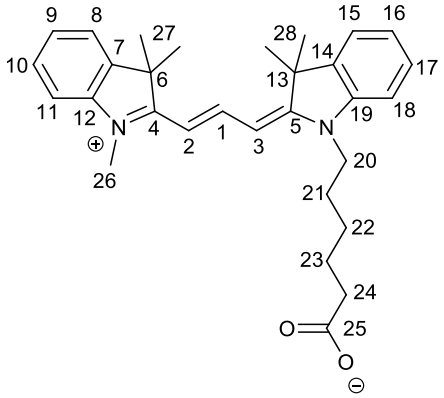

To resin **65** (1.1 g, 0.80 mmol) were added dry pyridine (5.0 mL), DIPEA (1.3 mL, 7.4 mmol), Ac_2O (0.7 mL, 7.4 mmol) and indolium salt **7** (35.0 mg, 0.10 mmol). The mixture was stirred at room temperature for 2 h. The solvent was removed by filtration and the resin washed with DCM (3 x 10.0 mL). The filtrates were combined and evaporated and the resulting solid was dissolved in DCM (15.0 mL) and washed with water (3 x 10.0 mL). After removal of the solvent *in vacuo*, a red solid was recovered and was purified by column chromatography [eluting solvent: DCM:MeOH (90:10)] to give a dark glassy red solid (37 mg, 81%).

HPLC (method 2) t_r = 5.6 min, purity 81% (ELSD).
MS (ES): calculated for $C_{30}H_{37}N_2O_2$ $[M+H]^+$ m/z 457.3. Found 457.2 (100%).
λ_{abs}= 547 nm, λ_{em}= 570 nm (MeOH).
^{1}H NMR (500 MHz, CD_3OD) δ: 8.51 (t, *J* = 13.5 Hz, 1H, **1**), 7.50 (d, *J* = 7.4 Hz, 2H, **8,15**), 7.39-7.42 (m, 2H, **10,17**), 7.30 (m, 4H, **9,11**, **16,18**), 6.43 (d, *J* = 13.5 Hz, 1H, **2 or 3**), 6.40 (d, 1H, *J* = 13.5 Hz, **2 or 3**), (m, 2H, **20**), 3.65 (s, 3H,**26**), 2.15 (t, 2H, *J* = 7.4 Hz, **24**), 1.82 (quintet, 2H, *J* = 7.8 Hz, **21**), 1.73 (s, 12H, **27,28**), 1.66 (quintet, 2H, *J* = 7.5 Hz, **23**), 1.44-1.50 (m, 2H, **22**).
^{13}C NMR (125MHz, CD_3OD) δ: 182.51 (**25**), 176.62 (**5**),176.11 (**4**) 152.09 (**1**), 144.24 (**12**), 143.43 (**7**), 142.31 (**19**), 142.09 (**14**), 130.12 (**10**), 130.00 (**17**), 126.82 (**9**), 126.73 (**16**), 123.53 (**8,15**), 112.64 (**11**), 112.31 (**18**), 103.83 (**2**), 103.72 (**3**),

51.52 (**6**), 50.63 (**13**) 45.21 (**20**), 38.64 (**24**), 31.82 (**26**), 28.34 (**21**), 28.30 (**27**), 28.21(**28**), 27.73 (**23**), 27.24 (**22**).
All data in agreement with the literature[89].

6.5.3 Solid-Phase Cyanine 5 Synthesis

4-[(E,2E)-3-methoxy-2-propenylidene]aminophenol PS (66)

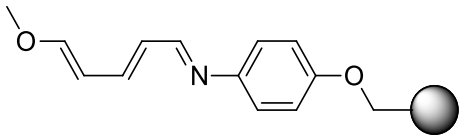

To resin **63** (2.0 g, 3.34 mmol) was added a solution of 1,1,3,3-tetramethoxypropane (7.4 mL, 45.1 mmol) and a solution of $BF_3 \cdot OEt_2$ (0.46 mL, 3.71 mmol) in dry DCM (9.0 mL) and the mixture stirred at room temperature for 6 h. Dry DIPEA (0.94 mL, 5.51 mmol) was added and the mixture stirred for a further 5 min. The resin was isolated by filtration, washed with DCM (3 x 20.0 mL), and dried *in vacuo* to give the product as a dark blue-black resin.

IR (υ) 1630 (C=N), 1219 (C-O) cm^{-1}.
All data in agreement with the literature[89].

2-[(1E,3E)-4-(4-hydroxyanilino)-1,3-butadienyl]-1,3,3-trimethyl-3*H*-indolium iodide (67)

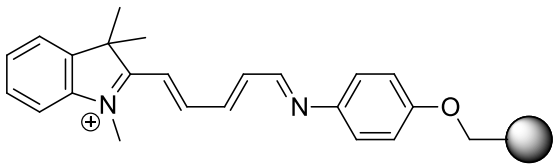

To resin **66** (1.0 g, 1.56 mmol) and indolium salt **9** (2.3 g, 7.6 mmol) was added DMF (8.0 mL) and the mixture stirred at 120 °C for 15 min under microwave

irradiation. After cooling, the resin was isolated by filtration, washed with DMF (3 × 10.0 mL) and DCM (3 × 10.0 mL), and dried *in vacuo* to give the product as a blue/black resin.

IR (υ) 1566 (C=N), 1505 (C=N), 1190 (C-N), 1171 (C-O) cm^{-1}.
All data in agreement with the literature[89].

2-((1E,3E,5E)-5-(1-(5-carboxypentyl)-3,3-dimethylindolin-2-ylidene)penta-1,3-dienyl)-1,3,3-trimethyl-3*H*-indolium iodide (60)

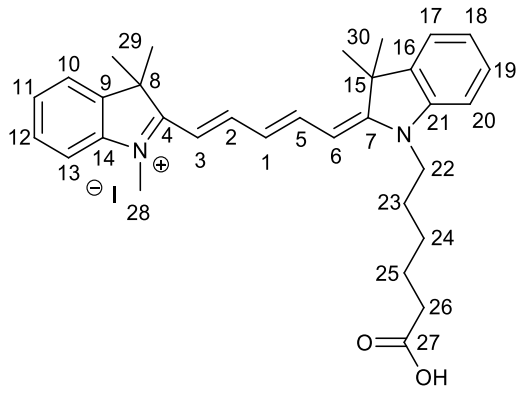

To resin **67** (1.1 g, 1.1 mmol) were added dry pyridine (7.0 mL), DIPEA (1.9 mL, 11 mmol), Ac_2O (1.0 mL, 11 mmol) and indolium salt **7** (50.0 mg, 0.14 mmol). The mixture was stirred at room temperature for 2 h. Afterwards the resin was removed by filtration and washed several times with DCM (4 x 10.0 mL). The filtrates were combined and evaporated and the resulting solid was dissolved in DCM (15.0 mL) and washed with water (3 x 10.0 mL). After removal of the solvent *in vacuo*, a blue solid formed and was purified by column chromatography [eluting solvent: DCM:MeOH (90:10)] to give **60** as a dark blue solid (57 mg, 84%).

HPLC (method 2) t_r = 6.0 min, Purity 91% (ELSD).
MS (ES): calculated for $C_{32}H_{40}N_2O_2$ $[M+H]^+$ m/z (%) 484.3. Found 484.3 (35%)
λ_{abs}= 640 nm, λ_{em}= 665 nm (MeOH); λ_{abs}= 648 nm, λ_{em}= 675 nm (DMSO),.

^{1}H NMR (500 MHz, MeOD) δ: 8.29 (t, J = 13.1 Hz, 2H, **2,5**), 7.50 (d, J = 7.5 Hz, 2H, **10,17**), 7.43-7.40 (m, 2H, **12,19**), 7.32-7.25 (m, 4H, **11,13,18,20**), 6.71 (dd, J = 9.6Hz, J = 18.2 Hz, 1H, **1**), 6.33 (t, J = 14.4 Hz, 2H, **3,6**), 4.14 (t, J = 7.5 Hz, 2H, **22**), 3.66 (s, 3H, **28**), 2. 33 (t, J = 7.3 Hz, 2H, **26**), 1.88-1.82 (m, 2H, **23**), 1.72 (s + m, 14H, **25,29,30**), 1.56-1.50 (m, 2H, **24**).

^{13}C NMR (125 MHz, MeOD) δ: 177.6 (**27**), 175.1 (**4**), 174.4 (**7**), 155.3 (**2**), 144.1 (**14**), 143.4 (**9**), 142.5 (**21**), 142.4 (**16**), 129.6 (**5**), 129.5 (**1**), 126.7 (**12**), 126.0 (**19**), 124.5 (**11**), 123.3 (**18**), 123.1 (**10**), 122.7 (**17**), 111.9 (**13**), 111.7 (**20**), 104.4 (**3**), 104.3 (**6**), 50.4 (**8**), 50.3 (**15**), 44.7 (**22**), 34.8 (**26**), 31.6 (**28**), 28.0 (**24**), 27.9 (**29**), 27.8 (**30**), 27.2 (**23**), 25.7 (**25**).

All data in agreement with the literature[89].

Aminomethyl and Boronic acid Functionalised Nanoparticles (68)

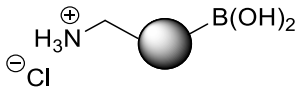

Styrene (122.0 µL, 1 mmol, freshly washed with 4 x 25% NaOH and 4 x brine), divinylbenzene (3.1 µL, 22 µmol freshly washed with 4 x 25% NaOH and 4 x brine), 4-vinylbenzylamine hydrochloride (5.9 mg, 35.0 µM), 4-vinylbenzylboronic acid (5.2 mg, 35.0 µM), 2,2-azobis (2-methylpropionamidine) dihydrochloride (V-50) (1.6 mg, 6.0 µmol) and $MgSO_4$ (0.4 mg, 3.0 µmol) were added to N_2 purged water (2.0 mL). The reaction mixture was stirred at 80 °C for 15 h. After cooling to room temperature, the particles were collected by centrifugation (15 min at 30000 g, eppendorf 5430R) and washed with DMF (3 x 2.0 mL), MeOH (3 x 2.0 mL) and water (3 x 2.0 mL). The particles were stored in water at a solid content of 20 mg/ml.

General Procedure for Pd-mediated Particle Conjugation (69)

Conjugation of iodated cargo was carried out by Suzuki-Miyaura cross-coupling. A solution of iodofluorescein (40.0 µL, 50 equiv.) in DMSO (4.0 µL) was prepared and

added to a suspension of $(HO)_2B/H_2N$ nanoparticles **68** (0.8 µmol, 1 equiv.) in PBS (1.0 mL, pH 7.4) and sonicated for 1 min. Afterwards, a catalyst stock solution (Table 5) were added and the reaction mixture shaken at 1400 rpm at 37 °C for 12 h. The particle mixture was washed in water (3 x 1.0 mL) and stored in PBS at a concentration of 10 mg/mL.

6.6 Experimental for Chapter 4

Ethyl (3-hydroxyphenyl) carbamate (72)

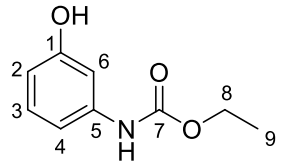

3-Aminophenol (50.0 g, 0.46 mol) was dissolved in hot EtOAc (175.0 mL). Ethyl chloroformate (21.7 mL, 0.23 mol) was added dropwise over 30 min while heating to reflux. The mixture was allowed to stir at reflux for a further 15 min after addition and then cooled. The solution was filtered and the solid washed with EtOAc before removal of the solvent to yield a white solid (4.0 g, 96%).

HPLC (method 2) t_r = 1.9 min, Purity 100% (ELSD).

MS (ES): calculated for $C_9H_{11}NNaO_3$ $[M+Na]^+$ m/z 204.1. Found 204.1 (100%).

Mp. 96 °C.

IR (υ): 3257 (O-H), 1685 (C=O), 1556 (N-H), 1449, 1249 (OC-O), 1223 (C-O), 1061 (C-N) cm^{-1}.

^{1}H NMR (500 MHz, DMSO-d6) δ: 9.46 (s, 1H, **NH**), 9.31 (s, 1H, **OH**), 7.03 – 6.98(m, 2H, **3, 6**), 6.84 (dd, J = 8.7, 1.5 Hz,1H, **4**) 6.37 (dd, J = 8.0, 1.7 Hz, 1H, **2**), 4.09 (quartet, J = 7.1 Hz, 2H, **8**), 1.23 (t, J = 7.1 Hz, 3H, **9**).

^{13}C NMR (126 MHz, DMSO-d6) δ: 158.13 (**1**), 153.88 (**7**), 140.74 (**5**), 129.79 (**3**), 109.88 (**4**), 109.45 (**2**), 105.76 (**6**), 60.46 (**8**), 15.01 (**9**).

All data in agreement with the literature[216]

7-[(ethoxycarbonyl)amino]-4-methyl-2-oxo-, ethyl ester (73)

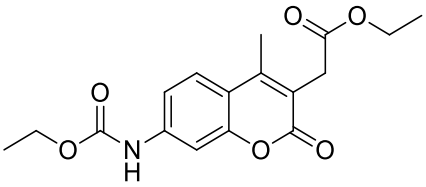

Carbonate **72** (2.0 g, 11 mmol) and diethylacetylsuccinate (2.2 mL, 0.11 mmol) were dissolved in 75% H_2SO_4 (5.0 mL). The mixture was stirred at room temperature for 3 h. Ice water was added (50.0 mL) and the filter cake was washed with cold water until the washings became ~ pH 7. The compound was confirmed by IR spectroscopy before taking compound to the next step.

IR (υ): 3285 (N-H), 1731 (C=O), 1683 (C=O), 1588, 1226 (OC-O), 1153 (C-O), 1060 (C-N) cm^{-1}.
Procedure followed from reference[228].

7-Amino-4-methylcoumarin-3-acetic acid (74)

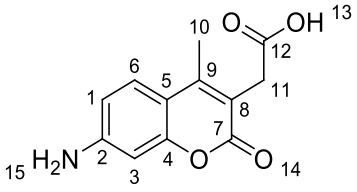

Carbonate **73** (0.3 g, 0.98 mmol) and $LiOH.H_2O$ (0.12 g, 4.9 mmol) were dissolved in a mixture of EtOH and H_2O (1:1, 25.0 mL) and stirred at reflux for 4 h. The solution was cooled and acidified with 2 M HCl to produce a pink precipitate which was washed with water. The 7-[(ethoxycarbonyl)amino]-4-methyl-2-oxo-2*H*-1-benzopyran-3-acetic acid (1.8 g, 6.2 mmol) and NaOH (2.5 g, 62.0 mmol) were the dissolved in H_2O (20.0 mL) and stirred under reflux. After 16 h, the solution was

cooled to room temperature and acidified with 2 M H_2SO_4 to give a white solid (1.15 g, 80%).

HPLC (method 2) t_r = 3.0 min, Purity 99% (ELSD).

MS (ES): calculated for $C_{12}H_{11}NNaO_4$ $[M+Na]^+$ m/z 256.1. Found 256.1.

Mp. 226 °C decomposed.

Absorption and Emission (H_2O) λ_{abs}= 325 nm, λ_{em}= 450 nm.

IR (υ): 3458 (N-H), 3358 (N-H), 3236 (O-H) 1677 (C=O), 1600 (HOC=O) cm^{-1}.

^{1}H NMR (500 MHz, DMSO-d6) *δ*: 12.34 (s, 1H, **13**), 7.47 (d, *J* = 8.7 Hz, 1H,**6**), 6.59 (dd, *J* = 8.7, 2.2 Hz, 1H, **1**), 6.42 (d, *J* = 2.2 Hz, 1H,**3**), 6.06 (s, 2H, **15**), 3.50 (s, 2H, **11**), 2.28 (s, 3H, **10**).

^{13}C NMR (126 MHz, DMSO-d6) *δ*: 172.52 (**12**), 161.93 (**7**), 154.53 (**2**), 152.95 (**4**), 150.13 (**9**), 126.87 (**6**), 113.27 (**8**), 111.86 (**5**), 109.57 (**1**), 98.83 (**3**), 32.92 (**11**), 15.26 (**10**).

All data in agreement with the literature[228]

7-Fmoc-Amino-4-methylcoumarin-3-acetic acid (75)

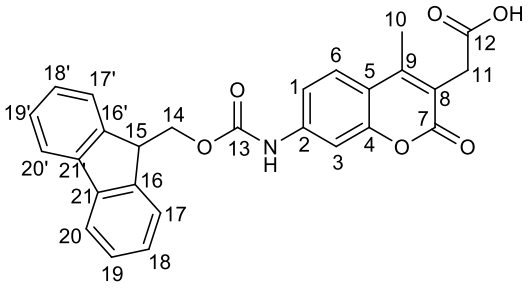

Coumarin **74** (0.5 g, 2.1 mmol) was dissolved in anhydrous DCM (3.0 mL). Freshly distilled TMS-Cl (0.5 mL, 4.3 mmol) was added and the solution cooled to 0 °C. Fmoc-OSu (0.8 g, 2.4 mmol) and DIPEA (0.56 mL, 4.3 mmol) were added and the solution refluxed for 3 h. After cooling, the solvent was evaporated and the product precipitated in Et_2O to give a yellow solid (0.98 g, 99%).

HPLC (method 2) t_r = 6.9 min, Purity 100% (ELSD).

Mp. 240 °C decomposed.

IR (ν): 3304 (O-H), 1746 (HOC=O), 1689 (C=O), 1615 (OC=O), 1053 (C-N) cm^{-1}.

^{1}H NMR (500 MHz, DMSO) δ: 12.45 (s, 1H, **OH**), 10.19 (s, 1H, **NH**), 7.93 (d, J = 7.5 Hz, 2H, **20,20'**), 7.79 – 7.72 (m, 4H **1,6,17,17'**), 7.55 (s, 1H, **NH**), 7.46-7.41 (m, J = 7.4 Hz, 3H, **3,19,19'**), 7.37 (td, J = 7.4, 0.9 Hz, 2H, **18,18'**), 4.57 (d, J = 6.5 Hz, 2H, **14**), 4.39 – 4.30 (m, 1H, **15**), 3.59 (s, 2H, **11**), 2.37 (s, 3H, **10**).

^{13}C NMR (126 MHz, DMSO) (Fmoc Ar together) δ: 171.98 (**12**), 161.31 (**7**), 153.72 (**13**), 152.91 (**4**), 149.31 (**9**), 144.14 (**2**), 142.55 (**16,16'**), 141.30 (**21,21'**), 128.20 (**18,18'**), 127.63 (**19,19'**), 126.67 (**17,17'**), 125.56 (**6**), 120.70 (**20,20'**), 117.95 (**1**), 115.14 (**8**), 114.99 (**5**), 104.86 (**3**), 66.38 (**14**), 47.03 (**15**), 33.19 (**11**), 15.40 (**10**).

2*H*-1-Benzopyran-4-methyl-5-acetamide,7-[[(2*S*)-2-amino-1-oxopropyl]amino]-2-oxo- (78)

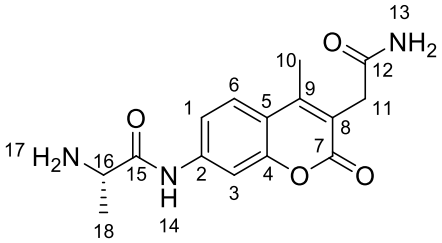

Coumarin **75** was attached onto the solid-phase by coupling to a polystyrene resin with rink-amide linker using standard coupling conditions. Fmoc deprotection was carried out with 20% piperidine in DMF followed by twice coupling to Fmoc-alanine-OH with 3 eq HATU and 3 eq DIPEA. Cleavage from the linker was carried out with TFA:DCM:TIS (95:2.5:2.5) and purification was carried out by preparative HPLC.

HPLC (method 2) t_r = 0.8 min, Purity 100% (ELSD).

MS (ES): calculated for $C_{15}H_{18}N_3O_4$ $[M+H]^+$ m/z 304.1. Found 304.0 (100%).

^{1}H NMR (500 MHz, MeOD) δ: 7.86 (d, J = 2.1 Hz, 1H, **3**), 7.80 (d, J = 8.8 Hz, 1H, **6**), 7.49 (dd, J = 8.8, 2.1 Hz, 1H,**1**), 4.11-4.06 (m, 1H, **16**), 3.67 (s, 2H, **11**), 2.47 s, 3H,**10**), 1.62 (d, J = 7.1 Hz, 3H,**18**).
^{13}C NMR (126 MHz, MeOD) δ: 173.68 (**12**), 168.24 (**15**), 162.26 (**7**), 152.84 (**4**), 149.98 (**2**), 140.75 (**9**), 125.74 (**6**), 118.60 (**1**), 116.77 (**5**), 115.53 (**8**), 106.55 (**3**), 33.18 (**16**), 16.04 (**11**), 14.03 (**18**), 12.26 (**10**).

2*H*-1-Benzopyran-4-methyl-5-acetamide,7-[[(2*R*)-2-amino-1-oxopropyl]amino]-2-oxo- (79)

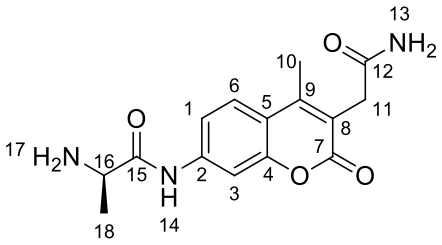

Procedure and purification for compound **78** repeated with use of Fmoc-D-Ala-OH.

HPLC (method 6) t_r = 1.1 min, Purity 88% (ELSD).
MS (ES): calculated for $C_{15}H_{18}N_3O_4$ $[M+H]^+$ m/z 304.1. Found 304.2 (100%).
^{1}H NMR (500 MHz, D_2O) δ: 7.79 (d, J = 8.3 Hz, 1H, **6**), 7.64 (s, 1H, **3**), 7.41 (d, J = 8.9 Hz, 1H, **1**), 3.65 (s, 2H, **11**), 3.15 – 3.10 (m, 1H, **16**), 2.42 (s, 3H, **10**), 1.35 (d, J = 5.5 Hz, 3H, **18**).

Appendix 1

All published material used in this thesis was adapted and re-printed with permissions for use electronically and on paper in the present thesis. A summary of all the acquired permissions is listed below.

Figure 1: R. Weissleder, M. J. Pittet, *Nature* **2008**, *452*, 580-589. **2).** Quon, S. S. Gambhir, *Journal of Clinical Oncology* **2005**, *23*, 1664-1673. **3)**. L. Figueiredo, H. Alencar, R. Weissleder, U. Mahmood, *International Journal of Cancer* **2006**, *118*, 2672-2677. **4)** P. J. Saeij, J. P. Boyle, M. E. Grigg, G. Arrizabalaga, J. C. Boothroyd, *Infection and Immunity* **2005**, *73*, 695-702. **5)** M. Rudin, R. Weissleder, *Nature Reviews Drug Discovery* **2003**, *2*, 123-131. **6)** D. E. Sosnovik, M. Nahrendorf, N. Deliolanis, M. Novikov, E. Aikawa, L. Josephson, A. Rosenzweig, R. Weissleder, V. Ntziachristos, *Circulation* **2007**, *115*, 1384-1391. **7)** L. V. Wang, S. Hu, *Science* **2012**, *335*, 1458-1462.

Figure 2: K. Politi, P.-D. Fan, R. Shen, M. Zakowski, H. Varmus, *Disease Models & Mechanisms* **2010**, *3*, 111-119.

Figure 3: R. L. Scherer, M. N. VanSaun, O. McIntyre, L. M. Matrisian, *Molecular Imaging* **2008**, *7*, 118-131.

Figure 4: C. Bremer, C.-H. Tung, R. Weissleder, *Nature Medicine* **2001**, *7*, 743-748.

Figure 5: V. Ntziachristos, E. A. Schellenberger, J. Ripoll, D. Yessayan, E. Graves, A. Bogdanov, L. Josephson, R. Weissleder, *Proceedings of the National Academy of Sciences of the United States of America* **2004**, *101*, 12294-12299.

Figure 6: R. M. Yusop, A. Unciti-Broceta, E. M. V. Johansson, R. M. Sánchez-Martín, M. Bradley, *Nature Chemistry* **2011**, *3*, 239-243.

Figure 9: A. P. de Silva, T. S. Moody, G. D. Wright, *Analyst* **2009**, *134*, 2385-2393.

Figure 10: H. He, M. A. Mortellaro, M. J. P. Leiner, R. J. Fraatz, J. K. Tusa, *Journal of the American Chemical Society* **2003**, *125*, 1468-1469.

Figure 11: M. Ethirajan, Y. Chen, P. Joshi, R. K. Pandey, *Chemical Society Reviews* **2011**, *40*, 340-362.

Figure 13: L. D. Lavis, R. T. Raines, *American Chemical Society Chemical Biology* **2008**, *3*, 142-155

Figure 14: H. Kobayashi, M. Ogawa, R. Alford, P. L. Choyke, Y. Urano, *Chemical Reviews* **2009**, *110*, 2620-2640.

Figure 15: S. B. Raymond, J. Skoch, I. D. Hills, E. E. Nesterov, T. M. Swager, B. J. Bacskai, *European Journal of Nuclear Medicine and Molecular Imaging* **2008**, *35*, 93-98.

Figure 16: M. Hintersteiner, A. Enz, P. Frey, A.-L. Jaton, W. Kinzy, R. Kneuer, U. Neumann, M. Rudin, M. Staufenbiel, M. Stoeckli, K.-H. Wiederhold, H.-U. Gremlich, *Nature Biotechnology* **2005**, *23*, 577-583.

Figure 19: D. Oushiki, H. Kojima, T. Terai, M. Arita, K. Hanaoka, Y. Urano, T. Nagano, *Journal of the American Chemical Society* **2010**, *132*, 2795-2801.

Figure 46: K. Ando, H. Kawaguchi, *Journal of Colloid and Interface Science* **2005**, *285*, 619-626.

Figure 47: Q. Tian, J. Hu, Y. Zhu, R. Zou, Z. Chen, S. Yang, R.-W. Li, Q. Su, Y. Han, X. Liu, *Journal of the American Chemical Society* **2013**.

Table 1: R. Weissleder, M. J. Pittet, *Nature* **2008**, *452*, 580-589.

Appendix 2

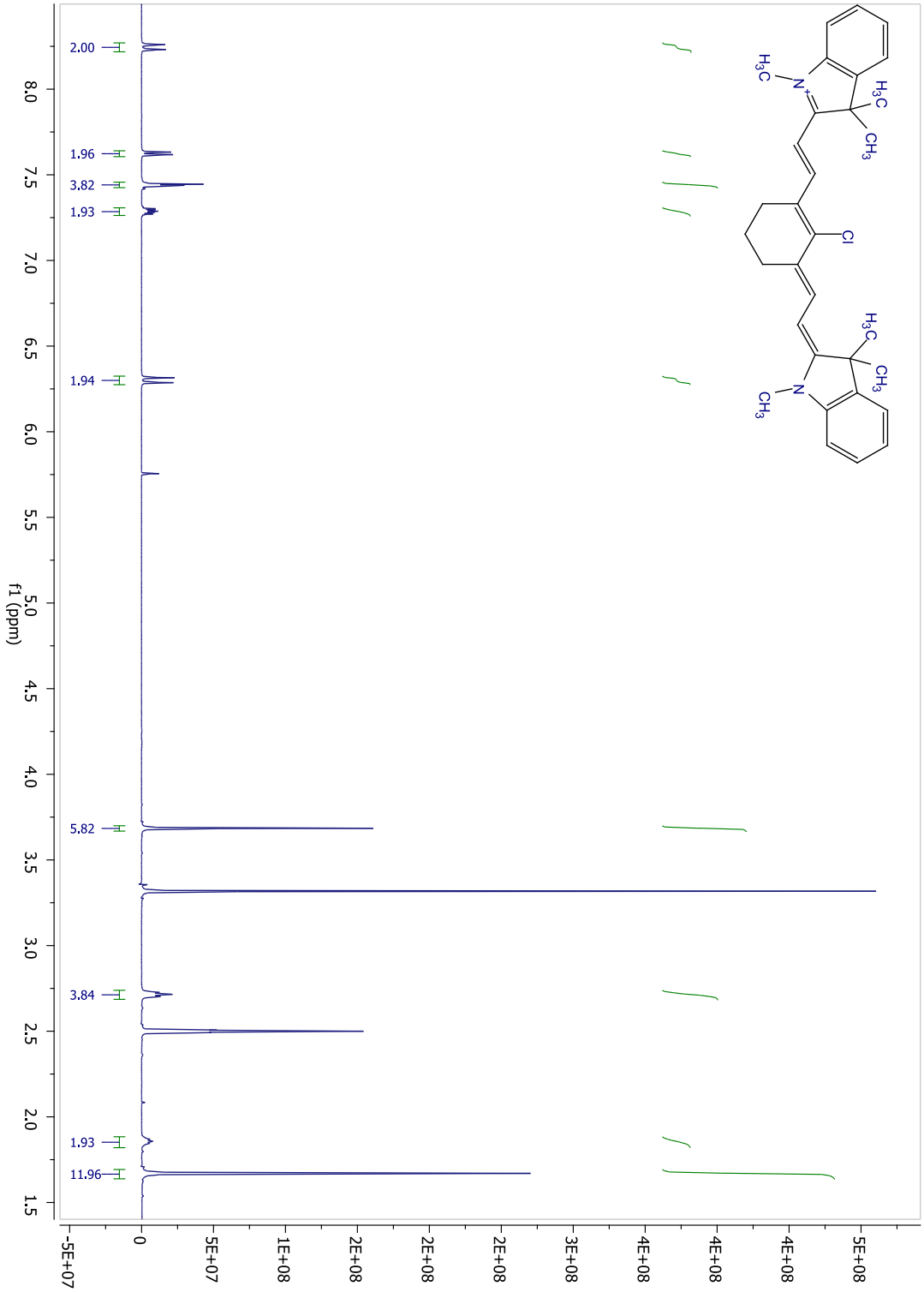
2.00
1.96
3.82
1.93
1.94
5.82
3.84
1.93
11.96
f1 (ppm)
8.0
7.5
7.0
6.5
6.0
5.5
5.0
4.5
4.0
3.5
3.0
2.5
2.0
1.5
-5E+07
0
5E+07
1E+08
2E+08
2E+08
2E+08
3E+08
4E+08
4E+08
4E+08
5E+08
H3C
N+
H3C
CH3
Cl
H3C
CH3
N
CH3

Appendix 3

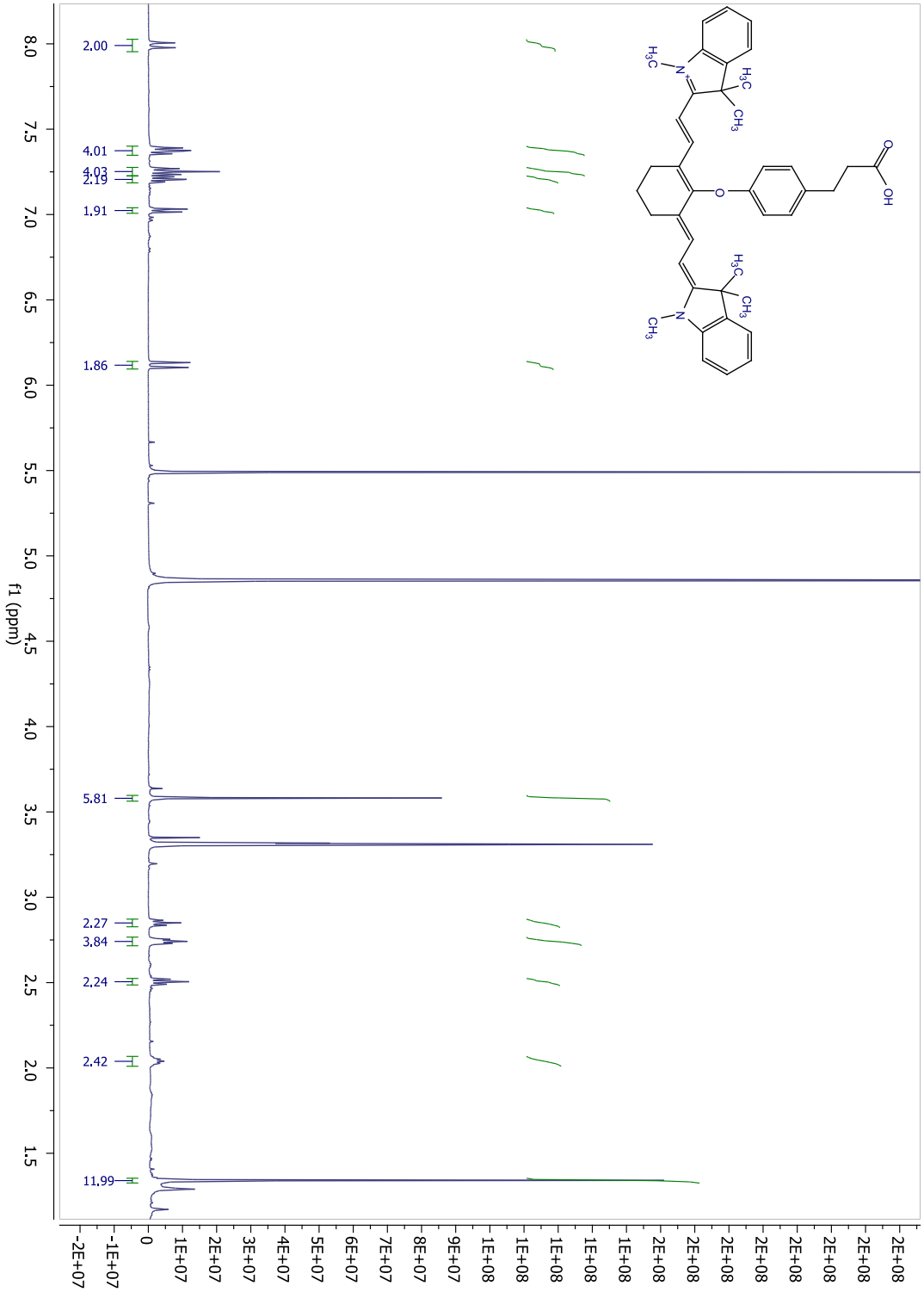
2.00
4.01
4.03
2.19
1.91
1.86
5.81
2.27
3.84
2.24
2.42
11.99
f1 (ppm)
8.0
7.5
7.0
6.5
6.0
5.5
5.0
4.5
4.0
3.5
3.0
2.5
2.0
1.5
-2E+07
-1E+07
0
1E+07
2E+07
3E+07
4E+07
5E+07
6E+07
7E+07
8E+07
9E+07
1E+08
1E+08
1E+08
1E+08
2E+08
2E+08
2E+08
2E+08
2E+08
2E+08
2E+08
H3C
N
CH3
H3C
CH3
O
O
OH
H3C
CH3
N
CH3

Appendix 4

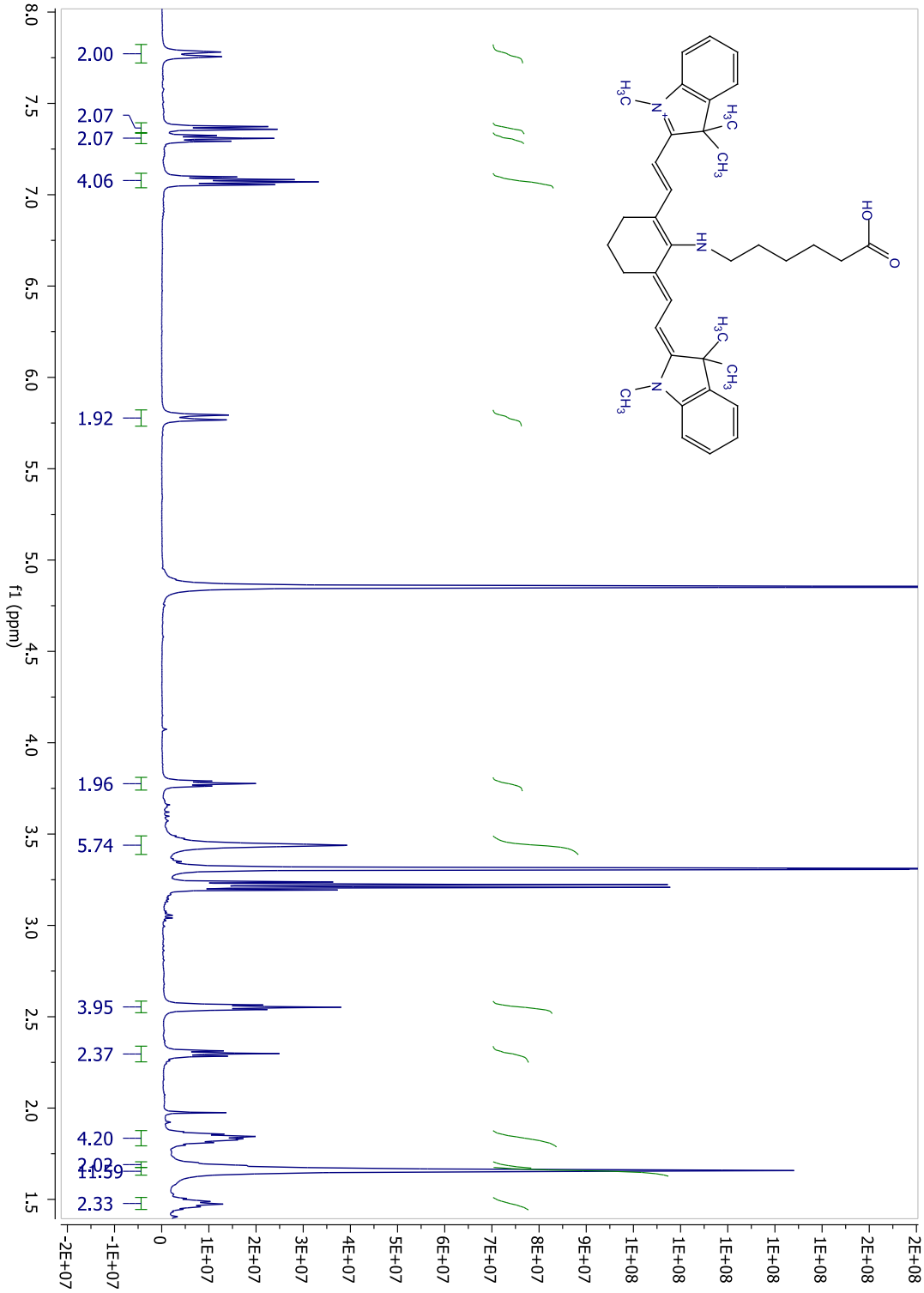
2.00
2.07
2.07
4.06
1.92
1.96
5.74
3.95
2.37
4.20
2.02
11.59
2.33
f1 (ppm)
8.0
7.5
7.0
6.5
6.0
5.5
5.0
4.5
4.0
3.5
3.0
2.5
2.0
1.5
-2E+07
-1E+07
0
1E+07
2E+07
3E+07
4E+07
5E+07
6E+07
7E+07
8E+07
9E+07
1E+08
1E+08
1E+08
1E+08
1E+08
2E+08
2E+08
H3C
N+
H3C
CH3
HN
HO
O
H3C
CH3
N
CH3

Appendix 5

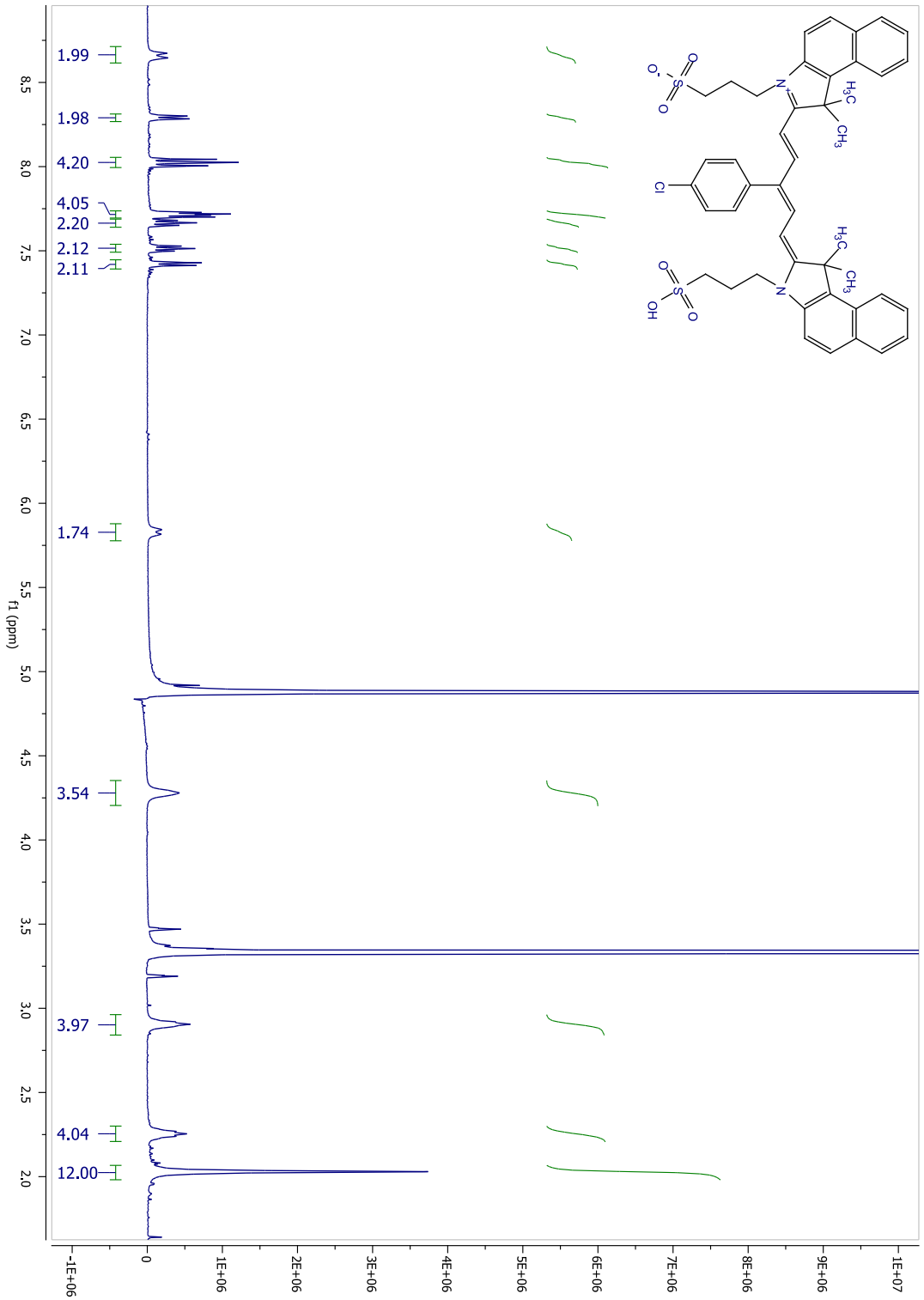
1.99
1.98
4.20
4.05
2.20
2.12
2.11
1.74
3.54
3.97
4.04
12.00
f1 (ppm)
8.5
8.0
7.5
7.0
6.5
6.0
5.5
5.0
4.5
4.0
3.5
3.0
2.5
2.0
-1E+06
0
1E+06
2E+06
3E+06
4E+06
5E+06
6E+06
7E+06
8E+06
9E+06
1E+07
O
S
O
O
N+
H3C
CH3
Cl
H3C
CH3
N
S
O
OH
O

References

[1] S. J. Eustace., E. Nelson., *British Medical Journal* **2004**, *328*, 1387.

[2] D. J. Brenner, E. J. Hall, *New England Journal of Medicine* **2007**, *357*, 2277-2284.

[3] T. Jones, *European Journal of Nuclear Medicine* **1996**, *23*, 207-211.

[4] aT. A. Holly, B. G. Abbott, M. Al-Mallah, D. A. Calnon, M. C. Cohen, F. P. DiFilippo, E. P. Ficaro, M. R. Freeman, R. C. Hendel, D. Jain, S. M. Leonard, K. J. Nichols, D. M. Polk, P. Soman, *Journal of Nuclear Cardiology* **2010**, *17*, 941-973; bW. J. Jagust, T. F. Budinger, B. R. Reed, *Archives of Neurology* **1987**, *44*, 258-262.

[5] H. Kobayashi, M. Ogawa, R. Alford, P. L. Choyke, Y. Urano, *Chemical Reviews* **2009**, *110*, 2620-2640.

[6] aS. M. Ametamey, M. Honer, P. A. Schubiger, *Chemical Reviews* **2008**, *108*, 1501-1516; bS. A. Hilderbrand, R. Weissleder, *Current Opinion in Chemical Biology* **2010**, *14*, 71-79.

[7] R. Weissleder, M. J. Pittet, *Nature* **2008**, *452*, 580-589.

[8] A. Quon, S. S. Gambhir, *Journal of Clinical Oncology* **2005**, *23*, 1664-1673.

[9] J.-L. Figueiredo, H. Alencar, R. Weissleder, U. Mahmood, *International Journal of Cancer* **2006**, *118*, 2672-2677.

[10] J. P. J. Saeij, J. P. Boyle, M. E. Grigg, G. Arrizabalaga, J. C. Boothroyd, *Infection and Immunity* **2005**, *73*, 695-702.

[11] M. Rudin, R. Weissleder, *Nature Reviews Drug Discovery* **2003**, *2*, 123-131.

[12] D. E. Sosnovik, M. Nahrendorf, N. Deliolanis, M. Novikov, E. Aikawa, L. Josephson, A. Rosenzweig, R. Weissleder, V. Ntziachristos, *Circulation* **2007**, *115*, 1384-1391.

[13] L. V. Wang, S. Hu, *Science* **2012**, *335*, 1458-1462.

[14] K. Politi, P.-D. Fan, R. Shen, M. Zakowski, H. Varmus, *Disease Models & Mechanisms* **2010**, *3*, 111-119.

[15] aR. Weissleder, *Science* **2006**, *312*, 1168-1171; bS. S. Gambhir, *Nature Reviews Cancer* **2002**, *2*, 683-693.

[16] aF. A. Jaffer, P. Libby, R. Weissleder, *Circulation* **2007**, *116*, 1052-1061; bF. A. Jaffer, R. Weissleder, *Circulation Research* **2004**, *94*, 433-445.

[17] J. Chen, C.-H. Tung, J. R. Allport, S. Chen, R. Weissleder, P. L. Huang, *Circulation* **2005**, *111*, 1800-1805.

[18] R. L. Scherer, M. N. VanSaun, O. McIntyre, L. M. Matrisian, *Mol Imaging* **2008**, *7*, 118-131.

[19] aJ. Tremoleda, M. Khalil, L. Gompels, M. Wylezinska-Arridge, T. Vincent, W. Gsell, *European Journal of Nuclear Medicine and Molecular Imaging Research* **2011**, *1*, 11; bP. J. Keller, *Science* **2013**, *340*; cB. J. Pichler, H. F. Wehrl, M. S. Judenhofer, *Journal of Nuclear Medicine* **2008**, *49*, 5S-23S; dE. M. Sevick-Muraca, *Annual Review of Medicine* **2012**, *63*, 217-231; eA. F. Chatziioannou, *Molecular Imaging & Biology* **2002**, *4*, 47-63.

[20] aF. M. Lambers, G. Kuhn, R. Muller, *BoneKEy Reports* **2012**, *1*; bG. Antoch, J. Kanja, S. Bauer, H. Kuehl, K. Renzing-Koehler, J. Schuette, A. Bockisch,

J. F. Debatin, L. S. Freudenberg, *Journal of Nuclear Medicine* **2004**, *45*, 357-365.

[21] A. Wagner, H. Mahrholdt, T. A. Holly, M. D. Elliott, M. Regenfus, M. Parker, F. J. Klocke, R. O. Bonow, R. J. Kim, R. M. Judd, *The Lancet* **2003**, *361*, 374-379.

[22] aR. J. Hargreaves, *Clinical Pharmacology and Therapeutics* **2008**, *83*, 349-353; bJ. K. Willmann, N. van Bruggen, L. M. Dinkelborg, S. S. Gambhir, *Nature Reviews Drug Discovery* **2008**, *7*, 591-607; cS. Gross, D. Piwnica-Worms, *Current Opinion in Chemical Biology* **2006**, *10*, 334-342.

[23] E. Bombardieri, L. Gianni, *European Journal of Nuclear Medicine and Molecular Imaging* **2004**, *31*, S179-S186.

[24] aV. Ntziachristos, C. Bremer, R. Weissleder, *European Radiology* **2003**, *13*, 195-208; bP. P. Ghoroghchian, M. J. Therien, D. A. Hammer, *Wiley Interdisciplinary Reviews: Nanomedicine and Nanobiotechnology* **2009**, *1*, 156-167; cJ. O. Escobedo, O. Rusin, S. Lim, R. M. Strongin, *Current Opinion in Chemical Biology* **2010**, *14*, 64-70.

[25] S. S. Gambhir, M. L. James, *Phys Rev* **2012**, *92*, 897-965.

[26] V. Ntziachristos, *Annual Review of Biomedical Engineering* **2006**, *8*, 1-33.

[27] U. Mahmood, C.-H. Tung, A. Bogdanov, R. Weissleder, *Radiology* **1999**, *213*, 866-870.

[28] C. Bremer, C.-H. Tung, R. Weissleder, *Nature Medicine* **2001**, *7*, 743-748.

[29] V. Ntziachristos, R. Weissleder, *Optics Letters* **2001**, *26*, 893-895.

[30] V. Ntziachristos, E. A. Schellenberger, J. Ripoll, D. Yessayan, E. Graves, A. Bogdanov, L. Josephson, R. Weissleder, *Proceedings of the National Academy of Sciences of the United States of America* **2004**, *101*, 12294-12299.

[31] R. H. Webb, in *Methods in Enzymology, Vol. Volume 307* (Ed.: P. M. Conn), Academic Press, **1999**, pp. 3-20.

[32] R. B. Sekar, A. Periasamy, *The Journal of Cell Biology* **2003**, *160*, 629-633.

[33] aF. Thielbeer, S. V. Chankeshwara, E. M. V. Johansson, N. Norouzi, M. Bradley, *Chemical Science* **2013**, *4*, 425; bX. Michalet, F. F. Pinaud, L. A. Bentolila, J. M. Tsay, S. Doose, J. J. Li, G. Sundaresan, A. M. Wu, S. S. Gambhir, S. Weiss, *Science* **2005**, *307*, 538-544.

[34] S. González, Z. Tannous, *Journal of the American Academy of Dermatology* **2002**, *47*, 869-874.

[35] M. Marvin, United States, **1961**.

[36] R. M. Yusop, A. Unciti-Broceta, E. M. V. Johansson, R. M. Sánchez-Martín, M. Bradley, *Nature Chemistry* **2011**, *3*, 239-243.

[37] H. Kashida, T. Takatsu, T. Fujii, K. Sekiguchi, X. Liang, K. Niwa, T. Takase, Y. Yoshida, H. Asanuma, *Angewandte Chemie International Edition* **2009**, *48*, 7044-7047.

[38] aL. Yuan, W. Lin, K. Zheng, S. Zhu, *Accounts of Chemical Research* **2013**, *46*, 1462-1473; bM. Liang, X. Liu, D. Cheng, K. Nakamura, Y. Wang, S. Dou, G. Liu, M. Rusckowski, D. J. Hnatowich, *Bioconjugate Chemistry* **2009**, *20*, 1223-1227.

[39] J. R. Johnson, B. Kocher, E. M. Barnett, J. Marasa, D. Piwnica-Worms, *Bioconjugate Chemistry* **2012**, *23*, 1783-1793.

[40] V. V. Didenko, *Biotechniques* **2001**, *31*, 1106-1121.

[41] L. Stryer, *Annual Review of Biochemistry* **1978**, *47*, 819-846.
[42] aA. P. de Silva, T. S. Moody, G. D. Wright, *Analyst* **2009**, *134*, 2385-2393; bA. P. de Silva, H. Q. N. Gunaratne, T. Gunnlaugsson, A. J. M. Huxley, C. P. McCoy, J. T. Rademacher, T. E. Rice, *Chemical Reviews* **1997**, *97*, 1515-1566.
[43] F. V. Englich, T. C. Foo, A. C. Richardson, H. Ebendorff-Heidepriem, C. J. Sumby, T. M. Monro, *Sensors* **2011**, *11*, 9560-9572.
[44] Y. Ooyama, A. Matsugasako, K. Oka, T. Nagano, M. Sumomogi, K. Komaguchi, I. Imae, Y. Harima, *Chemical Communications* **2011**, *47*, 4448-4450.
[45] Y. Urano, D. Asanuma, Y. Hama, Y. Koyama, T. Barrett, M. Kamiya, T. Nagano, T. Watanabe, A. Hasegawa, P. L. Choyke, H. Kobayashi, *Nature Medicine* **2009**, *15*, 104-109.
[46] H. He, M. A. Mortellaro, M. J. P. Leiner, R. J. Fraatz, J. K. Tusa, *Journal of the American Chemical Society* **2003**, *125*, 1468-1469.
[47] B. Valeur, M. r. N. Berberan-Santos, *Journal of Chemical Education* **2011**, *88*, 731-738.
[48] S. E. Braslavsky, *Pure and Applied Chemistry* **2006**, *79*, 293-465.
[49] A. Jablonski, *Nature* **1933**, *131*, 839-840.
[50] C. L. Amiot, S. P. Xu, S. Liang, L. Y. Pan, J. X. J. Zhao, *Sensors* **2008**, *8*, 3082-3105.
[51] M. Ethirajan, Y. Chen, P. Joshi, R. K. Pandey, *Chemical Society Reviews* **2011**, *40*, 340-362.
[52] W. H. Melhuish, *The Journal of Physical Chemistry* **1961**, *65*, 229-235.
[53] G. A. Crosby, J. N. Demas, *The Journal of Physical Chemistry* **1971**, *75*, 991-1024.
[54] A. T. R. Williams, S. A. Winfield, J. N. Miller, *Analyst* **1983**, *108*, 1067-1071.
[55] A. M. Brouwer, *Pure and Applied Chemistry* **2011**, *83*, 2213-2228.
[56] G. Weber, F. W. J. Teale, *Transactions of the Faraday Society* **1957**, *53*, 646-655.
[57] J. H. Brannon, D. Magde, *The Journal of Physical Chemistry* **1978**, *82*, 705-709.
[58] A. Pardo, D. Reyman, J. M. L. Poyato, F. Medina, *Journal of Luminescence* **1992**, *51*, 269-274.
[59] E. P. Kirby, R. F. Steiner, *The Journal of Physical Chemistry* **1970**, *74*, 4480-4490.
[60] K. K. Sanap, S. D. Samant, *Tetrahedron Letters* **2012**, *53*, 5407-5410.
[61] F. Thielbeer, *SynLett* **2012**, *23*, 1703-1704.
[62] K. Kolmakov, V. N. Belov, J. Bierwagen, C. Ringemann, V. MÃ¼ller, C. Eggeling, S. W. Hell, *Chemistry - A European Journal* **2010**, *16*, 158-166.
[63] M. C. Basheer, U. Santhosh, S. Alex, K. G. Thomas, C. H. Suresh, S. Das, *Tetrahedron* **2007**, *63*, 1617-1623.
[64] A. Loudet, K. Burgess, *Chemical Reviews* **2007**, *107*, 4891-4932.
[65] N. Norouzi, *SynLett* **2013**, *24*, 1307-1308.
[66] aS. Alex, U. Santhosh, S. Das, *Journal of Photochemistry and Photobiology A: Chemistry* **2005**, *172*, 63-71; bO. Malinkiewicz, T. Grancha, A. Molina-

Ontoria, A. Soriano, H. Brine, H. J. Bolink, *Advanced Energy Materials* **2013**, *3*, 472-477.

[67] aK. P. Divya, S. Sreejith, B. Balakrishna, P. Jayamurthy, P. Anees, A. Ajayaghosh, *Chemical Communications* **2010**, *46*, 6069; bP. Li, X. Duan, Z. Chen, Y. Liu, T. Xie, L. Fang, X. Li, M. Yin, B. Tang, *Chemical Communications* **2011**, *47*, 7755; cB. K. Datta, C. Kar, A. Basu, G. Das, *Tetrahedron Letters* **2013**, *54*, 771-774; dS. Deo, H. A. Godwin, *Journal of the American Chemical Society* **1999**, *122*, 174-175.

[68] aS. Luo, E. Zhang, Y. Su, T. Cheng, C. Shi, *Biomaterials* **2011**, *32*, 7127-7138; bX. Tian, K.-H. Baek, I. Shin, *Chemical Science* **2013**, *4*, 947.

[69] aA. E. Albers, B. C. Dickinson, E. W. Miller, C. J. Chang, *Bioorganic & Medicinal Chemistry Letters* **2008**, *18*, 5948-5950; bA. Gomes, E. Fernandes, J. L. F. C. Lima, *Journal of Biochemical and Biophysical Methods* **2005**, *65*, 45-80; cK. Kundu, S. F. Knight, N. Willett, S. Lee, W. R. Taylor, N. Murthy, *Angewandte Chemie International Edition* **2009**, *48*, 299-303.

[70] L. D. Lavis, R. T. Raines, *Ameriacan Chemical Societie Chemical Biology* **2008**, *3*, 142-155.

[71] Y. M. W. Janssen, B. Vanhouten, P. J. A. Borm, B. T. Mossman, *Laboratory Investigation* **1993**, *69*, 261-274.

[72] J. Rao, A. Dragulescu-Andrasi, H. Yao, *Current Opinion in Biotechnology* **2007**, *18*, 17-25.

[73] aD. L. Steffens, G. Y. Jang, S. L. Sutter, J. A. Brumbaugh, L. R. Middendorf, K. Mühlegger, E. R. Mardis, L. A. Weinstock, R. K. Wilson, *Genome Research* **1995**, *5*, 393-399; bS. A. Soper, J. H. Flanagan, Jr., B. L. Legendre, D. C. Williams, R. P. Hammer, *Institute of Electrical and Electronic Engineers Journal of Selected Topics in Quantum Electronics* **1996**, *2*, 1129-1139; cH. Kashida, T. Takatsu, T. Fujii, K. Sekiguchi, X. G. Liang, K. Niwa, T. Takase, Y. Yoshida, H. Asanuma, *Angewandte Chemie-International Edition* **2009**, *48*, 7044-7047; dY. Hara, T. Fujii, H. Kashida, K. Sekiguchi, X. Liang, K. Niwa, T. Takase, Y. Yoshida, H. Asanuma, *Angewandte Chemie International Edition* **2010**, *49*, 5502-5506.

[74] aS. B. Raymond, J. Skoch, I. D. Hills, E. E. Nesterov, T. M. Swager, B. J. Bacskai, *European Journal of Nuclear Medicine and Molecular Imaging* **2008**, *35*, 93-98; bM. Hintersteiner, A. Enz, P. Frey, A.-L. Jaton, W. Kinzy, R. Kneuer, U. Neumann, M. Rudin, M. Staufenbiel, M. Stoeckli, K.-H. Wiederhold, H.-U. Gremlich, *Nature Biotechnology* **2005**, *23*, 577-583.

[75] aU. Mahmood, R. Weissleder, *Molecular Cancer Therapeutics* **2003**, *2*, 489-496; bR. A. Sheth, R. Upadhyay, L. Stangenberg, R. Sheth, R. Weissleder, U. Mahmood, *Gynecologic Oncology* **2009**, *112*, 616-622.

[76] F. M. Hamer, *The Cyanine Dyes and Related Compounds, Vol. Chapter 1*, John Wiley & Sons, **1964**.

[77] B. Babo, *Journal für Praktische Chemie* **1857**, *72*, 73-88.

[78] L. Qun, L. Guo-Liang, P. Bi-Xian, L. Zheng-Xin, *Dyes and Pigments* **1998**, *38*, 211-218.

[79] aE. Berner., T. Jager., T. Lanz., F. Nuesch., J.-N. Tisserant., G. Wicht., H. Zhang., R. Hany., *Applied Physics Letters* **2013**, *102*, 183903; bR. Hany, B. Fan, F. A. de Castro, J. Heier, W. Kylberg, F. Nüesch, *Progress in Photovoltaics: Research and Applications* **2011**, *19*, 851-857.

[80] C. Anaya, N. Church, J. P. Lewis, *Proteomics* **2007**, *7*, 215-219.
[81] P.-A. Bouit, D. Rauh, S. Neugebauer, J. L. Delgado, E. D. Piazza, S. p. Rigaut, O. Maury, C. Andraud, V. Dyakonov, N. Martin, *Organic Letters* **2009**, *11*, 4806-4809.
[82] aJ. Li, K. Chen, H. Liu, K. Cheng, M. Yang, J. Zhang, J. D. Cheng, Y. Zhang, Z. Cheng, *Bioconjugate Chemistry* **2012**, *23*, 1704-1711; bL. E. Edgington, M. Verdoes, A. Ortega, N. P. Withana, J. Lee, S. Syed, M. H. Bachmann, G. Blum, M. Bogyo, *Journal of the American Chemical Society* **2013**, *135*, 174-182.
[83] Y. Lin, R. Weissleder, C.-H. Tung, *Bioconjugate Chemistry* **2002**, *13*, 605-610.
[84] aS. Gadde, E. K. Batchelor, A. E. Kaifer, *Chemistry – A European Journal* **2009**, *15*, 6025-6031; bG. B. Behera, P. K. Behera, B. K. Mishra, *Journal of Surface Science and Technology* **2007**, *23*, 1-31.
[85] M. Panigrahi, S. Dash, S. Patel, B. K. Mishra, *Tetrahedron* **2012**, *68*, 781-805.
[86] F. M. Hamer, *Journal of the Chemical Society* **1927**, *0*, 2796-2804.
[87] R. M. El-Shishtawy, P. Almeida, *Tetrahedron* **2006**, *62*, 7793-7798.
[88] aM. E. Jung, W.-J. Kim, *Bioorganic & Medicinal Chemistry* **2006**, *14*, 92-97; bJ. S. Minden, S. R. Dowd, H. E. Meyer, K. Stühler, *ELECTROPHORESIS* **2009**, *30*, S156-S161.
[89] M. Lopalco, E. N. Koini, J. K. Cho, M. Bradley, *Organic & Biomolecular Chemistry* **2009**, *7*, 856-859.
[90] B. Chipon, G. Clavé, C. Bouteiller, M. Massonneau, P.-Y. Renard, A. Romieu, *Tetrahedron Letters* **2006**, *47*, 8279-8284.
[91] aR. Nanjunda, E. A. Owens, L. Mickelson, S. Alyabyev, N. Kilpatrick, S. Wang, M. Henary, W. D. Wilson, *Bioorganic & Medicinal Chemistry* **2012**, *20*, 7002-7011; bK. I. E. McLuckie, M. Di Antonio, H. Zecchini, J. Xian, C. Caldas, B.-F. Krippendorff, D. Tannahill, C. Lowe, S. Balasubramanian, *Journal of the American Chemical Society* **2013**, *135*, 9640-9643.
[92] H. Hilal, J. A. Taylor, *Journal of Biochemical and Biophysical Methods* **2008**, *70*, 1104-1108.
[93] M. Y. Losytskyy, K. D. Volkova, V. B. Kovalska, I. E. Makovenko, Y. L. Slominskii, O. I. Tolmachev, S. M. Yarmoluk, *Journal of Fluorescence* **2005**, *15*, 849-857.
[94] aQ. Li, J. Tan, B.-X. Peng, *Molecules* **1997**, *2*, 91-98; bL. Strekowski, M. Lipowska, T. Górecki, J. C. Mason, G. Patonay, *Journal of Heterocyclic Chemistry* **1996**, *33*, 1685-1688; cL. Strekowski, M. Lipowska, G. Patonay, *The Journal of Organic Chemistry* **1992**, *57*, 4578-4580.
[95] X. Peng, F. Song, E. Lu, Y. Wang, W. Zhou, J. Fan, Y. Gao, *Journal of the American Chemical Society* **2005**, *127*, 4170-4171.
[96] aJ. T. Alander, I. Kaartinen, A. Laakso, T. Patila, T. Spillmann, V. V. Tuchin, M. Vernermo, P. Valisuo, *International Journal of Biomedical Imaging* **2012**, *2012*, 26; bS. L. Owens, *British Journal of Opthalmology* **1996**, *80*, 263-266.
[97] A. R. Cooke, D. D. Harrison, A. P. Skyring, *The American Journal of Digestive Diseases* **1963**, *8*, 244-250.
[98] K. Apel, H. Hirt, *Annual Review of Plant Biology* **2004**, *55*, 373-399.

[99] Y. J. Suzuki, H. J. Forman, A. Sevanian, *Free Radical Biology and Medicine* **1997**, *22*, 269-285.
[100] T. M. Paravicini, R. M. Touyz, *Diabetes Care* **2008**, *31*, S170-S180.
[101] S. Chen, Y. Su, J. Wang, *Cell Death and Disease* **2013**, *4*, e722.
[102] J.-I. Abe, I. Manabe, M. Aikawa, E. Aikawa, *International Journal of Inflammation* **2013**, *2013*, 2.
[103] H. Wiseman, B. Halliwell, *Biochemical Journal* **1996**, *313*, 17-29.
[104] M. L. Salin, J. M. McCord, *The Journal of Clinical Investigation* **1975**, *56*, 1319-1323.
[105] aM. D. Jacobson, *Trends in Biochemical Sciences* **1996**, *21*, 83-86; bT. M. Buttke, P. A. Sandstrom, *Immunology Today* **1994**, *15*, 7-10.
[106] D. Oushiki, H. Kojima, T. Terai, M. Arita, K. Hanaoka, Y. Urano, T. Nagano, *Journal of the American Chemical Society* **2010**, *132*, 2795-2801.
[107] aP. A. Gale, *Chemical Society Reviews* **2010**, *39*, 3746-3771; bR. M. Duke, E. B. Veale, F. M. Pfeffer, P. E. Kruger, T. Gunnlaugsson, *Chemical Society Reviews* **2010**, *39*, 3936-3953.
[108] aK. Kiyose, H. Kojima, Y. Urano, T. Nagano, *Journal of the American Chemical Society* **2006**, *128*, 6548-6549; bY.-D. Lin, Y.-S. Peng, W. Su, C.-H. Tu, C.-H. Sun, T. J. Chow, *Tetrahedron* **2012**, *68*, 2523-2526; cY. Ding, T. Li, W. Zhu, Y. Xie, *Organic & Biomolecular Chemistry* **2012**, *10*, 4201-4207.
[109] aB. Sui, B. Kim, Y. Zhang, A. Frazer, K. D. Belfield, *Amerian Chemical Societies Applied Materials & Interfaces* **2013**, *5*, 2920-2923; bX. Peng, Y. Wu, J. Fan, M. Tian, K. Han, *The Journal of Organic Chemistry* **2005**, *70*, 10524-10531; cS. Yamaguchi, S. Akiyama, K. Tamao, *Journal of the American Chemical Society* **2001**, *123*, 11372-11375.
[110] Z. Guo, S. Nam, S. Park, J. Yoon, *Chemical Science* **2012**, *3*, 2760.
[111] T.-K. Kim, D.-N. Lee, H.-J. Kim, *Tetrahedron Letters* **2008**, *49*, 4879-4881.
[112] R. Wang, F. Yu, L. Chen, H. Chen, L. Wang, W. Zhang, *Chemical Communications* **2012**, *48*, 11757-11759.
[113] S. M. Ametamey, M. Honer, P. A. Schubiger, *Chemical Reviews* **2007**, *108*, 1501-1516.
[114] aD. Wu, W. Huang, C. Duan, Z. Lin, Q. Meng, *Inorganic Chemistry* **2007**, *46*, 1538-1540; bY.-K. Yang, K.-J. Yook, J. Tae, *Journal of the American Chemical Society* **2005**, *127*, 16760-16761.
[115] Z. Xu, Y. Xiao, X. Qian, J. Cui, D. Cui, *Organic Letters* **2005**, *7*, 889-892.
[116] X. Peng, J. Du, J. Fan, J. Wang, Y. Wu, J. Zhao, S. Sun, T. Xu, *Journal of the American Chemical Society* **2007**, *129*, 1500-1501.
[117] H. Zheng, M. Yan, X.-X. Fan, D. Sun, S.-Y. Yang, L.-J. Yang, J.-D. Li, Y.-B. Jiang, *Chemical Communications* **2012**, *48*, 2243-2245.
[118] C. Tan, E. Atas, J. G. Müller, M. R. Pinto, V. D. Kleiman, K. S. Schanze, *Journal of the American Chemical Society* **2004**, *126*, 13685-13694.
[119] X. Chen, S.-W. Nam, G.-H. Kim, N. Song, Y. Jeong, I. Shin, S. K. Kim, J. Kim, S. Park, J. Yoon, *Chemical Communications* **2010**, *46*, 8953-8955.
[120] T. Myochin, K. Kiyose, K. Hanaoka, H. Kojima, T. Terai, T. Nagano, *Journal of the American Chemical Society* **2011**, *133*, 3401-3409.
[121] A. Wu, L. Duan, *Turkish Journal of Chemistry* **2011**, *35*, 475-479.

[122] aL. H. Song, E.J; Young, I.T and Tanke H.J, *Biophysical Journal* **1995**, *68*, 2588-2600; bJ. Widengren, R. Rigler, *Bioimaging* **1996**, *4*, 149-157.
[123] aB. L. Sprague, R. L. Pego, D. A. Stavreva, J. G. McNally, *Biophysical Journal* **2004**, *86*, 3473-3495; bJ. F. Pressley, N. B. Cole, T. A. Schroer, K. Hirschberg, K. J. M. Zaal, Lippincott-Schwartz, *Nature* **1997**, *389*, 81-85; cK. Braeckmans, L. Peeters, N. N. Sanders, S. C. De Smedt, J. Demeester, *Biophysical Journal* **2003**, *85*, 2240-2252.
[124] B. R. Renikuntla, H. C. Rose, J. Eldo, A. S. Waggoner, B. A. Armitage, *Organic Letters* **2004**, *6*, 909-912.
[125] G. A. Reynolds, K. H. Drexhage, *Journal of Organic Chemistry* **1977**, *42*, 885-888.
[126] aJ. H. Flanagan, S. H. Khan, S. Menchen, S. A. Soper, R. P. Hammer, *Bioconjugate Chemistry* **1997**, *8*, 751-756; bR. A. Rossi, *Accounts of Chemical Research* **1982**, *15*, 164-170.
[127] A. Samanta, M. Vendrell, R. Das, Y.-T. Chang, *Chemical Communications* **2010**, *46*, 7406-7408.
[128] L. Strekowski, J. C. Mason, J. E. Britton, H. Lee, K. Van Aken, G. Patonay, *Dyes and Pigments* **2000**, *46*, 163-168.
[129] H. Lee, J. C. Mason, S. Achilefu, *The Journal of Organic Chemistry* **2006**, *71*, 7862-7865.
[130] J. Han, A. Engler, J. Qi, C.-H. Tung, *Tetrahedron Letters* **2013**, *54*, 502-505.
[131] R. K. Das, A. Samanta, H.-H. Ha, Y.-T. Chang, *Royal Society of Chemistry Advances* **2011**, *1*, 573.
[132] X. Yang, C. Shi, R. Tong, W. Qian, H. E. Zhau, R. Wang, G. Zhu, J. Cheng, V. W. Yang, T. Cheng, M. Henary, L. Strekowski, L. W. K. Chung, *Clinical Cancer Research* **2010**, *16*, 2833-2844.
[133] G. A. Kullak-Ublick, M. G. Ismair, B. Stieger, L. Landmann, R. Huber, F. Pizzagalli, K. Fattinger, P. J. Meier, B. Hagenbuch, *Gastroenterology* **2001**, *120*, 525-533.
[134] aL. V. Johnson, M. L. Walsh, B. J. Bockus, L. B. Chen, *The Journal of Cell Biology* **1981**, *88*, 526-535; bK. Xu, S. Sun, J. Li, L. Li, M. Qiang, B. Tang, *Chemical Communications* **2012**, *48*, 684-686; cK. Xu, L. Wang, M. Qiang, L. Wang, P. Li, B. Tang, *Chemical Communications* **2011**, *47*, 7386.
[135] F. Yu, P. Li, G. Li, G. Zhao, T. Chu, K. Han, *Journal of the American Chemical Society* **2011**, *133*, 11030-11033.
[136] T. Mosmann, *Journal of Immunological Methods* **1983**, *65*, 55-63.
[137] G. Buller, W. Godfrey, *Molecular Probes - Invitrogen detection technologies* **2005**.
[138] aM. Bai, M. Sexton, N. Stella, D. J. Bornhop, *Bioconjugate Chemistry* **2008**, *19*, 988-992; bS. A. Hilderbrand, K. A. Kelly, R. Weissleder, C.-H. Tung, *Bioconjugate Chemistry* **2005**, *16*, 1275-1281.
[139] W. Pham, L. Cassell, A. Gillman, D. Koktysh, J. C. Gore, *Chemical Communications* **2008**, 1895.
[140] K. Kiyose, S. Aizawa, E. Sasaki, H. Kojima, K. Hanaoka, T. Terai, Y. Urano, T. Nagano, *Chemistry – A European Journal* **2009**, *15*, 9191-9200.
[141] F. Kratz, I. A. Müller, C. Ryppa, A. Warnecke, *ChemMedChem* **2008**, *3*, 20-53.

[142] J. L. M. Jourden, K. B. Daniel, S. M. Cohen, *Chemical Communications* **2011**, *47*, 7968.
[143] R. B. Silverman, *Accounts of Chemical Research* **1995**, *28*, 335-342.
[144] J. C. Shih, K. Chen, M. J. Ridd, *Annual Review of Neuroscience* **1999**, *22*, 197-217.
[145] A. E. Albers, K. A. Rawls, C. J. Chang, *Chemical Communications* **2007**, 4647.
[146] Y. Zhang, Y. Xu, S. Tan, L. Xu, X. Qian, *Tetrahedron Letters* **2012**, *53*, 6881-6884.
[147] K. R. F. Spring, T.J and Davidson, M.W, *Molecular Expressions* **2003**.
[148] I. Medical Isotopes, **2013**.
[149] N. C. Shaner, P. A. Steinbach, R. Y. Tsien, *Nature Methods* **2005**, *2*, 905-909.
[150] J. Kuruc, *Journal of Radioanalytical and Nuclear Chemistry* **1984**, *82*, 93-100.
[151] aF. G. Incorporated, **2012**, pp. 1-337; bT. M. Allen, P. R. Cullis, *Science* **2004**, *303*, 1818-1822.
[152] aR. Langer, *Nature* **1998**, *392*, 5-10; bN. A. Kshirsagar, *Indian Journal of Pharmacology* **2000**, *32*, 54-61.
[153] J. Folkman, D. M. Long, *Journal of Surgical Research* **1960**, *4*, 139-142.
[154] S. K. Sahoo, V. Labhasetwar, *Drug Discovery Today* **2003**, *8*, 1112-1120.
[155] aT. Moritero, Y. Oguro, Y. Honda, R. Wada, S. Hyon, Y. Ikada, *Investigative Opthalmology & Visual Science* **1991**, *32*, 1785-1790; bS. Freiberg, X. X. Zhu, *International Journal of Pharmaceutics* **2004**, *282*, 1-18.
[156] aY. Y. Yang, T. S. Chung, X. L. Bai, W. K. Chan, *Chemical Engineering Science* **2000**, *55*, 2223-2236; bJ.-F. Chen, H.-M. Ding, J.-X. Wang, L. Shao, *Biomaterials* **2004**, *25*, 723-727.
[157] S. S. Suri, H. Fenniri, B. Singh, *Journal of Occupational Medicine and Toxicology* **2007**, *2*, 1-6.
[158] aF. Thielbeer, S. V. Chankeshwara, M. Bradley, *Biomacromolecules* **2011**, *12*, 4386-4391; bP. Couvreur, P. Tulkenst, M. Roland, A. Trouet, P. Speiser, *Federation of European Biochemical Societies Letters* **1977**, *84*, 323-326.
[159] R. M. Sánchez-Martín, L. Alexander, M. Bradley, *Annals of the New York Academy of Sciences* **2008**, *1130*, 207-217.
[160] H. Goesmann, C. Feldmann, *Angewandte Chemie International Edition* **2010**, *49*, 1362-1395.
[161] aR. M. Rioux, H. Song, J. D. Hoefelmeyer, P. Yang, G. A. Somorjai, *The Journal of Physical Chemistry B* **2004**, *109*, 2192-2202; bA. J. Kell, R. L. Donkers, M. S. Workentin, *Langmuir* **2004**, *21*, 735-742.
[162] S. S. Kelkar, T. M. Reineke, *Bioconjugate Chemistry* **2011**, *22*, 1879-1903.
[163] aB. T. Luk, R. H. Fang, Z. L., *Theranostics* **2012**, *2*, 1117-1126; bZ. Liu, L. X., *Theranostics* **2012**, *2*, 235-237.
[164] D. B. Tada, L. L. R. Vono, E. L. Duarte, R. Itri, P. K. Kiyohara, M. S. Baptista, L. M. Rossi, *Langmuir* **2007**, *23*, 8194-8199.
[165] M. Bradley, L. Alexander, K. Duncan, M. Chennaoui, A. C. Jones, R. M. Sánchez-Martín, *Bioorganic & Medicinal Chemistry Letters* **2008**, *18*, 313-317.

[166] R. M. Sánchez-Martín, M. Cuttle, S. Mittoo, M. Bradley, *Angewandte Chemie International Edition* **2006**, *45*, 5472-5474.
[167] L. M. Alexander, R. M. Sánchez-Martín, M. Bradley, *Bioconjugate Chemistry* **2009**, *20*, 422-426.
[168] H. Bamnolker, S. Margel, *Journal of Polymer Science Part A: Polymer Chemistry* **1996**, *34*, 1857-1871.
[169] C. S. Chern, *Progress in Polymer Science* **2006**, *31*, 443-486.
[170] M. Egen, R. Zentel, *Macromolecular Chemistry and Physics* **2004**, *205*, 1479-1488.
[171] T. Delair, V. Marguet, C. Pichot, B. Mandrand, *Colloid Polym Sci* **1994**, *272*, 962-970.
[172] Q. Zhang, Y. Han, W.-C. Wang, L. Zhang, J. Chang, *European Polymer Journal* **2009**, *45*, 550-556.
[173] M. Han, X. Gao, J. Z. Su, S. Nie, *Nature Biotechnology* **2001**, *19*, 631-635.
[174] T. Taniguchi, N. Takeuchi, S. Kobaru, T. Nakahira, *Journal of Colloid and Interface Science* **2008**, *327*, 58-62.
[175] Y.-Y. Yang, T.-S. Chung, N. Ping Ng, *Biomaterials* **2001**, *22*, 231-241.
[176] F. Tronc, M. Li, J. Lu, M. A. Winnik, B. L. Kaul, J.-C. Graciet, *Journal of Polymer Science Part A: Polymer Chemistry* **2003**, *41*, 766-778.
[177] K. Ando, H. Kawaguchi, *Journal of Colloid and Interface Science* **2005**, *285*, 619-626.
[178] R. Bardhan, W. Chen, C. Perez-Torres, M. Bartels, R. M. Huschka, L. L. Zhao, E. Morosan, R. G. Pautler, A. Joshi, N. J. Halas, *Advanced Functional Materials* **2009**, *19*, 3901-3909.
[179] aS. P. Sherlock, S. M. Tabakman, L. Xie, H. Dai, *American Chemical Society Nano* **2011**, *5*, 1505-1512; bQ. Tian, J. Hu, Y. Zhu, R. Zou, Z. Chen, S. Yang, R.-W. Li, Q. Su, Y. Han, X. Liu, *Journal of the American Chemical Society* **2013**.
[180] X. Zhang, G. Zhang, B. Zhang, Z. Su, *Langmuir* **2013**.
[181] Y. Liu, T. Kobayashi, M. Iizuka, T. Tanaka, I. Sotokawa, A. Shimoyama, Y. Murayama, E. Otsuji, S.-i. Ogura, H. Yuasa, *Bioorganic & Medicinal Chemistry* **2013**, *21*, 2832-2842.
[182] A. M. Alkilany, C. J. Murphy, *Journal of Nanoparticle Research* **2010**, *12*, 2313-2333.
[183] M. Nurunnabi, K. J. Cho, J. S. Choi, K. M. Huh, Y.-k. Lee, *Biomaterials* **2010**, *31*, 5436-5444.
[184] K. M. Tsoi, Q. Dai, B. A. Alman, W. C. W. Chan, *Accounts of Chemical Research* **2012**, *46*, 662-671.
[185] L. Ye, K.-T. Yong, L. Liu, I. Roy, R. Hu, J. Zhu, H. Cai, W.-C. Law, J. Liu, K. Wang, J. Liu, Y. Liu, Y. Hu, X. Zhang, M. T. Swihart, P. N. Prasad, *Nature Nanotechnology* **2012**, *7*, 453-458.
[186] S. V. Chankeshwara, A. K. Chakraborti, *Organic Letters* **2006**, *8*, 3259-3262.
[187] F. Galindo, B. Altava, M. I. Burguete, R. Gavara, S. V. Luis, *Journal of Combinatorial Chemistry* **2004**, *6*, 859-861.
[188] K. Kundu, S. F. Knight, N. Willett, S. Lee, W. R. Taylor, N. Murthy, *Angewandte Chemie-International Edition* **2009**, *48*, 299-303.
[189] aN. Sharifi-Sanjani, M. Soltan-Dehghan, N. Naderi, A. Ranji, *Journal of Applied Polymer Science* **2004**, *94*, 1898-1904; bR. M. Sanchez-Martin, M.

Muzerelle, N. Chitkul, S. E. How, S. Mittoo, M. Bradley, *ChemBioChem* **2005**, *6*, 1341-1345.
[190] V. K. Sarin, S. B. H. Kent, J. P. Tam, R. B. Merrifield, *Analytical Biochemistry* **1981**, *117*, 147-157.
[191] N. Vogel, C. P. Hauser, K. Schuller, K. Landfester, C. K. Weiss, *Macromolecular Chemistry and Physics* **2010**, *211*, 1355-1368.
[192] aJ. M. Chalker, C. S. C. Wood, B. G. Davis, *Journal of the American Chemical Society* **2009**, *131*, 16346-16347; bN. Li, R. K. V. Lim, S. Edwardraja, Q. Lin, *Journal of the American Chemical Society* **2011**, *133*, 15316-15319.
[193] A. Hennig, H. Borcherding, C. Jaeger, S. Hatami, C. Würth, A. Hoffmann, K. Hoffmann, T. Thiele, U. Schedler, U. Resch-Genger, *Journal of the American Chemical Society* **2012**, *134*, 8268-8276.
[194] T. W. P. Kim, J and Hong, J, *Bulletin of the Korean Chemical Society* **2007**, *28*, 1221-1223.
[195] H. F. Gilbert, in *Advances in Enzymology and Related Areas of Molecular Biology*, John Wiley & Sons, Inc., **2006**, pp. 69-172.
[196] H. N. Schulz, B. B. Jørgensen, *Annual Review of Microbiology* **2001**, *55*, 105-137.
[197] W. Schumann, in *Dynamics of the Bacterial Chromosome*, Wiley-VCH Verlag GmbH & Co. KGaA, **2006**, pp. 1-27.
[198] C. Gram, *Fortschritte der Medecin* **1884**, *2*, 185-189.
[199] J. Ghosh, P. Larsson, B. Singh, B. M. F. Pettersson, N. M. Islam, S. N. Sarkar, S. Dasgupta, L. A. Kirsebom, *Proceedings of the National Academy of Sciences* **2009**, *106*, 10781-10786.
[200] D. Claus, *World Journal of Microbiology and Biotechnology* **1992**, *8*, 451-452.
[201] F. Fenollar, D. Raoult, *European Journal of Clinical Microbiology and Infectious Diseases* **2000**, *19*, 33-38.
[202] S. Halebian, B. Harris, S. M. Finegold, R. D. Rolfe, *Journal of Clinical Microbiology* **1981**, *13*, 444-448.
[203] M. Spengler, G. T. Rodeheaver, L. Richter, M. T. Edgerton, R. F. Edlich, *Journal of the American College of Emergency Physicians* **1978**, *7*, 434-438.
[204] T. Gregersen, *Applied Microbiology and Biotechnology* **1978**, *5*, 123-127.
[205] U. Blachman, G. L. Gilardi, M. J. Pickett, I. J. Slotnick, A. von Graevenitz, *Clinical Microbiology Newsletter* **1980**, *2*, 8.
[206] G. Cerny, *European journal of applied microbiology and biotechnology* **1976**, *3*, 223-225.
[207] A. L. James, J. D. Perry, A. Rigby, S. P. Stanforth, *Bioorganic & Medicinal Chemistry Letters* **2007**, *17*, 1418-1421.
[208] F. W. Kahn, J. M. Jones, *Journal of Infectious Diseases* **1987**, *155*, 862-869.
[209] C. MacAulay, P. Lane, R. Richards-Kortum, *Gastrointestinal Endoscopy Clinics of North America* **2004**, *14*, 595-620.
[210] R. L. Danner, K. A. Joiner, M. Rubin, W. H. Patterson, N. Johnson, K. M. Ayers, J. E. Parrillo, *Antimicrobial Agents and Chemotherapy* **1989**, *33*, 1428 - 1434.
[211] E. M. Stames, J. F. O'Toole, *Public Library of Science One* **2013**, *8*, e77234.

[212] P. T. Cristofoletti, F. A. Mendonça de Sousa, Y. Rahbé, W. R. Terra, *Federation of European Biochemical Societies Journal* **2006**, *273*, 5574-5588.
[213] A. Taylor, *The Journal of the Federation of American Societies for Experimental Biology* **1993**, *7*, 290-298.
[214] aL. Chen, W. Sun, W. Li, J. Li, L. Du, W. Xu, H. Fang, M. Li, *Analytical Methods* **2012**, *4*, 2661-2663; bM. Sakabe, D. Asanuma, M. Kamiya, R. J. Iwatate, K. Hanaoka, T. Terai, T. Nagano, Y. Urano, *Journal of the American Chemical Society* **2012**, *135*, 409-414; cL. Chen, W. Sun, J. Li, Z. Liu, Z. Ma, W. Zhang, L. Du, W. Xu, H. Fang, M. Li, *Organic & Biomolecular Chemistry* **2013**, *11*, 378.
[215] E. Kaiser, R. L. Colescott, C. D. Bossinger, P. I. Cook, *Analytical Biochemistry* **1970**, *34*, 595-598.
[216] D. J. Maly, F. Leonetti, B. J. Backes, D. S. Dauber, J. L. Harris, C. S. Craik, J. A. Ellman, *The Journal of Organic Chemistry* **2002**, *67*, 910-915.
[217] J. R. Mannekutla, B. G. Mulimani, S. R. Inamdar, *Spectrochimica Acta Part A: Molecular and Biomolecular Spectroscopy* **2008**, *69*, 419-426.
[218] J. Martinez, F. Azam, *Marine Ecology Progress Series* **1993**, *92*, 89-97.
[219] B. Korkmaz, T. Moreau, F. Gauthier, *Biochimie* **2008**, *90*, 227-242.
[220] K. Kawabata, T. Hagio, S. Matsuoka, *European Journal of Pharmacology* **2002**, *451*, 1-10.
[221] L. L. Walling, J. H. Fowler, M. Matsui, *Biol Chem* **2006**, *387*, 1535-1544.
[222] D. Zhang, J. Su, X. Ma, H. Tian, *Tetrahedron* **2008**, *64*, 8515-8521.
[223] M. Wang, M. Gao, K. D. Miller, G. W. Sledge, G. D. Hutchins, Q.-H. Zheng, *European Journal of Medicinal Chemistry* **2009**, *44*, 2300-2306.
[224] K. S. Chichak, A. J. Peters, S. J. Cantrill, J. F. Stoddart, *The Journal of Organic Chemistry* **2005**, *70*, 7956-7962.
[225] C. E. Schiaffo, P. H. Dussault, *The Journal of Organic Chemistry* **2008**, *73*, 4688-4690.
[226] N. Narayanan, G. Patonay, *The Journal of Organic Chemistry* **1995**, *60*, 2391-2395.
[227] K. Kiyose, S. Aizawa, E. Sasaki, H. Kojima, K. Hanaoka, T. Terai, Y. Urano, T. Nagano, *Chemistry - A European Journal* **2009**, *15*, 9191-9200.
[228] B. Wu, Z. Wang, Y. Huang, W. R. Liu, *ChemBioChem* **2012**, *13*, 1405-1408.

Publications

Chemical Science

RSC Publishing

EDGE ARTICLE

View Article Online
View Journal | View Issue

Palladium-mediated bioorthogonal conjugation of dual-functionalised nanoparticles and their cellular delivery†

Cite this: *Chem. Sci.*, 2013, 4, 425

Frank Thielbeer,‡ Sunay V. Chankeshwara,‡ Emma M. V. Johansson, Neil Norouzi and Mark Bradley*

Received 2nd June 2012
Accepted 9th October 2012

DOI: 10.1039/c2sc20706k

www.rsc.org/chemicalscience

Nanoparticles have gained considerable significance in the life sciences due to their ability to be internalised by living cells and the relative ease with which they can be functionalised with cargos ranging from molecular sensors to biomacromolecules. However, the scope of available bioconjugation methods is limited and new bioorthogonal methods are much sought after. Herein, we present dual functionalised $(HO)_2B/H_2N$-polymeric nanoparticles which can be conjugated *via* amide bond formation and/or Pd-mediated Suzuki–Miyaura cross-coupling in a chemoselective and bioorthogonal manner. These dual-functionalised particles were found to be efficiently taken up by mammalian cells without toxicity and were successfully employed in the cellular delivery and intracellular release of a "*turn-on*" molecular probe thereby demonstrating the potential use of the new particles for chemical biology applications.

Introduction

Intracellular delivery of functional macromolecules using nano and micro-sized polymeric particles is widely used in the life sciences due to their efficiency in being able to deliver cargos into cells in a benign manner.[1] Sensors conjugated to particles have, for example, been utilised to reveal important insights concerning the physiological state of a cell, such as intracellular pH,[2] ion concentrations,[3] and the functional states of proteins.[4] In addition, particles have been employed to deliver a wide range of bioactive compounds into cells including drugs,[5,6] proteins[7] and nucleic acids;[8,9] moreover; fluorescently labelled particles have been used to track and sort cells.[10,11]

Non-degradable polystyrene nanoparticles have been used *in vitro* cellular uptake[11a] and *in vivo* tracking[11b] experiments because of their non-immunogenic properties and low cytotoxicity. They have been used to track the stem cells in the generation of chimera, perhaps the most robust proof possible of non-toxicity.[11c] In addition, the particle's size and surface modification can easily be varied.[1,11a]

The ability to functionalise non-degradable nanoparticles such as polymeric, magnetic or quantum dots is extremely relevant due to their proposed biomedical applications. Such nanoparticles can be used as a multi-tasking platform, for instance, the combination of fluorescent markers and MRI contrast agents or photothermal therapy and hyperthermia agents would allow simultaneous diagnosis and therapeutic application of internalised nanoparticles.[12]

Typical bioconjugation techniques, such as thiol–maleimide addition or amide coupling reactions are applied in the construction of particle bioconjugates.[13,14] However, a variety of competing nucleophiles and electrophiles present in complex biomolecules hamper their use. Huisgen cycloaddition chemistry can be used to ligate alkyne-functionalised cargos onto azide-functionalised particles in a bioorthogonal fashion, but typically requires copper ion catalysis.[15,16] The efficient, selective and benign bioconjugation of cargo molecules onto nanoparticles therefore remains an important challenge, and one that becomes even more complex when particles are required to carry two or more cargos.[17] This can be achieved using particles with multiple bioorthogonal, functional groups on their surface. Stucky and co-workers have prepared dual-functionalised amine and azide particles[18] while Li *et al.* synthesised a block copolymer, containing amine, acylhydrazide and azide groups, which was used to coat and functionalise gold nanoparticles.[19]

Recently, we have demonstrated the synthesis and reaction monitoring of aminomethyl-functionalised nanoparticles which can be further derivatised with a variety of reactive functional groups.[20] However, to boost the particle properties, we aimed to introduce an additional functionality allowing chemoselective conjugation onto the particle's surface.

School of Chemistry, University of Edinburgh, West Mains Road, EH9 3JJ, Edinburgh, UK. E-mail: Mark.Bradley@ed.ac.uk; Fax: +44 (0)131 777 0344; Tel: +44 (0)131 650 4820

† Electronic supplementary information (ESI) available: Synthesis of VBAH, 5-iodofluorescein, anionic and NLS peptide-reporters, particle analysis, preparation of particles **13–16** (amide bond coupling and Pd-mediated coupling), ICP-OES analysis (for palladium and boron quantification), DTT-induced fluorescein release, histograms and microscopy images of cells following fluorescein-conjugated particle uptake, quantification of Cy5 fluorescence after incubation with dual-functionalised particles, MTT assays and HeLa cell data. See DOI: 10.1039/c2sc20706k

‡ These authors contributed equally to this work.

Inspired by the challenges and demands of synthesising novel nanoparticles while developing new conjugation techniques, herein we describe the development of dual $(HO)_2B$/H_2N-functionalised polymeric nanoparticles. Further, we investigated their derivatisation *via* orthogonal Pd-mediated Suzuki–Miyaura cross-coupling and amide bond formation, and demonstrate the benefits of these dual-functionalised nanoparticles by efficient cellular uptake, intracellular cargo liberation and organelle targeting.

Results and discussion

Particle synthesis

Lately, carbon–carbon bond formation *via* Pd-catalysed reactions, has been used to modify proteins,[21] label cell membranes,[22] and to carry out novel intracellular chemistry[23] in a manner that is fully orthogonal to amide bond formation. To the best of our knowledge Pd-mediated nanoparticle functionalisation has not been reported and we therefore targeted this approach to allow bioorthogonal nanoparticle conjugation.

The $(HO)_2B$/H_2N-particles (**5–8**) were prepared by emulsifier-free emulsion polymerisation of styrene **1**, cross-linker divinylbenzene **2** (2%), 4-vinylbenzylamine hydrochloride **3** (VBAH, 3%), and varying amounts of 4-vinylbenzylboronic acid **4** (VBA, 0–9%) (Scheme 1a). The particles **5–8** all had a hydrodynamic diameter between 200 and 260 nm as determined by dynamic light scattering (Scheme 1b, Table 1, Fig. S1†) regardless of the level of VBA incorporation. However, they showed varying polydispersity indices (PDI) (Table 1).

Particles **6**, polymerised with 3% VBA, had a PDI of 0.071, similar to particles **5** synthesised without VBA (0.060), both being classified as monodisperse (PDI < 0.1). Further increase in VBA levels lead to polydisperse particles with PDIs of 0.190 (6% VBA, **7**) and 0.313 (9% VBA, **8**) which were confirmed by scanning electron microscopy (Scheme 1b, Fig. S1†). Presumably, **7** and **8** were polydisperse resulting from increased acid–base interactions between VBAH **3** and VBA **4** disturbing the VBAH-mediated micelle formation during the polymerisation.[24]

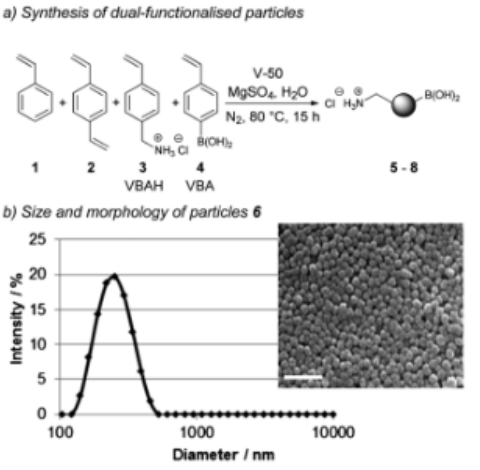

Scheme 1 Synthesis and analysis of dual-functionalised $(HO)_2B$/H_2N-particles *via* emulsifier-free emulsion polymerisation: (a) particle synthesis; and (b) size analysis of particles **6** by dynamic light scattering and scanning electron microscopy (240 nm, PDI 0.071). Scale bar equals 1 μm.

Table 1 Analysis of $(HO)_2B$/H_2N-particles

Particles	Size [nm] (PDI)	H_2N-groups [μmol g^{-1}]	$(HO)_2B$-group [μmol g^{-1}]
5 (0% VBA)	229 (0.060)	(82 ± 14)	(2 ± 1)
6 (3% VBA)	240 (0.071)	(129 ± 15)	(62 ± 1)
7 (6% VBA)	260 (0.190)	(163 ± 5)	(116 ± 2)
8 (9% VBA)	211 (0.313)	(76 ± 3)	(204 ± 1)

The dual-functionalisation of the nanoparticles was quantitatively verified by ninhydrin analysis for amine loading and ICP-OES analysis[25] for boronic acid loading levels (Table 1). The addition of 3% VBA in the synthesis gave particles **6** with a boronic acid loading of 62 μmol g^{-1}. An increase in VBA levels (6% or 9%) resulted in an approximately 2-fold (116 μmol g^{-1}, **7**) and 3-fold (204 μmol g^{-1}, **8**) increase in boron content. Due to the good polydispersity, in combination with the good boronic acid and aminomethyl loadings, particles **6** were selected for Pd-mediated conjugation and biological studies.

Palladium-mediated particle conjugation

In order to study Pd-mediated Suzuki–Miyaura cross-coupling onto the particles 5-iodofluorescein[10] **9** was coupled onto **6** (Scheme 2a) with various Pd salts screened in physiological buffers. This allowed monitoring of the conjugation reaction by increases in particle fluorescence in addition to a decrease in the boron content (Table S5†) with the best reaction conditions identified to be in PBS at 37 °C with the water soluble complex of 2-amino-4,6-dihydroxypyrimidine–$Pd(OAc)_2$ as catalyst.[26]

Following the coupling, two independent techniques, ICP-OES and flow cytometry, were applied to verify the degree of fluorescein conjugation. ICP-OES analysis of **10** revealed a 40% reduction in the boron content (Scheme 2b, dark grey columns), while flow cytometry analysis of **10** revealed a 500-fold increase in particle fluorescence compared to the precursor particles **6** (Scheme 2b, light grey columns). Two control reactions were run, one in which 5-iodofluorescein was replaced with fluorescein and a second in which the catalyst was removed from the reaction mixture. As expected, both control reactions resulted in unchanged boron content and particle fluorescence.

To confirm the reproducibility of palladium-mediated particle conjugation, the optimised conditions were performed on a model system in triplicate and the efficiency of conjugation was determined by measuring the boron consumption using ICP-OES. The conjugation reactions were highly reproducible (38 ± 4% conjugation efficiency). Quantitative yields were not achieved presumably due to the distribution of the boronic acid

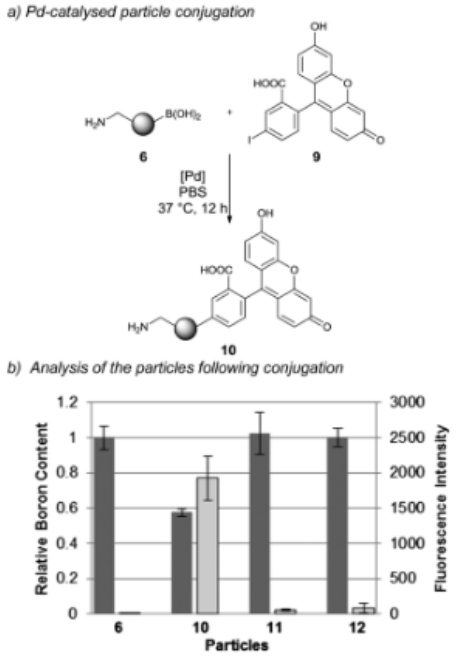

Scheme 2 Pd-catalysed particle conjugation: (a) $(HO)_2B/H_2N$-particle conjugation with 5-iodofluorescein using as a catalyst the sodium salt complex of $Pd(OAc)_2$ and 2-amino-4,6-dihydroxypyrimidine; and (b) analysis of particle conjugation by boron consumption (*via* ICP-OES analysis) and fluorescence intensity of particles (*via* flow cytometry) ($n = 3$). Dark grey = boron content and light grey = fluorescence intensity of particles.

groups between the particle's "surface" and "interior" with coupling to the latter increasingly more difficult due to the steric demands,[27] in agreement with recent reports that demonstrated that modifications of azide-functionalised nanoparticles with alkyne modified fluorescein by Cu-catalysed click chemistry was dependent on the polymerisation process, surfactants used and accessible azide groups.[28] Advantages of the Pd-mediated Suzuki–Miyaura cross-coupling over the Cu-catalysed click reaction are the benign nature of the Pd catalyst,[29] while oxidation of biological substrates has also been observed with Cu-catalysed click chemistry due to the hydrogen peroxide and superoxide radicals produced by copper ion mediated catalytic oxidation of sodium ascorbate by molecular oxygen.[16]

Palladium catalysed reactions have been used to modify proteins,[21] label cell membranes,[22] and to carry out novel intracellular chemistry[23] without any observed apparent toxicity or substrate sensitivity towards palladium. The above results thus confirmed the ability of Suzuki–Miyaura cross-coupling reactions to conjugate cargo molecules onto the $(HO)_2B/H_2N$-particles in a biocompatible manner.

Cellular uptake and viability

Following the successful Pd-mediated conjugation of fluorophore **9** onto the particles, the cellular uptake of the fluorescein conjugated particles **10** into HEK293T and HeLa cells was analysed by flow cytometry. This demonstrated successful internalisation of the particles with increasing particle concentrations lead to increasing intracellular fluorescence (Fig. 1, external fluorescence quenched with trypan blue.[30] For histograms and microscopy images see Fig. S5 and S6†). A 14-fold increase in cellular fluorescence was observed with the highest particle concentration (75 μg mL^{-1}) with no apparent cellular toxicity (Fig. S15†).

Boronic acid groups are known for their high affinity towards diols which has been used to develop glucose sensors.[31] As described above, the Pd-coupling is not quantitative leaving boronic acid groups on the nanoparticle surface. To investigate if the boronic acid groups could induce cellular toxicity, cell viability assays were also carried out with non-functionalised $(HO)_2B/H_2N$-nanoparticles **6** and demonstrated no cellular toxicity (Fig. S13†). These results demonstrated that the $(HO)_2B/H_2N$-nanoparticles, are readily functionalised by Suzuki–Miyaura cross-coupling, that the modified particles are efficiently taken up by the cells without any toxicity from the residual boronic acid particles and that Pd-levels on the particles are negligible.[32]

Bioorthogonal dual-functionalisation of the particles

The $(HO)_2B/H_2N$-nanoparticles **6** were subsequently dual functionalised to carry a Cy5 dye and cargo moiety which, upon cellular uptake, will be released from the particles (Scheme 3a). The Cy5 dye on the particles would enable cellular uptake quantification, while the cargo moiety (a peptide) was designed to contain a "*turn-on*" fluorescence signal that would only become active following intracellular release of the cargo. This was based on a cleavable disulphide linker connecting a fluorescence quencher (methyl red) and fluorescein to the cargo. Upon cellular uptake, intracellular cleavage of the disulphide bond would release the cargo from the particles allowing

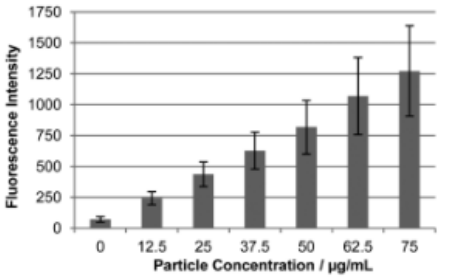

Fig. 1 Cellular uptake of Pd-mediated fluorescein conjugated particles **10** in HEK293T cells. Relative uptake by flow cytometry (external fluorescence was quenched by the addition of 2% trypan blue[30]). For microscopic images and histograms see Fig. S5 and S6†).

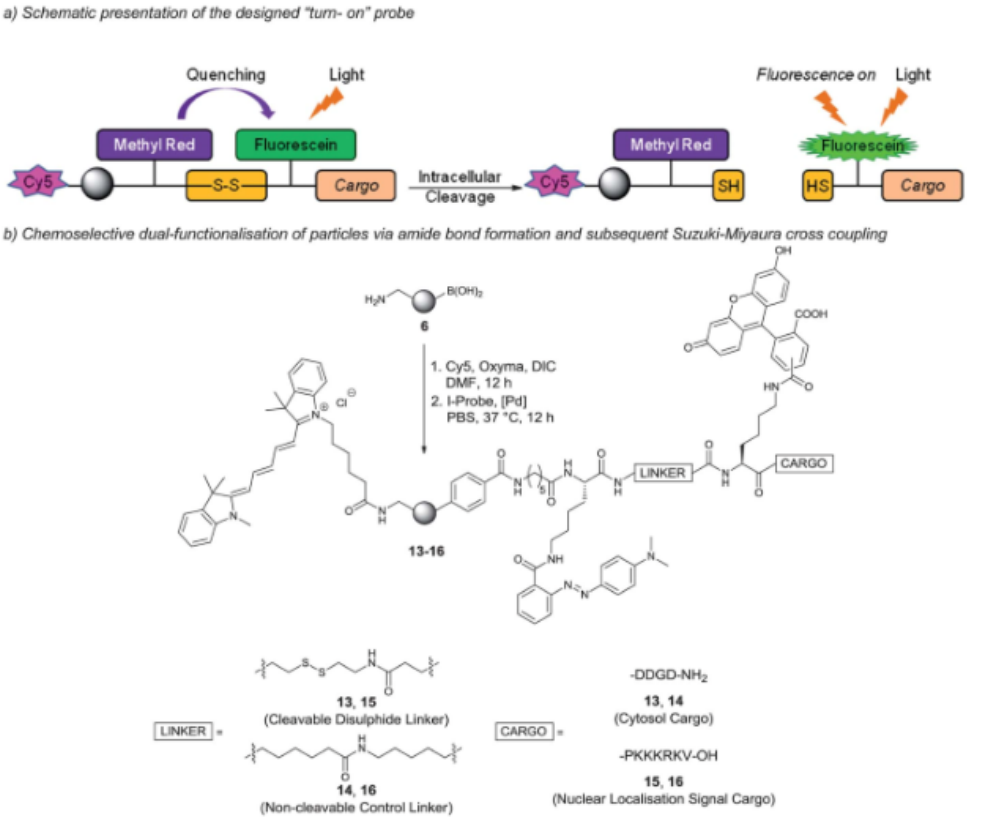

Scheme 3 Dual-functionalised particles and intracellular fluorescein release: (a) probe design and the mechanism of intracellular cargo release and fluorescence "*turn-on*"; (b) dual-functionalisation of particles by conjugation of Cy5 *via* amide formation and subsequent Suzuki–Miyaura cross-coupling of iodo-aryl probes onto particles. **13** = cytosol targeted probe and **15** = nucleus targeted probe (**14** and **16** are negative control probes with non-cleavable linkages).

"*turn-on*" of fluorescence (Scheme 3a) (as a control the disulphide bond was replaced with a hydrocarbon linkage). The cargo moiety was chosen to be a short anionic peptide sequence, DDGD, which would avoid leakage of the released fluorescein out of the cell.

The particle construct **13** was prepared by coupling Cy5 *via* carbodiimide chemistry while the $(HO)_2$B-groups on the particle surface allowed bioorthogonal conjugation of an unprotected peptide cargo containing an aryl-iodide *via* Suzuki–Miyaura cross-coupling (Scheme 3b, Fig. S2†). ICP-OES measurement of the particles revealed a decrease in the boron content for particles **13** (23%). The ability of **13** to release fluorescein was investigated *in vitro* by treatment with dithiothreitol (DTT) followed by analysis of the fluorescence of the particles supernatant. Fluorescence was only detected after DTT (10 mM) treatment of the disulphide-linked probe. As expected, control particles **14** did not release fluorescein (Fig. S3†).

Particles **13** and **14** were incubated with HEK293T and HeLa cells and cellular uptake monitored by flow cytometry detecting Cy5. The Cy5 fluorescence was equal for cells incubated with particles **13** and **14** confirming similar intracellular uptake (Fig. S8†). However, after 48 h incubation a intracellular fluorescence signal "*turn-on*" was detected, demonstrating the intracellular cleavage of the disulphide bond and subsequent release of the fluorescein peptide reporter from particles **13** (Fig. 2). Confocal fluorescence microscopy verified linker-dependent cargo release from the particles and cytosolic localisation (Fig. 3). In contrast, the control particles **14** did not release the fluorescent reporter (Fig. 2 and 3).

Finally, a particle construct was prepared with the intention of delivering the cargo into the cell nucleus. Thus a cargo containing the peptide PKKKRKV, a known nuclear localisation signal (NLS), and the previously described fluorescein–methyl red quencher system was conjugated onto the Cy5-labelled

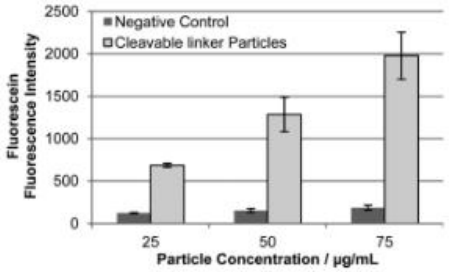

Fig. 2 Quantification of intracellular fluorescein release from particles in HEK293T cells as determined by flow cytometry after 24 h incubation. Light grey = disulphide-linked particles **13**; and dark grey = control particles **14**. ($n = 3$).

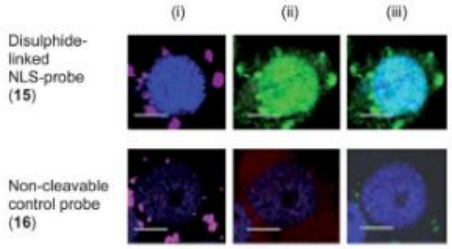

Fig. 4 Release of NLS-fluorescein construct and translocation into the nucleus of HEK293T cells from cleavable disulphide-linked particles **15** and from non-cleavable control particles **16** (50 μg mL^{-1}): (i) blue nucleus stain Hoechst 33342 ($\lambda_{ex} = 404$ nm), magenta: Cy5-labeled particles ($\lambda_{ex} = 633$ nm); (ii) blue: nucleus stain, red: cytoplasm stain celltracker red CMTPX ($\lambda_{ex} = 594$ nm), green: released NLS-fluorescein ($\lambda_{ex} = 488$ nm); and (iii) overlay. Scale bar: 25 μm.

particles affording particles **15** (cleavable disulphide linker) and the non-cleavable control **16** (Scheme 3b). The synthesis of the particles followed the previously established route *via* coupling of Cy5 onto $(HO)_2B/H_2N$-particles following the probe conjugation *via* Suzuki–Miyaura cross-coupling of an iodo-aryl tagged unprotected peptide (Scheme 3b).

As expected, uptake of particles **15** resulted in fluorescent "*turn-on*" in HEK293T and HeLa cells with fluorescein accumulated into the cell nucleus (Fig. 4). In contrast, the control particles **16** did not release the NLS-construct and fluorescein was not observed in the nucleus (Fig. 4). These studies demonstrate the advantages and applications of dual-functionalisation of particles. The attachment of an independent Cy5-label on the particles allowed quantitative measurement of cellular uptake of the particles while the cargo-sensor construct was readily conjugated to the particle and demonstrated intracellular release of the cargo by "*turn-on*" of fluorescence.

Conclusions

In conclusion, the preparation of dual-functionalised nanoparticles containing bioorthogonal boronic acid and aminomethyl groups was successfully demonstrated. The boronic acid groups on the particles allowed the conjugation of complex peptide-reporter cargos by Pd-mediated Suzuki–Miyaura cross-coupling. This conjugation method is reported for the first time and extends the repertoire of benign bioconjugation methods in a bioorthogonal fashion. The modified particles with attached cargos were successfully internalised into cells without cellular toxicity and the applications of these particles demonstrated by intracellular delivery and release of cargos with organelle targeting. Future applications of the dual-functionalised particles as well as the conjugation technique may address the awaiting challenges and opportunities in the field of nanoparticles in chemical biology.

Experimental section

Particle synthesis

Styrene **1** (122 μL, 1 mmol, freshly washed with 4 × 25% NaOH and 4 × brine), divinylbenzene **2** (3.1 μL, 22 μmol, 2 mol% with regards to styrene, freshly washed with 4 × 25% NaOH and 4 × brine), VBAH **3** (5.9 mg, 35 μmol, 3 mol%), 4-vinylbenzylboronic

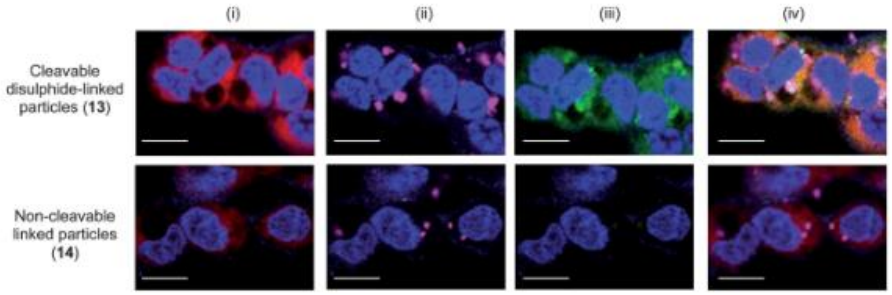

Fig. 3 Confocal fluorescence microscopy images of HEK293T cells following incubation with cytosol targeted probe **13** and non-cleavable control probe **14** (50 μg mL^{-1}). (i) Blue = nucleus stain Hoechst 33342 ($\lambda_{ex} = 404$ nm), red = cytoplasm stain celltracker red CMTPX ($\lambda_{ex} = 594$ nm); (ii) blue = nucleus stain, magenta = Cy5-labeled particles ($\lambda_{ex} = 633$ nm); (iii) blue = nucleus stain, green = released fluorescein ($\lambda_{ex} = 488$ nm); (iv) overlay. Scale bar: 50 μm.

acid **4** (0%; 3%: 5.2 mg, 35 μmol; 6% 10.4 mg, 70 μmol; 9% 15.5 mg, 105 μmol), 2,2-azobis (2-methylpropionamidine) dihydrochloride (V-50) (1.6 mg, 6 μmol) and $MgSO_4$ (0.4 mg, 3 μmol) were added to N_2 purged water (2 mL). The reaction mixture was stirred at room temperature under atmosphere of N_2 for 15 min and subsequently stirred at 80 °C for 15 h. Upon cooling to room temperature, the particles were collected by centrifugation (15 min at 30 000*g*, Eppendorf 5430R) and washed with DMF (3 × 2 mL), MeOH (3 × 2 mL) and water (3 × 2 mL). The particles were stored in water at a solid content of 20 mg mL^{-1}.

General procedure for Pd-mediated particle conjugation

Conjugation of iodated cargo was carried out by Suzuki–Miyaura cross-coupling. A solution of cargo (40 μmol, 50 equiv.) in DMSO (4 μL) was prepared and added to a suspension of $(HO)_2B/H_2N$-particles (0.8 μmol, 1 equiv.) in PBS (1000 μL, pH 7.4) and sonicated for 1 min. Afterwards, catalyst stock solution (2 μmol, 0.2 μL, 5%) were added and the reaction mixture shaken at 1400 rpm at 37 °C for 12 h. The particle mixture was washed in water (3 × 1 mL) and stored in PBS at a concentration of 10 mg mL^{-1}.

Cellular uptake

HEK293T and HeLa were plated in DMEM supplemented with 10% (v/v) heat inactivated fetal bovine serum, L-glutamine (4 mM) and antibiotics (100 units per mL penicillin and 100 units per L streptomycin) growth media in a 24-well plate at a density of 20 000 cells per well and grown for 24 h at 37 °C and 5% CO_2. Thereafter, particles in media (12.5–75 μg mL^{-1}) were added and incubated with the cells for 24 h. Cells were washed with PBS (2 × 350 μL) and incubated for a further 24 h. After incubation, cells were washed with PBS (2 × 350 μL), and imaged under a Leica DM IRB fluorescence microscope or fluorescence pictures were taken on a Leica SP5 confocal microscope. Zeiss 510 Meta software was used for digital acquisition. Images were processed using AutoQuant X software. Quantitative flow cytometric analysis was carried out following the above mentioned particle incubation procedure. Following washing, cells were harvested with trypsin/EDTA and analysed by flow cytometry (BD FACSAria using FlowJo Version 7.6.3 software for data analysis). Flow cytometry was carried out in triplicate and by addition of 2% trypan blue to quench any extracellular fluorescence.[30]

Acknowledgements

The authors would like to thank the MRC UK (F.T.), the European Commission for Marie Curie International Incoming Fellowship to S.V.C. (Project No. PIIF-GA-2009-254238) and Dr Annamaria Lilienkampf for helpful discussions.

Notes and references

1 (*a*) L. M. Alexander, S. Pernagallo, A. Livigni, R. M. Sánchez-Martín, J. M. Brickman and M. Bradley, *Mol. BioSyst.*, 2010, **6**, 399–409; (*b*) S. C. Balmert and S. R. Little, *Adv. Mater.*, 2012, **24**, 3757–3778, and references cited therein. A. Unciti-Broceta, J. J. Díaz-Mochón, R. M. Sánchez-Martín and M. Bradley, *Acc. Chem. Res.*, 2012, **45**, 1140–1152.
2 M. Bradley, L. Alexander, K. Duncan, M. Chennaoui, A. C. Jones and R. M. Sánchez-Martín, *Bioorg. Med. Chem. Lett.*, 2008, **18**, 313–317.
3 R. M. Sánchez-Martín, M. Cuttle, S. Mittoo and M. Bradley, *Angew. Chem., Int. Ed.*, 2006, **45**, 5472–5474.
4 K. Kim, M. Lee, H. Park, J.-H. Kim, S. Kim, H. Chung, K. Choi, I.-S. Kim, B. L. Seong and I. C. Kwon, *J. Am. Chem. Soc.*, 2006, **128**, 3490–3491.
5 J.-Z. Du, X.-J. Du, C.-Q. Mao and J. Wang, *J. Am. Chem. Soc.*, 2011, **133**, 17560–17563.
6 T. C. Yih and M. Al-Fandi, *J. Cell. Biochem.*, 2006, **97**, 1184–1190.
7 R. M. Sanchez-Martin, L. Alexander, M. Muzerelle, J. M. Cardenas-Maestre, A. Tsakiridis, J. M. Brickman and M. Bradley, *ChemBioChem*, 2009, **10**, 1453–1456.
8 L. M. Alexander, R. M. Sánchez-Martín and M. Bradley, *Bioconjugate Chem.*, 2009, **20**, 422–426.
9 J. G. Borger, J. M. Cardenas-Maestre, R. Zamoyska and R. M. Sanchez-Martin, *Bioconjugate Chem.*, 2011, **22**, 1904–1908.
10 F. Thielbeer, S. V. Chankeshwara and M. Bradley, *Biomacromolecules*, 2011, **12**, 4386–4391.
11 For the application of non-degradable nanoparticles see: (*a*) R. M. Sanchez-Martin, M. Muzerelle, N. Chitkul, S. E. How, S. Mittoo and M. Bradley, *ChemBioChem*, 2005, **6**, 1341–1345; (*b*) K. Dhaliwal, L. Alexander, G. Escher, A. Unciti-Broceta, M. Jansen, N. Mcdonald, J. M. Cardenas-Maestre, R. Sanchez-Martin, J. Simpson, C. Haslett and M. Bradley, *Faraday Discuss.*, 2011, **149**, 107–114; (*c*) A. Tsakiridis, L. M. Alexander, N. Gennet, R. M. Sanchez-Martin, A. Livigni, M. Li, M. Bradley and J. M. Brickman, *Biomaterials*, 2009, **30**, 5853–5861.
12 D. B. Tada, L. L. R. Vono, E. L. Duarte, R. Itri, P. K. Kiyohara, M. S. Baptista and L. M. Rossi, *Langmuir*, 2007, **23**, 8194–8199.
13 W. R. Algar, D. E. Prasuhn, M. H. Stewart, T. L. Jennings, J. B. Blanco-Canosa, P. E. Dawson and I. L. Medintz, *Bioconjugate Chem.*, 2011, **22**, 825–858.
14 J. M. Cardenas-Maestre, S. Panadero-Fajardo, A. M. Perez-Lopez and R. M. Sanchez-Martin, *J. Mater. Chem.*, 2011, **21**, 12735–12743.
15 R. K. Iha, K. L. Wooley, A. M. Nyström, D. J. Burke, M. J. Kade and C. J. Hawker, *Chem. Rev.*, 2009, **109**, 5620–5686.
16 V. Hong, S. I. Presolski, C. Ma and M. G. Finn, *Angew. Chem., Int. Ed.*, 2009, **48**, 9879–9883.
17 S. S. Kelkar and T. M. Reineke, *Bioconjugate Chem.*, 2011, **22**, 1879–1903.
18 Z. An, W. Tang, M. Wu, Z. Jiao and G. D. Stucky, *Chem. Commun.*, 2008, 6501–6503.
19 X. Li, J. Guo, J. Asong, M. A. Wolfert and G.-J. Boons, *J. Am. Chem. Soc.*, 2011, **133**, 11147–11153.
20 F. Thielbeer, K. Donaldson and M. Bradley, *Bioconjugate Chem.*, 2011, **22**, 144–150.
21 C. D. Spicer and B. G. Davis, *Chem. Commun.*, 2011, **47**, 1698–1700.

22 C. D. Spicer, T. Triemer and B. G. Davis, *J. Am. Chem. Soc.*, 2012, **134**, 800–803.
23 R. M. Yusop, A. Unciti-Broceta, E. M. V. Johansson, R. M. Sánchez-Martín and M. Bradley, *Nat. Chem.*, 2011, **3**, 241–245.
24 C. S. Chern, *Prog. Polym. Sci.*, 2006, **31**, 443–486.
25 N. Vogel, C. P. Hauser, K. Schuller, K. Landfester and C. K. Weiss, *Macromol. Chem. Phys.*, 2010, **211**, 1355–1368.
26 J. M. Chalker, C. S. C. Wood and B. G. Davis, *J. Am. Chem. Soc.*, 2009, **131**, 16346–16347.
27 A. Hennig, H. Borcherding, C. Jaeger, S. Hatami, C. Würth, A. Hoffmann, K. Hoffmann, T. Thiele, U. Schedler and U. Resch-Genger, *J. Am. Chem. Soc.*, 2012, **134**, 8268–8276.
28 K. Ouadahi, E. Allard, B. Oberleitner and C. Larpent, *J. Polym. Sci., Part A: Polym. Chem.*, 2012, **50**, 314–328.
29 D. A. Fleming, C. J. Thode and M. E. Williams, *Chem. Mater.*, 2006, **18**, 2327–2334.
30 V. L. Mosiman, B. K. Patterson, L. Canterero and C. L. Goolsby, *Cytometry*, 1997, **30**, 151–156.
31 H. Shibata, Y. J. Heo, T. Okitsu, Y. Matsunaga, T. Kawanishi and S. Takeuchi, *Proc. Natl. Acad. Sci. U. S. A.*, 2010, **107**, 17894–17898.
32 The residual Pd content of **10** was investigated by ICP-OES analysis and revealed 44 ng of palladium in 75 μg of particle suspension.

SYNLETT
Spotlight 435

This feature focuses on a reagent chosen by a postgraduate, highlighting the uses and preparation of the reagent in current research

Cyanine Dyes

Compiled by Neil Norouzi

Neil Norouzi was born in Edinburgh, UK, and studied Medicinal and Biological Chemistry at the University of Edinburgh, receiving his M.Chem degree in 2009. Currently, he is a PhD student working under the supervision of Professor Mark Bradley at the University of Edinburgh. His research involves the synthesis of near infra-red dyes and molecular imaging probes.

School of Chemistry, University of Edinburgh, King's Buildings, West Mains Road, Edinburgh, EH9 3JJ, UK
E-mail: N.Norouzi@sms.ed.ac.uk

Introduction

Cyanine dyes are highly conjugated, fluorescent molecules with absorption and emission wavelengths in the near infra-red region (700–900 nm). The simplest synthetic route to heptamethine cyanine dyes **1** (so-called because of the seven carbons in the conjugated backbone) was first described by Narayanan and Patonay who heated N-alkylated indolium salts **2** with 2-chloro-1-formyl-3-(hydroxyl methylene) (**3**) in a Vilsmeier-type reaction.[1] These heptamethine cyanine scaffolds can be readily modified through displacement of the labile chloride group by nucleophiles,[2,3,4] resulting in fluorescent molecules with varying quantum yields, extinction coefficients, and fluorescence maxima. Conjugation to biomolecules is achieved through chlorine substitution by 3-(4-hydroxyphenyl) propionic acid.

The resulting cyanine dye has a carboxylic acid moiety which can be coupled to an amine-containing compound via amide-bond formation. Enhanced aqueous solubility is typically achieved through sulfonation of the indole **2**. As biological tissue does not absorb strongly within the near infra-red window, cyanine fluorophores are ideal for in vivo optical imaging application,[5,6,7] while clinically, indocyanine green has been used for over 25 years in fluorescence angiography and opthalmology (mouse LD_{50} = 60 mg/kg).[8,9]

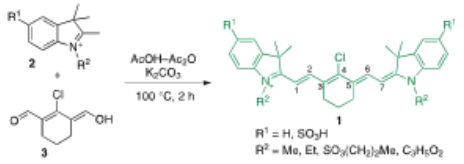

Scheme 1 Synthesis of heptamethine cyanine dyes **1**

Abstract

(A) *Necrosis Detection*
Necrotic tissue is found in a variety of disease states including cancer and sepsis[10] where levels of extracellular DNA are increased due to dead or dying cells. Murthy et al. described a hybrid heptamethine (IR-786)–bisbenzimidazole (Hoechst 33258)[11] probe that accumulates in necrotic tissue by binding to extracellular DNA.[2] In vivo analysis in mice ischemia–reperfusion models confirmed probe accumulation in necrotic tissue.[2]

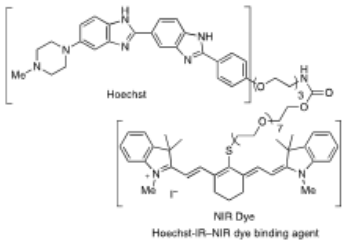

(B) *pH Sensor*
Nagano and co-workers synthesised a ratiometric, NIR heptamethine pH sensor. By using two excitation wavelengths (670 nm and 750 nm), the relative fluorescence intensities (λ_{em} = 780 nm) allowed pH values between 6 and 10 to be readily measured. Incubation of HeLa cells with the sensor resulted in staining of lysosomes and mitochondria with a demonstrable ability to monitor intracellular pH changes.[4]

SYNLETT 2013, 24, 1307–1308
Advanced online publication: 15.05.2013
DOI: 10.1055/s-0033-1338948; Art ID: ST-2013-V0442-V

(C) *Reactive Oxygen Species Detection*

Uncontrolled reactive oxygen species (ROS) are implicated in several inflammatory disease states.[12] Nagano and co-workers reported the real-time analysis of ROS by linking two NIR cyanine dyes with different oxidation potentials.[13] A turn on fluorescence signal was observed upon oxidation of the more susceptible cyanine dye as this removed the static quenching effect. A strong fluorescence signal was found after incubation with a variety of ROS such as the hydroxyl radical (·OH) using Fenton's reagent and superoxide ($O_2^{\cdot-}$) generated from xanthene oxidase.[13]

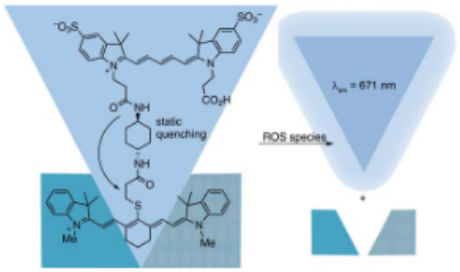

(D) *H_2S Molecule Sensor*

Hydrogen sulfide is known to be an important gaseous signaling molecule and is key in the regulation of blood pressure.[14] Zhang and co-workers developed a real-time NIR sensor for H_2S by incorporating 3-nitrophenol onto the heptamethine dye scaffold which resulted in photo-induced electron transfer (PET)[15] and quenching of the cyanine dye fluorescence.[3] This was liberated by nitro group reduction with hydrogen sulfide. Incubation with other reactive sulfide species such as glutathione and cysteine gave a far weaker fluorescence increase.

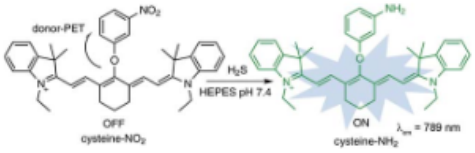

(E) *Silver Sensor*

Bioaccumulation of metal ions such as silver can demonstrate adverse biological effects due to binding to functional groups such as thiols.[16] Zheng, Jiang and co-workers developed a Ag^+ sensor based on a heptamethine cyanine motif that contained an adenine moiety.[17] Aggregation[18] of the cyanine dye with increasing concentrations of Ag^+ ions resulted in a fluorescence shift of 185 nm with a detection limit of 34 nM. High selectivity over other metal ions such as copper and iron was demonstrated.

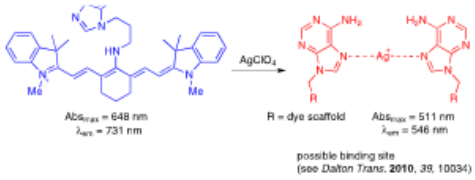

References

(1) Narayanan, N.; Lee, S.; Sy, J.; Patonay, G. *J. Org. Chem.* **1995**, *5*, 2391.
(2) Dasari, M.; Kim, D.; Lee, S.; Brown, M.; Davis, M.; Murthy, N. *Org. Lett.* **2010**, *12*, 3300.
(3) Wang, R.; Yu, F.; Chen, L.; Chen, H.; Wang, L.; Zhang, W. *Chem. Commun.* **2012**, *48*, 11757.
(4) Myochin, T.; Kiyose, K.; Hanaoka, K.; Kojima, H.; Terai, T.; Nagano, T. *J. Am. Chem. Soc.* **2011**, *133*, 3401.
(5) Fry, E. S. *Appl. Opt.* **2000**, *39*, 2743.
(6) Linder, K. E.; Metcalfe, E.; Nanjappan, P.; Arunachalam, T.; Ramos, K.; Skedzielewski, T. M.; Marinelli, E. R.; Tweedle, M. F.; Nunn, A. D.; Swenson, R. E. *Biocon. Chem.* **2011**, *22*, 1287.
(7) Thielbeer, F.; Chankeshwara, S. V.; Johansson, E. M. V.; Norouzi, N.; Bradley, M. *Chem. Sci.* **2013**, *4*, 425.
(8) Taichman, G. C.; Ph, D.; Hendry, P.; Keon, W. *Tex. Heart Inst. J.* **1987**, *14*, 133.
(9) Kodjikian, L.; Richter, T.; Halberstadt, M.; Beby, F.; Flueckiger, F.; Boehnke, M.; Garweg, J. G. *Graefe's Arch. Clin. Exp. Ophthalmol.* **2005**, *243*, 917.
(10) Amaravadi, R. K.; Thompson, C. B. *Clin. Cancer Res.* **2007**, *13*, 7271.
(11) Latt, S. A.; Stetten, G. *J. Histochem. Cytochem.* **1976**, *24*, 24.
(12) Valko, M.; Leibfritz, D.; Moncol, J.; Cronin, M. T. D.; Mazur, M.; Telser, J. *Int. J. Biochem. Cell Biol.* **2007**, *39*, 44.
(13) Oushiki, D.; Kojima, H.; Terai, T.; Arita, M.; Hanaoka, K.; Urano, Y.; Nagano, T. *J. Am. Chem. Soc.* **2010**, *132*, 2795.
(14) Yang, G.; Wu, L.; Jiang, B.; Yang, W.; Qi, J.; Cao, K.; Meng, Q.; Mustafa, A. K.; Mu, W.; Zhang, S.; Snyder, S. H.; Wang, R. *Science* **2008**, *322*, 587.
(15) Griesbeck, A. G.; Hoffmann, N.; Warzecha, K.-D. *Acc. Chem. Res.* **2007**, *40*, 128.
(16) Navarro, E.; Piccapietra, F.; Wagner, B.; Marconi, F.; Kaegi, R.; Odzak, N.; Sigg, L.; Behra, R. *Environ. Sci. Technol.* **2008**, *42*, 8959.
(17) Zheng, H.; Yan, M.; Fan, X.-X.; Sun, D.; Yang, S.-Y.; Yang, L.-J.; Li, J.-D.; Jiang, Y.-B. *Chem. Commun.* **2012**, *48*, 2243.
(18) Tan, C.; Atas, E.; Müller, J. G.; Pinto, M. R.; Kleiman, V. D.; Schanze, K. S. *J. Am. Chem. Soc.* **2004**, *126*, 13685.

